Coding and Multiple-Access over Fading Channels

by

Raymond Knopp

B. Eng. Honours Electrical Engineering
McGill University, Montreal, Canada 1992

M. Eng. Electrical Engineering
McGill University, Montreal, Canada 1994

Citizen of Canada

Submitted to the *Section Systèmes de Communication/Institut Eurécom*

Ecole Polytechnique Fédérale de Lausanne

in partial fulfillment of the requirements for the degree of

docteur ès sciences

Jury members

President:	Prof. M. Vetterli (EPFL)
Thesis supervisor:	Prof. P.A. Humblet (Eurécom)
Reviewers:	Dr. J.C. Belfiore (ENST)
	Dr. G. Caire (Politecnico di Torino)
	Dr. B.H. Fleury (ETHZ)
	Prof. J. Mosig (EPFL)
	Prof. Ch. Wellekens (Eurécom)

Lausanne/Sophia Antipolis
EPFL/Institut Eurécom
1997

Summary

The field of wireless radio communications is undoubtedly one of the most active and economically rewarding sectors in technology today. Existing terrestrial cellular networks already offer both voice and data services at reasonably affordable prices and there will soon be satellite networks which will offer communication services to and from any point on the globe.

This thesis takes a fundamental look at the communication problem over so-called fading channels which are the types of channels encountered in many radio communication systems. The main obstacle that the radio system designer has to cope with is the channel's underlying time-varying and time-dispersive nature. We strive towards a better understanding of the fundamental limits for the communication process over such channels and at the same time, wherever possible, indicate ways for approaching these limits with practical devices. Moreover, in many cases we use channel models which accurately describe the physical media, at the expense of giving up the possibility of presenting analytical solutions.

We show that the channel is prone to outages, in the sense that there is irreducible probability that reliable communication is impossible. These outages can only be avoided if there is some form of channel state feedback from the receiver to the transmitter. We discuss issues such as coding and power control and how they can be used jointly to improve performance both for long-term and short-term measures. Spread-spectrum systems are treated in a general sense and different coding alternatives are compared for such applications.

We examine coding schemes for a particular class of fading channels, known as block-fading channels and show that very practical codes can come close to fundamental limits on performance. Moreover, we have shown that there is a bound on the fundamental performance of such codes which depends on several design factors. We have found a series of block and trellis codes for moderate spectral efficiencies and present computer simulation of their performance.

The last part of this work is concerned with the multiple-access problem over such channels, which is the problem of sharing a common radio medium between a collection of user terminals wishing to communicate with a single base-station. We show that by performing a certain type of dynamic channel allocation using channel state information at the user terminals, we can achieve performances which surpass those of a non-fading environment. The development is simple and relies on the time-varying nature of the fading channel.

Résumé

Les télécommunications par transport hertzien constitue certainement un des domaines des plus actifs et lucratifs de la technologie moderne. Les réseaux cellulaires terrestres offrent déjà des services de transfert de parole et de données à des prix abordables et il y aura bientôt des réseaux de satellites qui offriront des services variés.

L'obstacle principal que doit surmonter l'ingénieur radio est que l'atténuation électromagnétique du signal émis est souvent une fonction des positions du transmetteur et du récepteur étant variables. D'autant plus, la géométrie de l'environnement introduit un effet dispersif du signal dans le temps. On essaiera de mieux comprendre les limites fondamentales du processus de communication sur ces *canaux à évanouissement* et, autant que faire se peut, d'indiquer des méthodes pratiques afin de s'y approcher.

On démontre que la probabilité de perte pour ces canaux est bornée par une valeur non-nulle, qui ne dépend pas de la complexité du codeur de canal, ce qui rend impossible une communication fiable. Ces pertes peuvent être éliminées seulement s'il existe un moyen de mettre le transmetteur au courant de l'état du canal à tout moment. On indique comment des systèmes de codage du canal et contrôle de puissance peuvent être combinés pour améliorer la performance selon des mesures à court et à long terme.

Le problème de codage du canal pour la famille des canaux à évanouissement en bloc est exposé. On démontre qu'il existe une borne fondamentale sur la performance qui dépend des choix d'implantation du système (modulation, taux de codage, délai de décodage, largeur de bande). Dans certains cas, on peut s'approcher de cette borne avec des codes très simples pour des efficacités spectrales modérées. On donne des exemples de codes en blocs et en trellis et on présente des simulations par ordinateur pour étudier leurs performances.

Dans la dernière partie de ce travail on traite l'accès-multiple sur les canaux à évanouissement, c'est-à-dire les méthodes pour partager le canal radio parmi un ensemble d'utilisateurs qui veulent communiquer simultanément avec une station de base centralisée. On démontre qu'en utilisant un méthode d'allocation dynamique du spectre qui exploite des mesures de l'atténuation de tous les canaux en parallèle, on peut atteindre des niveaux de performance qui dépassent même ceux du canal sans évanouissement.

Acknowledgements

First and foremost I wish to thank my supervisor, Professor Pierre Humblet, who gave me the opportunity to work on interesting problems at my own pace. His deep insight and experience in so many different areas was definitely a great help in understanding some of the finer points of digital communications. I am truly fortunate to have worked with him. The comments made by my jury members were very helpful and I am very grateful for their diligence in reviewing my thesis. Special thanks must go to Dr. Giuseppe Caire from the Politecnico di Torino, with whom I had many stimulating discussions during his stay at Eurécom. This collaboration was a great pleasure which I hope will continue in the future.

The financial aid provided by Eurécom and the Fonds FCAR (*Fonds pour la formation de chercheurs et l'aide à la recherche -Québec*) was greatly appreciated.

My friends in the Eurécom community have made my stay on the Côte d'Azur the most memorable experience of my life. Although I am leaving out many people, who I hope will not hold it against me, I wish to thank in particular for their friendship and kindness: Karim Maouche, Didier Samfat, Christian Blum, Alaa Dakroub, Christoph Bernhardt, Markos Troulis, Constantinos Papadias, Christian Bonnet, Dirk Slock, Ubli Mitra, Jörg Nonnenmacher, Stéphane Decrauzat and Philippe Gélin. Eurécom is a truly wonderful place which I hope will continue to grow and prosper.

My father's moral support was instrumental in my obtaining my doctorate. Everything I have accomplished is due to him. My late mother will always be in my heart and has always been able to guide me in her own special way. I wish to thank my grandmother who has always been a source of wisdom and encouragement.

Finally, I must thank Cathy. Her unfailing love and strength was an enormous help during the final stage of my studies. Putting up with me while I was hospitalized and the following month at home was not an easy task. I can only hope to play the same role in her life as she does in mine.

Contents

1 Introduction **1**

1.1 Thesis Outline 2

2 Mobile Radio Channels **5**

2.1 A Basic Overview of Radio Communications and Propagation Effects 5

2.2 Models for Path Loss and Shadowing 9

2.2.1 Path Loss in Free–Space 9

2.2.2 Measurement-based Models 10

2.2.3 Lognormal Shadowing 12

2.3 Short–term Fading 13

2.3.1 An Illustrative Example 13

2.3.2 The Gaussian Fading Model 15

2.4 Wideband channel models 21

2.4.1 Poisson arrival models 22

2.4.2 COST 207 models 23

2.4.3 Indoor Models 23

3 Signaling over Fading Channels **25**

3.1 Performance Measures 27

3.2 Diversity Reception 28

3.3 Narrow-band Information Signals over Doppler–Spread Channels 30

3.3.1 Optimal Receivers 32

3.3.2 Pairwise Error Probability - Binary Signals 35

3.3.3 Coded Quadrature Amplitude Modulated Signals 40

3.3.4 Interleaved Signals . . . 47
3.4 Wide-band Direct–Sequence Spread-Spectrum . . . 50
3.4.1 Receiver Structures . . . 51
3.4.2 RAKE Receiver Performance . . . 54
3.5 Multitone Signaling . . . 55
3.5.1 Multitone Receiver and Performance Criteria . . . 56
3.5.2 Multitone spread–spectrum . . . 57
3.6 Block Fading Channels . . . 58
3.6.1 System Model and Examples . . . 58

4 Mutual Information and Information Outage Rates 69
4.1 A generic time–varying channel model and basic definitions . . . 70
4.1.1 Block–Fading Channels . . . 74
4.2 Additive White Gaussian Noise (AWGN) Channels with Fading . . . 76
4.2.1 Calculating the Average Mutual Information . . . 76
4.2.2 Static Multipath Channels . . . 78
4.2.3 Multi-tone Signals . . . 80
4.2.4 Block–Fading AWGN Channels . . . 88
4.3 Chapter Summary . . . 89

5 Code Design for Block–Fading Channels 93
5.1 System Model and Outage Probability Analysis . . . 95
5.2 Maximum Code Diversity . . . 98
5.2.1 An introductory example . . . 105
5.2.2 Maximum Diversity Bound . . . 108
5.2.3 Block Codes . . . 110
5.2.4 Trellis Codes . . . 114
5.3 Computer simulation of various codes . . . 122
5.4 Chapter Summary . . . 123

6 Systems Exploiting Channel State Feedback 137
6.1 Variable Power Constant Rate Systems . . . 138
6.1.1 Multiple Receivers in Single–Path Rayleigh Fading . . . 138

6.1.2 Spread–Spectrum . . . 140
6.2 Variable Rate Schemes . . . 142
6.2.1 Average Information Rates . . . 142
6.2.2 Water–Filling . . . 143
6.3 Simple two–rate schemes with and without power control . . . 146
6.3.1 BER Comparison for Uncoded Transmission . . . 148
6.4 Average information rate with retransmissions . . . 154
6.5 Chapter Summary . . . 159

7 Multiuser Channels and Multiuser Diversity 163
7.1 Multiple–Access Channels without fading . . . 164
7.1.1 Orthogonal Multiplexing . . . 165
7.1.2 Non–Orthogonal Multiplexing . . . 167
7.1.3 Joint Detection on the MAC . . . 170
7.2 Outage Probability Analysis of Single–User Decoding in the Multiple–Access Channel with Multipath Fading . . . 175
7.3 Average Information Rates - Multiuser Diversity . . . 179
7.3.1 Generalizing the Single–User Average Mutual Information for the Fading MAC . 179
7.3.2 Systems Without Fast Power Control . . . 181
7.3.3 Channel State Feedback and Multiuser Diversity . . . 184
7.3.4 The Fading Channel Capacity Region . . . 186
7.3.5 Multiuser Diversity with Perfect Power Control . . . 194
7.4 Chapter Summary . . . 197

8 Conclusions and Areas for Further Research 203
8.1 Conclusions . . . 203
8.2 Areas for further research . . . 205

Chapter 1

Introduction

The field of wireless radio communications is undoubtedly one of the most active and economically rewarding sectors in technology today. Over the last decade we have all grown accustomed to seeing people walking in city streets with hand–held portable phones. Whether we are ready to accept it or not at this point, it is inevitable that we will all soon make use of some form of wireless communication. The existing terrestrial cellular networks already offer both voice and data services at reasonably affordable prices and there will soon be satellite networks which will offer communication services to and from any point on the globe.

The technology breakthroughs in *Very Large Scale Integration (VLSI)* have made this explosion we are witnessing today possible since they have paved the way for the implementation of all–digital signal processing in the radio transmitters and receivers. This, in turn, allows for very sophisticated communication techniques, such as digital modulation, equalization, error control coding and others which were very difficult and expensive to implement until now. With this powerful tool at our disposal, we can really take advantage of the enourmous wealth of knowledge that communication theorists have amassed since the pioneering work of Claude Shannon [Sha48a][Sha48b] first appeared. The result of his ideas has pushed digital communications over the telephone channel to the limit and there is no reason why the same cannot be accomplished on the mobile radio channel. The latter seems to be formidable task however, because of the underlying physical nature of the medium.

The goal of this thesis is to take a small step towards a better understanding of the fundamental limits for the communication process over a mobile radio channel and at the same time, wherever possible, indicate methods for approaching these limits with practical devices. We will see that the mobile radio channel is quite difficult to characterize, in comparison to wired channels, and as a result we often

have to resort to heuristic models to analyse certain situations.

1.1 Thesis Outline

The main obstacle that the radio system designer has to cope with is the channel's underlying time–varying and time–dispersive nature. This type of channel is commonly refered to as a *fading* channel. We have chosen to focus our study on the communication problem over such a channel. We have tried to keep our treatment as close to practical systems as possible without dwelling too much on theoretical details. We use propagation models from systems in use today to apply the theories we develop, with our primary objective being to gain insight into practical system design issues.

In order to better understand the physical nature of the medium we begin with a short chapter dealing with basic issues in radio propagation. It goes without saying that a sufficient understanding of the underlying physics is a prerequisite for achieving performance approaching fundamental limits. This is at the same time necessary to *define* the fundamental limits. We stress, however, that our treatment of radio propagation is by no means complete and is only meant to introduce the reader to the subject. At the same time, we define the propagation models used in the remainder of the work. We describe the three–scale model for the fluctuations of the radio signal strength as the receiver moves in space, which is composed of very short and very long–scale time–varying phenomena. We show that the time–dispersive nature of the channel also causes strong variations in the frequency spectrum of the radio signal, which is an important issue for wideband systems. We describe basic statistical models which characterize the time–varying and time–dispersive nature of the channels.

Chapter 3 deals with issues in signal design for fading channels for the different types of system alternatives. No new results are presented, but we treat many topics which are not included in standard texts on the subject but which have appeared in the litterature. This chapter is crucial for understanding the models and approaches for analysing fundamental limits in subsequent chapters. We define the notion of signal *diversity* and how it is related to the number of degrees of freedom needed to characterize the underlying channel process. We consider three basic ways of achieving diversity

1. Multireceiver Diversity

2. Time Diversity

3. Frequency Diversity

We show that each is due to a different phenomenon but all three are analysed in the same way and are essentially equivalent.

The fourth chapter defines the basic information theoretic quantities needed to determine the fundamental limits for communication over point–to–point fading channels. On wired channels, such as the telephone channel, which are practically time–invariant, the basic quantity defining the fundamental limit on the amount of information that can be transmitted is the *channel capacity* defined by Shannon [Sha48a][Sha48b]. The channel capacity is the maximum information rate in bits/second at which reliable communication is possible. In his theory, reliable communication was taken to mean that by appropriately coding the information at the transmitter, arbitrarily low probability of decoding error can be achieved. There is no guarantee, however, that the complexity of the decoding process is low, and generally it is not. We show that on a fading channel, no such maximum limit need exist and it is often the case that reliable communication, in Shannon's sense, is impossible. This fact is solely due to the time–varying nature of the channel.

If the transmitter has no *a priori* knowledge of the state of the channel at any given time and he is subject to some processing delay constraint, the communication is always corrupted by outages. These are due to the times when the signal strength drops to an unacceptable level during the transmission of the "short" message. By short we mean relative to the speed at which the channel fluctuates. Another explanation for the presence of outages in the communication process is that when insufficient processing time is available, we are not able to average (or spread information) over the different realizations of the channel.

In the fourth chapter we look at practical coding schemes for approaching the fundamental limits for a certain class of channels. These are called block–fading channels and from a practical point of view can represent a variety of systems. We are interested in finding error–control codes and bounds on the ultimate performance of practical codes with reasonable complexity which perform close to the fundamental limits defined in Chapter 4. We show that in some cases, this can be done without too much effort.

We then examine the case when channel state information is available at the transmission end in Chapter 5. We demonstrate that outages can be avoided in some cases using power control, or utilized effectively to conserve power and increase long–term information rates. We give simple examples of variable–rate schemes which can potentially come very close to optimal performance.

Chapter 6 deals with multiple–accessing. Simply put, this is a problem of allocating the energy of several independent users on the same physical channel. This can be done in various ways, and we

examine the achievable performance for the different alternatives on the fading channel. We focus our treatment on the *many–to–one* communication problem, which in cellular communications is called the *uplink*. Here many users share a common medium and transmit their information to the same receiver. We show that the achievable performance over a fading channel can actually surpass that of a non–fading channel because of the time/frequency–varying nature of the channel coupled with the fact that the medium has to be shared. The key lies in using an allocation strategy which forces the users to transmit only when their respective channel conditions are favourable, or equivalently, at points in time/frequency where reliable communication is more likely to take place.

Chapter 2

Mobile Radio Channels

This chapter gives a small introduction to the propagation characteristics of typical mobile radio channels, such as those encountered in today's personal communications systems (e.g. the *Global System for Mobile Communications (GSM)* [GSM90]). It is not a complete treatment of the subject and it is only meant to define the necessary propagation effects and models which will be used in the remainder of this thesis. More complete treatment of the subject can be found in classic books such as Lee [Lee82] and Jakes [Jak74]. Many of the recent advances in the characterization of the mobile radio channel has come out of European research, and the success of the GSM system came to a great extent as a result of it. A recent article which gives a very complete description of the the past and current European research results is Fleury [FL96].

In our treatment, we begin with a general description of the electromagnetic spectrum and the different bands in which today's and future systems lie. We then go on to explain the three scale models for the attenuation effects on typical land–mobile radio channels. Each effect is then treated in turn with an emphasis on the short–term attenuation characteristics, since the main goal of this thesis is to find communication methods which are robust in the presence of these characteristics. The basic statistical models for predicting signal fluctuations are described using a framework suitable for the analyses of later chapters. We describe a few generic propagation models for urban, rural and hilly terrain which we use for numerical computations throughout this thesis.

2.1 A Basic Overview of Radio Communications and Propagation Effects

Radio communications occupy a large part of the electromagnetic spectrum. As a result of international agreement the radio frequency spectrum is divided into the bands shown in Table 2.1 The VLF band

Frequency band	Frequency range
Extremely low frequency (ELF)	$<$ 3kHz
Very low frequency (VLF)	3-30kHz
Low frequency (LF)	30-300kHz
Medium frequency (MF)	300kHz-3MHz
High frequency (HF)	3-30MHz
Very high frequency (VHF)	30-300MHz
Ultra high frequency (UHF)	300MHz-3GHz
Super high frequency (SHF)	3-30GHz
Extra high frequency (EHF)	30-300GHz

Table 2.1: Radio Frequency Bands

is used only for very special applications such as communication with submarines and some navigation systems. In general, the bands below MF have limited application due to the large size of the transmitting antennas. The MF band is used for commercial AM broadcasting. The HF band is not used for land–mobile communications even though long–distance communication is possible due to reflections off the different layers of the ionosphere [Par92]. The unpopularity of this band is mainly due to the fact that the height of the different layers varies greatly as a function of the time of day, the season and the geographical location. The most common bands for mobile radio as well as FM radio and television broadcasting are the VHF and UHF bands. Communication is achieved mainly by a direct path and a ground reflected component. What makes these bands most challenging from the point of view of the system designer is that he must cope with the possibility of signal reflection, refraction and diffraction from natural and man–made obstructions. The SHF band is used mainly for satellite communications, point–to–point terrestrial links, radar and short–range communications. The EHF or millimeter–wave band is receiving considerably more attention recently in the literature because of the enormous amount of spectrum available for use. The main problems with this band, again from the point of view of the system designer, are scattering due to rain and snow and the strong absorption lines at 22GHz (water–vapour) and 60 GHz (oxygen). There are bands between these lines (absorption bands) which are currently being considered for mobile communications [BR97].

Let us take a closer look at the propagation effects on mobile radio channels by considering the outdoor communication scenario depicted in Figure 2.1. The antenna at point 1 radiatess an electromag-

netic wave which is the result of modulating a chosen carrier frequency by an information–bearing signal. The electric and magnetic fields for any given location (e.g. at receivers 2 and 3) at any given instant of time are a superposition of the fields of many waves resulting from reflections, refractions and diffractions of the transmitted wave off nearby and far–off objects referred to as *scatterers*. Scatterers may be buildings, mountains, trees or even mobile objects such as cars or trains. The name stems from the fact that these objects are not ideal reflectors due to the roughness of their surfaces which tends to cause diffuse scattering. Similar effects also occur in indoor and satellite channels. There is often no direct

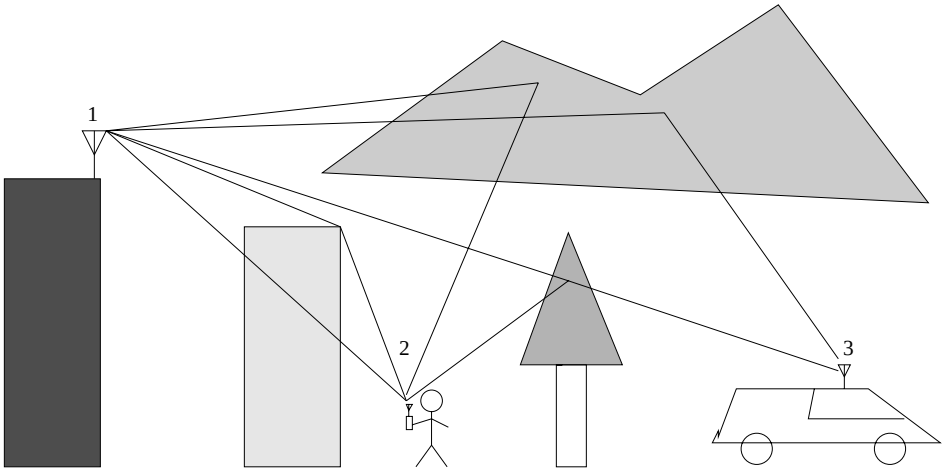

Figure 2.1: Outdoor Scenario

or *line–of–sight (LOS)* path between the transmitter and receiver or this path may be heavily attenuated or *shadowed* by a large object so that the received wavefront is due mainly to the diffuse components which are heavily location–dependent. This is especially true in built–up urban areas where the received energy at the mobile station is mostly results from diffraction. Since this is a worst–case situtation, the system designer must attempt to devise methods for dealing with non–LOS location dependent signal power fluctuations, or *signal fading*. The use of the term fading arises from the fact that the signal power varies in time as the mobile station moves. We remark, however, that in indoor environments the received signal power may vary in time even if the receiver is not in motion. This is because the scene can change to a great extent due to the presence of walking people or the opening and closing of doors or windows. This can also happen to a certain extent in outdoor systems due, for example, to trucks.

Signal fading also occurs in the frequency–domain. Because of the presence of multiple time–delayed replicas of the transmitted signal, we will see that the mobile radio channel may often be seen as a linear time-invariant filter for each location. As a result, there are some frequencies where the signal

power at the receiver is higher than others, so that the signal power *fades* in frequency.

One often models the location dependent propagation effects statistically. This allows the system designer to predict system performance, usually by averaging over the statistics of the received signal power or, equivalently, over all possible relative positions of the receiver/transmitter pair. The use of statistical models is not solely for mathematical convenience, since they were, for the most part, based on the results of empirical data. Later, different physical explanations for these measurements were used to develop the statistical descriptions. In a very simple sense, the source of randomness can be explained firstly by the fact that attenuation due to scattering off rough surfaces are random due to the position and electromagnetic properties of the objects. Secondly, the location of the mobile station has a certain degree of uncertainty.

One can distinguish three levels of signal attenuation which are due to *propagation path loss*, *shadowing* and *multipath propagation*. The first can sometimes be explained physically and can be accurately measured. The other two are usually modeled statistically.

Propagation path loss is dependent on the distance between the receiver and transmitter and is random only due to the position of the mobile station. For practical systems where the processing time of information bursts is not very long, the path loss, even for quickly moving objects, changes very little. Moreover, many systems are designed to offer the same quality of service independently of the distance between the mobile user and the basestation so that some form of power control is needed to counter the path loss and usually shadowing too.

Fading due to shadowing is slow, in the sense that it changes little over fairly large regions. The degree of variation is an issue which is constantly being debated. Some believe that it can be noticeable when the mobile moves only a few meters, as some paths are blocked by large objects such as trees or buildings. Shadowing and path loss can be seen as slow fluctuations of the mean signal power as the mobile moves and are virtually frequency–invariant. If we consider Figure 2.2 we see that for a far–off receiver/transmitter the long–term fading components are more or less constant within the differently shaded regions.

As we already mentioned, multipath propagation causes rapid power fluctuations as the mobile station moves, even over very short distances. For this reason, it is called *short–term* or fast fading. Since these fluctuations are heavily frequency–dependent the bandwidth of the transmitted signal is critical in describing the effects of multipath.

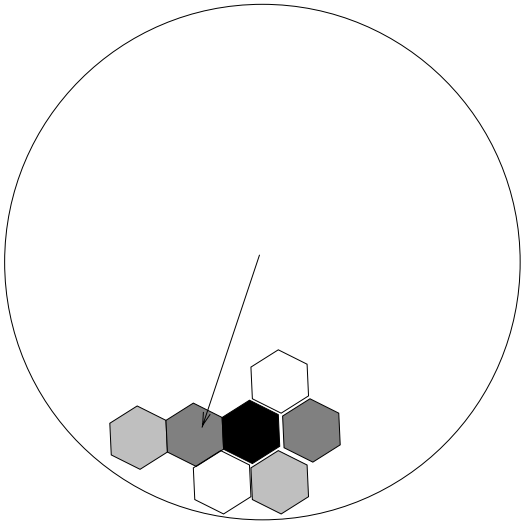

Figure 2.2: Long–term fading component

2.2 Models for Path Loss and Shadowing

The most widely employed mathematical models for path loss and shadowing came about from the results of numerous experimental studies in a wide variety of environments. Some more recent studies for dense urban areas, for example [WB88], are based on approximations using the theory of diffraction and some empirical corrections.

These models are extremely important for the planning phase during the deployment of a cellular network. The more accurate the model, the less the need for on–site measurements when placing base stations. In addition to these models, computer simulations based on optical approximations for electromagnetic propagation (ray–tracing [RH92][Kim97]) accurately describing the spatial distributions of the path loss/shadowing. These software tools are especially powerful for indoor systems, where the basic geometry of the environment is easily described.

2.2.1 Path Loss in Free–Space

Path loss in free–space can be analytically described by the *free–space transmission formula*

$$\frac{P_R}{P_T} = \left(\frac{\lambda}{4\pi d}\right)^2 G_T G_R \tag{2.1}$$

where P_R and P_T are the received and transmitted powers at the respective antennas, λ is the wavelength, d is the distance between the receiver and the transmitter in meters, while G_T and G_R are the antenna gains. This is useful in obtaining a rough idea of the true path loss in an outdoor environment. For

isotropic antennas $G_T = G_R = 1$ so that the path loss can be expressed in decibels as

$$L_{\rm FS} = 32.4 + 20\log_{10} d + 20\log_{10} f \quad \text{dB} \tag{2.2}$$

where d is now in kilometers and f is the frequency in MHz. We see that the power decays with 20 dB/decade in both frequency and distance. This means, first of all, that path loss is a virtually time–invariant phenomenon for practical mobile speeds. Secondly, it is also practically frequency–invariant. As an example, imagine a high data–rate system with carrier frequency 1.25 GHz and signalling bandwidth 10MHz. The path loss difference at the two extreme points of the signal bandwidth is $20\log_{10} 1.26/1.24 = .139$ dB. In reality, the presence of a strong reflection off the ground causes the power to decay with 40 dB/decade (or inverse $4^{\rm th}$ power) when the distance separating the transmitter and receiver is much larger than the heights of the two antennas. [Lee82].

2.2.2 Measurement-based Models

We now briefly describe a few classic models for the path loss which were based on measurements.

Okumura's Tokyo Model

The first empirical model for path loss in an urban area was proposed by Okumura [OOKF68]. It is based on extensive measurements made in Tokyo. It adjusts the free–space path loss equation with empirical constants depending on the heights of the fixed and mobile terminals and the type of terrain and area geometry (hilly, sloping, land–sea, presence of foliage and street orientation with respect to the fixed terminal). The path loss formula is given by

$$L_{\rm Okumura} = L_{\rm FS} + A_m(f,d) - H_B(h_B,d) - H_M(h_M,f) - K_U(f) - K \quad \text{dB} \tag{2.3}$$

where $L_{\rm FS}$ is the free–space path loss given in (2.2), $A_M(f,d)$ is a frequency and distance dependent factor indicating the median attenuation with respect to free–space loss in an urban area over quasi–smooth terrain. His measurements assumed a fixed terminal antenna height of $h_B = 200{\rm m}$ and mobile terminal antenna heigh of $h_M = 3{\rm m}$. $H_B(h_B,d)$ and $H_M(h_M,f)$ are the distance/frequency–dependent height gain factors, $K_U(f)$ is the so–called urbanization factor (depending on whether the environment is urban, suburban or an open area) and K is an additional term for taking account certain characteristics of the terrain (hilly, sloping, land-sea, foliage, etc.) These adjustment factors are all tabulated in curves for different environmental parameters [OOKF68].

Hata's and COST 231 Refinements

The main problem with Okumura's model is computing the different adjustment factors from tabulated data. Hata [Hat80] came up with the following formula which yields path–loss predictions which are almost indistinguishable from Okumura's without the need for these curves

$$L_{\text{Hata}} = 69.55 + 26.16 \log_{10} f - 13.82 \log_{10} h_B - A_m(h_M, f) + \tag{2.4}$$

$$(44.9 - 6.55 \log_{10} h_M) \log_{10} d + K_U(f) \quad \text{dB} \tag{2.5}$$

where

$$A_m(h_M, f) = (1.1 \log_{10} f - .7) h_M - (1.56 \log_{10} f - .8) \quad \text{dB} \tag{2.6}$$

is the correction factor for the mobile terminal's antenna height in a small or medium–sized city and

$$A_m(h_M, f) = \begin{cases} 8.29(\log 1.54 h_M)^2 - 1.1 & f \leq 200\text{MHz} \\ 3.2(\log 11.75 h_M)^2 - 4.97 & f \geq 400\text{MHz} \end{cases} \tag{2.7}$$

is the same factor for a large–sized city. The urbanization correction factor, $K_U(f)$, is zero in an urban area. In a suburban area it is given by

$$K_U(f) = -2(\log_{10}(f/28))^2 - 5.4 \quad \text{dB} \tag{2.8}$$

and in an open–area by

$$K_U(f) = -4.78(\log_{10} f)^2 + 18.33 \log_{10} f - 40.94 \quad \text{dB}. \tag{2.9}$$

This model is valid in the 150-1000 MHz frequency range and for distances of 1-20km. Also, the fixed terminal antenna height is 30-200m and for the mobile station 1-10m.

A similar model was proposed within the COST 231 project for the 1500-2000MHz frequency range for use in analyzing the DCS 1800 and PCS 1900 microcellular systems. We see that these empirical models aim at capturing the effects not predicted by the free–space transmission formula since the attenuation drops off with around 40 dB/decade and not 20 dB/decade.

Diffraction Models and Ray–Tracing

For microcellular and picocellular systems, the simple models for predicting path loss start to break down. This is due to several reasons, most notably the reduced height of the base stations. As shown in

Figure 2.1 , because of the presence of buildings and the fact that base stations are normally placed on the rooftops, the propagation path to the mobile station often is the result of a diffraction off the edge of a building. As a result, the empirical formulations based on Okumura's model had to be modified to take this new effect into account. We do not go into any details of these models except to make reference to the work of Walfisch and Bertoni [WB88] and Ikegami *et al* [IYTU84]. These methods were also used in the COST 207 and 231 projects [FL96]. For the case of rural mountainous areas, similar diffraction–based models are reviewed in Kürner *et al* [KCW93].

For indoor channels much less empirical modeling of path loss has been performed. One of the main problems is that the path loss properties vary greatly from one room to another or one corridor to another. For this reason, many computer simulation based studies using ray–tracing algorithms have been proposed [RH92][Kim97]. These algorithms use ray–optical approximations for reflections, refractions and diffractions to model the electromagnetic propagation within buildings. These are particularly appealing since the number of base stations required to service the location can be roughly determined and placed without having to resort to electromagnetic measurement. Their placement can then be adjusted once the system is in operation based on observed performance. In fact, some wireless companies sell systems which have signal–to–noise ratio measurement as a built–in feature in the handset to help in the placement of the base stations. Another possible advantage of Ray–Tracing algorithms is that the next generation of *intelligent buildings* can potentially be designed by architects with wireless communication in mind.

2.2.3 Lognormal Shadowing

The other long–term fading effect, called *shadowing* is a result of the fact that waves incident at the receiver are attenuated or vanish due to the presense of large objects. The characterization of this phenomenon is usually done statistically as for the short–term fading component described in the following sections. If we examine a typical average received power measurement as the mobile moves as in Figure 2.3, where the average is taken across distances of several hundreds of wavelengths. This averages–out the short–term fading component and leaves only the components due to path loss and shadowing which vary insignificantly over these intervals. It was found [ACM88] that the variation around the mean of this curve on a dB scale, which is the path–loss component, is approximately Gaussian with standard deviation, σ_{sh}, from 6–8 dB. The amplitude factor due to shadowing is therefore a lognormal random

variable given by

$$A_{\rm sh} = 10^{.1\sigma_{\rm sh}\zeta} \tag{2.10}$$

where ζ is a zero–mean Gaussian random variable with variance 1.

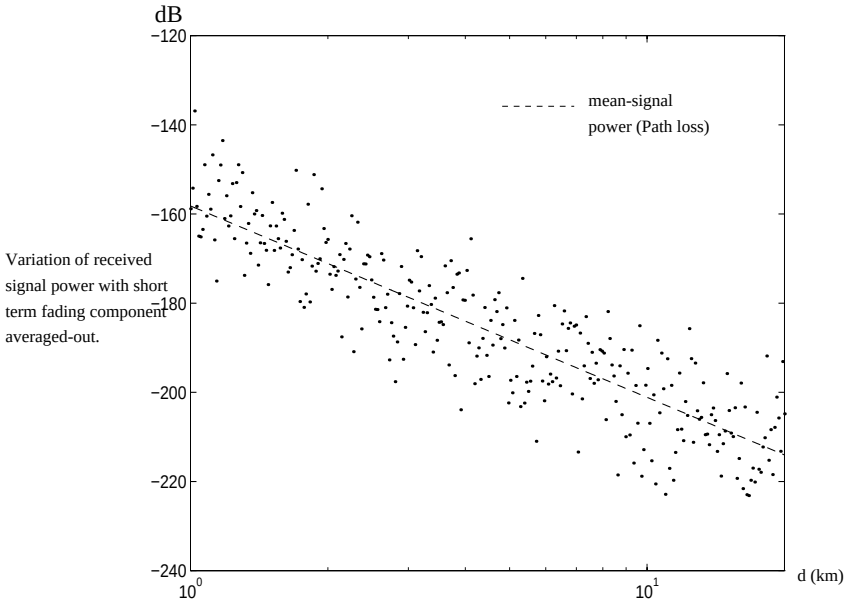

Figure 2.3: Variation of the mean signal strength

The spatial correlation of the shadowing component receives relatively little attention in the literature. Some authors make conjectures about these statistics [Ker96],[Gud91], however it is not clear whether there are any physical grounds to support them. Most seem to be chosen to simplify mathematical performance analysis, the goal only being to have a rough idea as to the effect of shadowing correlation.

2.3 Short–term Fading

2.3.1 An Illustrative Example

Let us first consider the short–term fading characteristics of the received signal for the simple 2–dimensional example shown in figure 2.4. We have a basestation with antenna height h_T and a mobile station with height h_M separated by x meters in the horizontal direction. The basestation transmits an unmodulated carrier with power P_T and frequency f_c. The path lengths are given by

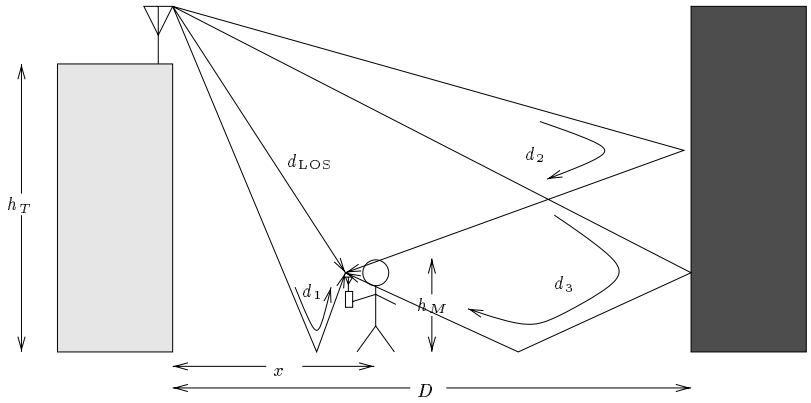

Figure 2.4: An illustrative example of short–term fading

$$d_{\mathrm{LOS}} = \sqrt{x^2 + (h_T - h_M)^2} \tag{2.11}$$

$$d_1 = \sqrt{x^2 + (h_T + h_M)^2}$$

$$d_2 = \sqrt{x^2 + 4D^2 - 4Dx + (h_T - h_M)^2}$$

$$d_3 = \sqrt{x^2 + 4D^2 - 4Dx + (h_T + h_M)^2}$$

and their corresponding phases are

$$\phi_i = \frac{2\pi f_c d_i}{c}$$

where $c = 3 \times 10^8$ m/s is the speed of light. We have assumed that the leftmost building is a perfect absorber so that no received energy is due to a reflection off of it. The ratio of received to transmitted power is therefore

$$\frac{P_R}{P_T} = \left(\frac{c}{4\pi f_c}\right)^2 \left| \frac{1}{d_{\mathrm{LOS}}} e^{j\phi_{\mathrm{LOS}}} + \frac{a_1}{d_1} e^{j\phi_1} + \frac{a_2}{d_2} e^{j\phi_2} + \frac{a_1 a_2}{d_3} e^{j\phi_3} \right|^2 \tag{2.12}$$

where a_1 and a_2 are the reflection coefficients of the ground and the rightmost building respectively . In Figure 2.5 we show the variation of the power ratio with distance assuming $h_T = 30$m, $h_M = 2$m, $D = 1$km, and $a_1 = a_2 = -1$(total reflection) and f_c =100MHz, 1GHz and 10GHz. We see that the received power fluctuates greatly as a function of the mobile position, especially as we approach the rightmost building where it exhibits an almost random behaviour. This behaviour is especially pronounced at higher carrier frequencies. This is due to the increasing complexity of the interference pattern as the powers of all paths start to become similar. For real mobile radio channels in urban environments where there are many paths this randomness is even more evident. In Figure 2.6 we show the frequency response in a 1MHz bandwidth starting at 1GHz. Here the fading effect in the frequency domain is evident and leads

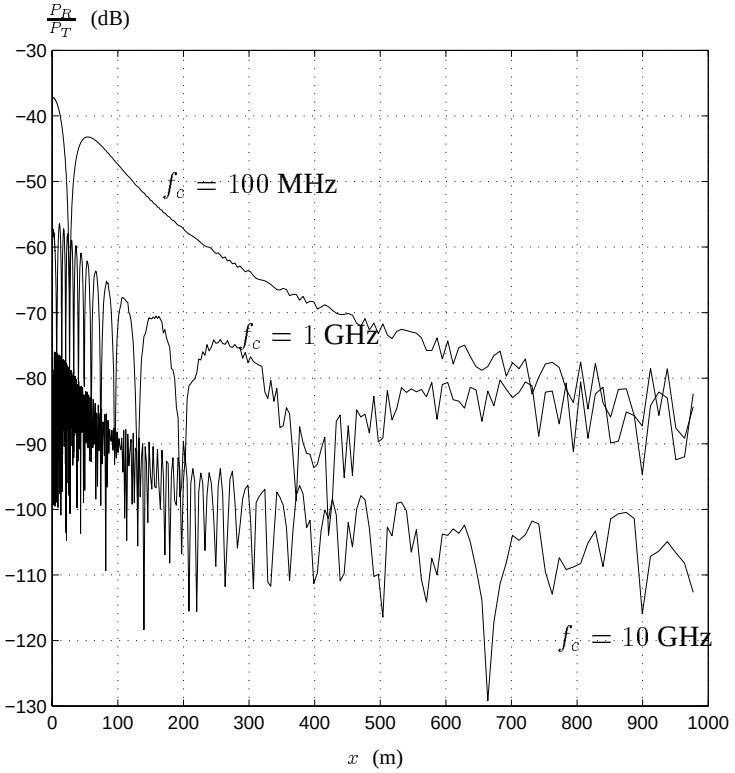

Figure 2.5: Received to transmitted power ratio as a function of mobile position

us to the notion of a *coherence bandwidth*, which indicates the signal bandwidth where the channel is practically flat or non time–dispersive. This allows the system designer to quantify the border between narrow and wideband signals. If we define *flat* as a 3dB bandwidth, then coherence bandwidth is on the order of 200 kHz for this example.

2.3.2 The Gaussian Fading Model

The statistical description of multipath propagation was given by Clarke [Cla68] and further refinements were done by Jakes [Jak74]. We summarize these results for both *static* and *dynamic* multipath channels. A static channel is one where the mobile station is stationary or virtually stationary and we are interested in a statistical description of the received power which does not change in time. A dynamic channel is one where the mobile station is moving with a specified velocity.

In the following chapters we will mainly be concerned with *block* static multipath channels. This is an approximation of a dynamic channel which changes very slowly so that it may be considered as static over blocks or intervals of time.

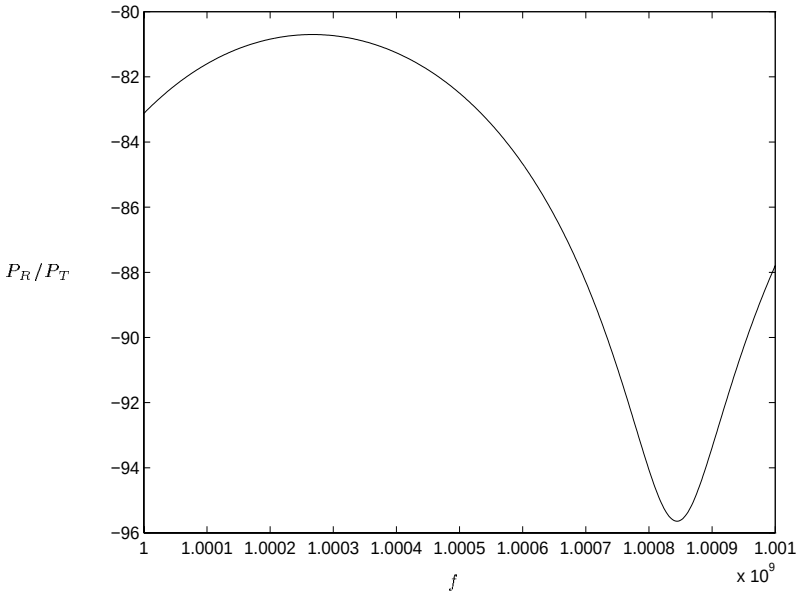

Figure 2.6: Frequency response at $x = 870$m

Static multipath channels

Assume we transmit a quadrature signal with complex envelope $\tilde{s}(t) = s_c(t) + js_s(t)$ by modulating the in–phase and quadrature carriers at frequency f_c. The signal fed to the transmitting antenna is given by

$$u(t) = s_c(t)\cos 2\pi f_c t - s_s(t)\sin 2\pi f_c t. \tag{2.13}$$

Considering only the electric field components of the electromagnetic wave at the receiving antenna, we write the received signal vector for a stationary receiver as

$$\mathbf{r}(t) = \begin{pmatrix} r^v(t) \\ r^h(t) \end{pmatrix} = k\mathrm{Re}\left\{\sum_{i=0}^{N} \mathbf{G}(\boldsymbol{\theta}_i)\mathbf{A}_i e^{j2\pi f_c t}\tilde{s}(t-d_i)\right\} \tag{2.14}$$

where k is a proportionality factor depending on the antenna characteristic. The angle $\boldsymbol{\theta}_i$ represents the two angles of arrival (i.e. azimuthal and elevation) of the i^{th} wave component at the receiver, $\mathbf{A}_i$ is a column vector holding its horizontal and vertical complex amplitudes and d_i its propagation delay. The 2×2 diagonal matrix $\mathbf{G}(\boldsymbol{\theta}_i)$ holds the horizontal and vertical field gains for the given angles of arrival. If the antenna is polarized in either of the vertical or horizontal direction, one of the diagonal elements is zero. The path index 0 corresponds to the LOS path, so that in the case where it is not present $\mathbf{A}_0 = \mathbf{0}$.

The complex envelope of $\mathbf{r}(t)$ is given by

$$\tilde{\mathbf{r}}(t) = k\sum_{i=1}^{N} \mathbf{G}(\boldsymbol{\theta}_i)\mathbf{A}_i\tilde{s}(t-d_i) \tag{2.15}$$

and its corresponding Fourier transform

$$\tilde{\mathrm{R}}(f) = k\tilde{S}(f)\sum_{i=1}^{N}\mathbf{G}(\boldsymbol{\theta}_i)\mathbf{A}_i e^{j2\pi f d_i} \tag{2.16}$$

From this point onward we assume the antenna is omnidirectional and polarized in the vertical direction so that $\mathbf{G}(\boldsymbol{\theta}) = \begin{pmatrix} 1 & 0 \\ 0 & 0 \end{pmatrix}$. For convenience we assume that the d_i are in increasing order. Dropping vector notation we may write $\tilde{R}(f) = k\tilde{S}(f)H(f)$ where $H(f)$ is a random frequency response (or filter) given by

$$H(f) = \sum_{i=0}^{N} A_i e^{j2\pi f d_i} \tag{2.17}$$

with covariance between frequency samples f_1 and f_2

$$\phi(f_1, f_2) = \phi(f_1 - f_2) = \mathrm{E}H(f_1)H^*(f_2) = \sum_{i=1}^{N}\mathrm{E}|A_i|^2 e^{j2\pi(f_1-f_2)d_i} \tag{2.18}$$

In writing this covariance functions, we have assumed that the path gains are independent zero–mean random variables which is usually known as the *uncorrelated scattering assumption*. This is justifiable since they are results of reflections off of rough surfaces [Lee82] whose electromagnetic properties have a certain degree of uncertainty. Provided that the number of paths is large, which is almost always the case and that a significant number of these contribute to the total received power, it is permissible to invoke the central limit theorem [Pap82] and approximate $H(f)$ as a Gaussian random variable for each f. We must stress, however, that the process $H(f)$ is not a Gaussian process. This follows from the fact that the Fourier transform is a linear operator and the process defined by the path strengths is not necessarily Gaussian. This approximation is very strongly corroborated by measurement [Jak74], and as a result is usually termed *Rayleigh fading* when no LOS path exists since the envelope of a zero–mean complex Gaussian random variable is Rayleigh distributed as

$$f_{|H|}^{\mathrm{Rayleigh}}(a) = \frac{2a}{\sigma_H^2}\exp\left(-\frac{a^2}{\sigma_H^2}\right), \quad a \geq 0 \tag{2.19}$$

where $\sigma_H^2 = \sum_{i=1}^{N}\mathrm{E}|A_i|^2$ is the total power of the random component of the received wavefront. In the case of a strong LOS path it is called *Ricean fading* since the mean of each $H(f)$ is A_0 so that the envelope has a Ricean distribution given by

$$f_{|H|}^{\mathrm{Rice}}(a) = \frac{2a}{\sigma_H^2}\exp\left(-\frac{a^2+|A_0|^2}{\sigma_H^2}\right)\mathrm{I}_0\left(\frac{2a|A_0|}{\sigma_H^2}\right), \quad a \geq 0 \tag{2.20}$$

where $\mathrm{I}_0(\cdot)$ is the zero–order modified Bessel function of the first kind. The ratio $K = |A_0|^2/\sigma_H^2$ is commonly referred to as the Ricean factor. The density and distribution functions of the energy at a given frequency $|H(f)|^2$ are usually more useful for calculation purposes and are given by

$$f_{|H|^2}^{\text{Rayleigh}}(a) = \frac{1}{\sigma_H^2} \exp\left(-\frac{a}{\sigma_H^2}\right), \quad a \geq 0 \tag{2.21}$$

$$F_{|H|^2}^{\text{Rayleigh}}(a) = 1 - \exp\left(-\frac{a}{\sigma_H^2}\right), \quad a \geq 0 \tag{2.22}$$

$$f_{|H|^2}^{\text{Rice}}(a) = \frac{K}{|A_0|^2} e^{-K(a+|A_0|^2)/|A_0|^2} \mathrm{I}_0\left(\sqrt{a}\frac{K}{|A_0|}\right), \quad a \geq 0 \tag{2.23}$$

$$F_{|H|^2}^{\text{Rice}}(a) = 1 - \mathrm{Q}_1\left(\sqrt{2K}, \sqrt{\frac{2aK}{|A_0|^2}}\right), \quad a \geq 0 \tag{2.24}$$

where $\mathrm{Q}_1(\cdot,\cdot)$ is the first order Marcum Q–function. Efficient numerical methods for calculating it are given in [Shn89]. In figure 2.7 we show the density functions of the received energy at a particular frequency as a function of K assuming the average received power is unity (i.e. $\sigma_H^2 + |A_0|^2 = 1$). We

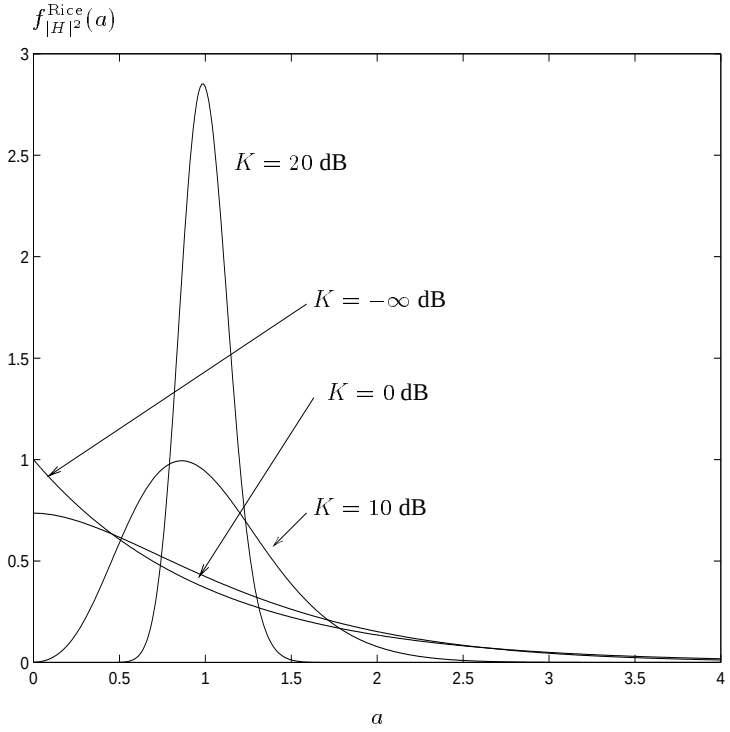

Figure 2.7: Ricean probability density for increasing K and normalized received energy

see that as K increases the channel becomes more and more deterministic. K is typically zero in urban environments but may rise to 6 dB in an indoor setting [Bul87]. If the transmitted signal $s(t)$ lies in a band $[f_c - W/2, f_c + W/2]$ and W is such that $\phi(u)$ is almost constant for $-W/2 \leq u \leq W/2$ (i.e.

$W(d_N - d_0) \ll 1$) then

$$\tilde{r}(t) \approx H(f_c)\tilde{s}(t - d_0) \tag{2.25}$$

This is a narrowband or single–path channel model.

There are other statistical models for fading which combine the shadowing and multipath phenomena. A popular one is the *Nakagami distribution* [Nak60]. The latter model is simply the square–root of Gamma distributed random variable.

Dynamic multipath channels

Let us now assume that the mobile station is moving with velocity v in the horizontal plane as shown in figure 2.8. This introduces a Doppler shift at each frequency f given by

$$\Delta f_i^D(f,t) = \frac{vf}{c}\cos(\theta_i(t)) \tag{2.26}$$

where $\theta_i(t)$ is the time–varying angle between the i^{th} incoming path (assumed to be traveling horizontally) and direction of motion of the mobile station. This 2–dimensional model is due to Clarke[Cla68]

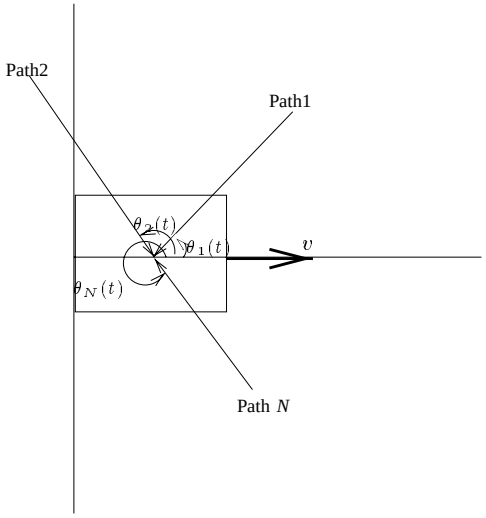

Figure 2.8: Two–dimensional Doppler model

and Jakes [Jak74]. An extension in 3–dimensions for which the significant conclusions regarding system design remain unchanged is considered by Aulin [Aul79]. If we consider modulating signals with bandwidths significantly less than the carrier frequency, which is always the case in mobile radio communications, then all frequencies are affected by virtually the same Doppler shift at any instant in time.

This allows us to write the complex envelope of the received signal as

$$\tilde{r}(t) = k \sum_{i=0}^{N} A(\theta_i(t)) e^{j2\pi\Delta f_i^D(f_c,t)t} \tilde{s}(t - d_i(t)) \tag{2.27}$$

In most cases where processing of $\tilde{r}(t)$ is done in a short timespan $d_i(t) \approx d_i$ so that the time–varying nature of the delays may be ignored. This is further justified by the fact that the amplitudes change much more quickly than do the delays. This assumes, of course, that the mobile speed is not very large, and therefore may not apply to some aeronautical or satellite channels. For simplicity let us focus on the narrowband signal case so that

$$\tilde{r}(t) \approx k \left\{ \sum_{i=0}^{N} A(\theta_i(t)) e^{j2\pi f_i^D(f_c,t)t} \right\} s(t - d_0) \tag{2.28}$$

As before, provided N is large enough and significant number of $A(\theta_i(t))$ contribute to the sum, the samples of the process $\alpha(t) = \sum_{i=0}^{N} A(\theta_i(t)) e^{j f_i^D(f_c,t)t}$ are approximately Gaussian. If the paths are results of far–off reflections, the Doppler shift for each path changes very slowly (i.e. $\theta_i(t)$ changes slowly) so that, at least on intervals of a certain length, we may justifiably approximate the process $\alpha(t)$ as a stationary Gaussian process with correlation function

$$R_\alpha(t,\tau) = \mathrm{E}\alpha(t)\alpha^*(t+\tau) = \sum_{i=0}^{N} \mathrm{E}|A(\theta_i)|^2 \mathrm{E} e^{j2\pi f_D \cos\theta_i \, \tau}, \tag{2.29}$$

where $\Delta f_D = v f_c / c$ is the maximum Doppler shift. In the classic model by Clarke and Jakes it is assumed that the angles of arrival are uniformly distributed on $[0, 2\pi)$ so that

$$\mathrm{E} e^{j2\pi f_d \cos\theta_i \, \tau} = \frac{1}{2\pi} \int_0^{2\pi} e^{j2\pi f_d \cos\theta_i \, \tau} d\theta_i = \mathrm{J}_0 \left(2\pi f_D \tau\right), \tag{2.30}$$

where $\mathrm{J}_0(\dot{})$ is the zero–order Bessel function. In the frequency domain the power spectrum of the fading process is

$$S_\alpha(f) = \begin{cases} \frac{\sigma_H^2}{2\pi} \sqrt{\frac{1}{f^2 - f_D^2}} & |f| < f_D, \\ 0 & \text{elsewhere.} \end{cases} \tag{2.31}$$

This is commonly referred to as the *land–mobile power spectrum* and is strongly corroborated by measurement [Jak74] in urban environments. It is shown in figure 2.9 where its characteristic peaks at the maximum Doppler shift f_D are evident. In rural or hilly urban areas the distribution of the angles of arrival may not be uniform and as a result the power spectrum will be quite different. The actual form of the Doppler spectrum is not that critical. It is rather its bandwidth which determines the extent of the

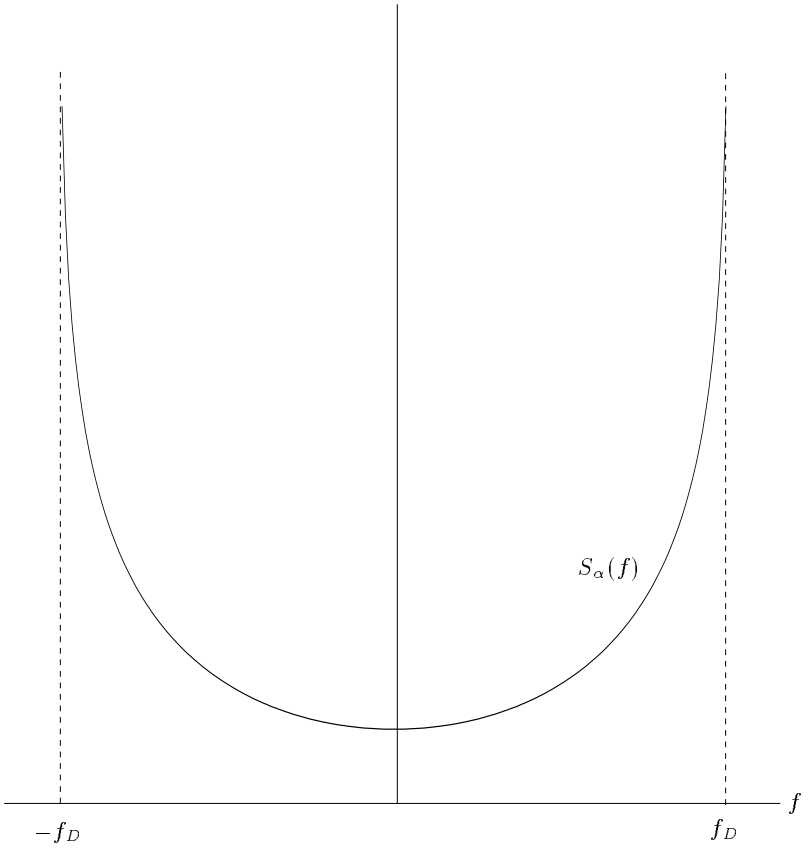

Figure 2.9: Land–mobile power spectrum

time–variation of the fading process. We will see in the following chapter that for performance analysis of such channels, the bandwidth of the fading process determines the number of degrees of freedom necessary to describe it statistically.

2.4 Wideband channel models

Up until this point we have not said anything about how different environments are characterized with respect to the distribution of the multipath energy. In a general sense, we may define the multipath intensity profile (MIP) as

$$\sigma(\tau) = \sum_{i=0}^{N} \mathrm{E}|A_i(t)|^2 \delta(\tau - d_i). \tag{2.32}$$

This describes the extent of the spread of multipath energy for a given environment. An important parameter is the *delay–spread* which is simply $d_N - d_0$. In order to predict the effect of multipath and to design systems to work well a target environment, there have been scores of models proposed for

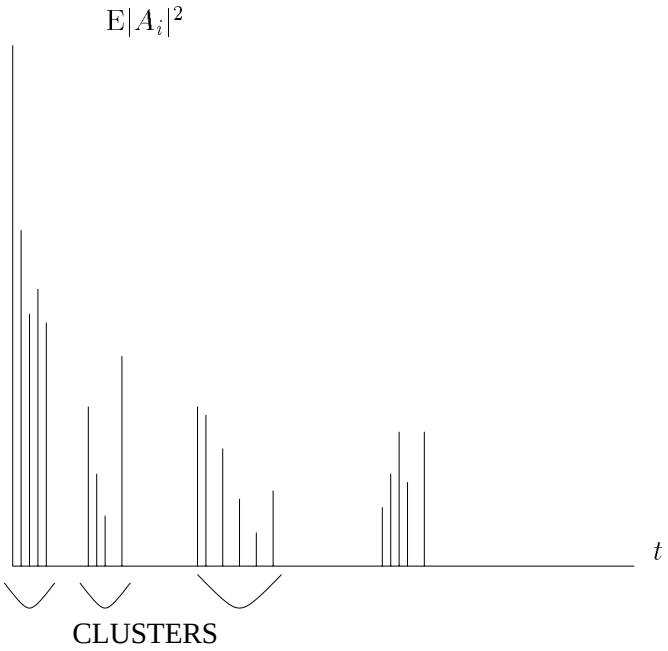

Figure 2.10: Clustering Effect of Multipath Channels

the MIP. These models attempt not to perfectly described a given multipath environment, since this is an impossible task, but rather to capture the key features from a series of measurements in the desired system setting (i.e. frequency band and physical environment). At the same time as being representative of a typical channel, they should be mathematically suitable for performing an analytical/simulation system performance analysis. Without going into too much detail of the different models, we briefly describe a few here.

2.4.1 Poisson arrival models

Turin [TCJ$^+$72] considered the static multipath channel for an urban environment and modeled the sequence of delays $\{d_i\}$ as a Poisson point process. The simplest approach is to consider a homogeneous process so that delay differences $\Delta d_i = d_i - d_{i-1}$ are i.i.d. exponential random variables. This, however, does not capture the clustering effect which is typical of real channels. We show this in figure 2.10. Each cluster corresponds to a series of scatterers closely located to each other. A simple non–homogeneous process was proposed to model this effect. This technique was later extended by Suzuki[Suz77] and Hashemi [Has79].

2.4.2 COST 207 models

In order to analyze the GSM cellular telephone system, a series of propagation studies were performed as part of the COST 207 project. These studies yielded a series of models for outdoor channels, denoted by TU(typical urban), RU(rural area) and HT(hilly terrain), which we show in Table 2.2. These are tap delay line models with regularly spaced taps which have the drawback that they are applicable only for a limited signaling bandwidth. We will see in the remainder of this thesis that the performance of a system depends on the degree of randomness of the channel which is closely related to the signaling bandwidth. For wideband analysis, such as for spread spectrum or slow frequency hopping systems these models are not necessarily applicable.

Each path has an associated Doppler which is not indicated in this table. For our purposes we will only use the static fading characteristics of these channels. Paths from local scatterers have been found to be accurately modeled by the classic land–mobile model given in 2.30. For those caused by distant scatterers in the BU and HT channels the Doppler spectrum have a particular two–lobe Gaussian Doppler spread under the assumption of two significant scatterers. We only include the MIP statistics since we will only use them for frequency–domain computations.

2.4.3 Indoor Models

Saleh and Valenzuela [SV87] consider a ncatenation of two Poisson point processes for describing the indoor propagation channel. One process defines the positions of clusters of paths and the second the positions of the paths within clusters. The modified Poisson process models described in section 2.4.1 were extended for typical indoor channels by Ganesh and Pahlavan in [GP89].

Rural Area (RU6)		Hilly Terrain (HT6)		Typical Urban (TU6)	
$d_i(\mu s)$	$\|A_i\|^2$ (dB)	$d_i(\mu s)$	$\|A_i\|^2$ (dB)	$d_i(\mu s)$	$\|A_i\|^2$ (dB)
0	0	0	0	0	-3
.1	-4	.1	-1.5	.2	0
.2	-8	.3	-4.5	.5	-2
.3	-12	.5	-7.5	1.6	-6
.4	-16	15	-8	2.3	-8
.5	-20	17.2	-17.7	5.0	-10

Typical Urban (TU12)		Hilly Terrain (HT12)	
$d_i(\mu s)$	$\|A_i\|^2$ (dB)	$d_i(\mu s)$	$\|A_i\|^2$ (dB)
0	-4	0	-10.01
.1	-3.01	.1	-8.01
.3	0	.3	-6
.5	-2.6	.5	-4.01
.8	-3	.7	.01
1.1	-5	1	0
1.3	-7	1.3	-4
1.7	-5	15	-8
2.3	-6.5	15.2	-9
3.1	-8.6	15.7	-10
3.2	-11	17.2	-12
5.0	-10	20	-14

Table 2.2: ETSI-COST 207 Channel Models

Chapter 3

Signaling over Fading Channels

Signal fading is arguably the most difficult phenomenon that radio communication system designers have to cope with. As we saw in Chapter 2, the average received signal strength can drop tens of decibels due to the destructive interference of delayed reflections of the transmitted signal [Jak74]. This is especially the case in non line–of–sight communications. Moreover, for slowly moving mobile transceivers, such "deep fades" result in unacceptably long periods of time where reliable communication is impossible.

In wide-band systems the receivers are sensitive enough to distinguish (or resolve) different faded replica of the transmitted signal, or *paths*, which can be used jointly to improve performance. In spread–spectrum based systems, such as IS–95 [IS992], where the signal bandwidth is much larger than the symbol rate, some paths can be combined by what is commonly referred to as a RAKE receiver [Pro95] to improve performance. Medium–band systems are subject to *intersymbol interference* (ISI) due to time dispersion so that the use of an equalizer also benefits from frequency–diversity. This is actually a situation where ISI is desirable.

In order to operate efficiently in such a hazardous environment, the system designer often opts to use so-called *diversity* methods. Simply put, the diversity is the number of independent replica of the transmitted signal that are made available to the receiver. In the absence of multiple antennas, this calls for the exploitation of either the frequency or the time-variation properties of the fading signal or both. The former can be called *frequency diversity*, and makes use of the amplitude of the transfer function of the channel in different parts of the spectrum. Frequency–diversity schemes are quite popular in multiuser systems due to the large amount of bandwidth that is available, and can be achieved in different ways.

Another way of exploiting frequency–diversity is to use coded narrow or medium–band signals

with *slow frequency–hopping*. This technique is used in the GSM system and its derivatives DCS 1800 and PCS 1900 [GSM90]. Here, the information is coded and interleaved over $F = 4$ (half–rate) or $F = 8$ (full–rate) blocks of length $N = 208$ or $N = 378$ symbols, and each block modulates a different carrier (ideally) according to some predefined hopping pattern. This is achieved by altering the FDMA allocation of users every block. It has the effect of ensuring that after deinterleaving any F *adjacent* received symbols modulated a different carrier. If the carriers are sufficiently separated, the resulting received symbols have uncorrelated strengths. It is well known that error–control coding can yield a significant diversity effect in such cases [Pro95].

Time diversity can also be exploited to some extent using interleaving even without frequency–hopping. Assuming that the receiver/transmitter is in motion, interleaving spreads the information across different channel strengths whose correlation depends on the mobile speed and interleaving delay. For example, the IS54 system [IS592] encodes the information and interleaves it over $F = 2$ blocks of length $N = 178$ separated by 20ms. For low mobile speeds this can result in highly correlated symbols after deinterleaving. For this reason, systems exploiting frequency diversity are more desirable when reliable performance is desired at low mobile speeds.

In this chapter we will consider the different ways signaling is performed over the various types of fading channels. There is nothing really new, but much of the material is presented in a way that is not found in most classic textbooks on digital communications. More precisely we look at the different diversity methods and show that performance criteria are computed in essentially the same way in each case. Once the signal has been characterized statistically, the computation of performance criteria is a question of performing an *eigenvalue analysis* of a kernel or quadratic form representing the energy of the received signal in some observation interval/bandwidth. The number of significant eigenvalues or *degrees of freedom* of the channel process in a given frequency band or time interval will play an important role.

We end with a generic model which is useful for describing many systems which operate with a small number of degrees of freedom or eigenvalues, which we call the *block–fading model*. In practice, this model is applicable to systems where processing is performed over a few different channel realizations which can result for instance from a *frequency–hopping* mechanism. Chapters 4 and 5 will treat the fundamental aspects of this model in more detail.

3.1 Performance Measures

Imagine a communication system where signal blocks or messages of duration T seconds are used to convey information from the sender to the receiver. We assume that a finite number, M, of message waveforms exist, which we denote by the set $\{x_m(t), m = 0, \cdots, M-1\}$. The amount of information per message is $\log_2 M$ bits so that the bit rate is

$$R = \frac{1}{T} \log_2 M \quad \text{bits/s} \tag{3.1}$$

For simplicity, we will assume that the receiver requires the entire message in order to make a decision about which message was sent, so that the processing or decoding delay is T seconds. In many systems, there is a limit to the tolerable decoding delay. A long decoding delay for voice telephony results in an unacceptable audible delay. Some data transmission protocols also have stringent decoding delay constraints due to some quality of service requirement or limited buffer size.

The message or *codeword error–rate* is a critical measure of the robustness of a coding scheme in noise. Under the assumption that messages are transmitted with equal probability it can be bounded from above using the union bound [Pro95]

$$P_e = \frac{1}{M} \sum_{m=0}^{M-1} \sum_{n=0}^{M-1} \text{Prob}(m \to n) \tag{3.2}$$

where $\text{Prob}(m \to n)$ is the called the *pairwise error probability (PEP)* between messages m and n and indicates the probability of decoding n given that m is transmitted if they were the only two possible messages.

The analysis of the PEP for systems working in a fading environment is usually based on characterizing the statistics of the total received energy in the interval $[-T/2, T/2]$. It is therefore not surprising that most formulations yield very similar forms for the PEP. The goal of this chapter is to describe different narrow and wide-band systems which we will refer to in the remainder of this thesis by defining the basic receiver structures and their performance measures. We begin by defining the notion of *diversity* using a simple two–channel receiver which can be seen as a dual–antenna receiver.

Throughout this chapter we express all transmitted and received messages as complex baseband signals representing the complex envelope of real signals centered at a certain carrier frequency.

3.2 Diversity Reception

Let us consider transmission of a binary message over *two* static independent single–path Rayleigh fading channels. Physically, this could represent a dual–antenna receiver where one antenna is vertically polarized the other is horizontally polarized and the receiver can process both polarizations. Here the receiver has access to two faded versions of the same signal which is known as *diversity reception*. The received signals can be written as

$$\mathbf{y}(t) = \begin{pmatrix} y_0(t) \\ y_1(t) \end{pmatrix} = \begin{pmatrix} \alpha_0 \\ \alpha_1 \end{pmatrix} x(t) + \begin{pmatrix} z_0(t) \\ z_1(t) \end{pmatrix}, \quad -T/2 \leq t \leq T/2 \tag{3.3}$$

where α_i are the two independent zero–mean complex circular symmetric Gaussian random variables, $x(t)$ is a binary message taking on values $x_0(t)$ and $x_1(t)$ with equal probability and $z_i(t)$ is additive white complex circular symmetric Gaussian noise with two–sided power spectral density N_0. Let us assume that the receiver is capable of perfectly estimating the α_i. Furthermore we take $\mathrm{E}|\alpha_i|^2 = 1$ so that any average attenuation factor is included in the transmitted signal energy $\mathcal{E}$ which now becomes the average received signal energy. In this case, the optimal receiver, in the sense of minimum probability of error, is the *maximum–likelihood* receiver [VT68]

$$\begin{aligned} \hat{m} &= \underset{m=0,1}{\operatorname{argmin}} \int_{-T/2}^{T/2} |\mathbf{y}(t) - \boldsymbol{\alpha} x_m(t)|^2 dt \\ &= \underset{m=0,1}{\operatorname{argmax}} \int_{-T/2}^{T/2} \mathrm{Re}\{y_{\mathrm{MR}}(t) x_m^*(t)\} - \frac{1}{2}\sqrt{|\alpha_0|^2 + |\alpha_1|^2}\,|x_m(t)|^2 \end{aligned} \tag{3.4}$$

where

$$y_{\mathrm{MR}}(t) = \frac{1}{\sqrt{|\alpha_0|^2 + |\alpha_1|^2}} \left(\alpha_0^* y_0(t) + \alpha_1^* y_1(t)\right) \tag{3.5}$$

is the *combined* received signal. The receiver in (3.4) is depicted in figure 3.1 and is known as a *maximal ratio combiner*. It has been given this name since the front end of the receiver combines the two diversity branches in such a way as to assure that the resulting signal takes most of its energy from the stronger branch. The rest of the circuit works as a regular maximum–likelihood receiver with fading strength equal to $\alpha_c = \sqrt{|\alpha_0|^2 + |\alpha_1|^2}$.

Another sub–optimal receiver structure known as *selection combining* uses a front end with combined signal

$$y_{\mathrm{SD}}(t) = y_i(t), i = \underset{j=0,1}{\operatorname{argmax}} |\alpha_j| \tag{3.6}$$

so that the combined signal strength is $\alpha_c = \max\{|\alpha_0|, |\alpha_1|\}$. The rest of the receiver is maximum–likelihood as with maximal–ratio combining. We will meet this structure again in Chapter 7 when we consider multiuser communications.

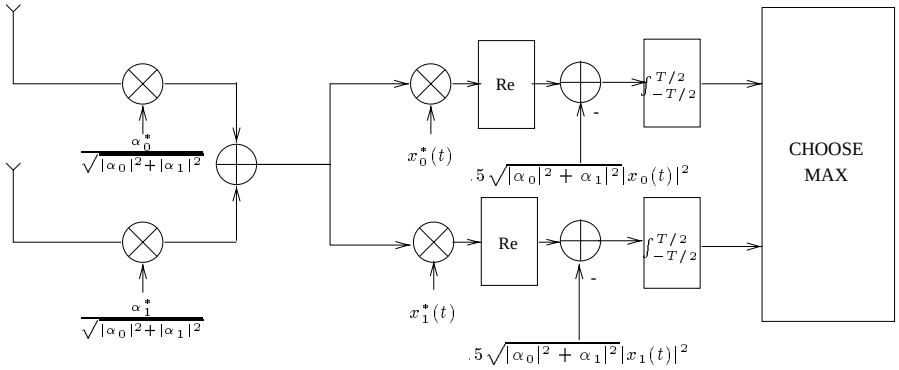

Figure 3.1: Maximal–ratio combining

Let us assume an antipodal system so $x_0(t) = -x_1(t)$ with $\int_{-T/2}^{T/2} |x_i(t)|^2 dt = \mathcal{E}$. The PEP conditioned on the fading level for maximum–likelihood reception is given by [VT68]

$$P_{e|\alpha_c}(0 \to 1) = \mathrm{Q}\left(\sqrt{2|\alpha_c|^2 \frac{\mathcal{E}}{N_0}}\right) \tag{3.7}$$

where $\mathrm{Q}(\cdot)$ is the area under the tail of a normalized Gaussian distribution given by

$$\mathrm{Q}(x) = \sqrt{\frac{1}{2\pi}} \int_x^\infty e^{-u^2/2} du \tag{3.8}$$

In order to calculate the average PEP we must average (3.7) over the density of $|\alpha_c|^2$. Let us first consider the selection combining case. The distribution function of the maximum of two unit-mean exponential random variables is given by

$$F^{\mathrm{SD}}_{|\alpha_c|^2}(u) = (1 - e^{-u})^2, \; u \geq 0 \tag{3.9}$$

so that its density is

$$f^{\mathrm{SD}}_{|\alpha_c|^2}(u) = 2e^{-u} - 2e^{-2u}, \; u \geq 0 \tag{3.10}$$

The effect of diversity is clear since the density of the average received power is small around the origin, so that a low *signal–to–noise ratio (SNR),* $\alpha_c \mathcal{E}/N_0$ is unlikely. Using the fact that

$$\int_0^\infty a\mathrm{Q}(\sqrt{u}) e^{-a\,u} du = .5 \left(1 - \sqrt{\frac{1}{1+2a}}\right) \tag{3.11}$$

we have that the average PEP for selection combining is given by

$$P_e^{\mathrm{SD}}(0 \to 1) = \mathrm{E}\left[\mathrm{Q}\left(\sqrt{2|\alpha_c|^2 \frac{\mathcal{E}}{N_0}}\right)\right] = .5\left(1 - 2\sqrt{\frac{\mathcal{E}/N_0}{1+\mathcal{E}/N_0}} + \sqrt{\frac{\mathcal{E}/N_0}{2+\mathcal{E}/N_0}}\right) \tag{3.12}$$

Turning to the case of maximal–ratio combining we see that $|\alpha_c|$ is the sum of two unit–mean exponential random variables so it has a central Chi-square distribution with 4 degrees of freedom. Thus, $|\alpha_c|^2$ has density

$$f_{|\alpha_c|^2}^{\mathrm{MR}}(u) = ue^{-u},\ u \geq 0. \tag{3.13}$$

It is shown in [Pro95, Chap 14] that

$$P_e^{\mathrm{MR}}(0 \to 1) = .25\left(1 - \sqrt{\frac{\mathcal{E}/N_0}{1+\mathcal{E}/N_0}}\right)^2\left(1 + .5\left(1 + \sqrt{\frac{\mathcal{E}/N_0}{1+\mathcal{E}/N_0}}\right)\right) \tag{3.14}$$

We plot the PEP for both cases as a function of the signal–to–noise ratio $\mathcal{E}/N_0$ in Figure 3.2. We also show the PEP if we use only one of the branches. In this case we have that $f_{|\alpha_c|^2}(u) = e^{-u},\ u \geq 0$ and

$$P_e(0 \to 1) = .5\left(1 - \sqrt{\frac{\mathcal{E}/N_0}{1+\mathcal{E}/N_0}}\right) \tag{3.15}$$

We see that by having two replicas of the transmitted signal, which are subject to independent channel realizations, we can significantly reduce the error–rate performance. In what follows we will see similar effects which are due to coding the information signal in such a way to take advantage of the time and/or frequency–selective nature of fading channels, without the need for multiple antennas. The number of diversity branches will become the number of degrees of freedom (either in time or in frequency or both) needed to characterize the fading process.

3.3 Narrow-band Information Signals over Doppler–Spread Channels

A narrow-band system, as shown in chapter 1, can often be described by the single–path time–varying fading channel as

$$y(t) = \alpha(t)x^{(m)}(t) + z(t), \quad |t| < T/2 \tag{3.16}$$

where $\alpha(t)$ is a circular symmetric zero–mean complex Gaussian process over the vector space of square–integrable functions over $[-T/2, T/2)$, $L^2(-T/2, T/2)$, with autocorrelation function $K_\alpha(t,u)$. This corresponds to Rayleigh fading which has no LOS path and holds if the bandwidth of $x(t)$ is much

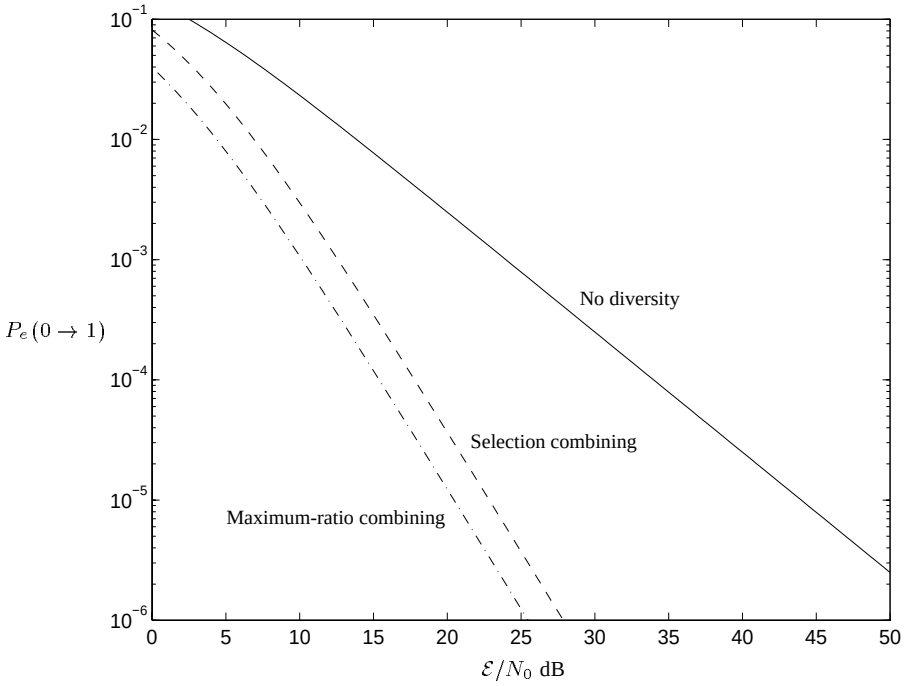

Figure 3.2: Diversity reception performance

less than the coherence bandwidth of the channel. We have assumed in (3.16) that the m^{th} codeword is transmitted. For channels of practical interest we may express $\alpha(t)$ in terms of its Karhunen–Loève expansion [DR58] as

$$\alpha(t) = \sum_{i=1}^{\infty} \alpha_i \phi_i(t), \tag{3.17}$$

where $\{\phi_i(t)\}$ is a complete orthonormal basis for $L^2(-T/2, T/2)$. The coefficients α_i are uncorrelated zero–mean Gaussian variables with variance $\mathrm{E}|\alpha_i|^2 = \lambda_i^{(\alpha)}$. The functions $\{\phi_i(t)\}$ and the non–negative numbers $\{\lambda_i^{(\alpha)}\}$ are the eigenvectors and their corresponding eigenvalues, respectively, of the linear mapping with kernel $K_\alpha(t,u)$, so that they satisfy

$$\lambda_i^{(\alpha)} \phi_i(t) = \int_{-T/2}^{T/2} K_\alpha(t,u)\phi_i(u)du. \tag{3.18}$$

This integral equation can be solved numerically for practical choices of $K_\alpha(t,u)$. We show the eigenvalues for the *land–mobile* model with omni–directional antennas which has $K_\alpha(t,u)$ given by $\mathrm{J}_0(2\pi(t-u))$ in Figure 3.3. For this example, we see that the kernel is effectively degenerate since it has around $D = \lceil 2f_D T + 1 \rceil$ significant eigenvalues. This is not surprising since $\alpha(t)$ is a process bandlimited to $[-f_D, f_D]$. The number of significant eigenvalues is definitely the most crucial parameter since it is the number of degrees of freedom necessary to characterize this process during $[-T/2, T/2]$. We will see

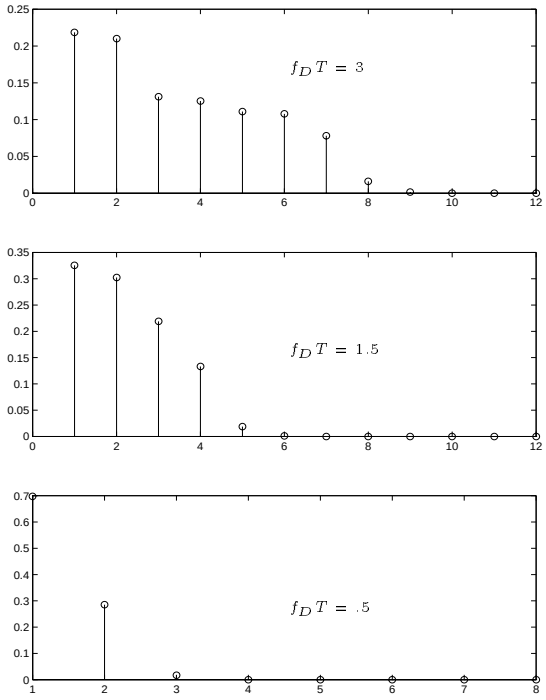

Figure 3.3: Eigenvalue spread for different $f_D T$

that this turns out to be equivalent, from the point of view of performance, to the number of diversity branches in a multiple antenna system. We consider the types of optimal receivers in Section 3.3.1 and their performance in Sections 3.3.2 and 3.3.3. Starting with the uncoded binary message case, we move on to coded systems with a discretized approximation for the fading process.

3.3.1 Optimal Receivers

We consider two possible receiver scenarios, one where the fading process is known perfectly to the receiver, and one where only its statistics are known. We will refer to the first case as a *coherent* receiver and to the second as a *non–coherent* receiver. We use the term non–coherent in a very general sense. Traditionally, it is reserved for detection without an absolute phase reference, whereas here we include the unknown signal amplitude as well. If the signal changes very quickly, it is often impossible to perform coherent detection. Nevertheless, it is still reasonable to consider a performance analysis in this case for comparison purposes.

Coherent Receivers

The optimal receiver assuming equally likely messages is the maximum–likelihood receiver we saw in (3.4) generalized for M–ary signals

$$\begin{aligned}\hat{m} &= \underset{m=0,\cdots,M-1}{\operatorname{argmin}} \int_{-T/2}^{T/2} |y(t) - \alpha(t)x^{(m)}(t)|^2 dt \\ \hat{m} &= \underset{m=0,\cdots,M-1}{\operatorname{argmax}} \int_{-T/2}^{T/2} \operatorname{Re}\left\{ y(t)\alpha^*(t)x^{*(m)}(t) \right\} dt - \frac{1}{2}\int_{-T/2}^{T/2} |\alpha(t)x^{(m)}(t)|^2 dt\end{aligned} \tag{3.19}$$

In the first case, the receiver simply chooses the weighted signal, $\alpha(t)x^{(m)}(t)$ which is closest in terms of *Euclidean distance,* whereas in the second case it chooses the message most correlated with the received signal biased by the energy of the message. Its performance analysis is left to Section 3.3.2.

Non–Coherent Receivers

The non–coherent detection problem is much more delicate, since it is a Gaussian signal detection problem. The difference between the two problems, in a few words, is that the information in the non–coherent case is hidden in the correlation function of the received signal and not the mean. We define the attenuated information signal $s^{(m)}(t) = \alpha(t)x^{(m)}(t)$, which is conditionally Gaussian given the hypothesis that the m^{th} waveform is transmitted. The conditional mean is zero (Rayleigh Fading) and the conditional correlation function is

$$K^{(m)}(t,u) = K_\alpha(t,u)x^{(m)}(t)x^{(m)}(u) \tag{3.20}$$

We now perform a Karhunen–Loève expansion on *each* $s^{(m)}(t)$ as

$$s^{(m)}(t) = \sum_{i=1}^{\infty} s_i^{(m)}\phi_i^{(m)}(t) \tag{3.21}$$

where $\{s_i^{(m)}, i = 1, \cdots, \infty\}$ are independent zero–mean circularly symmetric Gaussian random variables with variances $\{\lambda_i^{(m)}, i = 1, \cdots, \infty\}$ which satisfy

$$\lambda_i^{(m)}\phi_i^{(m)}(t) = \int_{-T/2}^{T/2} K^{(m)}(t,u)\phi_i^{(m)}(u)du \tag{3.22}$$

If we project the received signal on the first K of these basis functions we have

$$y_K^{(m)}(t) = \sum_{i=1}^{K} y_i^{(m)}\phi_i^{(m)}(t) \tag{3.23}$$

and

$$y(t) = \underset{K\to\infty}{\text{l.i.m.}}\, y_K^{(m)}(t) \tag{3.24}$$

The coordinates of the m^{th} representation are related by

$$y_i^{(m)} = s_i^{(m)} + z_i^{(m)} \tag{3.25}$$

where $z_i^{(m)}$ are i.i.d. complex Gaussian circularly symmetric random variables with variance N_0 and $\mathrm{E}y_i^{(m)}y_j^{(m)*} = (\lambda_i^{(m)} + N_0)\delta_{ij}$ so that the K–dimensional density function for $\mathbf{y}$ conditioned on the m^{th} input signal is

$$f_{\mathbf{Y}^{(m)}}(\mathbf{y}^{(m)}) = \left(\prod_{i=1}^{K} \frac{1}{\pi(\lambda_i^{(m)} + N_0)^{1/2}}\right) \exp\left(-\frac{1}{2}\sum_{i=1}^{K} \frac{|y_i^{(m)}|^2}{\lambda_i^{(m)} + N_0}\right) \tag{3.26}$$

The optimal detection rule under the assumption of equally–likely transmitted signals and the K–dimensional approximation is

$$\begin{aligned}
\hat{m}_K &= \underset{m=0,\cdots,M-1}{\text{argmax}}\, f_{\mathbf{Y}^{(m)}}(\mathbf{y}^{(m)}) \qquad (3.27)\\
&= \underset{m=0,\cdots,M-1}{\text{argmax}}\, \log f_{\mathbf{Y}^{(m)}}(\mathbf{y}^{(m)})\\
&= \underset{m=0,\cdots,M-1}{\text{argmax}} \sum_{i=1}^{K} \frac{|y_i^{(m)}|^2}{\lambda_i^{(m)} + N_0} + \sum_{i=1}^{K} \log\left(1 + \frac{\lambda_i^{(m)}}{N_0}\right)
\end{aligned}$$

Letting $K \to \infty$ yields

$$\hat{m} = \underset{m=0,\cdots,M-1}{\text{argmax}} \sum_{i=1}^{\infty} \frac{|y_i^{(m)}|^2}{\lambda_i^{(m)} + N_0} + \sum_{i=1}^{\infty} \log\left(1 + \frac{\lambda_i^{(m)}}{N_0}\right) \tag{3.28}$$

We would now like to express this in terms of the received signal and some filtering operation. The inverse kernel of the received signal correlation function under the m^{th} hypothesis is

$$Q_y^{(m)}(t,u) = \sum_{i=1}^{\infty} \frac{1}{\lambda_i^{(m)} + N_0} \phi_i^{(m)}(t)\phi_i^{*(m)}(u) \tag{3.29}$$

and is also the solution to the integral equation [VT68]

$$\int_{-T/2}^{T/2} Q_y^{(m)}(t,z) K_y^{(m)}(z,u)dz = \delta(t-u) \tag{3.30}$$

After expressing the coordinates $\{y_i^{(m)}\}$ as integrals, we obtain the decision rule

$$\hat{m} = \underset{m=0,\cdots,M-1}{\text{argmin}} \int_{-T/2}^{T/2}\int_{-T/2}^{T/2} y(t) Q_y^{(m)}(t,u) y^*(u)dtdu + \sum_{i=1}^{\infty} \log\left(1 + \frac{\lambda_i^{(m)}}{N_0}\right) \tag{3.31}$$

The rightmost term in (3.31) is the bias term for each decision statistic and is directly related to the energy of each input signal. Using the fact that $\log(1+x) \leq x$ it is upper bounded by $\mathcal{E}_m/N_0$ where $\mathcal{E}_m = \sum_{i=1}^{\infty} \lambda_i^{(m)}$ is the energy of the m^{th} weighted waveform.

The decision rule in (3.31) has a very interesting interpretation in terms of the theory of optimum linear filtering. After some manipulation [VT72], the decision rule may be cast into a form known as an *estimator–correlator* receiver. The decision rule now takes on the following form

$$\begin{aligned} \hat{m} &= \underset{m=0,\cdots,M-1}{\text{argmax}} \int_{-T/2}^{T/2} 2\text{Re}\left\{y(t)\hat{s}^{(m)}(t)\right\} - |\hat{s}^{(m)}(t)|^2 dt - \sum_{i=1}^{\infty} \log\left(1+\frac{\lambda_i^{(m)}}{N_0}\right) \\ &= \underset{m=0,\cdots,M-1}{\text{argmin}} \int_{-T/2}^{T/2} |y(t) - \hat{s}^{(m)}(t)|^2 dt + \sum_{i=1}^{\infty} \log\left(1+\frac{\lambda_i^{(m)}}{N_0}\right) \end{aligned} \tag{3.32}$$

where $\hat{s}^{(m)}(t)$ is optimal realizable point estimator for the attenuated message signal $s^{(m)}(t)$ given by

$$\hat{s}^{(m)}(t) = \int_{-T/2}^{t} h^{(m)}(t,u) y(u) du \tag{3.33}$$

The estimate for the instant t is based on the received signal in the interval $[-T/2, t]$ and the symmetric time–varying estimation filter $h^{(m)}(t,u)$ is the solution to the integral equation

$$N_0 h^{(m)}(t,u) + \int_{-T/2}^{t} h^{(m)}(t,z) K_s^{(m)}(z,u) dz = K_s^{(m)}(t,u), \ -T/2 \leq u \leq t \tag{3.34}$$

Another by–product of this realization is that the bias term is the estimation error of the filter

$$\sum_{i=1}^{\infty} \log\left(1+\frac{\lambda_i^{(m)}}{N_0}\right) = \frac{1}{N_0} \int_{-T/2}^{T/2} h^{(m)}(t,t) dt \tag{3.35}$$

which we will meet again when we consider average mutual information in the next chapter. This is also known as a *Fredholm determinant*.

The practical interpretation of this analysis is that we perform the same operation as in the coherent case, namely minimum distance or maximum correlation reception using the optimal linear estimate of the information process $s^{(m)}(t)$. The bias is different, however, and takes into account both the energy and associated mean–squared estimation error of each signal.

3.3.2 Pairwise Error Probability - Binary Signals

Here we perform performance analyses for the special case of binary message signals. We start with coherent case and then continue with one example of a non–coherent system. Suppose that there are two possible information signals, $x^{(0)}(t)$ and $x^{(1)}(t)$. We denote the conditional PEP by

$$\text{P}_{e|\alpha(t)}(0 \to 1) = \text{Prob}(\text{decide on } x^{(1)}(t) | x^{(0)}(t) \text{ transmitted}, \alpha(t)). \tag{3.36}$$

Using the decision rule in (3.19) the conditional PEP is given by [VT68]

$$\mathrm{P}_{e|\alpha(t)}(0 \to 1) = \mathrm{Q}\left(\sqrt{\frac{\int_{-T/2}^{T/2} |\alpha(t)(x^{(0)}(t) - x^{(1)}(t))|^2}{2N_0} dt}\right) \tag{3.37}$$

where $\int_{-T/2}^{T/2} |\alpha(t)(x^{(0)}(t) - x^{(1)}(t))|^2 dt$ is the Euclidean distance between the two weighted information signals.

Let us now consider a few examples. We start with antipodal signals, namely $x^{(0)}(t) = -x^{(1)}(t) = p(t)$ where $p(t)$ is chosen such that $\int_{-T/2}^{T/2} |p(t)|^2 = \mathcal{E}$ and for simplicity we choose a square pulse shape $p(t) = \sqrt{\mathcal{E}/T}, \;\; t \in [-T/2, T/2]$. We have, therefore, that the conditional PEP is given by

$$\mathrm{P}_{e|\alpha(t)}(0 \to 1) = \mathrm{Q}\left(\sqrt{\frac{2\mathcal{E}}{N_0} \frac{1}{T} \int_{-T/2}^{T/2} |\alpha(t)|^2 dt}\right) \tag{3.38}$$

Another example, which we will use later for comparison with the non–coherent case is *on–off keying (OOK)* where $x^{(0)}(t) = p(t)$ and $x^{(1)}(t) = 0$. Again we choose a square pulse, but this time with twice as much energy $p(t) = \sqrt{\frac{2\mathcal{E}}{T}}, \;\; t \in [-T/2, T/2]$ so that the average energy is still $\mathcal{E}$. Here we have

$$\mathrm{P}_{e|\alpha(t)}(0 \to 1) = \mathrm{Q}\left(\sqrt{\frac{\mathcal{E}}{N_0} \frac{1}{T} \int_{-T/2}^{T/2} |\alpha(t)|^2 dt}\right) \tag{3.39}$$

A final example is another orthogonal scheme using binary *Walsh–Hadamard pulses* where $x^{(0)}(t) = p(t)$ and $x^{(1)}(t) = \mathrm{sgn}(t)p(t)$ and $p(t)$ is as with antipodal. In this case, the conditional PEP is given by

$$\mathrm{P}_{e|\alpha(t)}(0 \to 1) = \mathrm{Q}\left(\sqrt{\frac{2\mathcal{E}}{N_0} \frac{1}{T} \int_{0}^{T/2} |\alpha(t)|^2 dt}\right) \tag{3.40}$$

In the three cases, we see that the conditional PEP is a function of the received power of the fading process over some time interval. This quantity is a random variable which we denote by

$$P_R(T) = \frac{1}{T} \int_{-T/2}^{T/2} |\alpha(t)|^2 dt \tag{3.41}$$

In the third example, we must remember to cut the time interval in half. In order to compute the average PEP we need the distribution of $P_R(T)$ which is found easily using the KL expansion for $\alpha(t)$. Replacing the $\{\alpha_i\}$ by their corresponding integrals we have that

$$P_R(T) = \frac{1}{T} \sum_{i=1}^{\infty} |\alpha_i|^2 \tag{3.42}$$

which is a sum of independent exponentially distributed random variables with means $\mu_i = \lambda_i/T$. It follows that the moment–generating function for $P_R(T)$ is given by

$$G_P(s) = \prod_{i=1}^{\infty} \frac{1}{1 - s\mu_i} \tag{3.43}$$

In most cases the μ_i are distinct so that we may perform a simple partial fraction expansion on $G_P(s)$ as

$$G_P(s) = \sum_{i=1}^{\infty} \frac{A_i}{1 - s\mu_i} \tag{3.44}$$

where $A_i = (1 - s\mu_i)G_P(s)|_{s=1/\mu_i} = \prod_{j \neq i} \frac{\mu_i}{\mu_i - \mu_j}$. By straightforward Laplace inversion we obtain the density function for $P_R(t)$

$$f_{P_R}(p) = \sum_{i=1}^{\infty} \frac{A_i}{\mu_i} \exp\left(-\frac{p}{\mu_i}\right) U(p) \tag{3.45}$$

where $U(p)$ is the unit–step function. It follows that the average PEP for antipodal signals is given by

$$\begin{aligned} \mathrm{P}_e(0 \to 1) &= \sum_{i=1}^{\infty} A_i \int_0^{\infty} \mathrm{Q}\left(\sqrt{\frac{2\mathcal{E}}{N_0} P_R(T)}\right) \exp\left(-\frac{p}{\mu_i}\right) dp \\ &= \sum_{i=1}^{\infty} \frac{A_i}{2} \left(1 - \sqrt{\frac{2\mathcal{E}\mu_i/N_0}{1 + 2\mathcal{E}\mu_i/N_0}}\right) \end{aligned} \tag{3.46}$$

The others are calculated in an identical fashion.

We now consider a bound on the average PEP. Using the Chernov bound on the $\mathrm{Q}(\cdot)$ function

$$\mathrm{Q}(x) \leq \frac{1}{2} e^{-x^2/2} \tag{3.47}$$

we may upper–bound the PEP using $G_P(s)$ as

$$\begin{aligned} \mathrm{P}_e(0 \to 1) &= \mathrm{E}\ \mathrm{Q}\left(\sqrt{\frac{2\mathcal{E}}{N_0} P_R(T)}\right) \\ &\leq \frac{1}{2} \mathrm{E}\ \exp\left(-\frac{\mathcal{E}}{N_0} P_R(T)\right) \\ &= \frac{1}{2} G_P\left(-\frac{\mathcal{E}}{N_0}\right) \\ &= \frac{1}{2} \prod_{i=1}^{\infty} \frac{1}{1 + \frac{\mathcal{E}}{N_0}\mu_i} \qquad (3.48) \\ &\approx \frac{1}{2} \left(\frac{N_0}{\mathcal{E}\chi}\right)^D \qquad (3.49) \end{aligned}$$

where $D = \left|\left\{\mu_i : \mu_i \gg \frac{N_0}{\mathcal{E}}\right\}\right|$ and

$$\chi = \left(\prod_{i=1}^{D} \mu_i\right)^{\frac{1}{D}} \tag{3.50}$$

The final approximation is valid only if a the total energy of the process is concentrated in a small number of eigenvalues. The parameter D is the number of significant eigenvalues with respect to the SNR and χ is their geometric mean. The upper bound has the characteristics of a *Bode plot* where D is the slope of the PEP vs. SNR curve on a log–log scale and is traditionally referred to as the *diversity order* of the system.

In Figure 3.4 we show the true PEP for antipodal signals for $f_D T = 0, .1$ and 1 along with the upper–bound in (3.48). We also show the straight-line approximations from (3.49) which show the similarity to a Bode plot. In Figure 3.5 we compare the PEP for the three examples. The performance

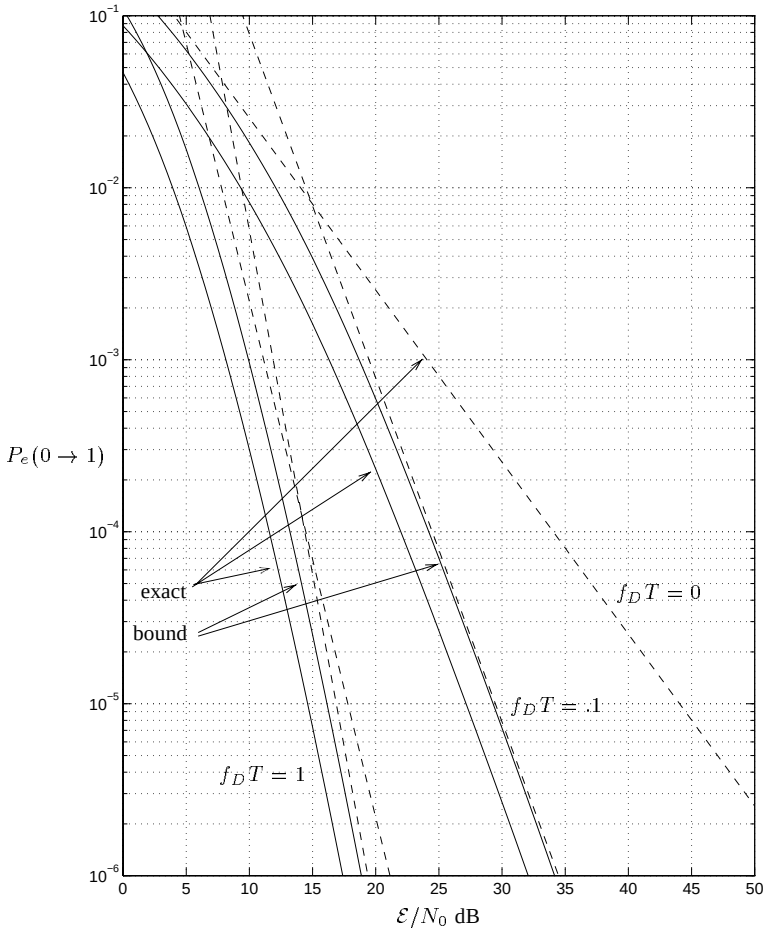

Figure 3.4: PEP and its upper–bound for antipodal signals

penalty in using a pulse shape where the energy of the difference signal is not equally distributed in $[-T/2, T/2]$ is evident, since the Walsh–Hadamard pulse performs much worse than the other two. This is due to the energy has a smaller number of significant eigenvalues which is seen in the curve for $f_D T = 3$ which has a smaller slope (i.e. less diversity). This is the first example of the importance of

the diversity order on the performance.

Performance of Non–Coherent Detection

Turning to the non–coherent case we assume from the outset that the number of eigenvalues is limited to D, in order to simplify the analysis. For antipodal modulation $\mathrm{P}_e(0 \to 1) = .5$ since $K_y^{(0)}(t,u) = K_y^{(1)}(t,u)$, which is typical for non–coherent problems. We should note that the optimal estimator cannot distinguish between signals which are identical except for a phase shift (i.e. $x^{(0)}(t) = e^{j\phi}x^{(1)}(t)$) since the received process has the same conditional correlation function. In general, a performance analysis

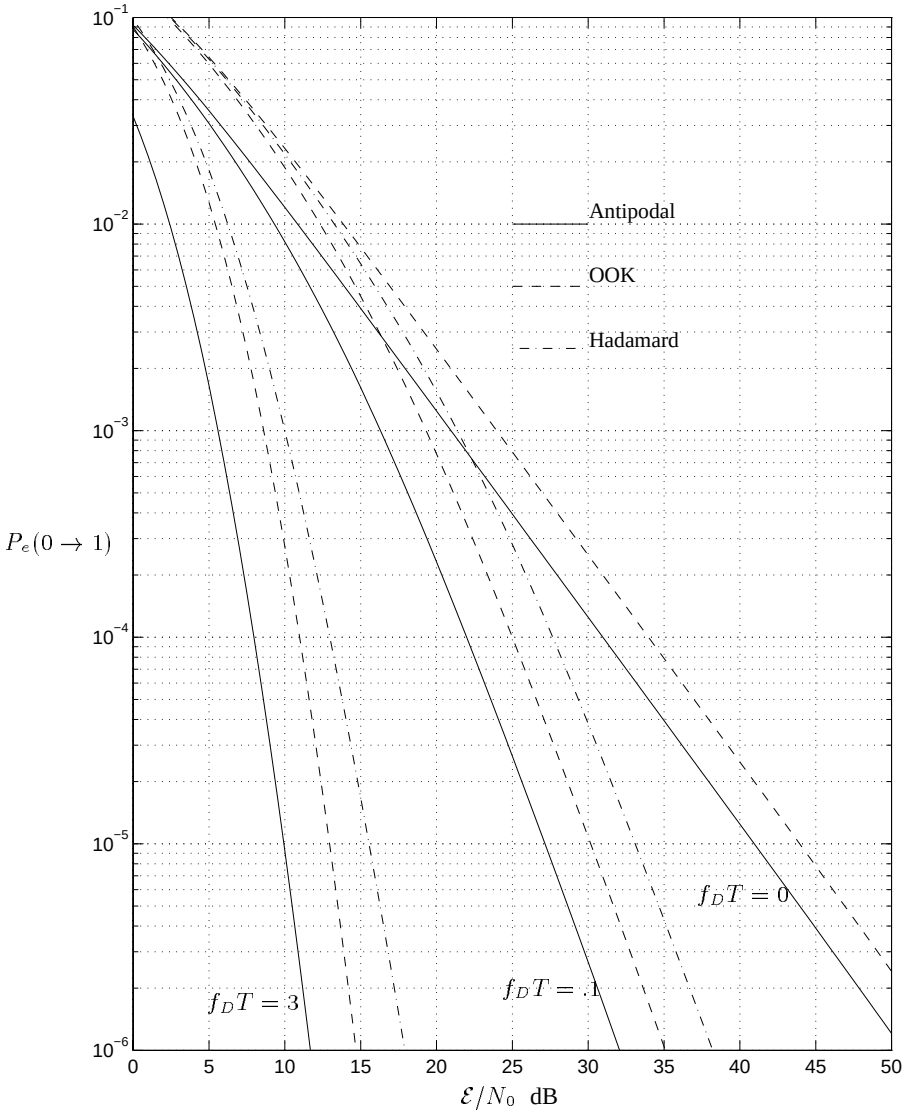

Figure 3.5: PEP for antipodal, Hadamard and OOK modulation

of Gaussian signal detection problems is difficult. The OOK example, however, is tractable with the degenerate kernel approximation. Here, $K_y^{(0)}(t,u) = \frac{2\mathcal{E}}{T}K_\alpha(t,u) + N_0\delta(t-u)$ and $K_y^{(1)}(t,u) = N_0\delta(t-u)$ so that

$$\mathrm{P}_e(0\to 1) = \mathrm{Prob}\left(\sum_{i=1}^{D}\frac{|y_i^{(0)}|^2}{\lambda_i^{(0)}+N_0} + \sum_{i=1}^{D}\log\left(1+\frac{\lambda_i^{(0)}}{N_0}\right) \geq \sum_{i=1}^{D}\frac{|y_i^{(1)}|^2}{N_0} \right. \\ \left. \Big| \, x^{(0)}(t) \text{ transmitted}\right) \tag{3.51}$$

In this case we may take $\phi_i^{(0)}(t) = \phi_i^{(1)}(t)$ so that $y_i^{(0)} = y_i^{(1)}$ which allows us to simply the decision rule as

$$\mathrm{P}_e(0\to 1) = \mathrm{Prob}\left(\sum_{i=1}^{D}\frac{\lambda_i^{(0)}}{N_0}|\beta_i|^2 \leq \sum_{i=1}^{D}\log\left(1+\frac{\lambda_i^{(0)}}{N_0}\right)\right) \tag{3.52}$$

where β_i are i.i.d. random variables with mean zero and variance 1. Normalizing the fading process so that $\mathrm{E}|\alpha(t)|^2 = 1$, we have that $\sum_{i=1}^{D}\lambda_i^{(1)} \approx 2\mathcal{E}$. This approximation can be made arbitrarily precise by increasing D. We now define the normalized eigenvalues $\mu_i = \lambda_i^{(0)}/2\mathcal{E}$ yielding

$$\begin{aligned}\mathrm{P}_e(0\to 1) &= \mathrm{Prob}\left(\sum_{i=1}^{D}\mu_i|\beta_i|^2 \leq \frac{N_0}{2\mathcal{E}}\sum_{i=1}^{D}\log\left(1+\frac{2\mathcal{E}}{N_0}\mu_i\right)\right) \\ &= \sum_{i=1}^{D}A_i\left(1-e^{-B/\mu_i}\right)\end{aligned} \tag{3.53}$$

where $B = \frac{N_0}{2\mathcal{E}}\sum_{i=1}^{D}\log\left(1+\frac{2\mathcal{E}}{N_0}\mu_i\right)$. This is plotted in Figure 3.6 as a function of the SNR and compared with the corresponding coherent case, where we see that for low fade rates the loss due to non–coherent detection is large.

3.3.3 Coded Quadrature Amplitude Modulated Signals

We now consider the possibility of performing non–coherent detection of non–binary messages, where the detection is performed across several symbols. We quickly realize that implementing the optimal receiver structures is a more or less an impossible task when M is large and the channel varies greatly during the duration of a message. Unfortunately, this is precisely the case of coded systems with *quadrature amplitude modulation (QAM)* on fast–fading channels. As a result, one must resort to some discretized approximation. We consider a piecewise constant approximation for the fading process as follows

$$\alpha(t) = \sum_{i=\left\lceil -\frac{N_s}{2}\right\rceil}^{\left\lceil \frac{N_s}{2}-1\right\rceil}\alpha_i q(t-iT/N_s) \tag{3.54}$$

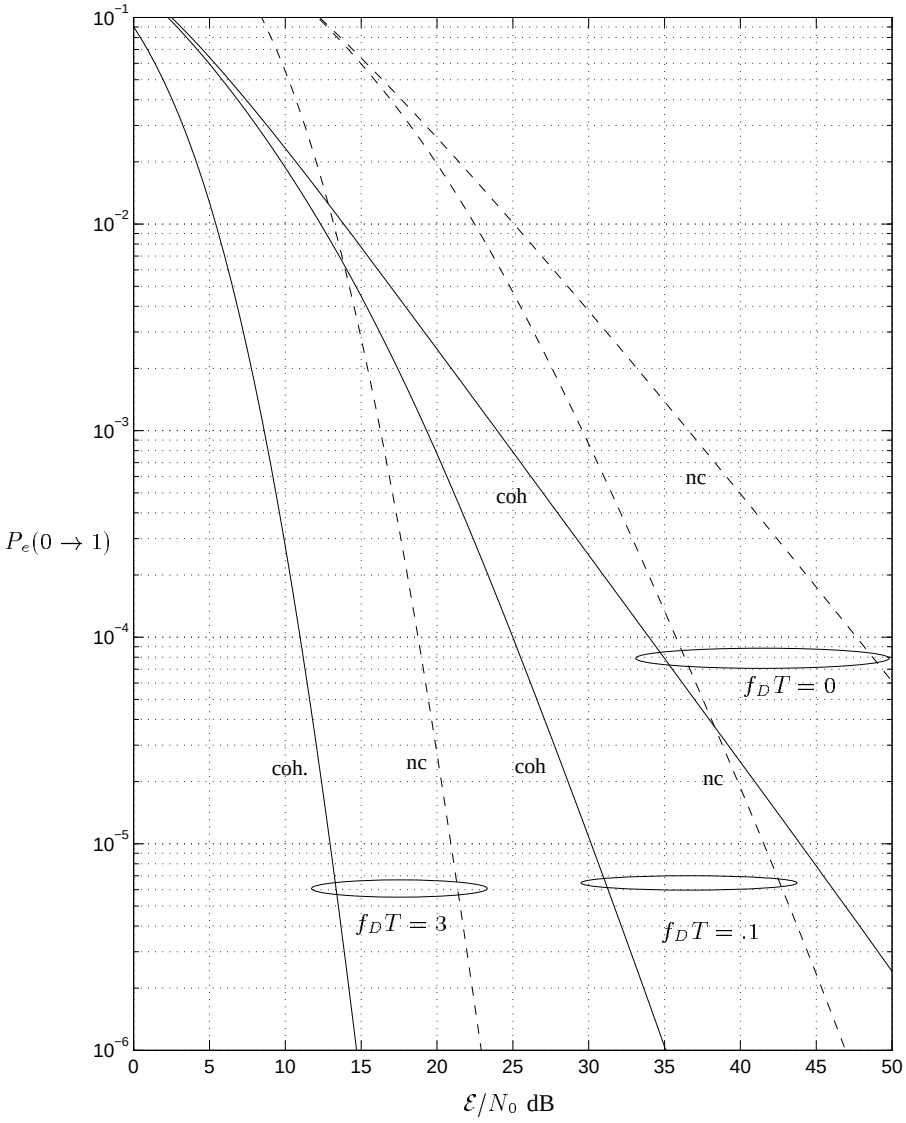

Figure 3.6: Performance of non-coherent OOK

where $q(t)$ is a rectangular pulse shape or *chip*

$$q(t) = \begin{cases} \sqrt{\frac{N_s}{T}} & t \in [0, T/N_s) \\ 0 & \text{elsewhere} \end{cases} \tag{3.55}$$

and N_s can be arbitrarily large. Provided that $f_D T \ll N_s$ this will be a close approximation to the actual fading process.

Now consider the QAM signal

$$x^{(m)}(t) = \sum_{i=-\lceil N_x/2 \rceil}^{\lceil N_x/2-1 \rceil} x_i^{(m)} p(t - iT/N_x) \tag{3.56}$$

with N_x being the number of coded symbols or *complex dimensions* used during the time–interval $[-T/2, T/2]$. The $x_i^{(m)}$ belong to an arbitrary complex alphabet and we assume that the pulse shape may be expressed as

$$p(t) = \sum_{i=0}^{N_s/N_x - 1} p_i q(t - iT/N_s) \tag{3.57}$$

with $\sum_{i=0}^{N_s/N_x-1} |p_i|^2 = 1$. The ratio $k = N_s/N_x$ is assumed to be an integer. We show a particular example where $N_s = 8$ and $N_x = 4$ in figure 3.7. This formulation allows us to express the detection

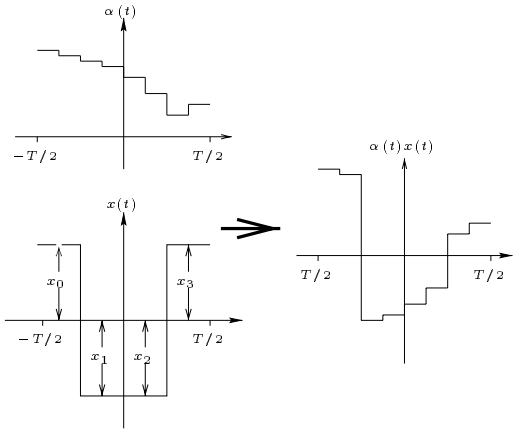

Figure 3.7: A QAM example with $N_s = 8$ and $N_x = 4$

problem vectorially as we now show. The received signal is given by

$$\begin{aligned} y(t) &= \alpha(t) x^{(m)}(t) + z(t) \\ &= \sum_{i=-\lceil N_s/2 \rceil}^{-\lceil N_s/2-1 \rceil} \alpha_i p_{i \bmod k} x_{i \div k} q(t - iT/N_s) + z(t) \end{aligned} \tag{3.58}$$

where $i \div k$ is taken to mean integer division. In complex circular symmetric white noise with power spectral density N_0, the set of statistics

$$y_i = \int_{-T/2}^{T/2} y(t) q(t - iT/N_s) dt \tag{3.59}$$

is sufficient for the detection of $x^{(m)}(t)$ since $\{q(t - iT/N_s), i = 0, \cdots, N_s\}$ forms a suitable basis for the signal. We may therefore write

$$\begin{aligned} \mathbf{y} &= \begin{pmatrix} y_0 \\ y_1 \\ \vdots \\ y_{N_s-1} \end{pmatrix} = \mathbf{X}^{(m)} \begin{pmatrix} \alpha_0 \\ \alpha_1 \\ \vdots \\ \alpha_{N_s-1} \end{pmatrix} + \begin{pmatrix} z_0 \\ z_1 \\ \vdots \\ z_{N_s-1} \end{pmatrix} \\ &= \mathbf{X}^{(m)} \boldsymbol{\alpha} + \mathbf{z} \end{aligned} \tag{3.60}$$

where z_i are zero–mean i.i.d. circular symmetric random variables with variance N_0 and

$$\mathbf{X}^{(m)} = \mathrm{diag}(p_0 x_0^{(m)}, p_1 x_0^{(m)}, \cdots, p_{k-1} x_0^{(m)}, p_0 x_1^{(m)}, \cdots p_{k-1} x_{N_x-1}^{(m)}) \tag{3.61}$$

Optimal Receiver Structure

Not surprisingly, this discrete–time system is completely analogous to the exact continuous–time model outlined earlier. Under hypothesis m the correlation matrix of $\mathbf{s}^{(m)} = \mathbf{X}^{(m)} \boldsymbol{\alpha}$ is

$$\mathbf{K}_s^{(m)} = \mathbf{X}^{(m)} \mathbf{K}_\alpha \mathbf{X}^{(m)*} \tag{3.62}$$

where $K_\alpha^{(ij)} = K_\alpha(iT/N_s, jT/N_s)$. The eigenvalues of $\mathbf{K}_\alpha$ are a close approximation to those of the kernel $K_\alpha(t, s)$ if N_x is sufficiently large. As before, we perform a KL expansion on $\mathbf{y}$ using the basis of eigenvectors of $\mathbf{K}_s^{(m)} = \mathbf{U}^{(m)} \boldsymbol{\Lambda}^{(m)} \mathbf{U}^{(m)*}$ yielding

$$\begin{aligned} \mathbf{y}^{(m)} = \mathbf{U}^{(m)*} \mathbf{y} &= \mathbf{U}^{(m)*} \mathbf{X}^{(m)} \boldsymbol{\alpha} + \mathbf{z}^{(m)} \\ &= \mathbf{x}'^{(m)} + \mathbf{z}^{(m)} \end{aligned} \tag{3.63}$$

with $\mathbf{K}_{x'}^{(m)} = \boldsymbol{\Lambda}^{(m)}$. The decision rule is identical to (3.28) with K replaced by $N_s - 1$. In terms of the original observation vector we have

$$\hat{m} = \underset{m=0,\cdots,M-1}{\mathrm{argmin}} \; \mathbf{y}^* \left(N_0 \mathbf{I} + \mathbf{K}_s^{(m)} \right)^{-1} \mathbf{y} + \log \det(N_0 \mathbf{I} + \mathbf{K}_s^{(m)}) \tag{3.64}$$

We note the similarity of this decision rule with (3.31).

Similarly to the continuous case we may express the decision rule in (3.64) in an estimator–correlator form using innovations. This type of approach is taken in [VT95]. The correlation matrix of received samples may be factored as $N_0\mathbf{I} + \mathbf{R}_s^{(m)} = \mathbf{L}^{(m)}\mathbf{L}^{(m)*}$, where $\mathbf{L}^{(m)}$ is an upper–triangular matrix, which is known as a *Cholesky factorization.* We now define the innovations vector $\mathbf{i}^{(m)} = \mathbf{\Gamma}^{(m)}\mathbf{y}$ where $\mathbf{\Gamma}^{(m)} = \mathbf{L}^{(m)^{-1}} = \sqrt{\mathbf{D}^{(m)}}\mathbf{P}^{(m)}$ and $\mathbf{P}^{(m)}$ is the N_s^{th}–order forward linear predictor for $\mathbf{y}$ under hypothesis m and $\mathbf{D}^{(m)}$ is a diagonal matrix containing the prediction errors for each y_i. The innovations vector has i.i.d. zero–mean Gaussian components with variance 1. It follows, therefore, that the decision rule may be written as

$$\hat{m} = \underset{m=0,\cdots,M-1}{\operatorname{argmin}} \mathbf{i}^{(m)*}\mathbf{i}^{(m)} + \sum_k \log d_k^{(m)} \tag{3.65}$$

For practical reasons, this form of the decision rule is convenient since it can be implemented recursively. We may define the metric $\Lambda(N_s) = \sum_{k=0}^{N_s-1} |i_k^{(m)}|^2 + \log d_k^{(m)}$ so that $\Lambda(k) = \Lambda(k-1) + |i_k^{(m)}|^2 + \log d_k^{(m)}$. If the fading process has very short memory (i.e. very fast fading) say L samples, then the computation of $i_k^{(m)}$ and $d_k^{(m)}$ depend only the $\{y_{k-L}, \cdots, y_k\}$ and therefore the Viterbi algorithm [For73] with 2^L states may be used effectively to decode the data sequence. This technique only becomes useful for fading speeds which do not occur in terrestrial mobile communication systems because of the slow mobile speed. In the future low–earth orbit mobile satellite systems however, these types of receiver structures may be interesting. The same holds true for aeronautical channels where fast Ricean fading is experienced due to scattering off the ocean surface. A difficult practical problem is that the complexity of the receiver structure is very dependent on the memory of the channel which is directly related to the mobile speed which changes in time.

We now examine the PEP which in this case is given by

$$\mathrm{P}_e(0 \to 1) = \mathrm{Prob}\left(|\mathbf{i}^{(1)}|^2 - |\mathbf{i}^{(2)}|^2 < \sum_k \log \frac{d_k^{(1)}}{d_k^{(2)}} \middle| \mathbf{X}^{(1)} \text{ transmitted} \right) \tag{3.66}$$

The random variable $z = |\mathbf{i}^{(1)}|^2 - |\mathbf{i}^{(2)}|^2 = \boldsymbol{\beta}^*\mathbf{Q}\boldsymbol{\beta}$ is a quadratic form of the Gaussian random vector $\boldsymbol{\beta} = \begin{pmatrix} \mathbf{i}^{(1)} \\ \mathbf{i}^{(2)} \end{pmatrix}$ with correlation matrix

$$\mathbf{K}_\beta = \begin{pmatrix} \mathbf{I} & \mathbf{L}^{(1)}\mathbf{\Gamma}^{(2)} \\ \mathbf{\Gamma}^{(2)*}\mathbf{L}^{(1)*} & \mathbf{I} \end{pmatrix} \tag{3.67}$$

and $\mathbf{Q} = \begin{pmatrix} \mathbf{I} & \mathbf{0} \\ \mathbf{0} & -\mathbf{I} \end{pmatrix}$. The moment–generating function for a quadratic form of correlated Gaussian

random variables is derived in [SBS66, App. B] which for z yields

$$\phi_z(s) = \prod_{k=0}^{N_s-1} \frac{1}{1 - s\lambda_i} \tag{3.68}$$

where the $\{\lambda_i\}$ are the eigenvalues of the matrix $\mathbf{R}_\beta\mathbf{Q}$. Denoting $z_{12} = \log \frac{d_k^{(1)}}{d_k^{(2)}}$ it follows that the PEP is given by

$$\begin{aligned} \mathrm{P}_e(0 \to 1) &= \frac{1}{2\pi j} \int_{-\infty}^{z_{12}} \int_{\sigma - j\infty}^{\sigma + j\infty} \phi_z(s) e^{-sz} ds dz \\ &= \frac{1}{2\pi j} \int_{\sigma - j\infty}^{\sigma + j\infty} \frac{\phi_z(s)}{s} e^{-sz_{12}} ds \end{aligned} \tag{3.69}$$

which can be computed numerically using Gauss Chebychev quadrature [BCTV96] or, in some cases, by the residue method.

Phase–Modulated Signals

For an important class of signals, namely those with phase modulated symbols (i.e. $|x_i|^2 = \mathcal{E}/T$), the bias terms may be neglected since they are all identical. When the fading is very slow (i.e. $f_D = 0$) it is easily shown using the matrix inversion lemma in this case that the decision rule reduces to the classic non–coherent detection rule

$$\hat{m} = \underset{m=0,\cdots,M-1}{\operatorname{argmax}} |\mathbf{y}^* \mathbf{x}^{(m)}| \tag{3.70}$$

Let us consider phase–modulated signals with rectangular pulse shapes $p(t)$. For an M–ary system, the coded symbols take on one of M values $\{e^{j\frac{2\pi a}{M}},\ a = 0, \cdots, M-1\}$. We assume detection can be performed on groups of $N_x \geq 2$ symbols. For a non–fading channel this type of multi–symbol non–coherent detection of uncoded M–DPSK modulation was considered in [DS90] and [LP91]. These results were extended for block–coded systems in [KL94] and for trellis–coded systems in [Rap96a]. Recently, Kofman *et al.* [KZS97a][KZS97b] have considered the design of binary convolutional for this application. We now briefly consider the general fading case where we have multiple fading levels per symbol, in order to show the difficulty in designing codes for this situation.

It is straightforward to show that the matrix $\mathbf{K}_\beta$ depends on $\mathbf{X}^{(m)}$ and $\mathbf{X}^{(n)}$ only through $\mathbf{X}^{(m)}\mathbf{X}^{(n)*}$ and consequently $\mathrm{Prob}(m \to n) = \mathrm{Prob}(q \to 0)$ where q is the codeword index corresponding to $\mathbf{X}^{(m)}\mathbf{X}^{(n)*}$ and 0 is the all–zero codeword. This holds true for any coding scheme where the set of codewords forms a group under complex component-wise multiplication.

We show the PEP with respect to the all–zero codeword $(1, 1, \cdots, 1)$ for QPSK modulation with three codewords of length $N_x = 4$ in Figure 3.8. The symbols, therefore, take on the values $\{1, j, -1, -j\}$. We chose fade rates of $f_D T_s = 1$ and 0 where $T_s = T/4$ and we used 5 discretization steps per symbol for the fading process. The three codewords are identical except for the positions of the non–zero symbols. On the static channel, therefore, the three have identical expressions for the PEP. We see that the positions of the non–zero symbols within the codeword are critical for the higher fade rate case. The code design problem is therefore much more difficult than for a static channel.

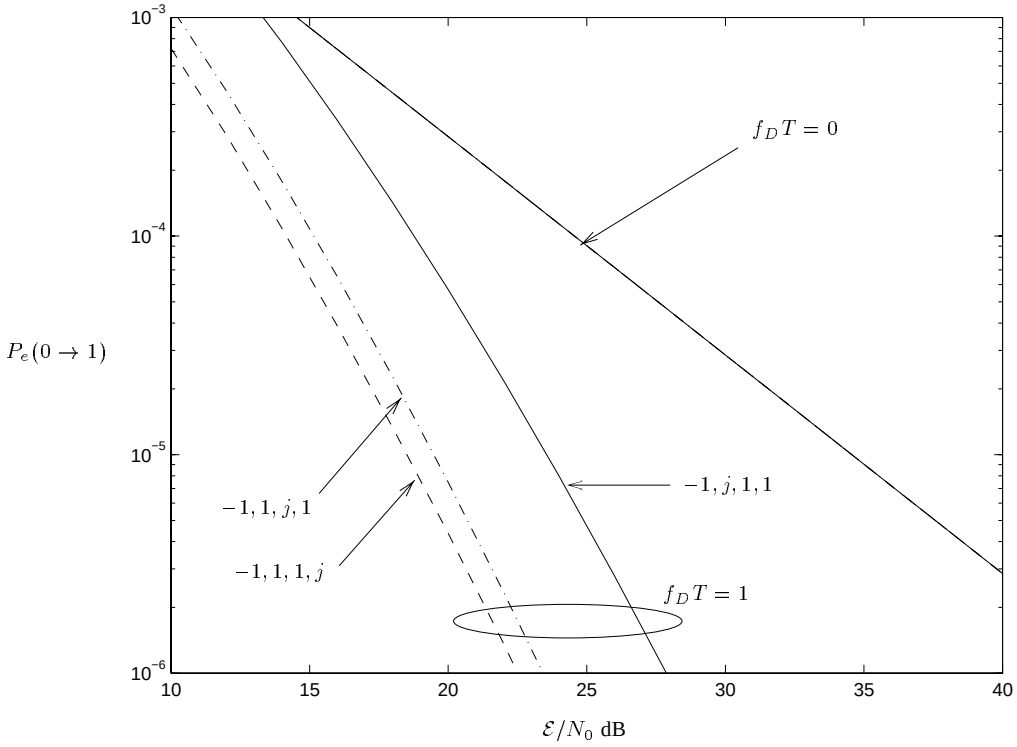

Figure 3.8: PEP for a non–coherent QPSK example

A practical solution to this problem would be to consider a concatenated coding scheme using a binary code and an interleaver (see the following section) whose output drives a simple M–ary code which is decoded non–coherently (ideally with a MAP decision rule on the individual bits) and deinterleaved. The bits passed to the binary decoder will have been subject to uncorrelated channel strengths so that traditional codes can be applied. This will become more clear after having read the following section.

3.3.4 Interleaved Signals

Let us now assume that the Doppler spread is significantly smaller than the signal bandwidth (i.e. $f_D T_s \approx 0$) and there is a modest or no time–delay constraint. A common method for achieving diversity is *interleaving*. We assume that coherent detection is possible because the channel varies very slowly. The simplest interleaving scheme is called *diagonal* or *periodic interleaving*. It is shown in Figure 3.9, where we also assume a discretized fading process. The coded symbols are placed into an $L \times N$ dimensional array columnwise and are read out rowwise before transmission. The interleaved signal is transmitted across a single–path channel and processed by a filter matched to the pulse shape $p(t)$. The samples at the output of the matched filter are fed into a similar array rowwise and read–out columnwise. The width of the array L determines the correlation of the variables α_i' at the output of the de-interleaver as well as the total decoding delay, LN. The depth of the interleaver, N, should be chosen to be larger than the memory of the code (for a block code, it would be the block length and for a convolutional code at least as long as the constraint length). This is because we want to avoid strong cyclic correlations, since two symbols separated by LT_s will be highly correlated. In many cases, a strict decoding delay constraint does not permit this type of arrangement and strong cyclic correlations are inevitable. We treat this situation in detail in Section 3.6 and Chapter 5.

In addition to coherent detection being possible in this case, it is often simple to achieve perfect knowledge of the α_i' at the receiving end. Under these assumptions, let us examine the PEP between two arbitrary codewords of length $N_x \leq N$ which is given by (using 3.36)

$$P_{e|\alpha_i'}(0 \to 1) = \mathrm{Q}\left(\sqrt{\frac{\sum_{i=0}^{N_x} |\alpha_i'|^2 |x_i^{(0)} - x_i^{(1)}|^2}{2N_0}}\right). \tag{3.71}$$

Defining $d_i^2(0,1) = |x_i^{(0)} - x_i^{(1)}|^2$ and $z = \sum_{i=0}^{N_x} |\alpha_i'|^2 d_i^2(0,1)/2N_0 = \boldsymbol{\alpha}^{*\prime}\mathbf{D}\boldsymbol{\alpha}'$ where $\boldsymbol{\alpha}' = \left(\alpha_0' \cdots \alpha_{N_x}'\right)$ and $\mathbf{D} = \mathrm{diag}\left\{d_i^2(0,1)\right\}$ we have that the moment–generating function for z is

$$\phi_z(s) = \prod_{i=0}^{N_x - 1} \frac{1}{1 - s\frac{\lambda_i}{2N_0}} \tag{3.72}$$

where $\{\lambda_i\}$ is the set of eigenvalues of $\mathbf{K}_{\alpha'}\mathbf{D}$. Consider the simplest case where $L \to \infty$ and $\mathbf{K}_{\alpha'} = \mathbf{I}$. This is known as *ideal* or *perfect interleaving* which assures that the α_i' are uncorrelated. In practice, this is achieved by choosing L to be larger than the coherence time of the fading process $\alpha(t)$. In this case we have that

$$\phi_z(s) = \prod_{i=0}^{d_H(0,1)-1} \frac{1}{1 - s\frac{d_i^2(0,1)}{2N_0}} \tag{3.73}$$

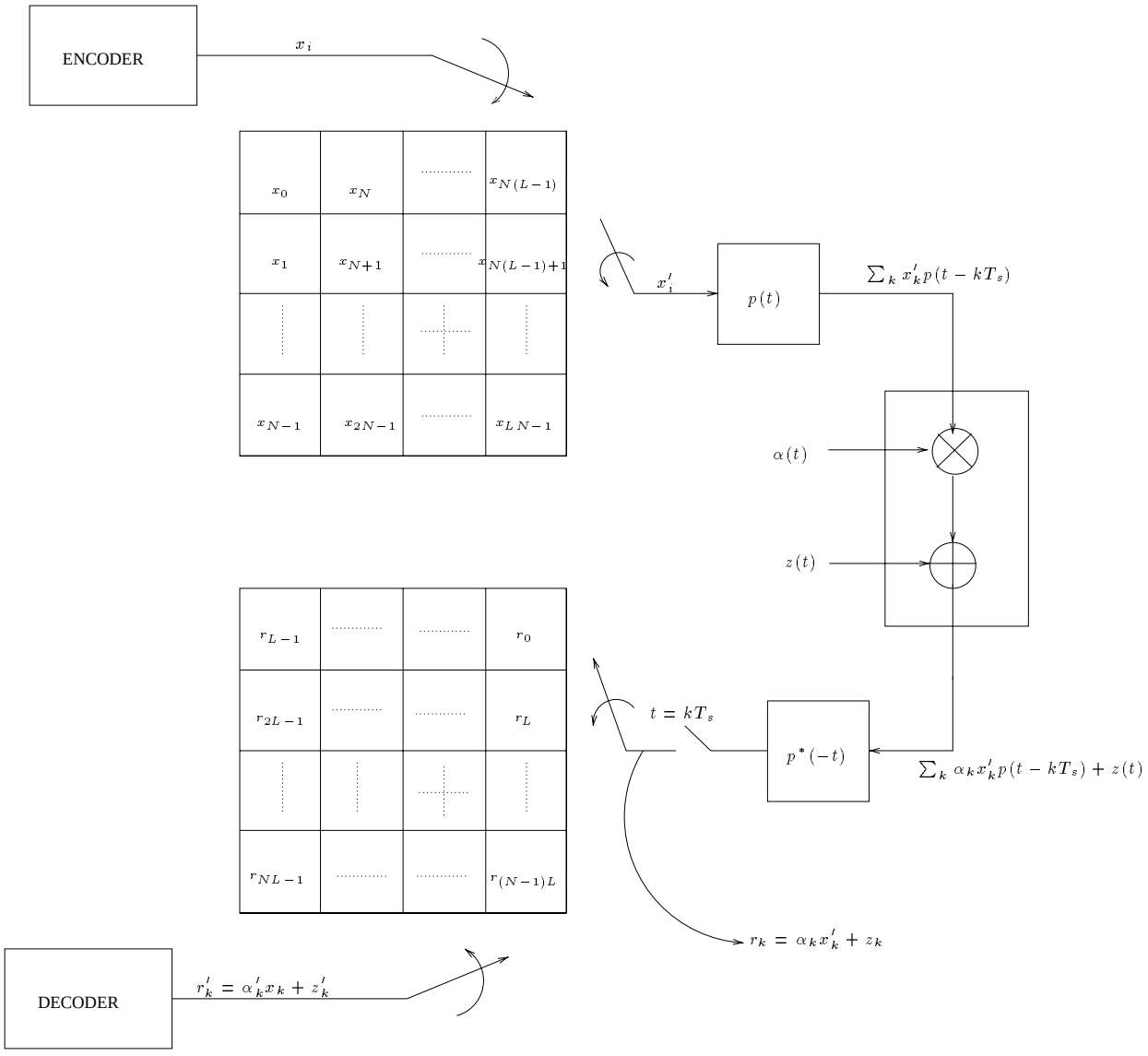

Figure 3.9: Periodic interleaving

where $d_H(0,1)$ is the *Hamming distance* between the two codewords on the symbol level. The average PEP can be computed numerically, and as before, we may consider the upper–bound in (3.48) which now becomes

$$P_e(0 \to 1) \leq \frac{1}{2} \prod_{i=0}^{d_H(0,1)} \frac{1}{1 + \frac{d_i^2(0,1)}{4N_0}} < \frac{1}{2} \left(\frac{4N_0}{\chi} \right)^{d_H(0,1)} \tag{3.74}$$

where $\chi = \left(\prod_{i=0}^{d_H(0,1)} d_i^2(0,1) \right)^{1/d_H(0,1)}$. An important observation is that the main performance indicator, $d_H(0,1)$, is a purely algebraic measure of the code symbols so that in order to maximize diversity we must simply maximize the Hamming distance. This is quite different from the non–fading case where Euclidean distance is the quantity to be maximized. The secondary parameter which acts as a gain in SNR is the geometric mean of the non–zero $d_i^2(0,1)$ which must lie between the minimum and maximum squared Euclidean distances of the underlying constellation.

When we do not have a perfect interleaving situation, which is almost always the case, we will say that the channel is *partially interleaved*. Let us now examine a numerical example to see the effect of symbol correlation on a partially interleaved channel. We choose $N = N_x = 8$ and assume L is chosen so that $f_D L T_s = .1, 1$ and ∞. The symbols are modulated using 8–PSK modulation. Figure 3.10 shows the PEP for two code sequences with respect to the all–zero codeword which differ only in the positions of the non–zero symbols. We see, as in the non–coherent case, that the PEP is heavily dependent on

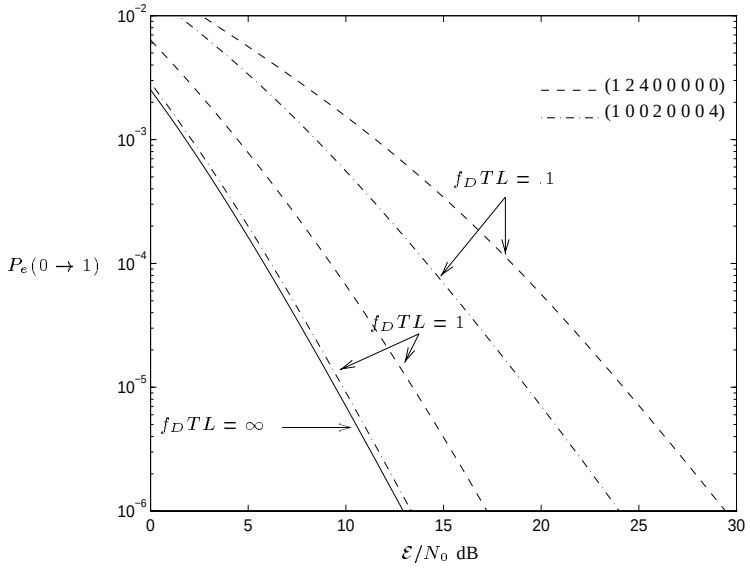

Figure 3.10: Effect of symbol positioning on the PEP

the positions of the non–zero symbols except in the perfectly interleaved case. The codeword with the

symbols evenly spaced performs better since the positions become less correlated as their separation increases. As a result, the code design problem is more complex than simply maximizing the Hamming distance. Fortunately we will see that by appropriately choosing the interleaver dimensions, we can turn this correlated channel problem into a *block fading channel* for which code design is simpler. We consider this in Section 3.6 and Chapter 5.

3.4 Wide-band Direct–Sequence Spread-Spectrum

Now we will consider schemes which exploit diversity in the frequency domain by using wide–band signals. Let us examine wide-band signals strictly band-limited to W Hz transmitted over a static multipath channel

$$h(t) = \sum_{i=1}^{P} \alpha_i \delta(t - d_i). \tag{3.75}$$

We now look at a particular class of wide-band signals known as *direct sequence spread–spectrum (DSSS)* signals. Here, we use more physical bandwidth than necessary to convey the information signal. A DSSS pulse–shape ideally band-limited to W Hz may be expressed as

$$s(t) = \sum_{i=0}^{N_c-1} c_i \frac{\sin \pi W(t - i/W)}{\pi W(t - i/W)} \tag{3.76}$$

which is a bandlimited version of a classical DSSS system. Most transmission schemes have bandlimiting filters before transmission, so even if the original DSSS signal was rectangular, the actual transmitted signals look more like (3.76). The transmitted signal is given by

$$x^{(m)}(t) = \sum_{k} x_k^{(m)} s(t - kT_s) \tag{3.77}$$

where $N_c = WT_s$ is the spreading factor assumed to be an integer and T_s is the symbol time. We see that N_c is simply the number of degrees of freedom for a signal band-limited to W Hz and approximately time–limited to T_s seconds. The c_i are called *chips* and are usually chosen to be a *pseudo–noise (PN)* ± 1 sequence. The vector formed by the chip sequence is therefore the basis vector for a one–dimensional subspace of the space of signals band-limited to W and approximately time–limited to T_s in which the transmitted signal lies. In essence, we have just described a repetition coding scheme with code-rate $1/N_c$. Although not DSSS, we could equally well choose to code several adjacent information symbols jointly while keeping the same overall code-rate (or bandwidth expansion factor). A much more elaborate extension of this idea is used on the up-link of the IS-95 CDMA mobile cellular telephone

system [IS992], and turns out to be a much better way to spread spectrum. The main difference between the two approaches is that, in the latter case, the waveform for each symbol belongs a subspace with a dimension greater that one. The advantages of this type of low–rate coding is considered by Viterbi for a non–fading channel in [Vit90]. The effect in terms of performance on a multipath channel is significant and will be treated in the next chapter more closely.

There are important reasons to spread spectrum in certain situations. The traditional application was military communications. The spread signal has a *low probability of intercept* character; since the information is spread across a large bandwidth, a narrow-band interfer or receiver interprets it as white noise. This property is also useful in situations where several systems must coexist in the same frequency band.

3.4.1 Receiver Structures

Examining a block of N_x transmitted signals, the received signal may be written as

$$r(t) = \sum_{k=0}^{N_x-1} x_k^{(m)} \left\{ s(t - kT_s) * h(t) \right\} + z(t) \tag{3.78}$$

The autocorrelation function of the pulse–shape is given by

$$\begin{aligned} \rho_s(\tau) &= \int_{-\infty}^{\infty} s(t)s(t+\tau)dt \qquad (3.79) \\ &= \int_{-\infty}^{\infty} \sum_{i=0}^{N_c} \sum_{j=0}^{N_c} c_i c_j \frac{\sin \pi W(t - j/W + \tau)}{\pi W(t - j/W + \tau)} \frac{\sin \pi W(t - i/W)}{\pi W(t - j/W)} dt \\ &= \sum_{i=0}^{N_c} \sum_{j=0}^{N_c} c_i c_j \frac{\sin \pi W(\tau - (j-i)/W)}{\pi W(\tau - (j-i)/W)} \qquad (3.80) \end{aligned}$$

This is plotted in Figure 3.11 for a few choices of PN pulse shapes with increasing N_c. Assuming perfect knowledge of the channel response and equal energy signals, the maximum–likelihood receiver in this case can be written as

$$\hat{m} = \underset{m=0,\cdots,M-1}{\operatorname{argmax}} \operatorname{Re} \left\{ \int_{-\infty}^{\infty} r^*(t) \sum_{k=0}^{N_x-1} x_k^{(m)} \left\{ s(t - kT_s) * h(t) \right\} dt \right\} \tag{3.81}$$

Since all signals are band-limited to W Hz we may express this decision rule in terms of the samples

$$\begin{aligned} \hat{m} &= \underset{m=0,\cdots,M-1}{\operatorname{argmax}} \operatorname{Re} \left\{ \sum_{n=0}^{N_c N_s - 1} r^*(n/W) \sum_{k=0}^{N_s-1} x_k^{(m)} \left\{ s(n/W - kT_s) * h_W(n/W) \right\} \right\} \\ &= \underset{m=0,\cdots,M-1}{\operatorname{argmax}} \operatorname{Re} \left\{ \sum_{n=0}^{N_c N_s - 1} r^*(n/W) \sum_{l=0}^{L-1} \sum_{k=0}^{N_s-1} x_k^{(m)} h_W(l/W) s((n-l)/W - kT_s) \right\} \end{aligned} \tag{3.82}$$

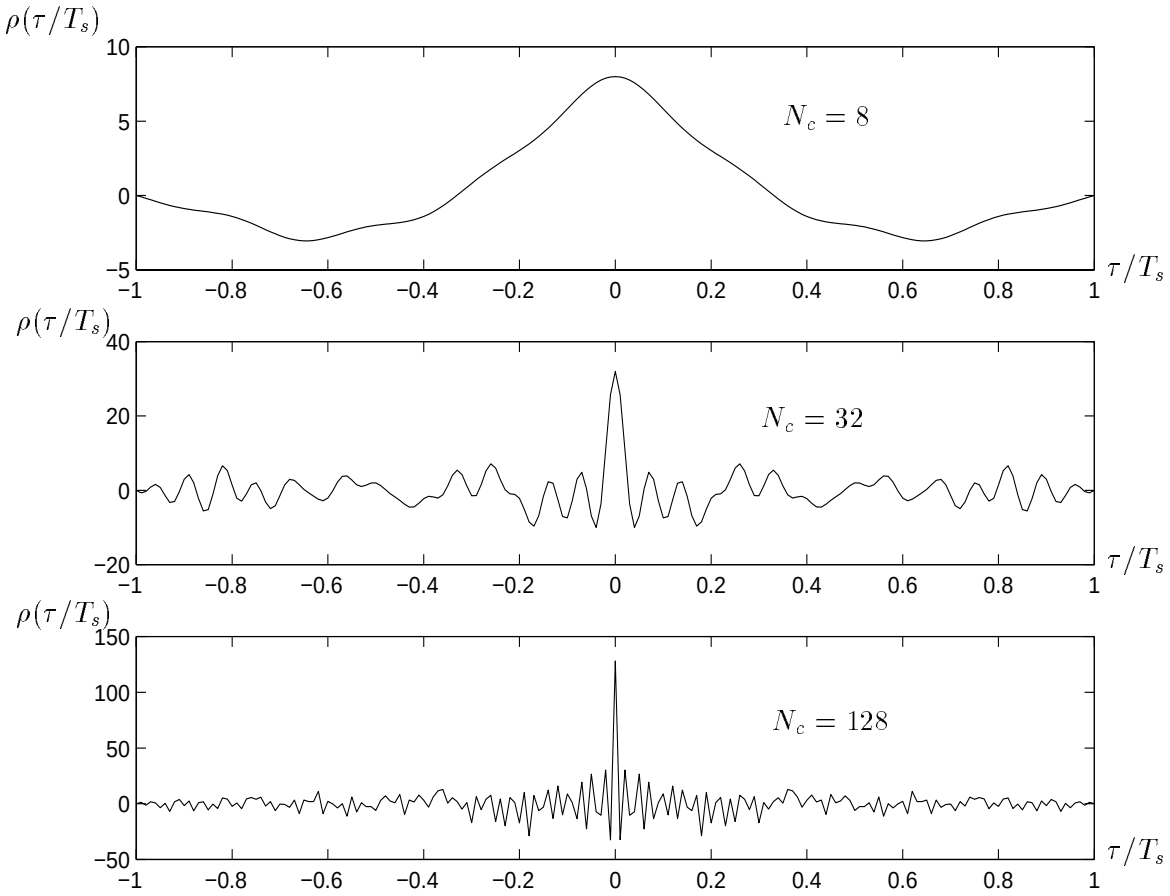

Figure 3.11: DSSS autocorrelation functions

where $h_W(t)$ is the ideally low–pass filtered version of $h(t)$ given by

$$h_W(t) = \sum_{i=1}^{P} \alpha_i \frac{\sin \pi W(t-d_i)}{\pi W(t-d_i)} \tag{3.83}$$

and L is the number of significant $h_W(n/W)$ (i.e. $\sum_{l=0}^{L-1} \mathrm{E}|h_W(n/W)|^2 > \epsilon$). Provided the number of paths is large the $h_W(n/W)$ are accurately modeled by correlated Gaussian random variables having an autocorrelation matrix $\mathbf{K}_h$ with components

$$\begin{aligned} K_h^{(ij)} &= \mathrm{E} h_W(i/W) h_W^*(j/W) \\ &= \sum_{k=1}^{P} \mathrm{E}|\alpha_k|^2 \frac{\sin \pi WT(\frac{i}{WT} - \frac{d_k}{T})}{\pi WT(\frac{i}{WT} - \frac{d_k}{T})} \frac{\sin \pi WT(\frac{j}{WT} - \frac{d_k}{T})}{\pi WT(\frac{j}{WT} - \frac{d_k}{T})} \end{aligned} \tag{3.84}$$

where we have used the uncorrelated scattering assumption (i.e. $\mathrm{E}\alpha_i \alpha_j^* = \mathrm{E}|\alpha_i|^2 \delta_{ij}$.) Essentially, we have reduced the system to the transmission of a discrete–time signal $x(i/W)$ over a discrete–time finite impulse response channel $h(i/W), i = 0, \cdots, L-1$. We must stress, however, that the channel

coefficients are highly correlated. It is common in the literature when using discrete–time multipath models to assume uncorrelated taps which can yield highly optimistic performance results. To see the extent of this correlation consider the ETSI TU channel described in Chapter 2 with $T_s = 104.67\mu$s. The significant number of taps in the filter response and the correlation matrices for different $N_c = WT_s$ for the first 5 taps are shown in Table 3.1.

WT_s	Number of significant taps	Correlation of taps 1-5
8	2	$\begin{pmatrix} 0.9671 & 0.0726 & -0.0331 & 0.0214 & -0.0159 \\ 0.0726 & 0.0153 & -0.0065 & 0.0041 & -0.0030 \\ -0.0331 & -0.0065 & 0.0028 & -0.0018 & 0.0013 \\ 0.0214 & 0.0041 & -0.0018 & 0.0011 & -0.0008 \\ -0.0159 & -0.0030 & 0.0013 & -0.0008 & 0.0006 \end{pmatrix}$
32	3	$\begin{pmatrix} 0.7554 & 0.1662 & -0.0689 & 0.0423 & -0.0307 \\ 0.1662 & 0.1701 & -0.0284 & 0.0197 & -0.0145 \\ -0.0689 & -0.0284 & 0.0231 & -0.0109 & 0.0075 \\ 0.0423 & 0.0197 & -0.0109 & 0.0057 & -0.0040 \\ -0.0307 & -0.0145 & 0.0075 & -0.0040 & 0.0028 \end{pmatrix}$
128	8	$\begin{pmatrix} 0.3822 & 0.1321 & -0.0627 & 0.0400 & -0.0286 \\ 0.1321 & 0.3040 & -0.0066 & 0.0060 & -0.0058 \\ -0.0627 & -0.0066 & 0.1278 & -0.0053 & 0.0055 \\ 0.0400 & 0.0060 & -0.0053 & 0.0586 & -0.0056 \\ -0.0286 & -0.0058 & 0.0055 & -0.0056 & 0.0519 \end{pmatrix}$

Table 3.1: Significant taps and tap correlation

We now make a critical assumption which holds true in many spread–spectrum applications by taking $L \ll N_c$ which means that the channel is practically free of multipath induced *intersymbol interference (ISI)*. In the example we just mentioned this is definitely the case since the delay spread is on the order of 5μs. Under this assumption, the proportion of received energy in $[kT_s, (k+1)T_s]$ due to symbols $x_i^{(m)}$, $i \neq k$ is neglible so that the decision rule may be approximated by

$$\hat{m} = \underset{m=0,\cdots,M-1}{\operatorname{argmax}} \operatorname{Re}\left\{ \sum_{k=0}^{N_s-1} \sum_{n=0}^{N_c-1} \sum_{l=0}^{L-1} x_k^{(m)} r^*(kT_s + n/W) h_W(l/W) s((n-l)/W) \right\} \tag{3.85}$$

We may define the set of sufficient statistics

$$r_k = \sum_{n=0}^{N_c-1} \sum_{l=0}^{L-1} r^*(kT_s + n/W) h_W(l/W) s((n-l)/W) \tag{3.86}$$

so that the decision rule becomes

$$\hat{m} = \underset{m=0,\cdots,M-1}{\operatorname{argmax}} \operatorname{Re} \left\{ \sum_{k=0}^{N_s-1} r_k^* x_k^{(m)} \right\} \tag{3.87}$$

The operation in (3.86) is known as a *coherent RAKE* receiver since it acts like a garden rake on the multipath components by combining their energies in the same fashion as the maximal–ratio combiner we considered in Section 2.1.

3.4.2 RAKE Receiver Performance

Let us assume that message $\{x_k^{(0)}\}$ is sent so that

$$\begin{aligned} r_k &= \sum_{n=0}^{N_c-1} \left(x_k^{(0)} \sum_{l=0}^{L-1} h_W^*(l/W) s((n-l)/W) + z(n/W) \right) \sum_{l'=0}^{L-1} h_W(l'/W) s((n-l')/W) \\ &= x_k^{(0)} \sum_{l=0}^{L-1} \sum_{l'=0}^{L-1} h_W(l'/W) h_W^*(l/W) \rho_s((l-l')/W) + \sum_{n=0}^{N_c-1} \sum_{l=0}^{L-1} h_W(l/W) s((n-l)/W) z(n/W) \\ &= x_k^{(1)} \mathbf{h}^* \mathbf{P} \mathbf{h} + z_k \end{aligned} \tag{3.88}$$

where $\mathrm{E}|z_k|^2 = N_0 \sum_{l=0}^{L-1} |h_W(l/W)|^2 \approx N_0$, $\mathbf{h} = \begin{pmatrix} h_W(0) & \cdots & h_W((L-1)/W) \end{pmatrix}^{\mathrm{T}}$ and $P^{i,j} = \rho_s((i-j)/W)$. As before, the PEP between arbitrary code sequences conditioned on a particular channel realization is given by

$$P_{e|\mathbf{h}}(0 \to 1) = \mathrm{Q}\left(\sqrt{\frac{||\mathbf{x}^{(0)} - \mathbf{x}^{(1)}||^2}{2N_c N_0} \mathbf{h}^* \mathbf{P} \mathbf{h}} \right) \tag{3.89}$$

where we have included the normalization factor N_c which takes into account the bandwidth expansion factor. The quadratic form $\alpha = \mathbf{h}^* \mathbf{P} \mathbf{h}$ has moment–generating function

$$\phi_\alpha(s) = \prod_{l=0}^{L-1} \frac{1}{1 - s\lambda_l} \tag{3.90}$$

and λ_l are now the eigenvalues of $\mathbf{K}_h \mathbf{P}$. Evaluation of the average PEP is identical to the coherent case outlined described earlier. In Figure 3.12 we plot the average PEP vs. the signal–to–noise ratio per information bit for uncoded antipodal signals for different values of the spreading gain WT_s. The effect of spreading on the performance is evident. The number of significant eigenvalues at the SNR shown for the three spreading bandwidths are 2,3 and 6 which roughly correspond to the slopes of the three curves.

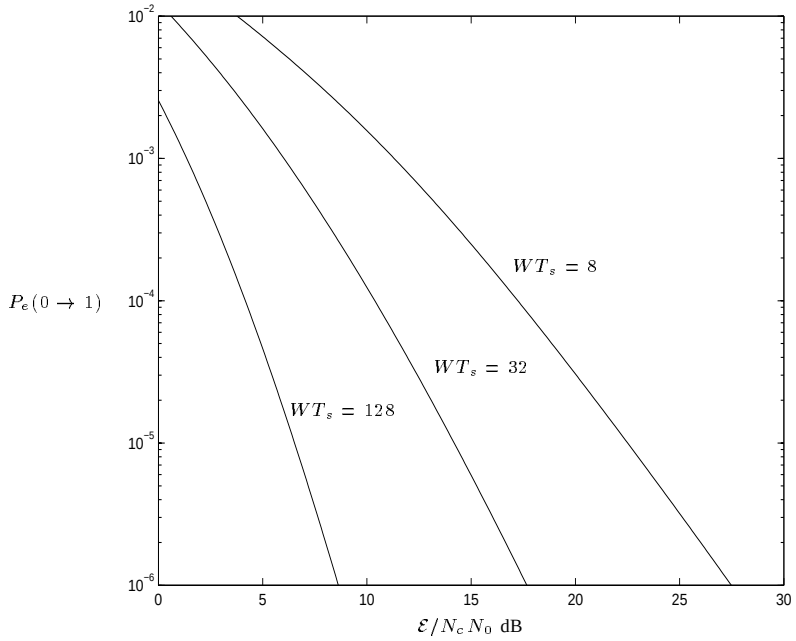

Figure 3.12: DSSS performance for different spreading gains

3.5 Multitone Signaling

We now consider another wideband approach where the signals are described directly in the frequency domain. As before, we assume complex baseband band-limited signals with a two–sided bandwidth of W hertz. Let us expand the transmitted signal in time and frequency as

$$x(t) = \sum_{s=0}^{S-1} \sum_{n=0}^{N-1} x_{s,n} \theta_{s,n}(t) \tag{3.91}$$

where the time/frequency or *multitone* basis functions are

$$\theta_{s,n}(t) = \sqrt{W_B} e^{j\pi f_s t} \frac{\sin \pi W (t - n/W_B)}{\pi W_B (t - n/W_B)}, \tag{3.92}$$

$f_s = -W/2 + (s - 1/2)W_B$ and $W_B = W/S$. These basis functions are simply sampling functions for signals band-limited to W_B hertz around f_s. Although we have chosen the sampling functions as a basis set, any set of (sufficiently) band-limited time/frequency orthogonal functions will suffice (for instance raised–cosine pulses). We stress that this is a subset of the set of signals band-limited to $[-W/2, W/2]$, since we assume that they are flat in any sub-band of bandwidth W_B. This is not a significant restriction, since the sub-bands can be made arbitrarily small. This type of modulation scheme is often also referred to as *orthogonal frequency–division multiplexing (OFDM).*

One of the main practical problems with this type of signaling is the high peak–to–average power ratio when a large number of sub-bands are used. This is especially problematic in wireless applications since there is a need for highly linear power amplifiers over the large dynamic range of the signal. A clever way to reduce the dynamic range of the signal when the number of sub-bands is not too large is to use specially designed coding schemes which reduce the peak–to–average power ratio [WJ95],[VN96].

3.5.1 Multitone Receiver and Performance Criteria

The received signal may now be written as

$$y(t) = \sum_{s=0}^{S-1} \sum_{n=0}^{N-1} x_{s,n} h_s(t - n/W_B) + z(t), \tag{3.93}$$

where $h_s(t)$ is the portion of the channel response in sub-band s given by

$$h_s(t) = \int_{f_s - W_B/2}^{f_s + W_B/2} e^{j2\pi ft} H(f) df, \tag{3.94}$$

and $H(f)$ is the Fourier Transform of $h(t)$. Projecting the output on $\{\theta_{f,n}(t)\}$ yields

$$y_{s,n} = \sum_{n'=0}^{N-1} x_{s,n'} h_{s,n,n'} + z_{s,n} \tag{3.95}$$

where

$$h_{s,n,n'} = \int_{f_s - W_B/2}^{f_s + W_B/2} H(f) e^{j \frac{2\pi(n-n')}{W_B} f} df \tag{3.96}$$

We assume that W_B is small enough (or equivalently F is large enough) to assure that $d_L W_B \ll 1$, where d_L is the delay spread, yielding

$$h_{s,n,n'} \approx H(f_s) \delta_{n,n'} \tag{3.97}$$

For this assumption to be valid in practice, we require that W_B be much less than the coherence bandwidth of the channel as described in Chapter 2.

The frequency autocorrelation function of the channel response $H(f)$ was given in Chapter 2 and denoted $\phi(f_1 - f_2)$. We now denote the autocorrelation matrix for the sub-band strengths by

$$\mathbf{K}_H = \begin{pmatrix} \phi(0) & \phi(W/S) & \phi(2W/S) & \cdots & \phi((S-1)W/S) \\ \phi(W/S) & \ddots & \ddots & \ddots & \phi((S-2)W/S) \\ \phi(2W/S) & \ddots & \ddots & \ddots & \vdots \\ \vdots & \ddots & \ddots & \ddots & \vdots \\ \phi((S-1)W/S) & \phi((S-2)W/S) & \cdots & \cdots & \phi(0) \end{pmatrix} \tag{3.98}$$

This significant eigenvalues of this matrix are good approximations to those of the corresponding kernel $\phi(f1 - f2)$ [VT68]. The conditional PEP in this case between arbitrary sequences $x_{s,n}^{(0)}$ and $x_{s,n}^{(1)}$ is given by

$$P_{e|h}(0 \to 1) = \mathrm{Q}\left(\sqrt{\frac{d^2(0,1)}{2N_0}}\right) \tag{3.99}$$

where

$$\begin{aligned} d^2(0,1) &= \sum_{n=0}^{N-1}\sum_{s=0}^{S-1} |x_{s,n}^{(0)} - x_{s,n}^{(1)}|^2 |H(f_s)|^2 \\ &= \sum_{s=0}^{S-1} |H(f_s)|^2 d_s^2(0,1) \end{aligned} \tag{3.100}$$

where $d_s^2(0,1)$ is the Euclidean distance between the signal components in sub-band s. The performance computation is identical to earlier coherent cases and the moment–generating function of the pairwise distance is given by

$$\phi_d(s) = \prod_{i=0}^{S-1} \frac{1}{1 - s\lambda_i} \tag{3.101}$$

where λ_i are now the eigenvalues of $\mathbf{K}_H\mathbf{D}$ with $\mathbf{D} = \mathrm{diag}(d_s^2(0,1))$. Not surprisingly, this is an analogous result to the partially–interleaved narrow-band channel and similarly with appropriate interleaving can be cast into the framework the block–fading channel discussed in section 3.6.

3.5.2 Multitone spread–spectrum

As in the case of DSSS, let us now assume that each codeword $x(t)$ lies in a $W_L T$–dimensional subspace of the WT–dimensional signal space, so that the number of Shannon dimensions is less than the number of degrees of freedom that the channel has to offer. For simplicity, we take $W_L = KW_B$ with K being some integer so that the spreading factor is S/K. Here we opt to perform spreading in the frequency domain. This has been considered by several authors such as [Van95]. We denote the K–dimensional information vector for a given time coordinate n by $\mathbf{u}_n$ and write the corresponding F–dimensional frequency vector as

$$\mathbf{x}_n = \mathbf{G}\mathbf{u}_n \tag{3.102}$$

where $\mathbf{G} = \begin{pmatrix} \mathbf{g}_1 & \cdots & \mathbf{g}_K \end{pmatrix}$ is the *spreading matrix.* In order to preserve the input energy, we take the $\mathbf{g}_i$ to have unit–norm.

For illustration purposes, let us consider the simplest case when $K = 1$. We assume further a simple binary antipodal modulation scheme without any additional channel coding so that $u_n = \pm\sqrt{\mathcal{E}}$. The maximum–likelihood receiver for each u_n is simply

$$\hat{m} = \underset{m=-1,1}{\operatorname{argmax}} \sum_{s=0}^{S-1} y_{s,n}^{*} H(f_s) g_{0,s} \sqrt{\mathcal{E}} m \tag{3.103}$$

This can be seen as the multitone equivalent of the RAKE receiver or a maximal ratio combiner of the sub-band components [SBS66]. The minimum distance between transmitted sequences conditioned on the channel state is therefore

$$d^2(0,1) = 4\mathcal{E} \sum_{s=0}^{S-1} |H(f_s)|^2 \tag{3.104}$$

and the PEP is readily calculated.

3.6 Block Fading Channels

We now consider a general model for representing systems with a finite number of degrees of freedom which can appropriately be characterized in a block stationary fashion. This will be very useful for analysing many different types of systems in a generic fashion. It can accomodate both time and frequency diversity with narrow or wide–band signals.

3.6.1 System Model and Examples

Consider transmission scheme in Figure 3.13. The information bits are coded/modulated into F blocks of length N symbols so that codewords have length NF symbols and are denoted by

$$\mathbf{c} = \begin{pmatrix} c_{0,0} & c_{0,1} & \cdots & c_{0,N-1} & c_{1,0} & \cdots & c_{F-1,N-1} \end{pmatrix}. \tag{3.105}$$

In practice the coded symbols are formed by a combination of either a block or convolutional encoder and an interleaver. The interleaver serves to spread the information evenly over the F blocks so that very high complexity codes are not needed. Except when explicitly stated otherwise, we will consider the interleaver as part of the encoder.

Each block is then PAM modulated as

$$u_f(t) = \sum_{n=0}^{N-1} \sqrt{\mathcal{E}} c_{f,n} s(t - nT), f = 0, 1, \cdots, F-1 \tag{3.106}$$

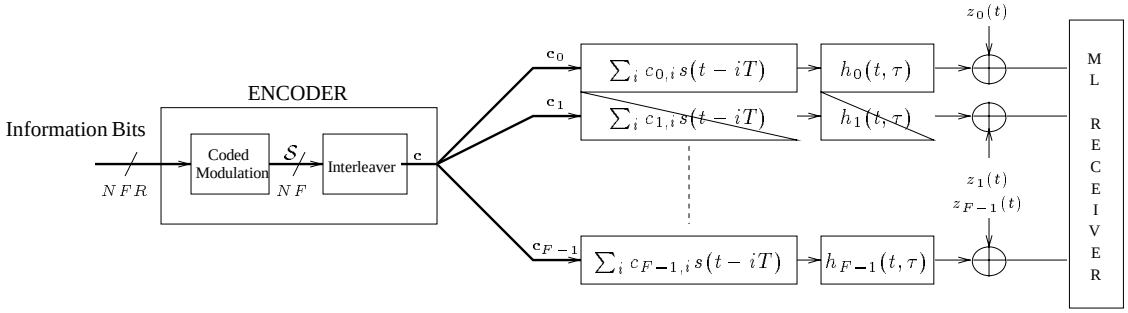

Figure 3.13: Block–Fading System Model

where $s(t)$ is some unit–energy pulse shape, and $\mathcal{E}$ is the energy per coded symbol. The blocks are transmitted over different time–varying channels, so that the complex baseband received signals before processing are given by

$$r_f(t) = u_f(t) * h_f(t,\tau) + z_f(t), t \in [0, NT], f = 0, 1, \cdots, F-1 \tag{3.107}$$

where $h_f(t,\tau)$ is the channel response at time t to an impulse at time τ on the f^{th} channel, and $z(t)$ is complex white Gaussian noise with power spectral density N_0.

In what follows we will assume that the F channel realizations are correlated, although it may well be the case in some systems that they can be taken to be uncorrelated. A system where this model is appropriate is the *Global System for Mobile Communication (GSM)*. Here, blocks modulate $F = 4$ (half–rate) or $F = 8$ (full–rate) carriers whose spacing is larger than the coherence bandwidth, resulting in virtually uncorrelated blocks. This is achieved by changing the frequency allocation scheme in F adjacent TDMA frames and is known as *slow frequency–hopping*. The number of blocks is determined by the tolerable decoding delay ΔT. Such a system with $F = 4$ is depicted in Figure 3.14(a). For reasonable mobile speeds, the channel is stationary during the block. The practical advantages of such a system are firstly that reliable coherent communication is possible. Secondly and more importantly, the amount of diversity is independent of the rate of channel variation, since it is a result of exploiting frequency–selectivity. For mobile telephony, this is crucial since the majority of calls are made at low speed. Another example is the IS54 standard where coding is performed across $F = 2$ TDMA blocks separated in time by 20ms so they become less correlated for high mobile speeds. In complete analogy with the frequency–based scheme, we may call this *time–hopping* and an example with $F = 2$ is illustrated in Figure 3.14(b).

We now assume that the time–variation of the channel is slow (i.e. that the coherence time is greater than the duration of a block) so that that the channel path strengths can be taken to be constant

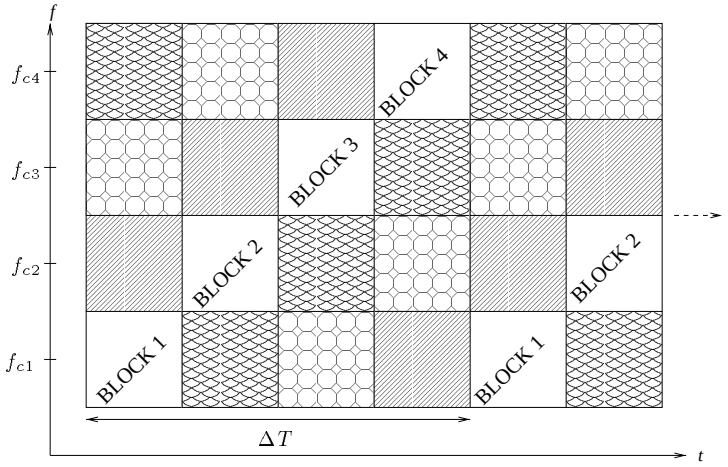

(a)

(b)

Figure 3.14: Frequency and time–hopping

over blocks. We therefore express the complex baseband channel response for each block as

$$h_f(t) = \sum_{l=0}^{L-1} \sigma_{f,l}\delta(t - d_{f,l}), \tag{3.108}$$

where $\sigma_{f,l}$ and $d_{f,l}$ are the complex attenuation and delay of the l^{th} path in the f^{th} block. As before we will use the COST 207 models for numerical calculations. The channel realizations are assumed to be random from block to block but known without error to the receiver. We assume the statistics of the $\sigma_{f,l}$ to be independent of f and further that

$$\mathrm{E}\left(\sigma_{f,l} - \overline{\sigma_{f,l}}\right)\left(\sigma_{f',l'} - \overline{\sigma_{f',l'}}\right)^* = \varrho_{f,f'}\overline{\sigma_l^2}\delta_{l,l'}, \tag{3.109}$$

where $\varrho_{f,f'}$ is the correlation coefficient between blocks f and f'. We have, therefore, that different paths are uncorrelated but that the strengths for a given path are correlated, in general, from block to block. Furthermore, we assume that the path strengths are normalized as $\sum_{l=0}^{L-1}\overline{\sigma_l^2} = 1$, so that the average attenuation is included in the transmitted signal strength.

The received signal is processed by a maximum–likelihood decoding rule as

$$\underset{m=0,\cdots,2^{FNR}-1}{\arg\min} \sum_{f=0}^{F-1} \int_0^{NT} \left| r_f(t) - \sum_{f=0}^{F-1} u_f^{(m)}(t-NT) * h_f(t,\tau) \right|^2 dt. \tag{3.110}$$

Decoding in this fashion is too complex to be carried out in practice, and it is usually done in two steps, depending on the relationship between the coherence bandwidth of the channel and the bandwidth of $s(t)$. In medium-band systems like GSM where the multipath induces intersymbol interference, a sub–optimal approach is taken by first equalizing the F channels with a soft–output algorithm (e.g. soft–output Viterbi equalization [HH89]). These outputs are then deinterleaved and passed to a Viterbi decoder to retrieve the information bits. In narrow-band systems such as IS-54, the channel has ISI not extending over more than one symbol time, so that either a very simple equalizer or none at all is needed prior to deinterleaving/decoding. In wide-band systems with little ISI, equalization is also not required and some of the multipath can be exploited with a RAKE receiver prior to decoding as we outlined earlier.

Many systems which use coding schemes over a fading channel with a finite number of degrees of freedom can be cast into the framework. We mentioned earlier that this was both the case for the partially–interleaved narrow-band channel and the static multitone channel. Let us consider this more closely now that we have defined them precisely. In the partially–interleaved narrow-band case, the number of degrees of freedom was around $F = \lceil 2f_D T + 1 \rceil$ where $T = NLT_s$ was the total decoding delay. Similarly the number of degrees of freedom for the multitone case was around $F = \lceil W d_L + 1 \rceil$. Suppose now we use an interleaver with depth $N = F$ and width $L = T/(FT_s)$. This arrangement is close to the block–fading channel with F blocks each containing L symbols. Every set of F adjacent symbols are virtually uncorrelated at the receiver and symbols separated by multiples of F symbols (i.e. belonging to the same block) are strongly correlated. Without this choice for the interleaver, the coding problem was difficult because the location of non–zero symbols in the error–event was critical in the expression for the PEP. We will show in the remainder of this section that for the block–fading channel this is not a problem and in Chapter 5, how high performance codes can be designed.

Denoting the codewords as $\mathbf{c} = \begin{pmatrix} \mathbf{c}_0 & \mathbf{c}_1 & \cdots & \mathbf{c}_{F-1} \end{pmatrix}$, the PEP conditioned on a particular set of channel realizations is given by

$$P_{e|h_i(t)}(0 \to 1) = \mathrm{Q}\left(\sqrt{d^2(0,1)\frac{\mathcal{E}}{2N_0}} \right), \tag{3.111}$$

where $d^2(0,1)$ is the squared Euclidean distance between the code sequences given by

$$\begin{aligned} d^2(0,1) &= \sum_{f=0}^{F-1} \int_0^{NT} \left| \sum_{n=0}^{N-1} \sum_{l=0}^{L-1} \left(c_{f,n}^{(0)} - c_{f,n}^{(1)} \right) \sigma_{f,l} s(t - nT - d_{f,l}) \right|^2 dt \\ &= \sum_{f=0}^{F-1} \sum_{n,n'=0}^{N-1} \sum_{l,l'=0}^{L-1} \left(c_{f,n}^{(0)} - c_{f,n}^{(1)} \right) \sigma_{f,l} \sigma_{f,l'}^* \left(c_{f,n'}^{(0)*} - c_{f,n'}^{(1)*} \right) \rho_s \left((n-n')T + (d_{f,l} - d_{f,l'}) \right) \\ &= \sum_{f=0}^{F-1} (\mathbf{c}_f^{(0)} - \mathbf{c}_f^{(1)}) \left\{ \sum_{l,l'=0}^{L-1} \sigma_{f,l} \alpha_{f,l'}^* \mathbf{P}_{f,l,l'} \right\} (\mathbf{c}_f^{(0)} - \mathbf{c}_f^{(1)})^* \end{aligned} \tag{3.112}$$

where $P_{f,l,l'}^{(ij)} = \rho_s \left((i-j)T + (d_{f,l} - d_{f,l'}) \right)$ and $\rho_s(t)$ is given by (3.79). This can be simplified to the quadratic form

$$\begin{aligned} d^2(0,1) &= \sum_{f=0}^{F-1} \boldsymbol{\sigma}_f^* \boldsymbol{\Xi}_f(0,1) \boldsymbol{\sigma}_f \\ &= \begin{bmatrix} \boldsymbol{\sigma}_0^* & \boldsymbol{\sigma}_1^* & \cdots & \boldsymbol{\sigma}_{F-1}^* \end{bmatrix} \begin{bmatrix} \boldsymbol{\Xi}_0(a,b) & 0 & 0 & \cdots & 0 \\ 0 & \boldsymbol{\Xi}_1(a,b) & 0 & \cdots & 0 \\ 0 & 0 & \ddots & 0 & 0 \\ \cdots & \cdots & \cdots & \cdots & \cdots \\ 0 & \cdots & 0 & 0 & \boldsymbol{\Xi}_{F-1} \end{bmatrix} \begin{bmatrix} \boldsymbol{\sigma}_0 \\ \boldsymbol{\sigma}_1 \\ \cdots \\ \boldsymbol{\sigma}_{F-1} \end{bmatrix} \end{aligned} \tag{3.113}$$

$$= \boldsymbol{\sigma}^* \boldsymbol{\Xi} \boldsymbol{\sigma}, \tag{3.114}$$

where $\Xi_f^{(ll')}(0,1) = (\mathbf{c}_f^{(0)} - \mathbf{c}_f^{(0)}) \mathbf{P}_{f,l,l'} (\mathbf{c}_f^{(0)} - \mathbf{c}_f^{(1)})^*$, and $\boldsymbol{\sigma}_f = \left(\sigma_{f,0} \cdots \sigma_{f,L-1} \right)^{\mathrm{T}}$. Again we have a quadratic form of a correlated Gaussian random vector so that the moment–generating function of $z = d^2(0,1) \frac{\mathcal{E}_s}{2N_0}$ is

$$\Phi_z(s) = \prod_{i=0}^{d_{\mathrm{H}}^F L - 1} \frac{1}{1 - s\lambda_i \mathcal{E}_s / 2N_0}, \tag{3.115}$$

where $\{\lambda_i\}$ are the *non–zero* eigenvalues of the matrix

$$\mathbf{R}_\sigma \boldsymbol{\Xi} = \begin{bmatrix} \boldsymbol{\Sigma}\boldsymbol{\Xi}_0(0,1) & \varrho_{1,0}\boldsymbol{\Sigma}\boldsymbol{\Xi}_1(0,1) & \ldots & \varrho_{F-1,0}\boldsymbol{\Sigma}\boldsymbol{\Xi}_{F-1}(0,1) \\ \varrho_{0,1}\boldsymbol{\Sigma}\boldsymbol{\Xi}_0(0,1) & \boldsymbol{\Sigma}\boldsymbol{\Xi}_1(0,1) & \ldots & \varrho_{F-1,1}\boldsymbol{\Sigma}\boldsymbol{\Xi}_{F-1}(0,1) \\ \cdots & \cdots & \cdots & \cdots \\ \varrho_{0,F-1}\boldsymbol{\Sigma}\boldsymbol{\Xi}_0(0,1) & \varrho_{1,F-1}\boldsymbol{\Sigma}\boldsymbol{\Xi}_1(0,1) & \ldots & \boldsymbol{\Sigma}\boldsymbol{\Xi}_{F-1}(0,1) \end{bmatrix}, \tag{3.116}$$

and d_{H}^F is the number of non–zero $\boldsymbol{\Xi}_f(0,1)$ (or equivalently the *Hamming distance* between $\mathbf{c}^{(a)}$ and $\mathbf{c}^{(b)}$ with the symbols taken as the sub–vectors $\mathbf{c}_f$) and $\Sigma = \mathrm{diag}(\overline{\sigma_0^2}, \overline{\sigma_1^2}, \cdots, \overline{\sigma_{L-1}^2})$.

For the even simpler case where the blocks are uncorrelated (i.e. $\varrho_{f,f'} = \delta_{f,f'}$) (3.115) can be written as

$$\Phi_z(s) = \prod_{i=0}^{d_{\mathrm{H}}^F} \prod_{l=0}^{L-1} \frac{1}{1 - s\eta_{i,l}\mathcal{E}_s/2N_0}, \tag{3.117}$$

where $\eta_{i,l}$ is the l^{th} eigenvalue of the non–zero matrix $\mathbf{\Delta}_i = \mathbf{\Sigma}\mathbf{\Xi}_i(0,1)$. For very wide-band systems without ISI (i.e. the bandwidth of $s(t)$ is much larger than the coherence bandwidth and the symbol rate), $\mathbf{P}_{f,l,l'} \approx \delta_{ll'}\mathbf{I}$ so that $\eta_{f,l} = \overline{|\sigma_{f,l}|^2} d^2\left(\mathbf{c}_f^{(0)}, \mathbf{c}_f^{(1)}\right)$. For narrow-band systems without ISI (i.e. $|d_{f,l} - d_{f,l'}| \ll T$) $\mathbf{P}_{f,l,l'} \approx \mathbf{I}$ so that $\eta_{f,l} = d^2\left(\mathbf{c}_f^{(0)}, \mathbf{c}_f^{(1)}\right)\delta_l$. These are the two limiting cases for the diversity offered by multipath. The first corresponds to when it can be completely resolved, and the second when it cannot be resolved at all. The theoretical performance of a system will fall somewhere between the performance of these two limits which are straightforward to compute. The diversity factor due to coding is d_{H}^F and is completely independent of the extent of multipath, as long as the channels are independent. This means that from the point of view of code design, it is sufficient to consider only a narrow-band channel which greatly simplifies the problem. We note, however, in contrast to the perfectly interleaved case the diversity factor due to coding is limited to F and does not grow with the length of the codewords. These issues will be the focus of Chapter 5.

The computation of the average PEP is identical to the earlier cases once the eigenvalues have been determined. We have computed it exactly for narrow, medium and wide-band pulse shapes and chose examples inspired the IS–54, GSM and IS–95 cellular radio systems which respectively fall into these three categories. The narrow–band pulse shape is a root raised cosine with roll–off .35 and $T = 41.15\mu s$ while the medium–band is GMSK with $BT = .3$ and $T = 3.69\mu s$ (see Feher [Feh95] regarding GMSK.) For the wide-band pulse shape we used an FIR filtered 128 chip/symbol PN sequence with $T = 164.16\mu s$, with the filter coefficients taken from the IS–95 specifications [IS992]. We also compute the PEP for an un-filtered PN pulse to identify the loss due to filtering. The goal is not to compare the systems, since this is by no means a fair comparison, but to determine to what degree the multipath can be exploited on typical channels. In Figures 3.15–3.17 we show the PEP vs. $\mathcal{E}_s/N_0$ for the TU, RA and HT responses given in Chapter 2 along with the significant eigenvalue spread. We have assumed $F = 2$ blocks of length $N = 100$ antipodal symbols with $d^2(\mathbf{c}_0^{(0)}, \mathbf{c}_0^{(1)}) = 4$ and $d^2(\mathbf{c}_1^{(0)}, \mathbf{c}_1^{(1)}) = 8$, so that there two sets of eigenvalues corresponding to the two blocks. In all cases the narrow-band system is almost completely unresolved and has two significant eigenvalues equal to the two Euclidean distances between the codewords. The medium-band system benefits greatly from multipath, especially on the urban and hilly channels which have delay spreads extending over several symbols. This shows the effect that

equalization can have in a multipath environment. The wide-band pulse exploits the multipath to a great extent, but it is still far from being completely resolved. Moreover, there is a noticeable loss due to filtering. In Fig. 3.18 we examine the effect of correlation between $F = 2$ blocks with the narrow–band pulse shape. Surprisingly, even with a correlation coefficient as high as .5, there is very little degradation.

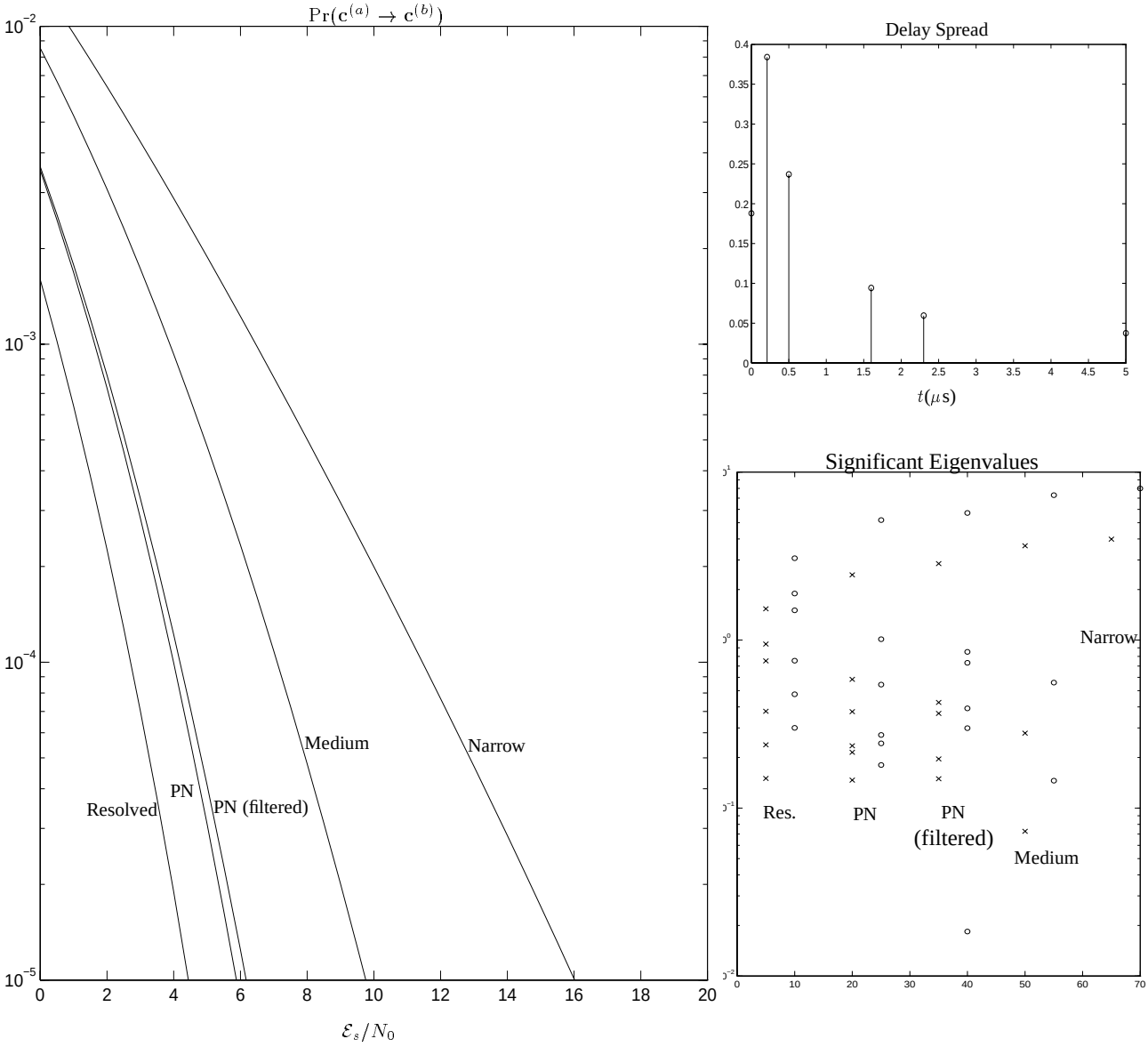

Figure 3.15: PEP and eigenvalues for the TU channel

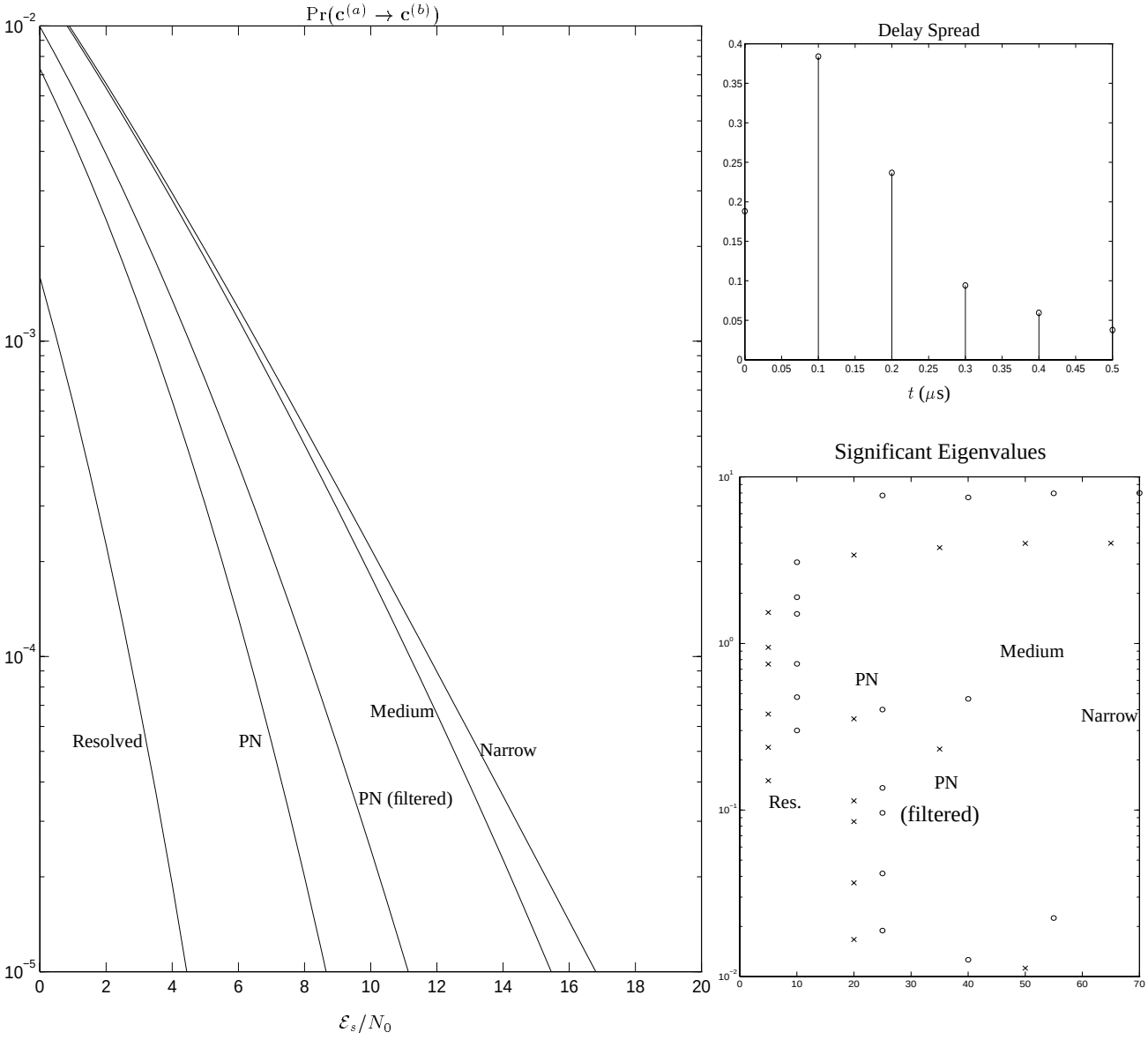

Figure 3.16: PEP and eigenvalues for the RU channel

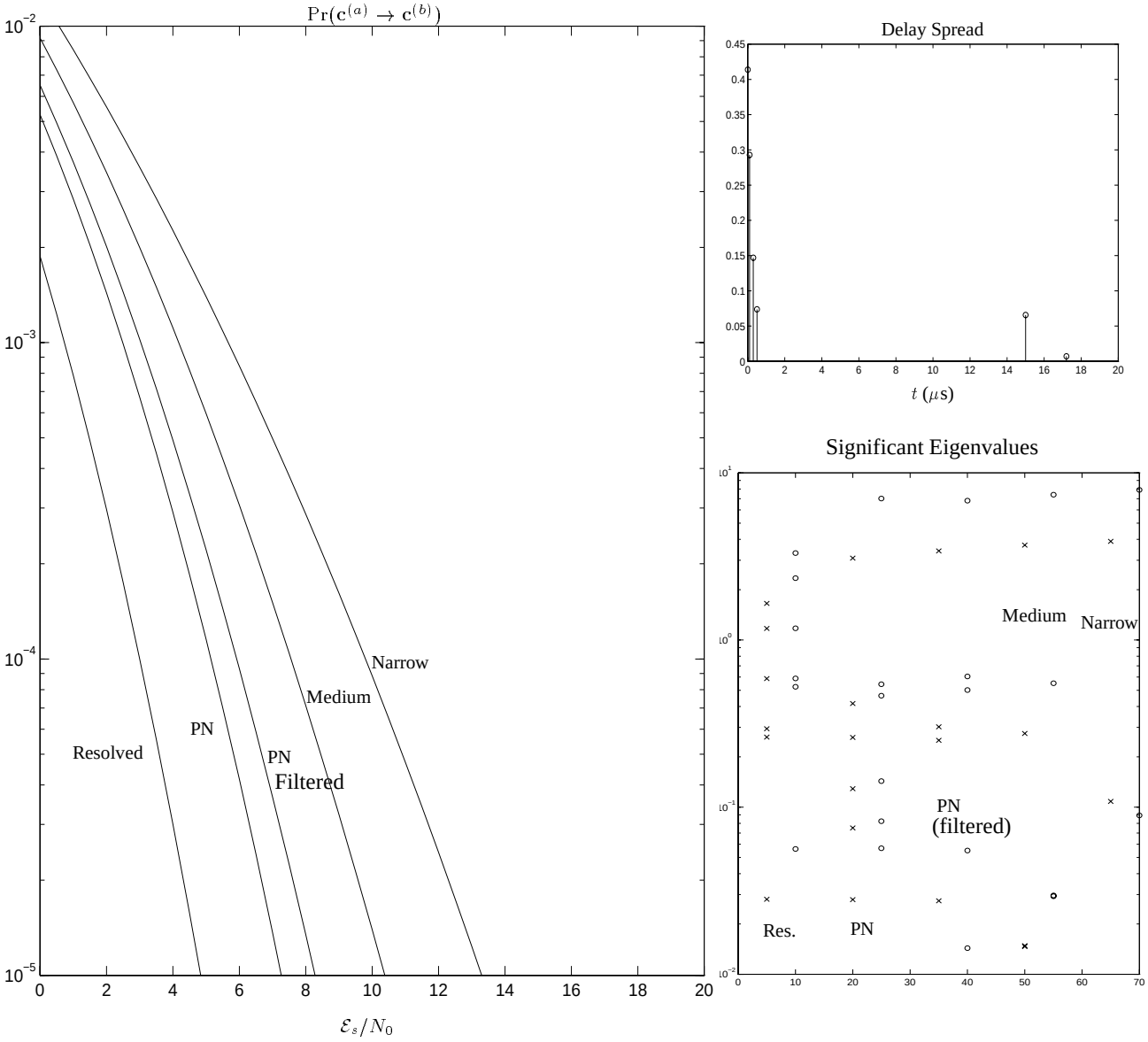

Figure 3.17: PEP and eigenvalues for the HT channel

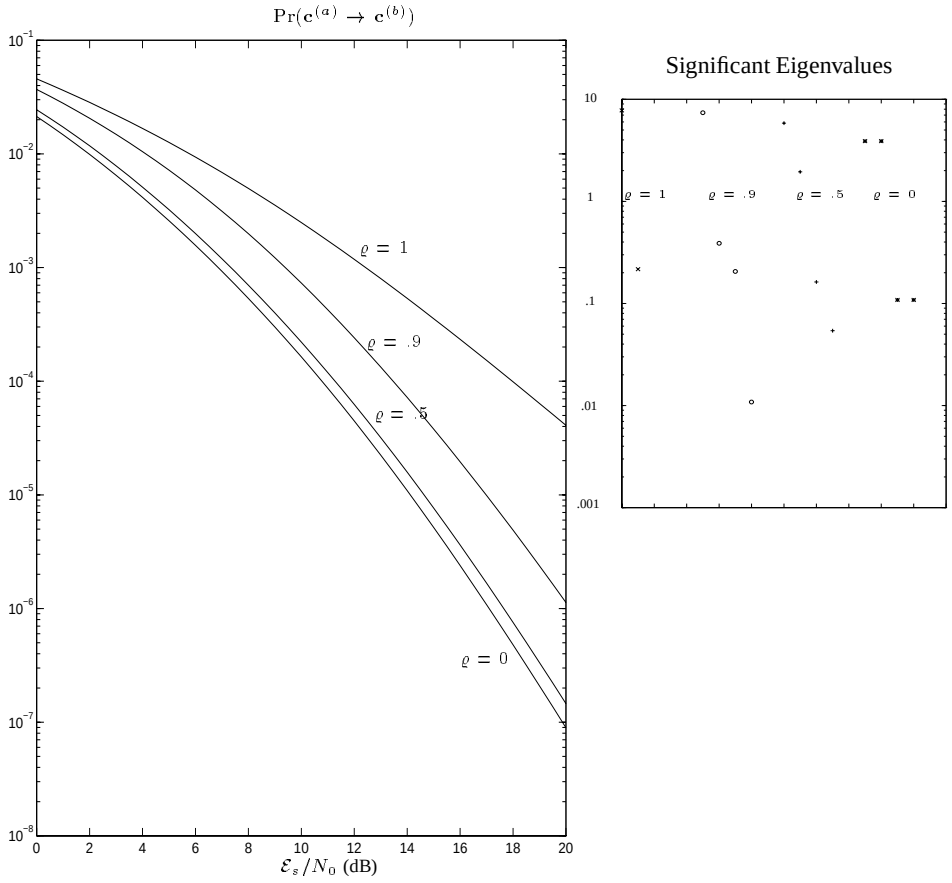

Figure 3.18: PEP and eigenvalues for a 2 block example

Chapter 4

Mutual Information and Information Outage Rates

In this chapter we take a fundamental look at the achievable performance for the coded systems described in Chapter 2 and we restrict our treatment to single–user channels. The multiuser case will be considered in Chapter 7. To this end we use information–theoretic techniques to analyze the average probability of codeword error and the achievable information rates under different system model assumptions. We rely heavily on some previous work and extend their results. First is the classic text by Gallager [Gal68] which is referenced often in this chapter. Second is the recent work by Ozarow *et al.* defining the concept of *information outage probability*[OSSW94]. We will see that for systems with a time–delay constraint that this quantity is crucial in defining system performance limits. This is often the case in mobile radio systems.

We first describe a generic discrete–time model for time–varying channels in order to describe the role of *average mutual information* and how it naturally leads to the information outage probability and to a lower–bound on the achievable error–rate performance. We then turn our attention to the additive white Gaussian noise channel with fading described in Chapter 2. We consider the case of systems operating without channel state feedback and give numerical examples of the information outage rates.

4.1 A generic time–varying channel model and basic definitions

Consider the discrete–time communication system in Figure 4.1 which operates over N_x dimensions and has code-rate

$$R = \frac{\log_2 M}{N_x} \quad \text{bits/dim}, \tag{4.1}$$

where M is the number of codewords used by the transmitter. The input symbols $\{x_k,\ k = 0, \cdots, N_x - 1\}$ are drawn from a continuous real alphabet $\mathcal{S}_X \subseteqq \mathbb{R}$. The N_x input symbols are transmitted across a channel $\mathcal{C} : \mathcal{X} \to \mathcal{Y}$ with transition probability $f_{\mathbf{Y}|\mathbf{X},H}(\mathbf{y}|\mathbf{x}, h)$ which depends on an auxiliary random variable H. This plays the role of the state of the channel during transmission of the N_x symbols or *codeword*. We denote the distribution function of the channel state by $F_H(h)$. The channel output symbols belong to another continuous alphabet $\mathcal{S}_Y \subseteqq \mathbb{R}$ which need not be the same as $\mathcal{S}_X$. We will assume throughout that the receiver has complete knowledge of the channel state H, and that, in this chapter, the transmitter has no access to this information.

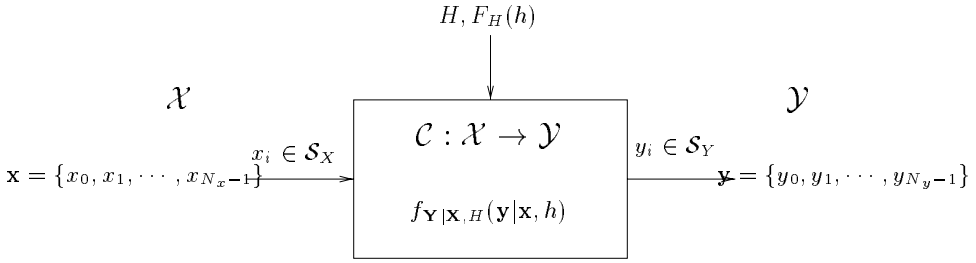

Figure 4.1: Generic fading channel model

Since there is no channel state feedback, the transmitter and receiver agree beforehand on acceptable choices for R and $f_{\mathbf{X}}$ and do not modify them during the course of communication. We first recall an upper–bound on the ensemble average probability of codeword error (i.e. taken over all possible codes chosen at random) conditioned on the channel state H. We denote this probability by $\overline{P_{\text{ens}|H}}$. From [Gal68] we have the following theorem and note that the only deviation from its original form is the additional conditioning on the channel state H.

Theorem 1 (Gallager)

An input source with N_x–dimensional joint probability density $f_{\mathbf{X}}(\mathbf{x})$ transmitting over a channel with transition probability $f_{\mathbf{Y}|\mathbf{X},H}(\mathbf{y}|\mathbf{x}, h)$ depending on an auxiliary random variable H has an ensemble average probability of codeword error taken conditioned on H which is upper–bounded by

$$\overline{P_{\text{ens}|H=h}} \leq 2^{-N_x(\mathrm{E}_0(\rho, f_{\mathbf{X}}, H=h) - \rho R)} \tag{4.2}$$

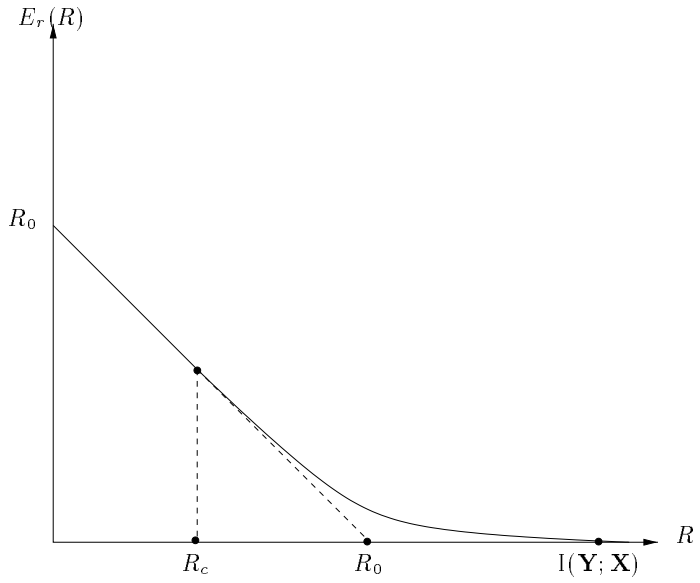

Figure 4.2: A typical random coding exponent curve

where

$$\mathrm{E}_0(\rho, f_{\mathbf{X}}, H=h) = -\frac{1}{N_x}\log_2 \int_{\mathbf{y}} \cdots \int \left(\int_{\mathbf{x}} \cdots \int f_{\mathbf{X}}(\mathbf{x}) f_{\mathbf{Y}|\mathbf{X},H}(\mathbf{y}|\mathbf{x},h)^{\frac{1}{1+\rho}} d\mathbf{x} \right)^{1+\rho} d\mathbf{y}, \tag{4.3}$$

R is given by (4.1) and ρ is arbitrary in $[0,1]$.

The quantity in (4.3) is commonly referred to as the *Gallager function*. The exponent in (4.2) is always maximized over ρ to yield the tightest upper bound. The maximum for each H is denoted

$$\mathrm{E}_r(R, f_{\mathrm{X}}, H=h) = \max_{0\le\rho\le 1} \mathrm{E}_0(\rho, f_{\mathrm{X}}, H=h) - \rho R, \tag{4.4}$$

When it is maximized over the input distribution, $f_{\mathbf{X}}$, it is known as the random coding exponent. Its typical shape is shown in figure 4.2 and it can normally only be expressed in parametric form.

There is a straight–line portion between $[0, R_c(H)]$ where $R_c(H)$ is known as the *critical rate* and is given by $R_c(H) = \left.\frac{\partial \mathrm{E}_0(\rho, f_{\mathrm{X}}, H=h)}{\partial \rho}\right|_{\rho=1}$. The random coding exponent in this region is $E_r(R, f_{\mathrm{X}}, H = h) = R_0(H) - R$ where $R_0(H) = \mathrm{E}_0(1, f_{\mathrm{X}}, H = h)$ is known as the *cutoff–rate*. The maximum value of R for which the random coding exponent remains non–negative is $R = \left.\frac{\partial \mathrm{E}_0(\rho, f_{\mathrm{X}}, H=h)}{\partial \rho}\right|_{\rho=0} = \mathrm{I}(\mathbf{Y};\mathbf{X}|H = h) = \mathrm{I}_H$ is the *average mutual information* between the input and output vectors condi-

tioned on a *particular realization* $H = h$ of the channel state. It is given by

$$\mathrm{I}_H = \frac{1}{N_x} \int_{\mathbf{x}} \cdots \int \int_{\mathbf{y}} \cdots \int f_{\mathbf{X}}(\mathbf{x}) f_{\mathbf{Y}|\mathbf{X},H}(\mathbf{y}|\mathbf{x},h) \log_2 \frac{f_{\mathbf{Y}|\mathbf{X},H}(\mathbf{y}|\mathbf{x},h)}{\int_{\mathbf{x}} \cdots \int f_{\mathbf{X}}(\mathbf{x}) f_{\mathbf{Y}|\mathbf{X},H}(\mathbf{y}|\mathbf{x},h) d\mathbf{x}} d\mathbf{y} d\mathbf{x} \ \text{bits/dim}. \tag{4.5}$$

We must stress that this is not a conditional mutual information functional and to avoid confusion we have used a slightly different notation. The conditional average mutual information between $\mathbf{Y}$ and $\mathbf{X}$ is $\mathrm{I}(\mathbf{Y};\mathbf{X}|\mathbf{H}) = \mathrm{E}_H \mathrm{I}_H$. We will see the importance of this functional later.

The first important observation is that I_H is a random variable. This means that, depending on the nature of the underlying channel process, it is possible that $\mathrm{I}_H < R$ for some realizations of H. For this reason, it is more appropriate to express the bound in (4.2) as

$$\overline{P_{\text{ens}|H=h}} \leq \begin{cases} 1 & \mathrm{I}_H < R \\ 2^{-N_x E_r(R, f_{\mathbf{X}}, H=h)} & \mathrm{I}_H \geq R \end{cases} \tag{4.6}$$

We may now bound the code–ensemble average probability of error as

$$\overline{P_{\text{ens}}} = \mathrm{E}_H \overline{P_{e|H}} \leq P_{\text{out}}(R, f_{\mathbf{X}}) + \int_{h:I_H \geq R} 2^{-N_x E_r(R, f_{\mathbf{X}}, H=h)} dF_H(h) \tag{4.7}$$

where

$$P_{\text{out}}(R, f_{\mathbf{X}}) = \text{Prob}(I_H < R). \tag{4.8}$$

Since the code ensemble average error–probability is upper–bounded by the right–hand side of (4.7) there is at least one code for which (4.7) holds. Unlike the time–invariant channel case, however, the irreducible term in (4.7) ($P_{\text{out}}(R, f_{\mathbf{X}})$) is independent of the number of code dimensions N_x and therefore casts some doubt as to whether arbitrarily small error probabilities can be achieved.

To get an idea of the achievable performance we now express the average codeword error probability for a particular code (i.e. not an ensemble average) as

$$\begin{aligned} \overline{P_e} &= \overline{P_{e|I_H \geq R}} \left(1 - P_{\text{out}}(R, f_{\mathbf{X}})\right) + \overline{P_{e|I_H < R}} P_{\text{out}}(R, f_{\mathbf{X}}) \\ &\geq \overline{P_{e|I_H < R}} P_{\text{out}}(R, f_{\mathbf{X}}) \end{aligned} \tag{4.9}$$

Practically speaking, this lower–bound on $\overline{P_e}$ is meaningful if we consider what is known as the strong converse to the coding theorem:

Theorem 2 ([Wol78])

The probability of codeword error conditioned on the channel state, H when $R > I_H$ is lower–bounded by

$$P_{e|H} > 1 - \frac{4A(h)}{N_x(R - \mathrm{I}(\mathbf{X};\mathbf{Y}|H=h))^2} - 2^{-\frac{N_x(R-\mathrm{I}(\mathbf{X};\mathbf{Y}|H=h))}{2}} \tag{4.10}$$

where $A(h)$ is a finite positive constant independent of N_x and the number of codewords M.

As a result of this theorem, for $R > I_H$ we have that $P_{e|H=h}$ must tend to 1 with increasing N_x for *all* codes. This result can be extended to show [Gal68] that $P_{e|H}$ must tend to 1 exponentially in N. In our context, this ensures that $\overline{P_{e|I_H<R}} \approx 1$ if N_x is large so that $\overline{P_e} \gtrapprox P_{\mathrm{out}}(R, f_{\mathbf{X}})$. In the limit $N_x \to \infty$ we have that $\overline{P_e} = P_{\mathrm{out}}(R, f_{\mathbf{X}})$ since the inequalities in (4.7) and (4.10) converge. Ozarow *et al*[OSSW94] recognized the importance of $P_{\mathrm{out}}(R, f_{\mathbf{X}})$ for systems operating over fading channels but its relationship with the achievable codeword error probability was not explicitly shown.

The reader may wonder whether why this is an important result since the use of the strong converse says nothing about the error probability of the individual source symbols or the *symbol error rate*. We note, however, that for many practical systems which are burst or block oriented, it is precisely the codeword error rate that is important. This is true for the transmission of some forms of digitized speech and in packet data communications. Typically, data is arranged into bursts and then coded for transmission using both error correction and error detection techniques. At the receiver the information burst is decoded and then checked for data integrity using the error detection scheme. If the burst is deemed intact, the data is passed to the next level of the system. On the other hand, if the data is corrupted then the burst is often discarded or a retransmission is requested. Provided the number of symbols in the burst (N_x) is large and a sophisticated coding scheme is used, $P_{\mathrm{out}}(R, f_{\mathbf{X}})$ will be a good indicator of the achievable codeword error rate performance.

The weak converse (Fano's inequality) yields a less useful lower bound on the codeword error probability since it only shows that $P_{e|I_H>R}$ is bounded away from zero when in an outage state. From [CT91] we have explicitly that

$$P_e \geq 1 - \frac{1}{N_x R} - \frac{I_H}{R}, \;\; I_H < R, \tag{4.11}$$

so that the average probability of codeword error is lower bounded by

$$\overline{P_e} \geq \left(1 - \frac{1}{N_x R}\right) P_{\mathrm{out}}(R, f_{\mathbf{X}}) - \frac{1}{R}\int_{h:I_H \leq R} I_H dF_H(h). \tag{4.12}$$

It is, however, more useful for obtaining a lower–bound to the bit error probability, P_b. It is shown in [Bla87] that the bit error probability conditioned on $I_H > R$ satisfies

$$\mathcal{H}(P_{b|I_H>R}) \geq 1 - \frac{I_H}{R} \tag{4.13}$$

where $\mathcal{H}(\cdot)$ is the binary entropy function

$$\mathcal{H}(x) = -x\log_2(x) - (1-x)\log_2(1-x). \tag{4.14}$$

The expression in (4.13) is only valid when the information source has maximum entropy. This yields the lower bound on the bit error probability

$$P_b \geq \int_{h:I_H \leq R} \mathcal{H}^{-1}\left(1 - \frac{I_H}{R}\right) dF_H(h), \tag{4.15}$$

where $\mathcal{H}^{-1}(\cdot)$ is taken to mean the smaller of the two roots of (4.13).

4.1.1 Block–Fading Channels

In some cases the information outage probability may be zero. We will see that this can occur when the transmitter has *a priori* knowledge of the channel state and can adjust either R or $f_{\mathbf{x}}$ accordingly. Another instance where this is the case is when coding can be performed across many channel states, say F, as shown in figure 4.3. Here each block uses N dimensions so that $N_x = NF$. Under the assumption that the F channel outputs $\mathbf{y_i},\ i = 0, \cdots, F-1$ are independent then the total average mutual information conditioned on the F channel states is

$$I_{\{H_0,H_1,\cdots,H_{F-1}\}} = \frac{1}{NF}\sum_{i=0}^{F-1} \mathrm{I}(\mathbf{Y}_i;\mathbf{X}_i|H_i = h_i) \triangleq \frac{1}{F}\sum_{i=0}^{F-1} I_{H_i}. \tag{4.16}$$

This is simply the block–fading channel we consider in section 3.6 on a more abstract level. This is also referred to as a block–interference channel by McEliece and Stark in [MS84], who considered different interference models, including the Rayleigh fading channel. If the set of channel realizations is an ergodic sequence then in the limit $F \to \infty$ we fall back on the traditional conditional average mutual information since

$$I_\infty = \lim_{F\to\infty} \frac{1}{F}\sum_{i=0}^{F-1} I_{H_i} = \mathrm{E}_H I_H = \mathrm{I}(\mathbf{Y};\mathbf{X}|\mathbf{H}), \tag{4.17}$$

and consequently

$$P_{\mathrm{out}}(R, f_{\mathbf{X}}) = \mathcal{I}(\mathrm{I}(\mathbf{Y};\mathbf{X}|\mathbf{H}) < R), \tag{4.18}$$

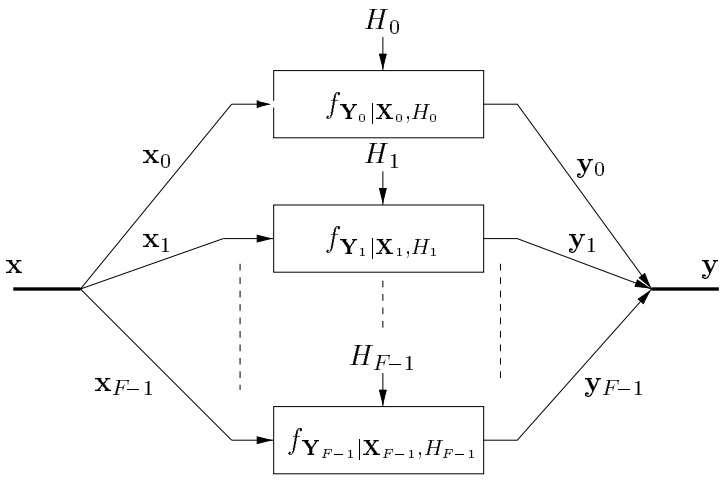

Figure 4.3: Block–Fading channel model

where $\mathcal{I}(\cdot)$ is the indicator function. Here the conditional average mutual information is maximum data rate at which arbitrarily small error–rates can be achieved. The result in (4.17) was first established by Ericson [Eri70] for the perfectly–interleaved narrow–band channel (i.e. $N = 1$).

The work of McEliece and Stark [MS84] focused on the relationship between the cutoff–rate and the average mutual information as a function of the length of the blocks N and whether or not channel state information is made available to the receiver. Their conclusions are that the cutoff rate (R_0) is not an acceptable performance measure since it tends to zero with increasing N. The conditional average mutual information, on the other hand, is independent of N, when channel state information is available. McEliece and Stark therefore conjecture that R_0 is a more appropriate measure of the *decoding delay* as opposed to decoding complexity. They did not consider the case when only a finite number of channel realizations are available in the case of very long blocks.

Kaplan and Shamai [KSS95] add to the results of McEliece and Stark [MS84] by specializing their treatment to the Rayleigh fading channel. They perform a very detailed analysis of the exponential nature of the ensemble average codeword error probability. In the case of no delay constraint where F can be arbitrarily large, they show that not only does R_0 decrease with N, but so does the entire reliability function curve. The conditional average mutual information remains unchanged as was found in [MS84]. It is noted that no exponential behaviour of the codeword error probability results when F is finite and outage probability computations based on R_0 and average mutual information are performed. The former case is defined similarly to (4.8) as

$$P_{\text{out}}(R, f_{\mathbf{X}}) = \text{Prob}(R_0(H) < R). \tag{4.19}$$

The behaviour of this measure is similar to (4.8) except that the outages are noticeably higher. It has less theoretical justification than (4.8) and may yield pessimistic results. Traditionally [Mas74],[Vit79] R_0 was taken to be the highest rate at which practical coding schemes can be implemented on ergodic channels. Humblet [Hum85] showed that on a direct detection optical channel there exist reasonably simple codes whose rates exceed those predicted by R_0 with acceptably low error probability. In recent years, the invention of *turbo codes* [BGT93] has given rise to practical evidence that R_0 may not be a practical limit even on a Gaussian channel. We will see in the next chapter that some practical codes, which are not even as complex as turbo codes, can come very close to (4.8) when the number of blocks is small which shows that mutual information outage is sometimes more appropriate in our case as well. The main reason for this is that when the number of blocks (or degrees of freedom) is small, $P_{\text{out}}(R)$ is quite high and even fairly simple codes have average error probabilities on the order of $P_{\text{out}}(R)$ when $I_H > R$ (i.e. when the system is not operating in an outage situation.)

4.2 Additive White Gaussian Noise (AWGN) Channels with Fading

We would now like to apply the ideas of the previous section for a communication system modeled by

$$y(t) = \int_{-T/2}^{T/2} x(\tau)h(t,\tau)d\tau + z(t) = s(t) + z(t) \tag{4.20}$$

The continuous–time random message sent across the channel by the transmitter, $x(t)$, is time–limited to $[-T/2, T/2]$ and has correlation function $K_x(t,u)$. The channel is modeled by a time–variant filter, $h(t,\tau)$, which is response at time t to an impulse at time τ, and has duration (delay spread) T_h. The noise signal, $z(t)$, is a complex, zero–mean, circular symmetric Gaussian process with correlation function $K_z(t,\tau) = N_0\delta(t-\tau)$ and $y(t)$ is the signal at the receiver. We assume that the channel response is known perfectly to the receiver.

4.2.1 Calculating the Average Mutual Information

The received signal in the absence of noise, $s(t)$, can be expressed in terms of its Karhunen-Loève expansion

$$s(t) = \sum_{i=1}^{\infty} s_i\phi_i(t) \tag{4.21}$$

where s_i are independent random variables with variance $\lambda_i(T,H)$ which, along with the basis $\{\phi_i(t : T,H),\ -T_o/2 \le t \le T_o/2\}$, are the solution to

$$\lambda_i(T,H)\phi_i(t:T,H) = \int_{-T_o/2}^{T_o/2} K_s(t,u)\phi_i(u:T,H)du \tag{4.22}$$

with $K_s(t,u) = \int_{-T/2}^{T/2}\int_{-T/2}^{T/2} K_x(\tau,\tau')h(t,\tau)h^*(u,\tau')d\tau d\tau'$ and where $T_o = T+T_h$. Note that we have explicitly indicated the dependence of the eigenvalues and eigenfunctions on the codeword duration and the channel state. This expansion allows us to write (4.20) equivalently as

$$y_i = s_i + z_i \tag{4.23}$$

where y_i and z_i are projections of the received signal and noise on the signal basis $\{\phi_i(t : H)\}$ given by

$$[y_i, z_i] = \int_{-T/2}^{T/2} [y(t), z(t)]\phi_i(t : T,H)dt, \tag{4.24}$$

where since the noise is white, the z_i are independent and have variance N_0. We have assumed that the channel response is known perfectly to the receiver and thus can, at least in principle, determine the message which was transmitted from $s(t)$. As a result, we are interested in the quantity

$$\begin{aligned} I_{T,H} &= \frac{1}{T}\mathrm{I}(S(t);Y(t)|H(t,\tau) = h(t,\tau)) \\ &= \frac{1}{T}\sum_{i=1}^{\infty}\mathrm{I}(S_i;Y_i|H(t,\tau) = h(t,\tau)) \ \ \text{bits/s} \end{aligned} \tag{4.25}$$

We have been rather cavalier in writing (4.25) and this deserves some explanation. In reality it only holds in a mean–square sense since the KL expansion is a mean–square representation of the process. It was shown by Kadota *et al* [KZZ71] that $I_{T,H}$ is simply the mean–squared error of the optimal point estimator of the process $s(t)$

$$I_{T,H} = \frac{1}{T}\int_{-T_o/2}^{T_o/2} \mathrm{E}|s(t) - \hat{s}(t)|^2 dt, \tag{4.26}$$

where

$$\hat{s}(t) = \int_{-T_o/2}^{t} g(t,u)y(u)du \tag{4.27}$$

where $g(t,u)$ is the solution to the integral equation

$$g(t,u) + \int_{-T_o/2}^{t} g(t,z)K_s(z,u)dz = K_s(t,u). \tag{4.28}$$

If $x(t)$ is a Gaussian process we saw in Chapter 3 when we were dealing with the Gaussian signal detection problem that

$$I_{T,H} = -\frac{1}{T}\int_{-T_o/2}^{T_o/2} g(t,t)dt = \frac{1}{T}\sum_{i=0}^{\infty}\log_2\left(1+\frac{\lambda_i(T,H)}{N_0}\right) \text{ bits/s}. \tag{4.29}$$

We quickly run into difficulties using this general approach to solve the problem at hand since in order to compute the outage probability we need the statistical description of $I_{T,H}$. While the numerical computation of $I_{T,H}$ for a particular channel realization is straightforward, the computation of its distribution is a hopeless task. We will now consider different approaches to determine the mutual information between the input and output signals in (4.20) for specific channel models.

4.2.2 Static Multipath Channels

We begin with an analysis of static multipath channels. We use the term static in the sense that they are stationary for the duration of a codeword so

$$h(t,\tau) = \begin{cases} h(t-\tau) & -T/2 \le \tau \le T/2,\ -T_o \le t \le T_o/2 \\ 0 & \text{elsewhere} \end{cases}$$

In the limit of large codeword duration (i.e. $T \to \infty$), the stationarity of the channel response assures that $K_s(t,\tau) = K_s(t-\tau)$. If we assume further that the channel response is band-limited then by invoking the *Szegö eigenvalue distribution theorem* [GS83] yields

$$I_H = \lim_{T\to\infty} I_{T,H} = \int_{-W/2}^{W/2}\log_2\left(1+\frac{1}{N_0}S_s(f)\right)df \text{ bits/s} \tag{4.30}$$

where $S_s(f)$ is the power spectrum of the information process at the output of the channel given by

$$S_s(f) = S_x(f)|H(f)|^2,\ \ -W/2 \le f \le W/2. \tag{4.31}$$

In a simple sense, this theorem just says that the countable set of eigenvalues $\lambda_i(T,H)$ approaches the power spectrum of the random process, if it is stationary. Assuming an input process bandlimited to $[-W/2, W/2]$, we introduce the average power constraint on the input process as

$$\int_{-W/2}^{W/2} S_x(f)df \le P. \tag{4.32}$$

Since average mutual information is a non–increasing function of T, for a finite T it follows that $I_{T,H} \ge I_H$ and consequently that $P_{\text{out}}(R,T) \le P_{\text{out}}(R)$. For large WT both will practically hold with equality, since as the number of significant eigenvalues increases they become a very close approximation to the squared–magnitude of the channel response [VT68].

Narrow–band channels

We now use (4.30) to determine the information outage probability for a narrow–band channel example. If the bandwidth W is considerably less that the coherence bandwidth of the multipath channel, then we showed in Chapter 2 that $|H(f)|^2 = \alpha,\ -W/2 \leq f \leq W/2$. Let us assume that the transmitted signal is chosen to be flat in $[-W/2, W/2]$ as $S_x(f) = P/W$. The information outage probability is therefore given by

$$\begin{aligned} P_{\text{out}}(R) &= \text{Prob}(W^{-1} I_H < R) \\ &= \text{Prob}\left(\alpha \leq (2^R - 1)\frac{WN_0}{P}\right) \\ &= 1 - F_\alpha\left((2^R - 1)\frac{WN_0}{P}\right) \end{aligned} \tag{4.33}$$

which in unit–mean square Rayleigh fading gives

$$P_{\text{out}}(R) = 1 - \exp\left(-(2^R - 1)\frac{WN_0}{P}\right) \tag{4.34}$$

This was found by Ozarow *et al* in [OSSW94]. For the more general case of Ricean fading with unit average attenuation we have from Chapter 2

$$P_{\text{out}}(R) = 1 - \text{Q}_1\left(\sqrt{2K}, \sqrt{2(2^R - 1)\frac{WN_0}{P}(1 + K)}\right) \tag{4.35}$$

We plot (4.35) in figure 4.4 as the Ricean factor increases for an SNR of $10\log_{10}\left(\frac{P}{WN_0}\right) = 10$dB. The non–fading channel is indicated by a dashed line which is the standard Gaussian channel capacity

$$C_G = W\log_2\left(1 + \frac{P}{WN_0}\right) \quad \text{bits/s} \tag{4.36}$$

We see that low codeword error–rates are practically impossible even with a significant LOS component. As we mentioned in Chapter 2, Ricean factors on the order of 6 dB are common in indoor applications so that severe degradation can still be expected. We only begin to approach a non–fading channel with a very strong LOS component. For a non–flat channel closed–form solutions such as (4.35) are unlikely to exist except in very special cases. Ozarow *et al* [OSSW94] have considered a two–path channel of the form

$$h(t) = \alpha_0\delta(t) + \alpha_1\delta(t - d). \tag{4.37}$$

They showed that if d is a multiple of $1/W$, then $P_{\text{out}}(R)$ can be expressed in terms of the Lobaschevski functions. For other values of d it must be computed numerically. Nevertheless, important conclusions

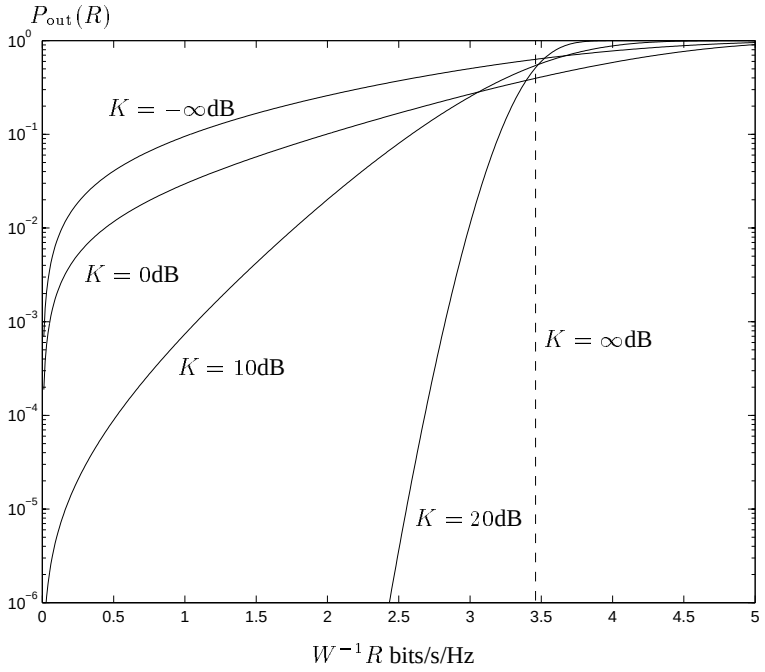

Figure 4.4: Information Outage Probability for Ricean Fading and Narrow–band Signals for $P/WN_0 = 10$ dB

concerning the effect of multiple–paths were drawn. In general, the added diversity significantly reduces $P_{\text{out}}(R)$. In order to gain more insight we now consider non–flat channels using the multi-tone signal model from Chapter 3 which allows for simpler numerical computation.

4.2.3 Multi-tone Signals

In order to use the multi-tone system model which was described in Chapter 3, we must drop the assumption of time–limited signals. We now have a situation characterized by WT dimensions. As long as WT is large, the proportion of signal energy outside of $[-T/2, T/2]$ is negligible so that we may consider codewords as being practically time–limited. The multi-tone model is mathematically convenient for analysing wide-band systems, even if the actual system does not use multi-tone modulation. This is especially true if the bandwidth of the sub–bands is small, since the set of multi-tone basis functions is almost sufficient for characterizing arbitrary band-limited signals. Another possible system which is appropriately characterized in this fashion is a multiuser orthogonal frequency–hopping system with coding which allocates sub-bands equally to all users. A wide-band *time–division multiple access (TDMA)* system with equalization (either in the time domain or via multi-tone) would also be subject to the same performance limits.

We recall that the channel input/output relationship is of the form

$$y_{s,n} = h_s x_{s,n} + z_{s,n},\ s = 0, \cdots, S-1,\ n = 0, \cdots, N-1 \tag{4.38}$$

where s is the sub-band index, n is the time index and the $\{z_{s,n}\}$ are i.i.d. zero–mean circular–symmetric complex Gaussian random variables with variance N_0. The number of complex dimensions is $N_x = NS = WT$. Under the assumption of independent $x_{s,n}$ we have that

$$I_H = \frac{1}{NS}\sum_{s=0}^{S-1}\sum_{n=0}^{N-1}\log_2\left(1+\frac{1}{N_0}\overline{|x_{s,n}|^2}|h_s|^2\right)\ \text{bits/dim} \tag{4.39}$$

$$= \frac{W}{NS}\sum_{s=0}^{S-1}\sum_{n=0}^{N-1}\log_2\left(1+\frac{1}{N_0}\overline{|x_{s,n}|^2}|h_s|^2\right)\ \text{bits/s.} \tag{4.40}$$

The power constraint becomes

$$\sum_{s=0}^{S-1}\sum_{n=0}^{N-1}\overline{|x_{s,n}|^2} \leq PT \tag{4.41}$$

As before we assume a flat signal spectrum with $\overline{|x_{s,n}|^2} = \frac{PT}{NS} = \frac{P}{W}$ so that

$$I_H = \frac{1}{S}\sum_{s=0}^{S-1}\log_2\left(1+\frac{P}{WN_0}|h_s|^2\right)\ \text{bits/dim} \tag{4.42}$$

$$= \frac{W}{S}\sum_{s=0}^{S-1}\log_2\left(1+\frac{P}{WN_0}|h_s|^2\right)\ \text{bits/s.} \tag{4.43}$$

The information outage probability corresponding to (4.42) is given by

$$P_{\text{out}}(R) = \text{Prob}\left(\frac{1}{S}\sum_{s=0}^{S-1}\log_2\left(1+\frac{P}{WN_0}|h_s|^2\right) < R\right) \tag{4.44}$$

and its computation must be carried out numerically by Monte–Carlo integration by creating random S–dimensional Gaussian vectors with correlation matrix given by (3.98). In figure 4.5 we show $P_{\text{out}}(R)$ for an SNR of $\frac{P}{WN_0} = 10$dB and spectral efficiency .5 bits/dim as a function of the number of carriers employed in the system. We have assumed that the bandwidth is SW_B, and each sub-band has bandwidth $W_B = 9.6$kHz. The TU12 ETSI channel model was used, so that the flat sub-band assumption holds (the coherence bandwidth is on the order of 200kHz). We see that for fairly modest spectral efficiencies, a wide-band system (i.e. $S \geq 16$) has a significantly lower achievable probability of error than a narrow–band system. We will see in Chapter 7 when we discuss multiuser systems that it is for this reason that multiple–access schemes like TDMA or FDMA/TDMA with slow frequency–hopping where signals occupy the entire system bandwidth are at a significant advantage over FDMA which uses narrow–band signals.

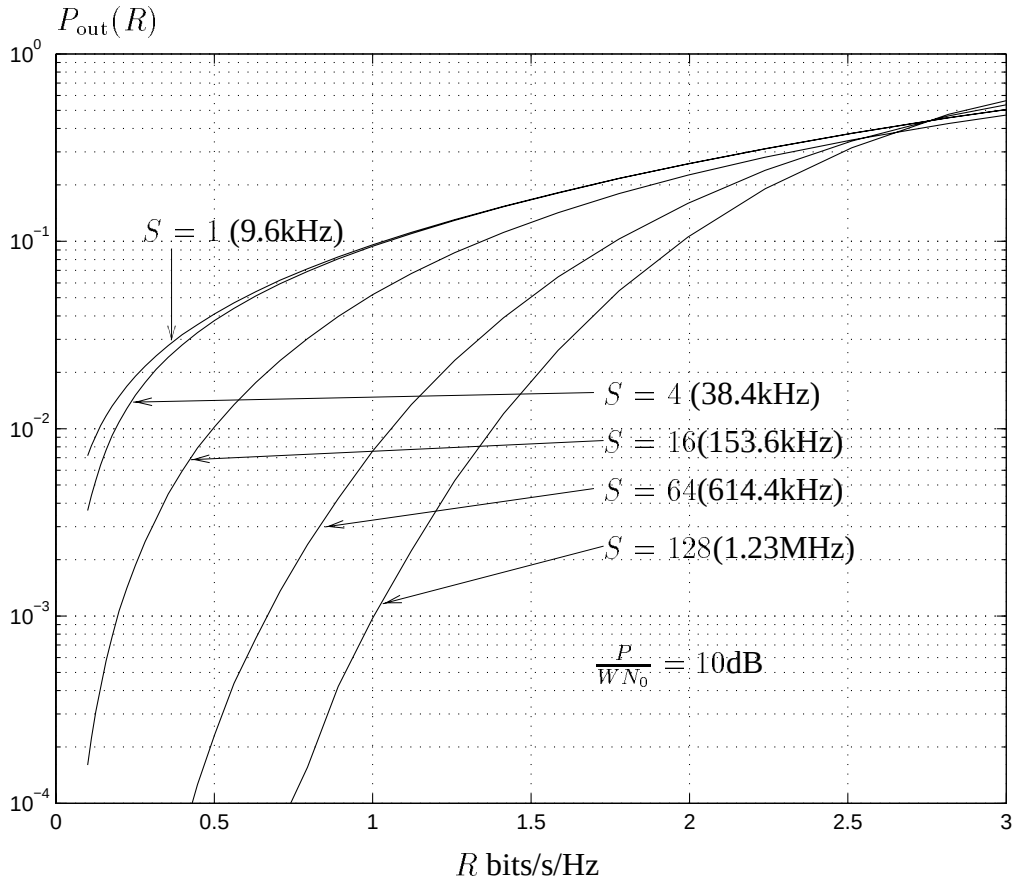

Figure 4.5: $P_{\text{out}}(R)$ as a function of bandwidth for $P/(WN_0) = 10$dB

$S = 1$ (9.6kHz)	$S = 4$ (38.4kHz)	$S = 16$ (153.6kHz)	$S = 64$ (614.4kHz)	$S = 128$ (1.2288MHz)
1	0.9953	0.9357	0.6926	0.5242
			0.1961	0.2222
				0.1103
		0.0614	0.0772	0.0619
				0.0493
			0.0230	0.0222
	0.0047	0.0028	0.0107	0.0094

Table 4.1: Significant eigenvalues for different bandwidths using the TU12 ETSI model

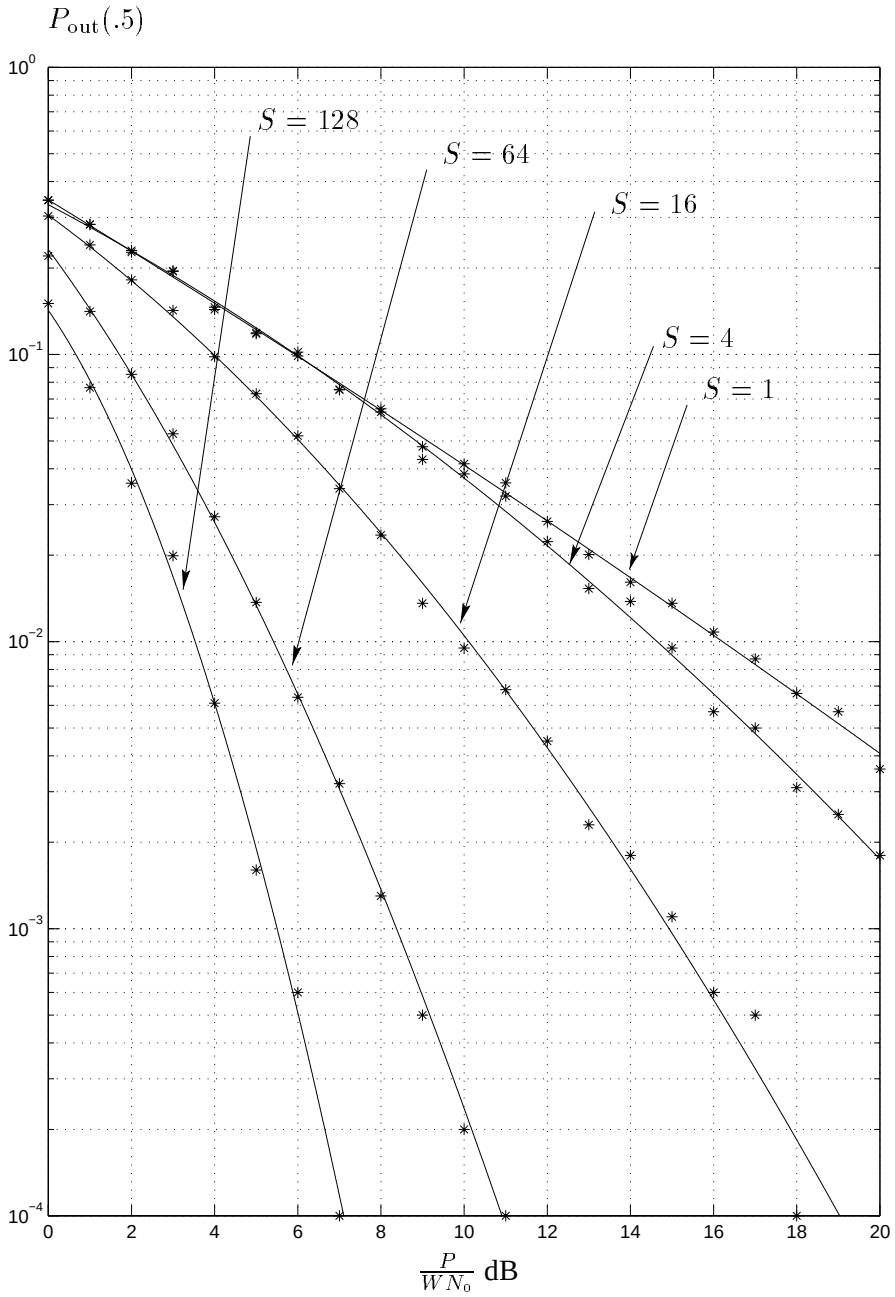

Figure 4.6: $P_{\text{out}}(.5)$ as a function of SNR and bandwidth

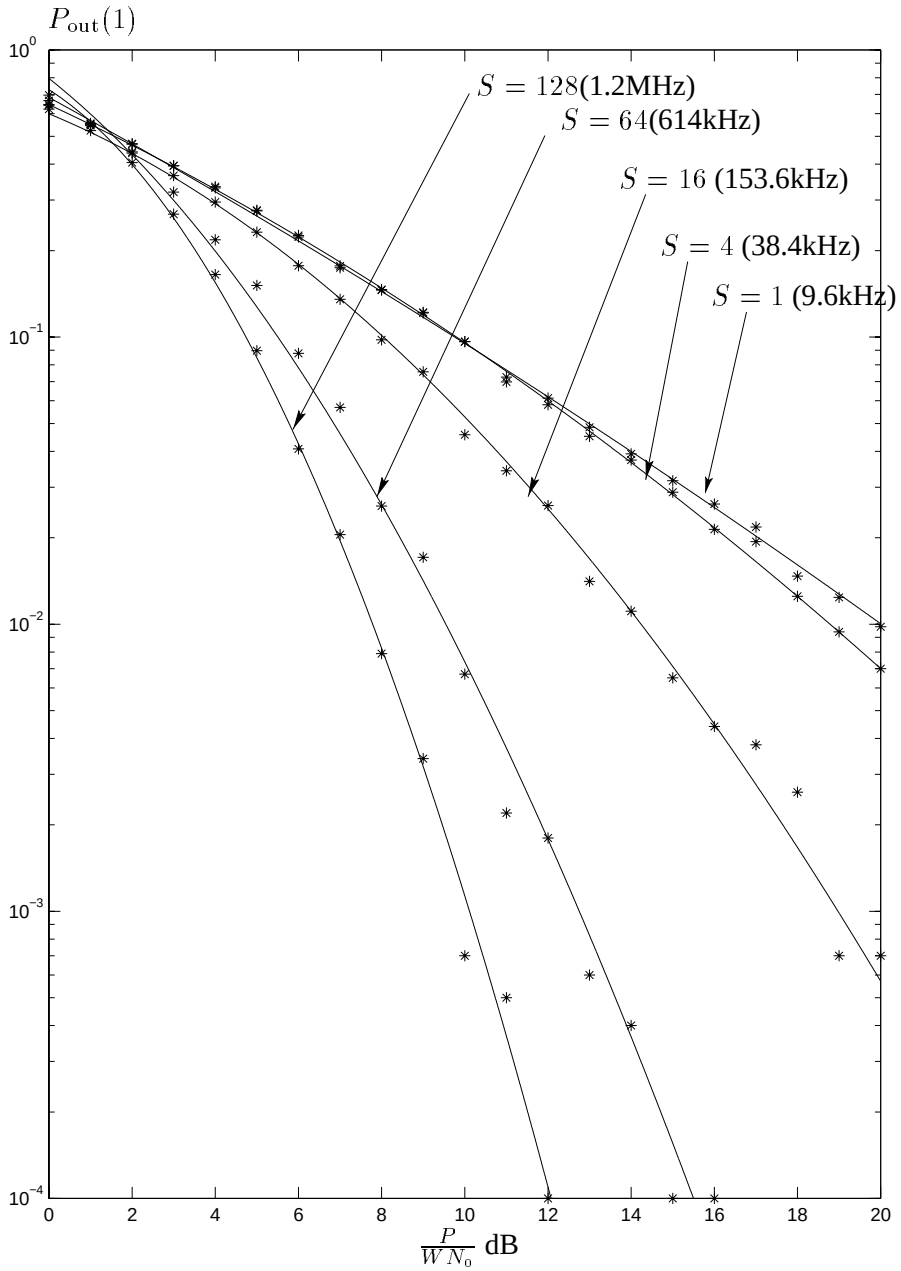

Figure 4.7: $P_{\text{out}}(1)$ as a function of SNR and bandwidth

In spite of the large difference between narrow and wide–band signals, the spectral efficiency for reasonable outage rates is still only on the order of 1 bit/dim even for a fairly high diversity system. The system with $S = 128$ which uses the entire 1.2288MHz still only achieves an outage rate of 10^{-3} at $R = 1$ bit/dim. To see the effect of diversity more concretely consider figures 4.6 and 4.7, where we plot $P_{\text{out}}(R)$ as a function of the SNR. We find that the slopes of the curves in the high SNR region are on the order of the number of significant eigenvalues for the channel bandwidth which are shown in Table 4.1. We note that the simulation points have been interpolated with a curve of best fit.

Spread–Spectrum Signals

Let us now examine spread–spectrum signals using the multitone model with spreading factor S. The received signal to be considered here is

$$\mathbf{y}_n = \begin{pmatrix} h_0 g_0 \\ h_1 g_1 \\ \vdots \\ h_{S-1} g_{S-1} \end{pmatrix} u_n + \mathbf{z}_n \tag{4.45}$$

where $\{g_s\}$ is the spreading–sequence satisfying $\sum_{s=0}^{S-1} |g_s|^2 = 1$. We assume uniform spreading so that $|g_s|^2 = 1/S$ and, in turn, the power constraint becomes

$$\sum_{n=0}^{N-1} \overline{|u_n|^2} \leq PT. \tag{4.46}$$

We may transform the problem using the *singular value decomposition* of $\begin{pmatrix} h_0 g_0 & \cdots & h_{S-1} g_{S-1} \end{pmatrix}^{\mathrm{T}} = \mathbf{U}\mathbf{\Sigma}\mathbf{V}^*$. The matrix $\mathbf{V}$ is simply 1, Σ is an N–dimensional vector with one non–zero entry equal to $\sqrt{\frac{1}{S}\sum_{s=0}^{S-1} |h_s|^2}$ and $\mathbf{U}$ is some unitary matrix. The received signal and noise vectors can be transformed as $\mathbf{y}' = \mathbf{U}^*\mathbf{y}$ and $\mathbf{z}' = \mathbf{U}^*\mathbf{z}$ so that the F frequency dimensions collapse into one and the channel may be written equivalently as

$$y'_n = \sqrt{\frac{1}{S}\sum_{s=0}^{S-1} |h_s|^2}\, u_n + z'_n \tag{4.47}$$

where z'_n are still zero–mean circular symmetric complex Gaussian random variables with variance N_0. The resulting average mutual information is given by

$$\begin{aligned} I_H &= \mathrm{I}\left(\{U_0,\cdots,U_{N-1}\};\{\mathbf{Y}_0,\cdots,\mathbf{Y}_{N-1}\}|\{H_s=h_s,\ s=0,\cdots,S-1\}\right) \ \text{bits/dim} \\ &= \mathrm{I}\left(\{U_0,\cdots,U_{N-1}\};\{Y'_0,\cdots,Y'_{N-1}\}|\{H_s=h_s,\ s=0,\cdots,S-1\}\right) \ \text{bits/dim} \\ &= \frac{1}{NS}\sum_{n=0}^{N-1}\log_2\left(1+\frac{PT}{NN_0}\frac{1}{S}\sum_{s=0}^{S-1}|h_s|^2\right) \ \text{bits/dim} \\ &= \frac{1}{S}\log_2\left(1+\frac{P}{WN_0}\sum_{s=0}^{S-1}|h_s|^2\right) \ \text{bits/dim} \qquad (4.48) \\ &= \frac{W}{S}\log_2\left(1+\frac{P}{WN_0}\sum_{s=0}^{S-1}|h_s|^2\right) \ \text{bits/s} \qquad (4.49) \end{aligned}$$

From (4.48) we see that the optimal receiver from the point of view of average mutual information is a maximal–ratio combiner (or RAKE receiver) of the sub–band channels. Moreover, $P_{\mathrm{out}}(R)$ is easily computed in closed–form since the argument of the logarithm is a quadratic form of correlated Gaussian random variables. In the case of Rayleigh fading we have

$$\begin{aligned} P_{\mathrm{out}}(R) &= \mathrm{Prob}\left(\sum_{s=0}^{S-1}|h_s|^2 < \frac{WN_0}{P}\left(2^{RS}-1\right)\right) \\ &= \sum_{s=0}^{S-1}A_s\left(1-\exp\left(-\left(2^{RS}-1\right)\lambda_i\frac{WN_0}{P}\right)\right) \qquad (4.50) \end{aligned}$$

where $\{\lambda_s\}$ are the eigenvalues of $\mathbf{K}_H$ and $A_s=\prod_{j\neq s}\frac{\lambda_s}{\lambda_s-\lambda_j}$. We have assumed, of course, that there are no repeated eigenvalues. In figure 4.8 we show $P_{\mathrm{out}}(R)$ for different spreading gains and signal–to–noise ratios of $\frac{P}{WN_0}=0$ dB. A high noise level such as this is typical in many spread–spectrum applications such as a fully–loaded *code–division multiple–access (CDMA)* system where additive noise is primarily due to other users sharing the same bandwidth. We will discuss this more in Chapter 7. We also show the Monte–Carlo simulation of (4.44) for this SNR. The scheme represented by (4.42) is a general coding scheme which we may choose to have operate at a low rate in spread–spectrum applications. The scheme represented by (4.48) is low–rate by design, in the sense that it is not ever meant to be used at a high rate. We note that for spectral efficiencies on the order of $1/S$ bits/dim there is a slight advantage to using a non–trivial low–rate coding scheme as opposed to PN spreading. This difference is greater in multiuser applications (i.e. CDMA) as we will show in Chapter 7. The real advantage of low–rate coding in single–user systems comes when we want to have more spectrally efficient schemes which use the same total bandwidth. At an information outage probability of 10^{-3} with $S=128$ (1.2288MHz) we see that a

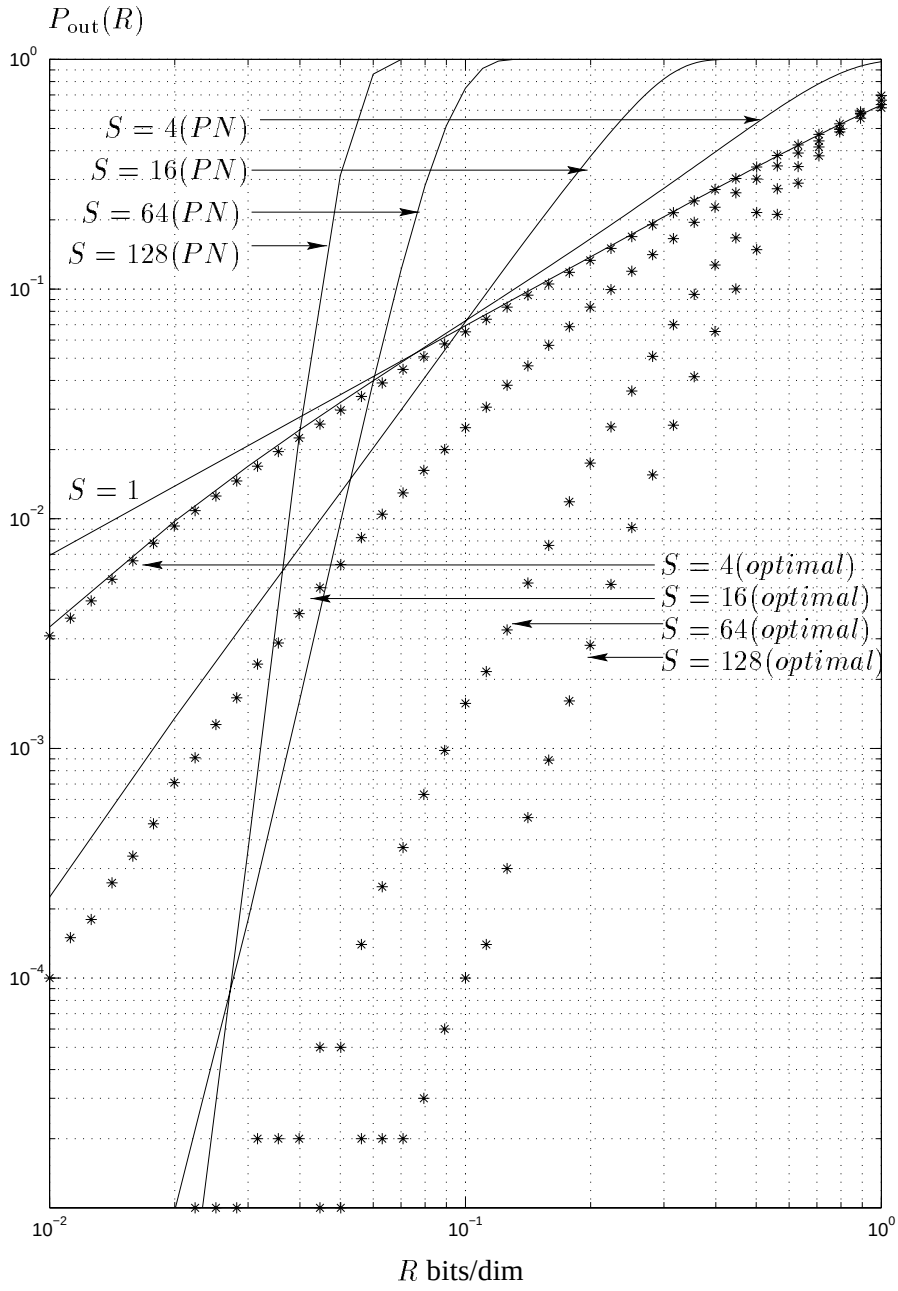

Figure 4.8: Comparison of low–rate coding and PN spreading $P/WN_0 = 0$ dB

fivefold increase in spectral efficiency is possible using a sophisticated coding/spreading scheme. These types of low–rate coding systems are discussed for non–fading channels in [Vit90][Hui84].

4.2.4 Block–Fading AWGN Channels

Let us now examine the block–fading AWGN channel where each block is transmitted across a single–path or frequency–flat channel with signals band-limited to W Hz. This would be the case, for instance, in a slow–frequency hopping system with narrow-band signals. We devote more attention to this channel when we consider code design in the next chapter. Generalizing (4.30) to the case of F blocks each having indepedent and identically distributed channel responses $H_i(f) = \alpha_i$, we have using (4.16),

$$I_{H_0,\cdots,H_{F-1}} = \frac{W}{F}\sum_{f=0}^{F-1}\log_2\left(1+\frac{P}{WN_0}\alpha_i\right). \tag{4.51}$$

As in the multi-tone case, $P_{\rm out}(R)$ must be calculated numerically. The independence of the channel gains in each block allow us to perform this calculation via an F–fold convolution of the density function of $\log_2\left(1+\frac{P}{WN_0}\alpha\right)$ (the derivative of (4.33)). A Chernov upper–bound is also found in [KSS95]. In figure 4.9 we plot $P_{\rm out}(R)$ for $\frac{P}{WN_0} = 10$dB for unit–mean Rayleigh fading in each block. We see as before that coding across several degrees of freedom (in this case the independent block fading levels) has a significant diversity effect in the outage probability. We show $P_{\rm out}(1)$ as a function of the SNR in figure 4.10, where we note that the curves have an inverse $F^{\rm th}$ power behaviour in the SNR.

For the case of perfect interleaving or an unlimited number of independent frequency bands and no delay constraint, the conditional average mutual information (4.17) on an AWGN channel with unit–mean Rayleigh fading is given by

$$\begin{aligned} I_\infty &= W\int_0^\infty \log_2\left(1+\alpha\frac{P}{WN_0}\right)e^{-\alpha}d\alpha \\ &= \frac{We^{\frac{WN_0}{P}}}{\ln 2}\mathrm{E}_1\left(\frac{WN_0}{P}\right), \ \ \text{bits/s} \end{aligned} \tag{4.52}$$

where $\mathrm{E}_1(x)$ is the first order exponential integral [AS65] given by

$$\mathrm{E}_1(x) = \int_x^\infty \frac{1}{u}e^{-u}du. \tag{4.53}$$

Although Lee [Lee90] showed I_∞ to be given by (4.52), it was also computed numerically much earlier by Ericson [Eri70], without explicit mention of the exponential integral function. We also show I_∞ in Figure 4.9 along with the non–fading channel capacity in (4.36). Even for a fairly high diversity system, the practical information rates are very far from those of an ergodic or perfectly–interleaved system.

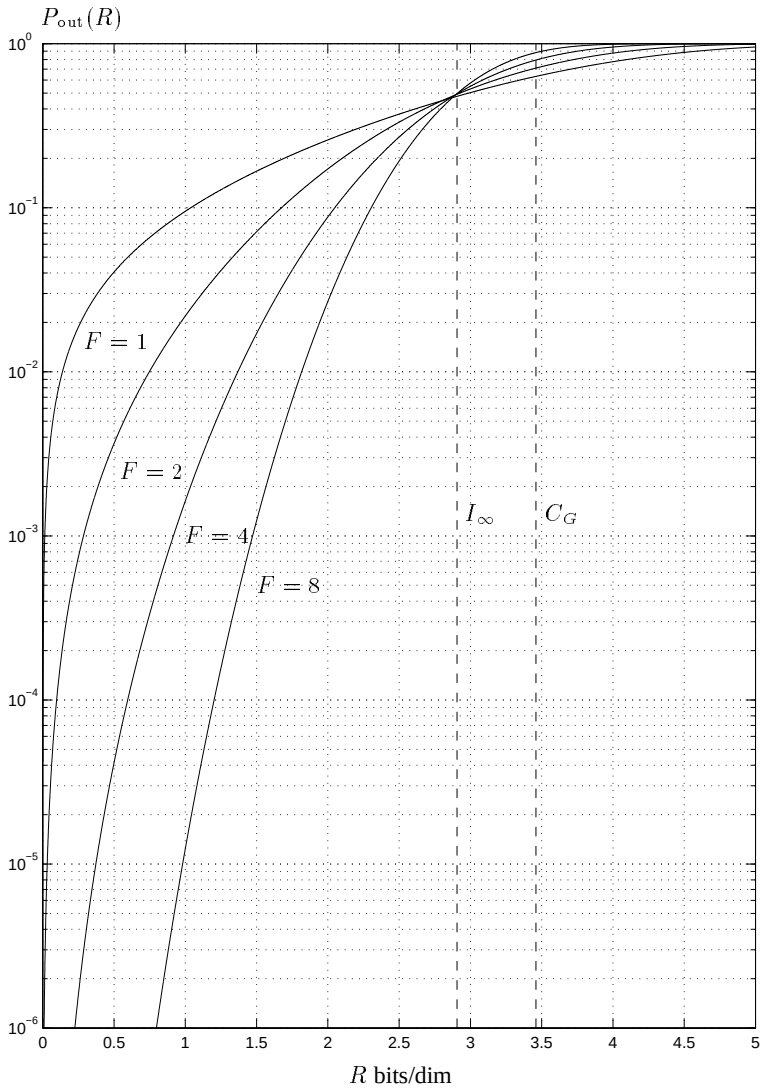

Figure 4.9: Information outage probabilities for Rayleigh fading for increasing F

This shows that ergodic channel measures are very optimistic when only a small number of degrees of freedom characterize the fading process.

4.3 Chapter Summary

This chapter examined fundamental limits for systems operating over fading channels. We began with a general discussion of the achievable probability of codeword error for fading channels which cannot be treated in an ergodic stationary manner. This is typically the case when the system is subject to a decoding delay as well a finite–bandwidth constraint. The main problem with such channels is that the

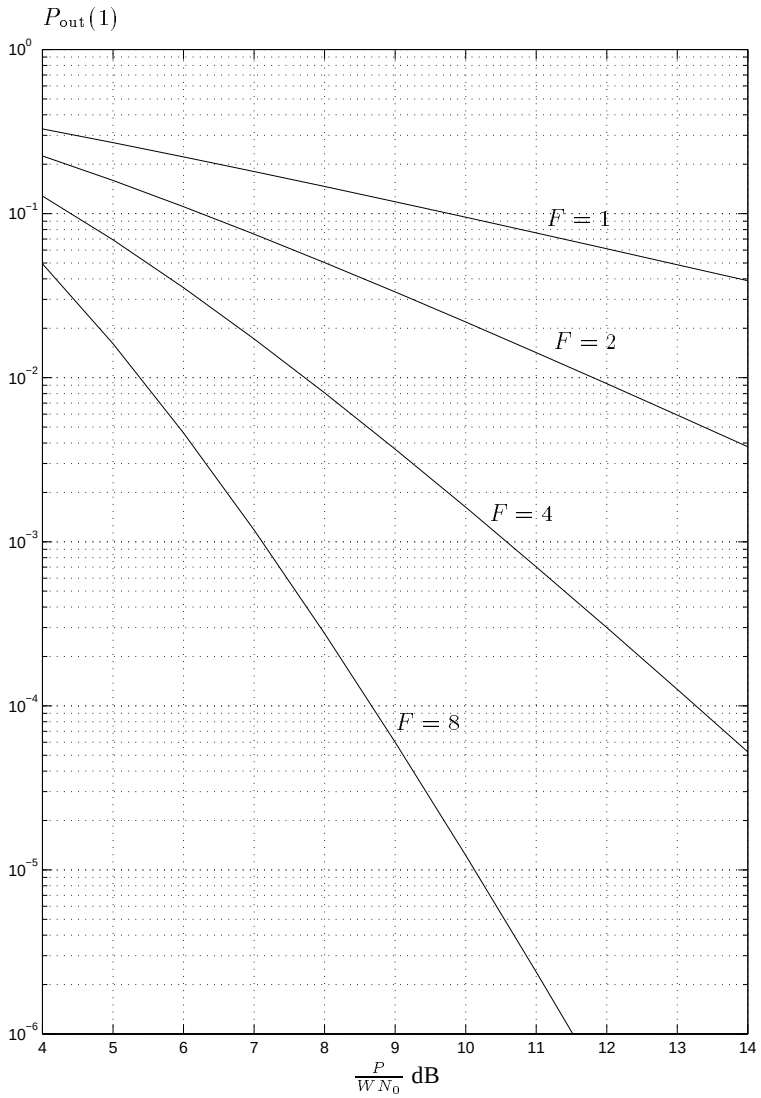

Figure 4.10: Information outage probabilities vs. SNR for Rayleigh fading

fading process cannot be sufficiently averaged during the decoding process, and as a result a channel capacity does not exist. It was shown that the probability of codeword error is bounded away from zero by a quantity called the *information outage probability*. This is the probability that the instantaneous average mutual information between the transmitted and received codeword is less than the information rate agreed upon by the communicating parties. When channel ergodicity cannot be exploited, it becomes a lower–bound to the achieveable codeword error–rate.

Using models for static multipath fading channels, we showed that the *information outage probability* exhibits a diversity effect similar to the pairwise–error–probability analyses we performed in Chapter 2. The codeword error–rate performance cannot be made arbitrarily small and decreases as the D^{th}

power of the signal–to–noise ratio, where D is the number of degrees of freedom or eigenvalues needed to characterize the fading process during the transmission of the codeword. We used the TU12 ESTI channel response model with the multitone representation of a wide–band transmission system to evaluate achievable spectral efficiency. We showed that with signals with a bandwidth of 1.2288MHz we could expect spectral efficiencies on the order of 2 bit/s/Hz with codeword error–rates of 10^{-3}. Transmission schemes such as frequency–hopping with coding or wide–band bursty transmission (such as TDMA) can exploit this bandwidth efficiently. Narrowband signals suffer hopelessly from lack of diversity. Using the same model, we considered spread–spectrum signals operating at a low signal–to–noise ratio. We found that when designed to operate at a spectral efficiency which is the inverse of the spreading gain, there is a slight advantage to using a non–trivial low–rate coding scheme as opposed to PN spreading, which can be seen as repetition coding. The main advantage for using low–rate coding comes when more bandwidth efficient schemes are required (i.e. for high data rate spread spectrum applications), where very large reductions in codeword error–rate can be achieved.

We have not considered the issue of imperfect estimation of the channel at the receiver. This clearly will have the effect of reducing achievable data rates across the channel. These issues are treated for time–varying channels in [Med95].

Chapter 5

Code Design for Block–Fading Channels

In the last chapter we were interested in defining the information–theoretic framework for communication over general fading channels. We did not, however, give any examples of practical coding schemes for approaching the performances given in our analyses. We now consider such issues for the particular class of systems appropriately modeled by the so–called *block–fading channel*. As we already mentioned in the two previous chapters this is an accurate model for systems where the channel state for blocks of length N symbols, and decoding only be performed on a finite and small number, F, of such blocks. In applications like GSM or IS54 N is quite large (hundreds of symbols) and there is a constraint on the interleaving depth due to a stringent processing delay requirement. Even in the absence of such delay constraints, there may be a maximum number of uncorrelated channel realizations (for instance FDMA slots in GSM). Both amount to the same thing, namely that the number of uncorrelated channel realizations over which coding is performed, F, is small, so that as we saw in the previous chapter, the channel may not be treated in an ergodic and stationary manner.

Most work dealing with code design for fading channels assumes an ideal interleaving situation [Pro95, BDMS91] which, in the context of block–fading channels, is equivalent to letting F tend to infinity. On ergodic channels parallel concatenated codes have proven to be effective [BGT93] and offer astoundingly good performance. For near–optimal performance, however, they can be quite complex for some applications. In addition, codes designed for ergodic channels need not be effective when applied to a system where F is small, which is often the case in PCS applications. Our goal here is to find coded–modulation schemes using relatively simple constellations and encoders/decoders of reasonable complexity which are especially well–suited for non–ergodic channels. We will show that there are reasonably simple codes for low spectral efficiencies (<2 bits/dim) which can achieve close to optimal

performance. This is appropriate in light of the results of the previous chapter where we showed that for typical wide–band urban channels (i.e. around 1MHz bandwidth), we cannot expect to be able to transmit at much more than 1 bit/dim at an SNR of 10dB.

Besides slow frequency–hopping systems, another application of a block–fading model is in fast frequency–hopping systems where N is small (on the order of a few symbols). The work of Kaplan *et al.* in [KSSK95] considers coding for these systems *without* a constraint on the number of frequencies over which the signal can hop. This amounts again to an ideal interleaving situation, where the fast frequency–hopping pattern takes the place of the interleaver. The work of Lapidoth in [Lap94] addresses the construction and performance of binary codes *matched* to the depth of the interleaver (or number of blocks) which, as in our case, is assumed to be small. This introduces strong cyclic correlations in the sequence to be decoded. Lapidoth's analysis was performed using an *erasure–channel* model of a fading channel and for various interleaving techniques.

In [LWK93] the coding problem was treated for the block fading channel. They showed that in order for the diversity order to be maximum (i.e. F) the code rate (in input/output symbols) must not exceed $1/F$. We will extend these results by considering arbitrary diversity orders. For the case of trellis codes with rate $1/F$ they consider an analytical approach for determining the pairwise error probability based on a generalized transfer function from the state diagram of the code. Trellis codes based on linear convolutional codes with M–PSK modulation and $F = 2$ blocks are considered and a few low–complexity examples are given. This approach was also recently considered for rate $1/F$ binary convolutional codes with antipodal signals over Ricean channels by Malkamaki and Leib in [ML97].

The work of Giraud and Belfiore [GB96] and Boutros *et al.* [BVRB96] examines the coding problem for fading channels from a different point of view. They both focus of the design of multidimensional lattice constellations which, using sufficient interleaving, are assumed to have an independent fading strengths in each dimension. The specially designed constellations have the property that the diversity order is equal to the number of dimensions. We will discuss these schemes in the context of our work shortly, since they can be applied directly to the block–fading channel.

We begin with a simplified discrete–time system model for the code design problem and perform an information outage probability analysis for the case of non–Gaussian discrete signal alphabets. Recall that in the last chapter we always assumed the transmitter used a continuous Gaussian symbol alphabet. The goal of this analysis is to gain insight regarding the choice of signal constellation size on the achievable codeword error–rate performance. We then examine the coding problem from the point of view of the diversity order. We show that the block–fading channel can be considered as a non–binary coding

scheme with block length F with N dimensional symbols. It follows that the diversity order, d_{H}^{F}, can be upper–bounded using standard techniques, and it turns out that the *Singleton bound* is the most appropriate of such techniques. We show how it can be used to determine the maximum diversity as a function of the information rate in bits/dim, the number of fading blocks F and the size of the signalling constellation. A code which meets the Singleton bound is known as a *Maximal Distance Seperable (MDS) code,* and therefore any MDS code achieves maximum diversity. Using the Singleton bound as target diversity order for any coded system, we provide examples for codes which achieve it. We first consider block codes and multidimensional constellations followed by trellis codes. Results of computer searches for maximal–diversity trellis codes of varying complexity for binary and non–binary constellations are given. We end with some computer simulations of some of the reported codes and compare them to codes already in use at the present time.

5.1 System Model and Outage Probability Analysis

We saw in Chapter 3 that the performance of the block–fading channel, in the case of uncorrelated blocks, is due to two factors which act independently. This is first the relation between the underlying signaling pulse shape and the multipath delay spread. The second is the effect of coding, more precisely the minimum Hamming distance between pairs of signals on a block–basis. Because of this separation between the two factors, it is sufficient to consider the simplest channel model which allows us to analyse the effects of coding without having to worry about the pulse–shape/multipath relationship. We therefore assume a narrow–band pulse shape so that there is no ISI due to multipath and amplitude statistics are Rayleigh. In addition, we assume the coded symbols belong to a real–valued symbol alphabet $\mathcal{S} \subseteq \mathbb{R}$ (i.e. each symbol uses 1 signaling dimension.) Extending this analysis to complex symbols is straightforward and brings no significant additional insight into the problem. Moreover, this allows us to determine how close we can expect to get to the performance of the continuous Gaussian symbol case with simple constellations.

We show the discrete–time channel model in figure 5.1. Assuming a system having F channels with blocks of length N symbols we have codewords occupying NF dimensions written as

$$\mathbf{c}_m = \left(c_{0,0}, c_{0,1}, \cdots, c_{0,N-1}, c_{1,0}, \cdots, c_{F-1,N-1}\right), \; m = 0, 1, \cdots, M-1, \tag{5.1}$$

where M is the size of the codebook. Each block is assumed to have a channel gain $\alpha_f, \; f = 0, \cdots, F-1$ which is the same for each symbol in the block and independent from block to block. Under the Rayleigh

assumption each channel gain is exponentially distributed with unit mean as

$$f_{\alpha_f}(u) = e^{-u}, u \geq 0. \tag{5.2}$$

The receiver uses a filter matched to the chosen pulse–shape which is sampled at the symbol rate so that we may may write the continuous–time problem equivalently as

$$r_{f,n} = \sqrt{\alpha_f} c_{f,n} + z_{f,n}\ , f = 0, \cdots, F-1,\ n = 0, \cdots, N-1, \tag{5.3}$$

where the $z_{f,k}$ are i.i.d. zero–mean real Gaussian random variables with variance $N_0/2$. Let the NF–dimensional vectors $\mathbf{r}$ and $\mathbf{z}$ denote the received signal and noise samples and $\mathbf{r}_f$, $\mathbf{c}_{m,f}$ and $\mathbf{z}_f$ the samples in each block $f = 0, \cdots, F-1$. We take for granted that the transmitter and receiver have agreed beforehand to use a codebook having M codewords so that the information rate is $R = (\log_2 M)/NF$ bits/dimension. We denote the F–dimensional vector of signal amplitudes by $\boldsymbol{\alpha}$, and assume that there is no feedback path for channel state information so that the transmitter has no *a priori* knowledge of $\boldsymbol{\alpha}$.

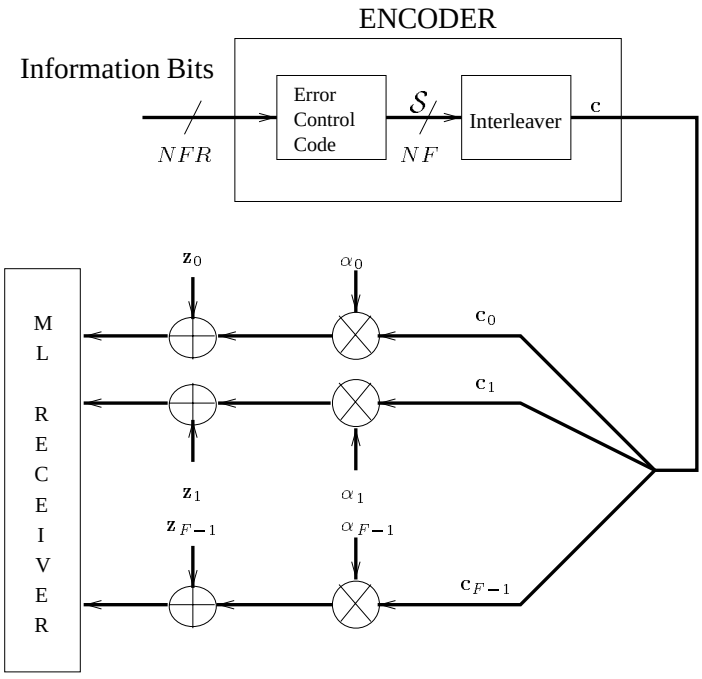

Figure 5.1: Discrete–time system model

We begin with an outage probability analysis for general non–Gaussian symbol alphabets in order to see the effects of using pragmatic constellations. From the results of Chapter 2, in order to compute

the average probability of codeword error, we must consider the average mutual information functional

$$I_H = \frac{1}{NF}\mathrm{I}(\mathbf{C};\mathbf{R}|\mathbf{A}=\boldsymbol{\alpha}) = \frac{1}{NF}\int_{\mathbf{c}\in\mathcal{S}^{NF}}\int_{-\infty}^{\infty} f_{\mathbf{R},\mathbf{C}|\mathbf{A}}(\mathbf{r},\mathbf{c}|\boldsymbol{\alpha})\cdot \log_2\frac{f_{\mathbf{R}|\mathbf{C},\mathbf{A}}(\mathbf{r}|\mathbf{c},\boldsymbol{\alpha})}{f_{\mathbf{R}|\mathbf{A}}(\mathbf{r}|\boldsymbol{\alpha})}d\mathbf{r}d\mathbf{c} \quad \text{bits/dimension}. \tag{5.4}$$

using which we can compute the information outage probability

$$P_{\text{out}}(R) = \text{Prob}(I_H < R). \tag{5.5}$$

This quantity defines the practical lower–limit to the codeword error–rate in the limit of large NF. We recall that under an average power constraint

$$\sum_{n=0}^{N-1}\sum_{f=0}^{F-1}\overline{c_{n,f}^2} < NF\mathcal{E}_s, \tag{5.6}$$

the quantity I_H is maximum for independent Gaussian symbols and is given by

$$I_H = \frac{1}{F}\sum_{f=0}^{F-1}\frac{1}{2}\log_2\left(1+\frac{2\alpha_f\mathcal{E}_s}{N_0}\right)\text{bits/dim}. \tag{5.7}$$

We have already computed the corresponding information outage probability in this case numerically. In a practical sense, this quantity is useful for assessing the potential performance gains afforded by the use of large constellations. For small constellations with equiprobable and independent symbols, $P_{\text{out}}(R)$ can similarly be computed numerically using [Bla87]

$$I_H = \log_2|\mathcal{S}| - \frac{1}{F|\mathcal{S}|}\sum_{f=0}^{F-1}\sum_{s_i\in\mathcal{S}}\int_{-\infty}^{\infty}\frac{1}{\sqrt{\pi N_0}}\exp\left(-\frac{1}{N_0}r^2\right)\cdot \tag{5.8}$$

$$\log_2\sum_{s_j\in\mathcal{S}}\exp\left(-\frac{1}{N_0}\left[(r-\alpha_f(s_j-s_i))^2 - r^2\right]\right)dr \quad \text{bits/dimension} \tag{5.9}$$

The simplest modulation scheme to consider is uniformly–spaced *Amplitude Modulation(AM)*, which is shown in figure 5.2.

In Figs. 5.3–5.7 we show the information outage probability now as a function of the the signal–to–noise ratio per information bit $\mathcal{E}_b/N_0$ (where $R\mathcal{E}_b = \mathcal{E}_s$) for both small AM constellations and Gaussian signals. We see that by doubling the constellation size with respect to the minimum constellation which achieves the desired information rate, we quickly approach the performance achievable with a continuous Gaussian input signal. This is similar to the effect of coding with expanded signal sets on the non–fading AWGN channel [Ung82]. We notice also that the diversity (i.e. the slope of the error–rate curve) is reduced for small constellations. In other words, constellation expansion can increase diversity. In some

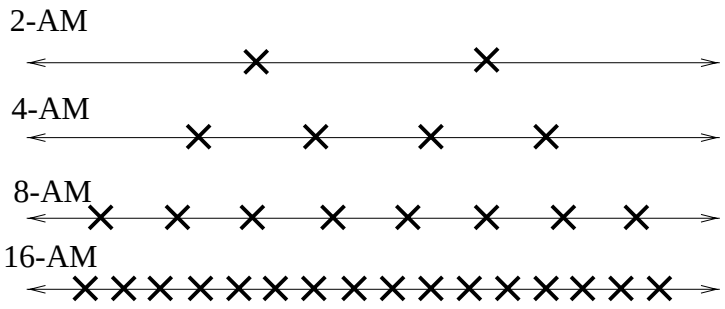

Figure 5.2: AM Modulation

cases, the increase can be very significant (e.g. 1.5 bits/dim with 4 or 8 AM.) In the following section we derive a bound on the diversity which allows us to quantify this observation more precisely.

In Figure 5.8 we show the lower bound on the bit–error probability given in (4.15). Again we see the same effect from constellation expansion but that the error rates are two orders of magnitude lower. We will see that this bound is much less indicative of practical bit error rates than P_{out} is for block error rates.

5.2 Maximum Code Diversity

This section addresses the issue of designing coded–modulation schemes which attain maximum code diversity (d_{H}^{F}) for a given number of uncorrelated blocks and information rate. Using the techniques from Chapter 2, we recall that the conditional pairwise–error probability between two arbitrary codewords is given by

$$P_{e|\boldsymbol{\alpha}}(\mathbf{c}^{(a)} \to \mathbf{c}^{(b)}) = \mathrm{Q}\left(\sqrt{\frac{d^2(a,b)}{2N_0}}\right). \tag{5.10}$$

For the system at hand the Euclidean distance between the two codewords conditioned on the channel state is

$$d^2(a,b) = \sum_{f=0}^{F-1} \alpha_f d_f^2(a,b) \tag{5.11}$$

and

$$d_f^2(a,b) = \sum_{n=0}^{N} (c_{f,n}^{(a)} - c_{f,n}^{(b)})^2. \tag{5.12}$$

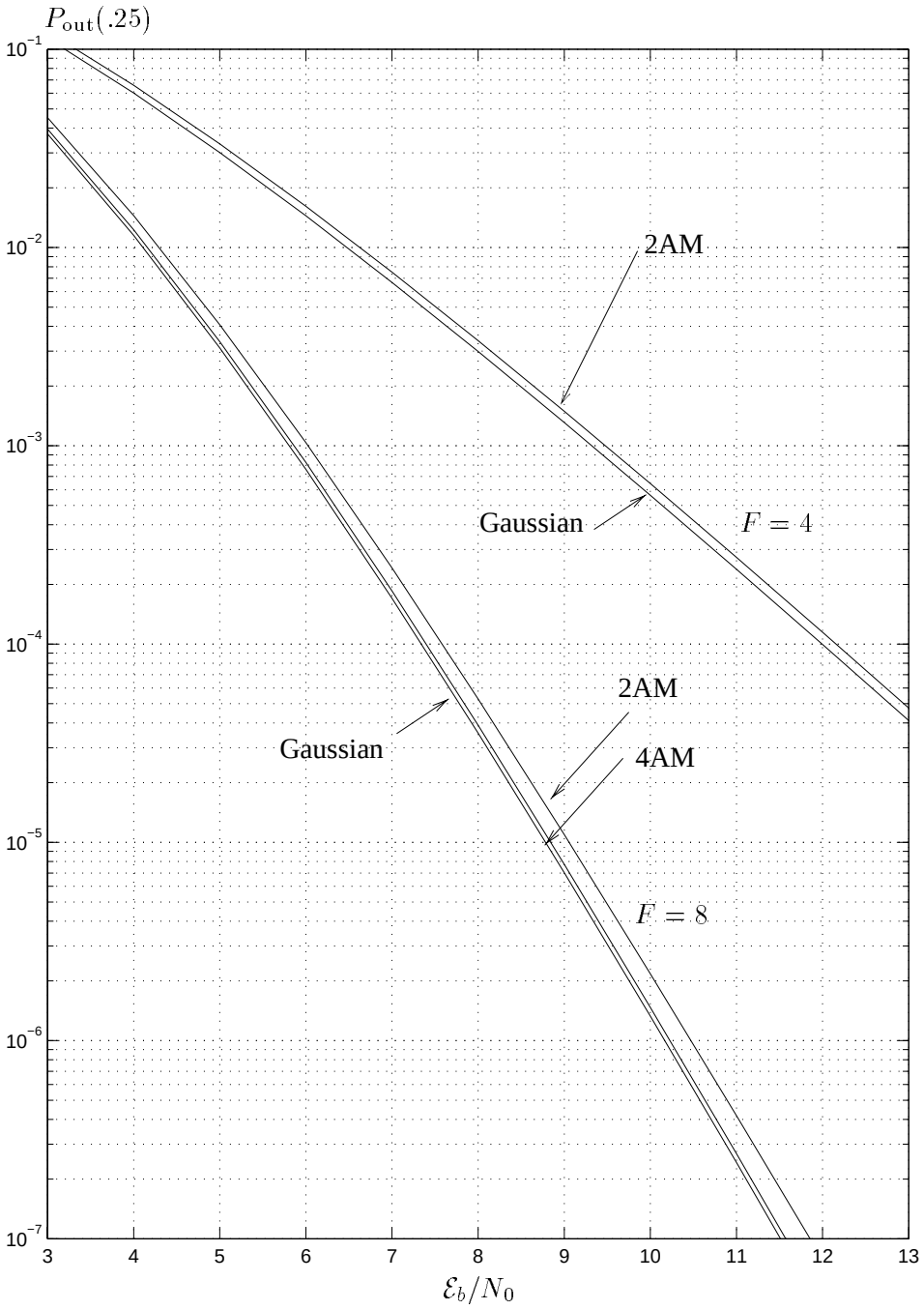

Figure 5.3: Information Outage Probabilities ($R = .25$ bits/dim)

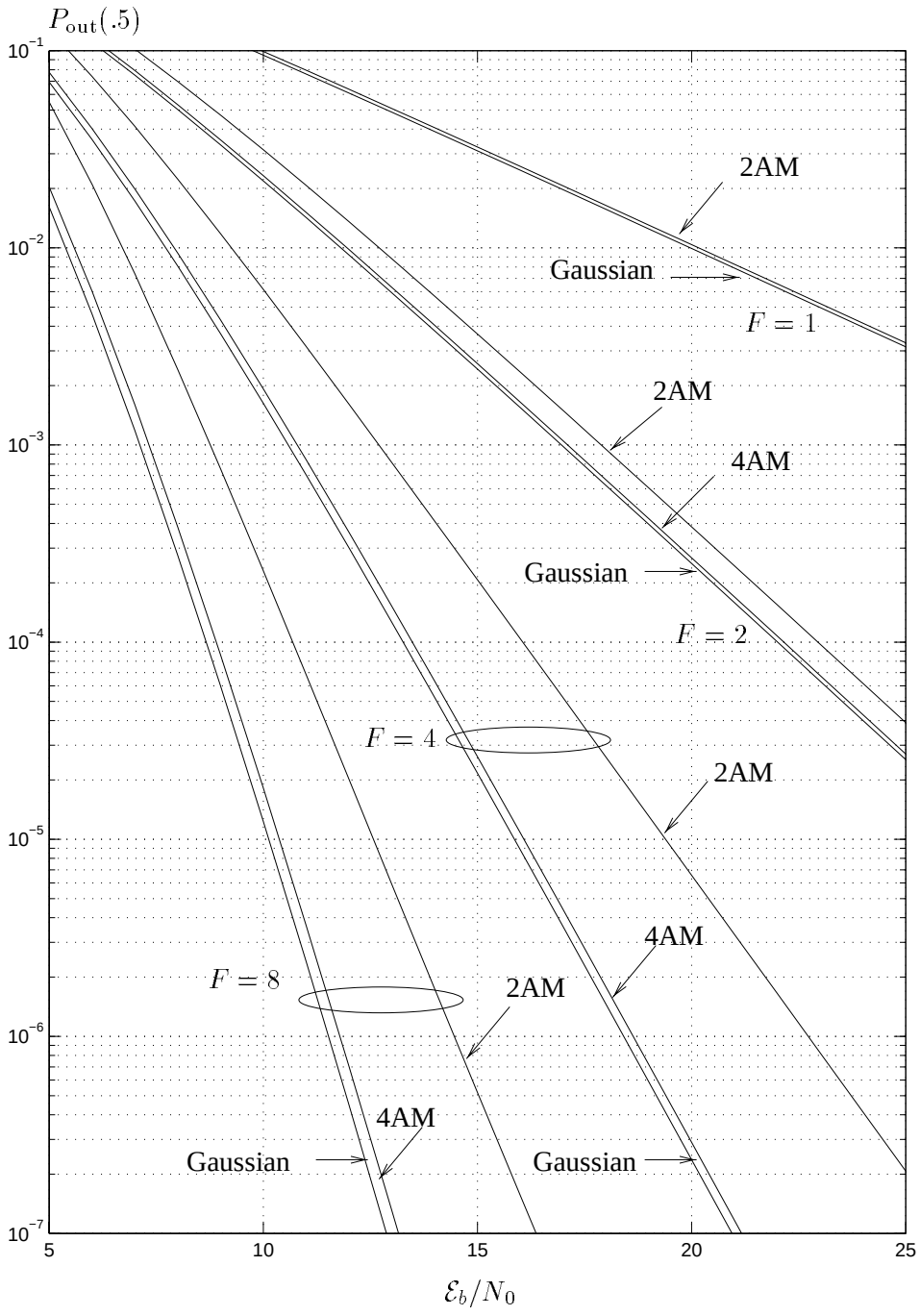

Figure 5.4: Information Outage Probabilities ($R = .5$ bits/dim)

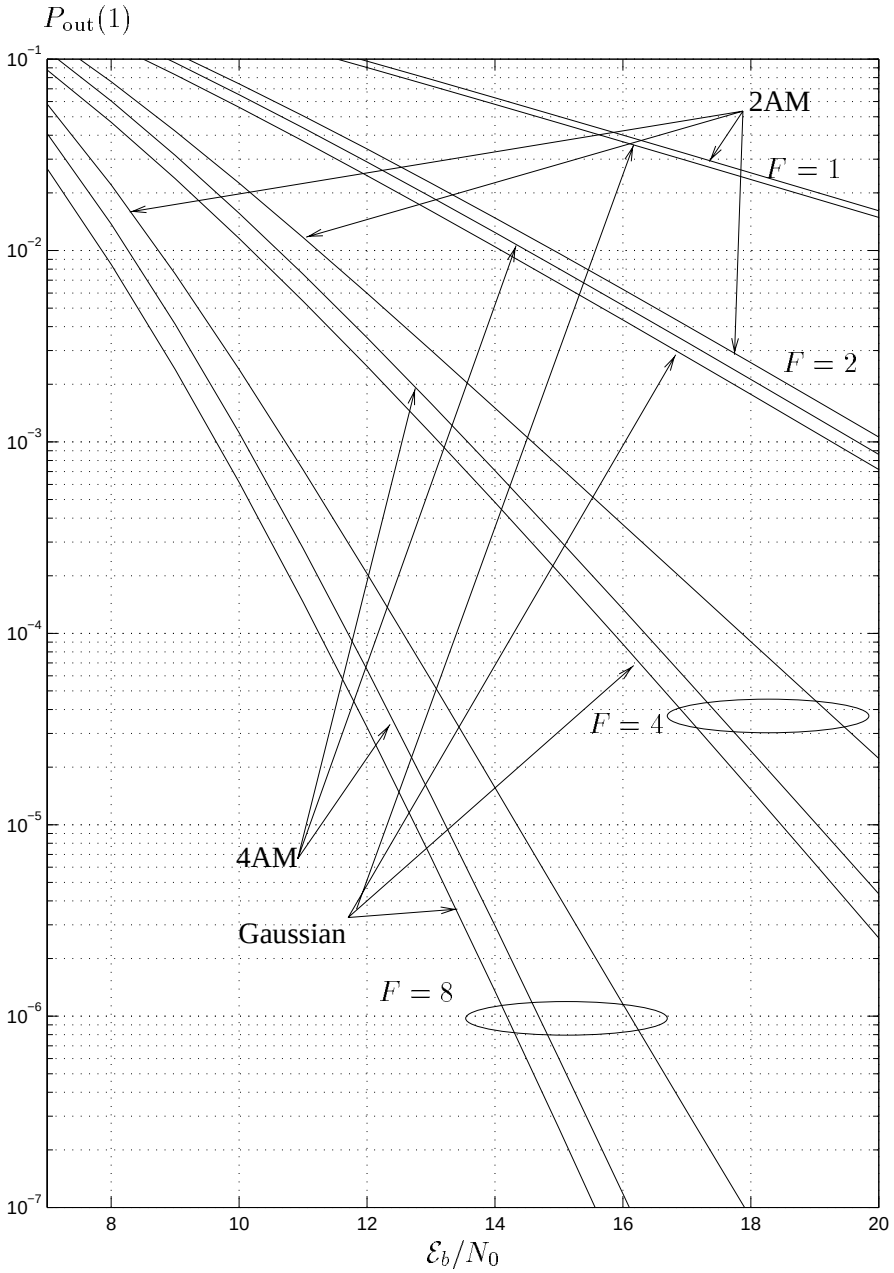

Figure 5.5: Information Outage Probabilities ($R = 1$ bit/dim)

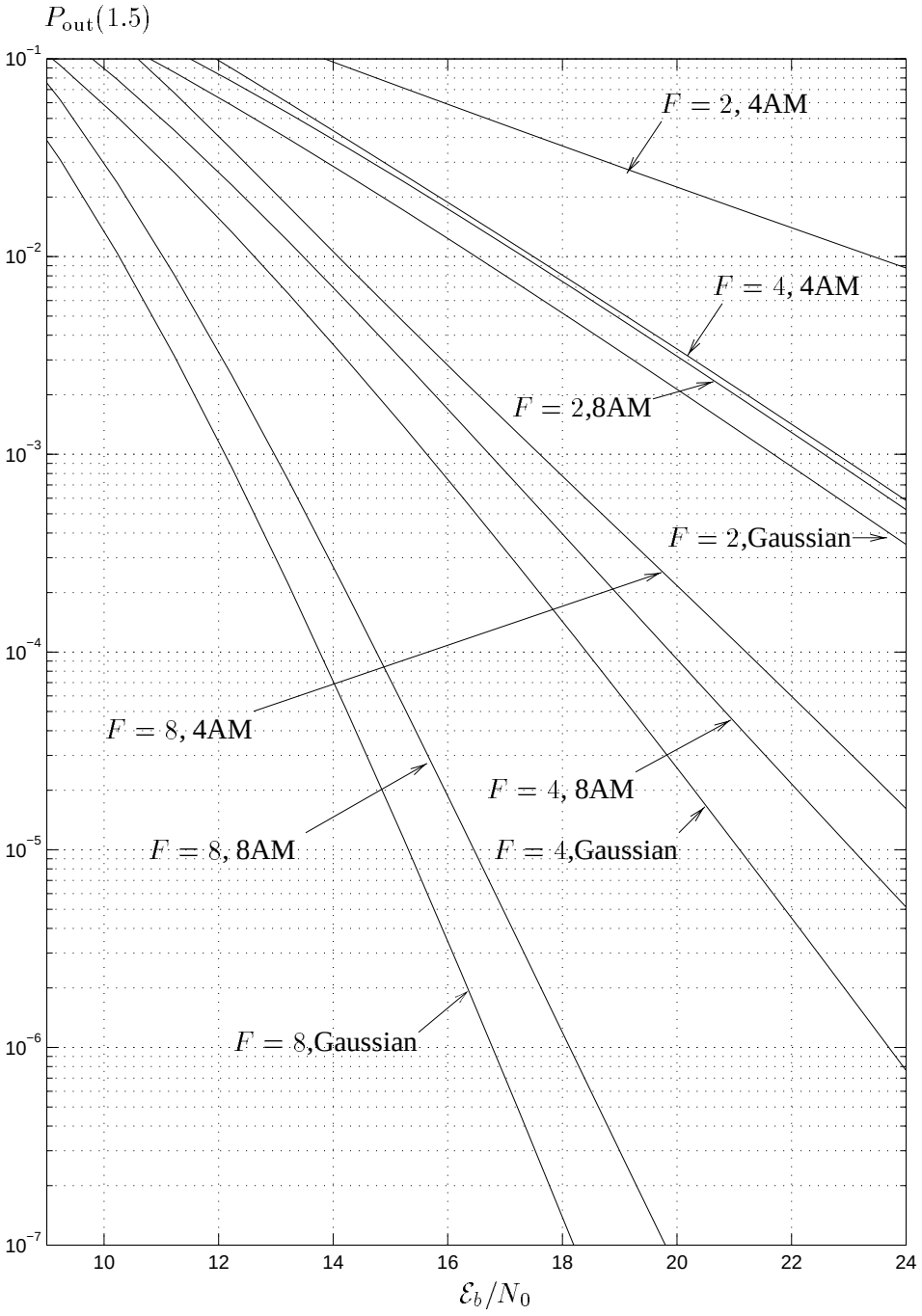

Figure 5.6: Information Outage Probabilities ($R = 1.5$ bits/dim)

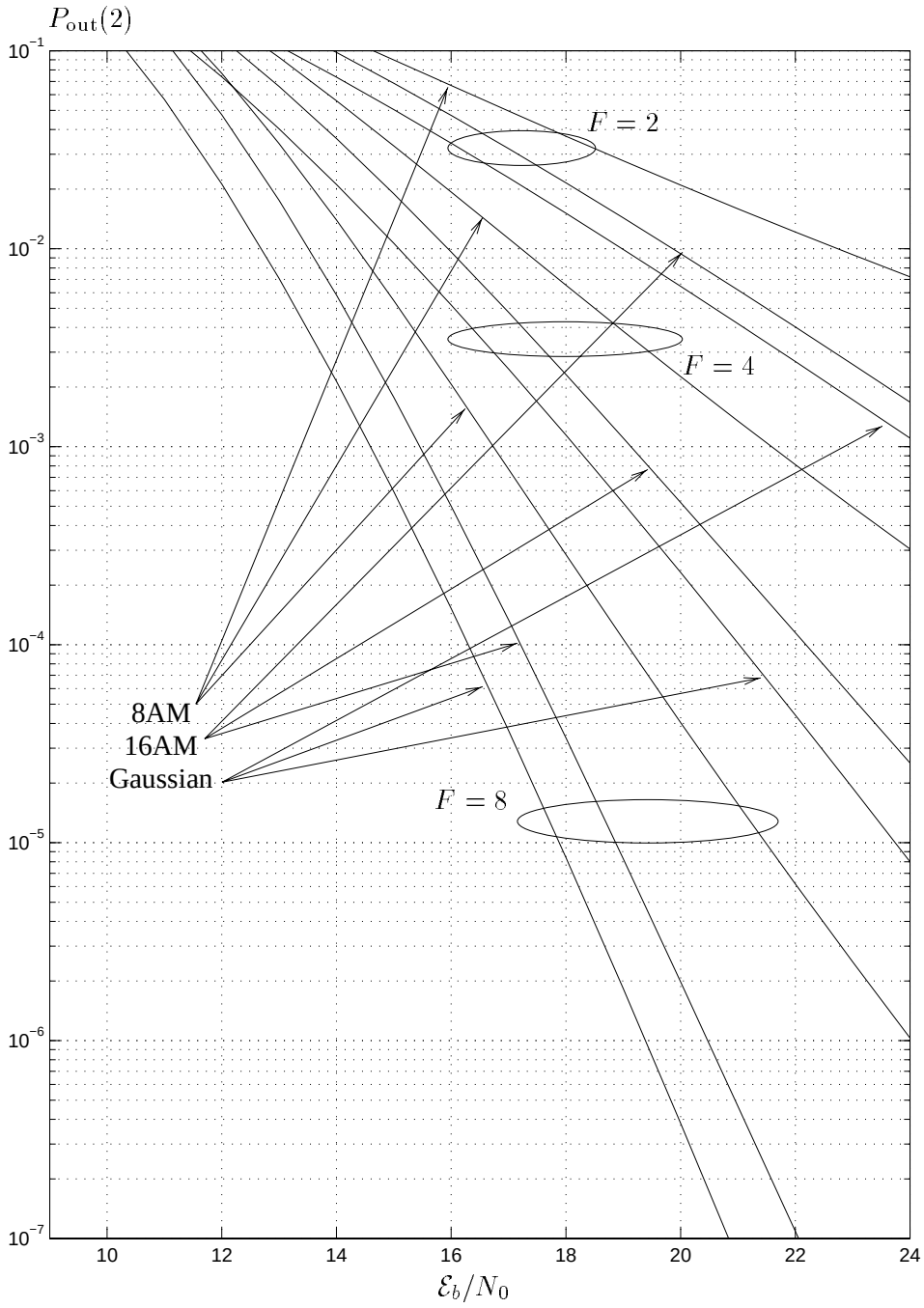

Figure 5.7: Information Outage Probabilities ($R = 2$ bits/dim)

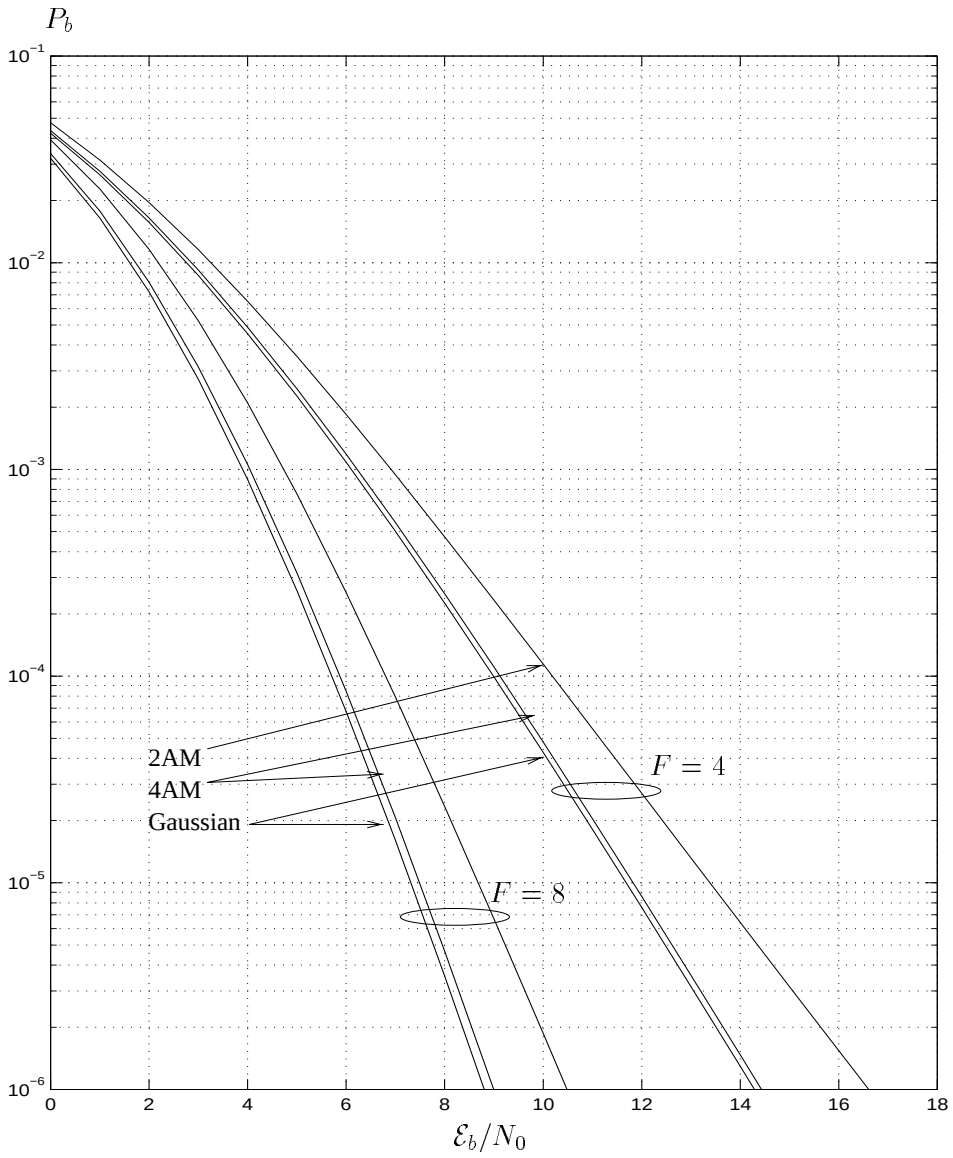

Figure 5.8: Lower Bound to Bit–Error Probability ($R = .5$ bits/dim)

Defining the variable $z = d^2(a,b)/(2N_0)$ we have that its moment–generating function is given by

$$\begin{aligned} G_z(s) &= \prod_{f=0}^{F-1} \frac{1}{1 - s\frac{d_f^2(a,b)}{2N_0}} \\ &= \prod_{i=0}^{d_{\mathrm{H}}^F(a,b)-1} \frac{1}{1 - s\frac{\mu_i}{2N_0}} \end{aligned}$$

where $\{\mu_i\}$ are the non–zero block Euclidean distances $\{d_f^2(a,b)\}$ and $d_{\mathrm{H}}^F(a,b)$ is the Hamming distance between the codewords on a block basis. The average PEP is therefore

$$P_e(\mathbf{c}^{(a)} \to \mathbf{c}^{(b)}) = \mathrm{E}_{\boldsymbol{\alpha}} P_{e|\boldsymbol{\alpha}}(\mathbf{c}^{(a)} \to \mathbf{c}^{(b)}) \leq .5 G_z\left(-\frac{1}{2}\right) = \prod_{i=0}^{d_{\mathrm{H}}^F(a,b)-1} \frac{1}{1 + .5\mu_i} \tag{5.13}$$

We saw in Chapter 2 that in these cases, the error probability curve decreases as the inverse $d_{\mathrm{H}}^{F\,\mathrm{th}}$ power of the signal–to–noise ratio, so clearly $d_{\mathrm{H}}^F(a,b)$ is the most critical performance indicator. Nevertheless, the secondary parameter

$$\chi(a,b) = \left(\prod_{i=0}^{d_{\mathrm{H}}^F(a,b)-1} \mu_i \right)^{1/d_{\mathrm{H}}^F(a,b)} \tag{5.14}$$

acts as a SNR gain factor which also must be considered. It is simply the *geometric mean* of the Euclidean distances $d_f^2(a,b)$.

From the average PEP we may invoke the union bound on the probability of error for an arbitrary code as

$$P_e = \frac{1}{M} \sum_{a=0}^{M-1} \sum_{b=0}^{M-1} P_e(\mathbf{c}^{(a)} \to \mathbf{c}^{(b)}), \tag{5.15}$$

and if the code is *geometrically uniform* [For91],

$$P_e = \sum_{b=0}^{M-1} P_e(\mathbf{c}^{(0)} \to \mathbf{c}^{(b)}). \tag{5.16}$$

This just means that the probability of error is indenpendent of the codeword that is being transmitted and there is no loss of generality in assuming that any one particular codeword is continuously transmitted.

5.2.1 An introductory example

We now consider a simple illustrative example which shows that the code design problem is different from the classic approach of maximizing the Hamming or Euclidean distances. In practice, the encoder

includes an interleaver, although in theory it is not required. The reason for its use is simply to reduce the computational complexity of the encoding and decoding processes. We require that the F degrees of freedom appear in the span of a codeword (or memory of a trellis code) which is assured by interleaving without needed very long codes (many states.) We will assume that the interleaver is of the diagonal type as described in Chapter 3 with depth F. If we denote the sequence at the output of the encoder by $\mathbf{q} = \{q_0, q_1, \cdots\}, q_k \in \mathcal{S}$, at the output of the interleaver the coded symbols in each block will be $\mathbf{c}_0 = \{q_0, q_F, \cdots, q_{kF}, \cdots\}, \cdots, \mathbf{c}_f = \{q_f, q_{F+f}, \cdots q_{kF+f}, \cdots\}$.

Let us examine the rate 1/2 binary convolutional code with binary modulation (.5 bits/dim) employed in the full–rate GSM standard shown in Fig.5.9. The output bits are interleaved over $F = 8$ blocks transmitted on widely spaced carriers, so that the channel strength in each block will be fairly uncorrelated from those in the other blocks. The minimum free Hamming distance path

$$\mathbf{q} = \{0, 0, \cdots, 0, 0, 1, 1, 0, 1, 0, 0, 1, 1, 1, 1, 0, 0, \cdots, 0\} \tag{5.17}$$

has $d_{\text{free}} = 7$ (after deinterleaving) and is shown along with the blocks over which each bit were transmitted. As for the symbols in each block, we have

$$\begin{aligned}
\mathbf{c}_0 &= \{0, \cdots, 0, 1, 1, 0, \cdots, 0\} \\
\mathbf{c}_1 &= \{0, \cdots, 0, 1, 1, 0, \cdots, 0\} \\
\mathbf{c}_2 &= \{0, \cdots, 0\} \\
\mathbf{c}_3 &= \{0, \cdots, 0, 1, 0, \cdots, 0\} \\
\mathbf{c}_4 &= \{0, \cdots, 0\} \\
\mathbf{c}_5 &= \{0, \cdots, 0\} \\
\mathbf{c}_6 &= \{0, \cdots, 0, 1, 0, \cdots, 0\} \\
\mathbf{c}_7 &= \{0, \cdots, 0, 1, 0, \cdots, 0\}
\end{aligned}$$

so that this path achieves $d_{\text{H}}^{8} = 5$. It turns out that this is also the minimum diversity path for this code and, as we shall soon see, that there is no other code which achieves a higher diversity order with binary modulation and $R = 1/2$ bits/dim.

Kaplan *et al.* [KSSK95] consider a similar trellis coding problem for an uninterleaved binary fast–frequency hopping system, without a constraint on the number of hopping frequencies. Their system model assumes that the hopping period extends over J ($J < 3$) trellis branches of a rate $1/n$ trellis code so that by grouping together the output bits over the J branches, we may see this as a J/Jn code. This

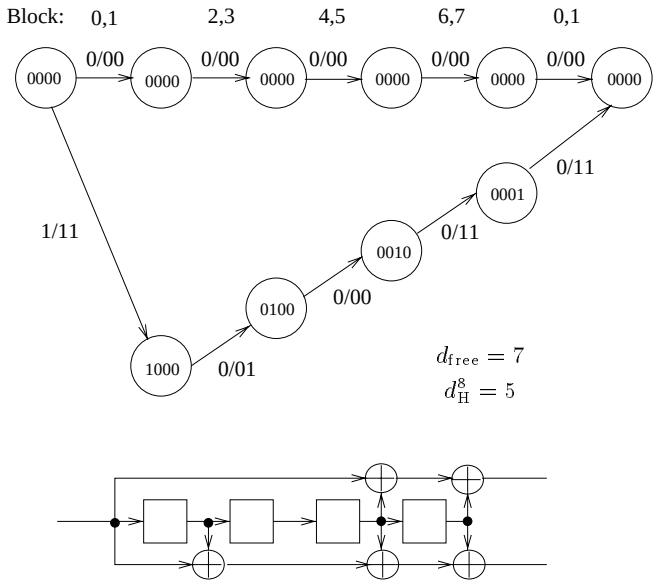

Figure 5.9: Minimum diversity/weight error event for full–rate GSM,

code design problem is quite different from the one we treat in this chapter for two reasons. Firstly, as the code complexity increases, the diversity also increases, since it is not fundamentally limited by a finite number of degrees of freedom. In fact, Kaplan *et al.* [KSSK95] give a bound on the diversity as a function of the number of states of the encoder. Secondly, the code search procedure is simpler since, although there is no interleaving, the frequency–hopping takes the place of an ideal interleaver using J adjacent bits at a time. In the case we treat here, the cyclic nature of the correlations can yield very long code sequences with low diversity. We are therefore often required to scan the trellis to a great depth to assure that these codewords are not in the code. This is easily explained with an example: consider the 16–state rate 1/2 code with generators $g_1 = (10101)$ and $g_2 = (11111)$ which has $d_{\mathrm{free}} = 6$. Let us use it on a channel with $F = 8$. An input $(10\cdots0)$ yields $(11011101110\cdots0)$ which has $d_{\mathrm{H}}^{8} = 6$. Similarly $(1010\cdots0)$ yields $(110100000001110\cdots0)$ with $d_{\mathrm{H}}^{8} = 5$ and $(101010\cdots0)$ yields $(110100001100000111 0\cdots0)$ with $d_{\mathrm{H}}^{8} = 4$. This example shows that it is possible that long low diversity codewords with high d_{free} can exist and have to be accounted for. We have found that in some cases they can be much longer than in this example. Even for this example an input of $(1010001010\cdots0)$ yields a codeword with $d_{\mathrm{H}}^{8} = 4$.

5.2.2 Maximum Diversity Bound

We begin by deriving a upper–bound on d_{H}^F taken over all codeword pairs as a function of R and the constellation size. Although d_{H}^F is the principle asymptotic indicator of the PEP for any coding scheme, we must keep in mind that it does not necessarily accurately indicate the total probability of error for low signal–to–noise ratios.

In order to determine the minimum pairwise d_{H}^F, it is convenient to group together the N symbols which are transmitted in the same block, and view them as a super-symbol over $\mathcal{S}^N$. The codeword is then a vector of length F super-symbols. Using this interpretation, d_{H}^F is simply the Hamming distance in $\mathcal{S}^N$. This reduces the analysis to one of non–binary block codes with a fixed block length F, and therefore all traditional bounding techniques apply.

An important first observation is that the highest rate code which achieves $d_{\mathrm{H}}^F = F$ has $R = \frac{1}{F}\log_2|\mathcal{S}|$ bits/dim. This follows directly from the fact that no two codewords can have identical symbols in the same position if $d_{\mathrm{H}}^F = F$. We can achieve this, for example, using a repetition code over $\mathcal{S}^N$, or the multidimensional constellations of Giraud and Belfiore [GB96] and Boutros *et al.* [BVRB96], which we will consider shortly. This was also remarked in [LWK93].

The question remains, therefore, how close we can get to $d_{\mathrm{H}}^F = F$ with high–rate codes and simple constellations. The answer lies in the Singleton bound [Sin64] which is proven in this context, for the sake of completeness, in the following theorem:

Theorem 3 (Singleton Bound)

Any code $\mathcal{C}$ of rate R bits/dim with M codewords consisting of F blocks of length N symbols from a one–dimensional alphabet $\mathcal{S}$ has d_{H}^F satisfying

$$d_{\mathrm{H}}^F \leq 1 + \left\lfloor F\left(1 - \frac{R}{\log_2|\mathcal{S}|}\right)\right\rfloor. \tag{5.18}$$

Proof: Let k ($0 < k \leq F-1$) denote the integer value satisfying $|\mathcal{S}|^{N(k-1)} < M \leq |\mathcal{S}|^{Nk}$, where $M = 2^{NFR}$. Consider any set of $k-1$ coordinates, for instance $i = 0, 1, \cdots, k-2$. Since $M > |\mathcal{S}|^{N(k-1)}$ there are necessarily at least two codewords, $\mathbf{x}, \mathbf{y} \in \mathcal{C}$ such that $\mathbf{x}_i = \mathbf{y}_i, \forall i \in \{0, 1, \cdots, k-2\}$. It follows that $d_{\mathrm{H}}^F \leq F - k + 1$ and therefore that

$$M \leq |\mathcal{S}|^{N(F - d_{\mathrm{H}}^F + 1)}. \tag{5.19}$$

Using the fact that d_{H}^F must be an integer yields (5.18). ■

We show the bound on d_{H}^F as a function of $R/\log_2|\mathcal{S}|$ and F in Fig. 5.10, where the value of F for each curve is simply the horizontal intercept.

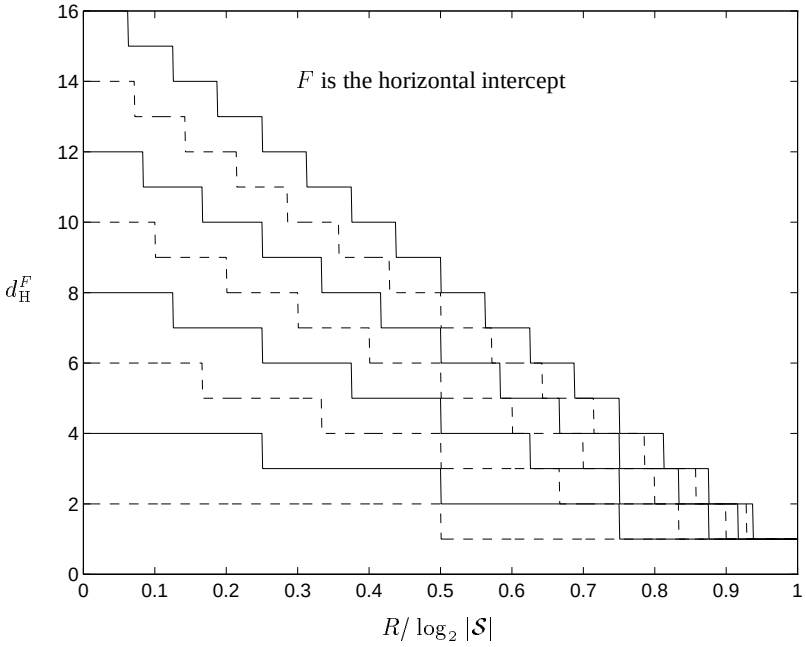

Figure 5.10: Singleton bound on d_{H}^{F} as a function of $R/\log_2|\mathcal{S}|$

The first interesting result of this analysis is that the shape of the constellation is not important with regard to the code diversity since it is a completely algebraic measure of the performance. The class of *maximum distance separable codes* (MDS) therefore play a large role in this context. An MDS code is one which meets the Singleton bound, such as the *Reed–Solomon (RS) codes*. There is a downside, however, which is that the block length of the code is constrained to be F which means that many existing codes cannot necessarily be used effectively. Shortly, however, we give some examples of codes which can be used with practical choices for F and guarantee maximum diversity. Secondly, and more importantly, we see what was remarked earlier in the information–theoretic analysis concerning constellation expansion. Take for example transmission at $R = .5$ bits/dimension over $F = 8$ blocks as in full–rate GSM . With binary modulation ($|\mathcal{S}| = 2$), the maximum pairwise diversity is 5, which incidently is what is achieved by the coding scheme used in GSM. With quaternary modulation we see that it can be increased to 7. Examining the slopes of the information outage curves in Fig. 5.4 we see that both results agree. On the downside, for high code rates (> 2 bits/dimension) very large symbol alphabets are required to achieve high asymptotic diversity. For example, with $F = 8$ and $R = 3$ bits/dimension, a 16-point constellation can only achieve a diversity of $d_{\mathrm{H}}^{8} = 3$. To achieve $d_{\mathrm{H}}^{8} = 7$ a constellation with 4096 points per dimension is needed. Since these are only asymptotic results, they may be somewhat pessimistic at low signal–to–noise ratios. We see from the information outage curves

that this is indeed the case, since the slopes of the curves start to decrease towards their asymptotic value as the SNR increases.

5.2.3 Block Codes

Let us first consider some examples of linear block codes of codeword length F with k information symbols, so that the rates of the codes are $R = \frac{k}{F}\log_2|\mathcal{S}|$ bits/dim. For this case the Singleton bound assures that $d_{\mathrm{H}}^F \leq F - k + 1$.

Repetition codes

As we already pointed out, the simplest possible coding scheme for achieving diversity F is repetition coding. A generalized repetition code for the case $N = 1$ has generator matrix $\mathbf{G} = \begin{pmatrix} 1 & 1 & \cdots & 1 \end{pmatrix}$ so that codewords are formed as

$$\mathbf{c} = u\mathbf{G} \tag{5.20}$$

where $u \in \mathcal{S}$. The number of codewords is $M = |\mathcal{S}|$ and the spectral efficiency is $\log_2|\mathcal{S}|/F$ bits/dim.

Multidimensional Constellations

The multidimensional lattice codes considered by Giraud and Belfiore [GB96] and Boutros *et al.* [BVRB96] are perfectly suited for the block–fading channel, since they consider constellations over a finite and small number of dimensions. Each dimension has an independent signal attenuation, and therefore in the context of the block–fading model, this is equivalent to letting F be the number of dimensions and $N = 1$. In [GB96] the constructed codes have dimensionality $2 \leq F \leq 8$ and $M = 2^{2F}$ points (codewords) which have diversity F. We show a particular constellation carved out of a hexagonal lattice for the case $F = 2$ in figure 5.11(a). If we project the points of the lattice for this example on each dimension, we obtain a one–dimensional constellation with $|\mathcal{S}| = 16$ points. The lattice may therefore be considered as a block code with $F = 2$ over this one–dimensional alphabet. This code therefore satisfies the Singleton bound with equality and uses the smallest constellation size to achieve $d_{\mathrm{H}}^2 = 2$. The repetition code for $F = 2$ using a 16-AM constellation looks different (see figure 5.11(b)), but has the same number of codewords and spectral efficiency. It makes much less efficient use of the signal space, however, which has a significant effect on the Euclidean distance between signal points, and thus on the secondary performance measure, χ. In general, when the multidimensional constellations are projected onto the coordinate axes,

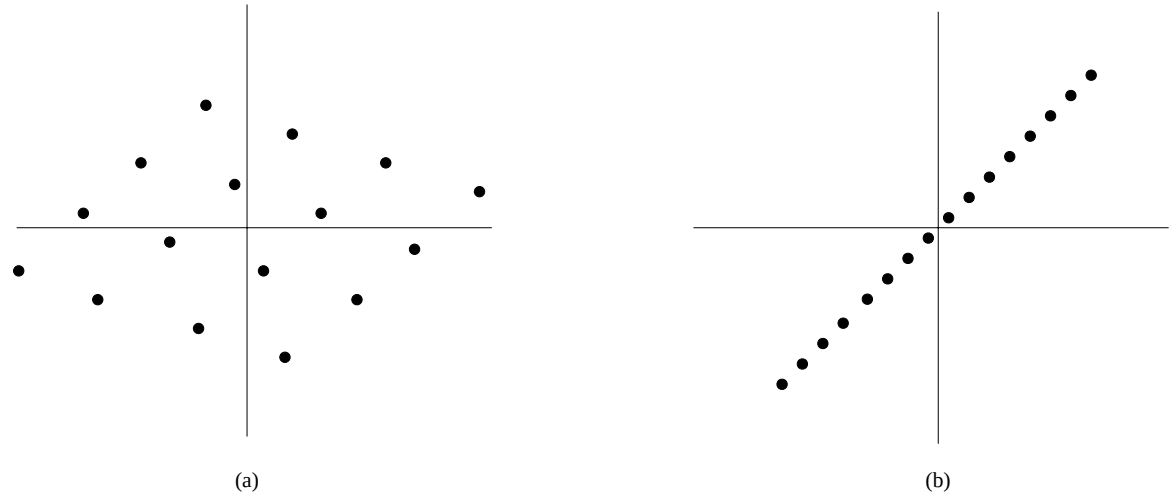

Figure 5.11: Giraud and Belfiore's 2-dimensional Lattice constellation *vs.* repetition coding

they produce non–uniformly spaced AM constellations. Another simple two–dimensional example to illustrate this point is the rotated QPSK constellation shown in figure 5.12 with spectral efficiency 1 bit/dim which was considered by Boullé and Belfiore in [BB92]. They showed that by rotating the constellation by $\pi/8$, the inherent diversity of the constellation is 2 and χ is maximum, under the assumption, of course, that both dimensions undergo independent channel realizations. We show the projection of the constellation on each axis where we note that it is a non–uniform 4AM constellation. In what follows we will consider the combination of a trellis code with uniform AM constellations, however, in light of this observation, it may also be appropriate to consider non–uniformly spaced constellations in order to improve performance. Boutros *et al.* [BVRB96] applied this rotation idea to known lattices which work well on the Gaussian channel to yield constellations with high diversity on the fading channel.

The parameter χ for these constellations is limited because of the fact that $N = 1$. In order to achieve higher coding gain, therefore, they must be concatenated with an error–control code, which will reduce the spectral efficiency of the system. Moreover, this places a significant burden on the receiver if high diversity is sought since the constellation itself is difficult to decode. In section 5.2.4, we take a different approach by considering simple constellations with binary trellis codes for achieving high diversity. This has the advantage of yielding larger values for χ since coding is performed across a larger number of symbols per block (i.e. $N > 1$.)

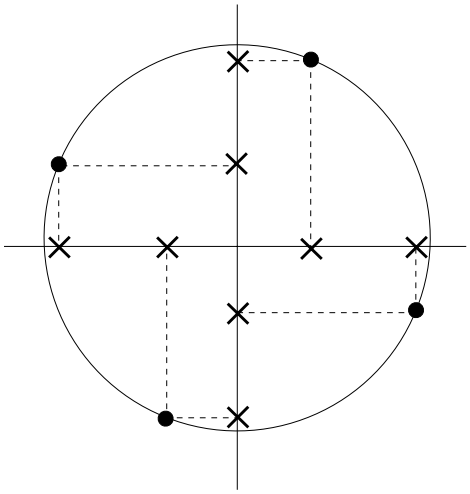

Figure 5.12: Rotated QPSK constellation

Short non–binary codes

We now consider MDS code families for systems having $F = 4, 6, 8$ formed by either shortening or lengthening RS codes such that they have block length F. Shortening RS codes by removing information symbols results in a code with the same d_{H}^{F} as the base code[Wil96]. Similarly, it is shown in [Wol69] that up to 2 information symbols can be added to an RS code without changing d_{H}^{F}. For the case $F = 6$ we also consider a particular less complex extended Hamming code which is also MDS. The combination of the constraints imposed by the structure of the codes and the number of blocks in the system does not assure minimal complexity, nor the flexibility of choosing arbitrary symbol alphabets. Another negative aspect is that the purely algebraic structure of the codes pays no attention to the other less critical performance indicator, χ.

Example A : $F = 4$

Consider a family of codes with rate $R = k/4$ bits/dimension for use with binary modulation. Assuming we form symbols over GF(4) by forming pairs of bits from the same block, we start with the $(3, k-1)$ RS code over GF(4) with $d_{\mathrm{H}}^{4} = 5 - k$ and lengthen it to $(4, k)$. Following [Wol69] the resulting parity check matrix for this code family is

$$\mathbf{H} = \begin{pmatrix} 1 & 1 & \alpha & \alpha^2 \\ 0 & 1 & \alpha^2 & (\alpha^2)^2 \\ \vdots & \vdots & \vdots & \vdots \\ 0 & 1 & \alpha^k & (\alpha^k)^2 \end{pmatrix}. \tag{5.21}$$

These codes achieve maximum diversity for $k/4$ bits/dim with binary modulation. Clearly, we could also use the same code with a quaternary symbol alphabet to achieve $R = k/2$ bits/dimension and keep the same diversity. Here we see the first example of the effect of constellation expansion; if we take $k = 2$ and binary modulation we have $R = .5$ bits/dim and $d_{\mathrm{H}}^4 = 3$. With $k = 1$ and quaternary modulation the information rate is still $.5$ bits/dim but $d_{\mathrm{H}}^4 = 4$.

Example B : $F = 6$

We now examine another family of codes with binary modulation and $R = k/6$ bits/dim for the case when $F = 6$. Consider the $(7, k+1)$ family of RS codes over GF(8), having $d_{\mathrm{H}}^6 = 7 - k$. The parity check matrix for a shortened code family $(6, k)$ is given by

$$\mathbf{H} = \begin{pmatrix} 1 & \alpha & \alpha^2 & \cdots & \alpha^5 \\ 1 & \alpha^2 & (\alpha^2)^2 & \cdots & (\alpha^2)^5 \\ \vdots & \vdots & \vdots & \vdots & \vdots \\ 1 & \alpha^k & (\alpha^k)^2 & \cdots & (\alpha^k)^5 \end{pmatrix}. \tag{5.22}$$

This shortened family achieves maximum diversity for binary modulation and $R = k/6$ bits/dim. We can also use this family with 8-ary modulation to yield $R = k/2$ bits/dim and the same diversity level. It is interesting to point out that although the codes are optimal in an MDS (maximum diversity) sense, there may be other less complex codes which are also MDS. For example, the (6,3) extended Hamming code over GF(4) with generator matrix

$$\mathbf{G} = \begin{pmatrix} 1 & 0 & 0 & 1 & 1 & 1 \\ 0 & 1 & 0 & 1 & \alpha & \alpha^2 \\ 0 & 0 & 1 & 1 & \alpha^2 & \alpha \end{pmatrix}, \tag{5.23}$$

is also MDS with $d_{\mathrm{H}}^6 = 4$. It is much less complex than the (6,3) shortened RS code outlined above (64 codewords instead of 512). Moreover, it can be used with a quaternary signal set.

Example C : $F = 8$

As a final example we consider the case of a code family with $R = k/8$ bits/dimension when $F = 8$ and $N = 3$. Similarly to when $F = 4$, we look at the $(7, k-1)$ family of Reed–Solomon codes over GF(8), having $d_{\mathrm{H}}^8 = 9 - k$. The parity check matrix for the lengthened code family $(8, k)$ is given

by

$$\mathbf{H} = \begin{pmatrix} 1 & 1 & \alpha & \alpha^2 & \cdots & \alpha^6 \\ 0 & 1 & \alpha^2 & (\alpha^2)^2 & \cdots & (\alpha^2)^6 \\ \vdots & \vdots & \vdots & \vdots & \vdots & \vdots \\ 0 & 1 & \alpha^k & (\alpha^k)^2 & \cdots & (\alpha^k)^6 \end{pmatrix}. \tag{5.24}$$

This family achieves maximum diversity for binary modulation and $R = k/8$ bits/dim. As before, we can also use this family with 8–ary modulation yield $R = 3k/8$ bits/dim and the same diversity level.

5.2.4 Trellis Codes

In the GSM system today, as previously mentioned, rate 1/2 binary trellis (convolutional) codes are used. This is mainly due to the computational simplicity of implementing the Viterbi algorithm with soft decisions. The Singleton bound is also applicable to convolutional codes, since they can always be interpreted as very long block codes. In fact, in systems like GSM the convolutional codes are used in a block fashion by appending trailing zeros to the information sequence, and a one–shot decoding of the entire block is performed.

Let us consider two examples of trellis codes with M–ary constellations. We have been unable to find simple design rules for such codes which guarantee maximum diversity, as well as high values for χ. Similar problems occur when trying to apply Ungerböck's techniques [Ung82] to perfectly interleaved Rayleigh channels. The main problem with Ungerböck's construction is the parallel transitions in the trellis representation of the codes imply that the diversity order is 1. Divsalar and Simon [DS88] came up with a way around this problem by describing some multi–dimensional trellis codes for 8–PSK modulation. They were designed for perfectly interleaved channels, but suffer from very low diversity orders, and therefore offer very poor performance. Schlegel and Costello [SC89] proposed new 8–PSK trellis codes for perfectly interleaved channels using such techniques, but these only offer high diversity for a large number of states ($>$64). In the multidimensional approach, the trellis still has parallel transitions, but several output dimensions are associated with each branch. Provided the parallel transitions have large mutual Hamming distances, diversity is increased.

We can apply the same multi–dimensional approach to a block–fading channel if we let the number of output dimensions in each branch be F. We illustrate this with the two 2–state trellises in figure 5.13 for $F = 4$, both having .5 bits/dim. The trellis in figure 5.13(a) uses binary modulation and the one in figure 5.13(b) quaternary AM modulation. We have assumed unit energy constellations and we denote

the Euclidean distance between points separated by i positions by d_i^2. Here we have two codes which

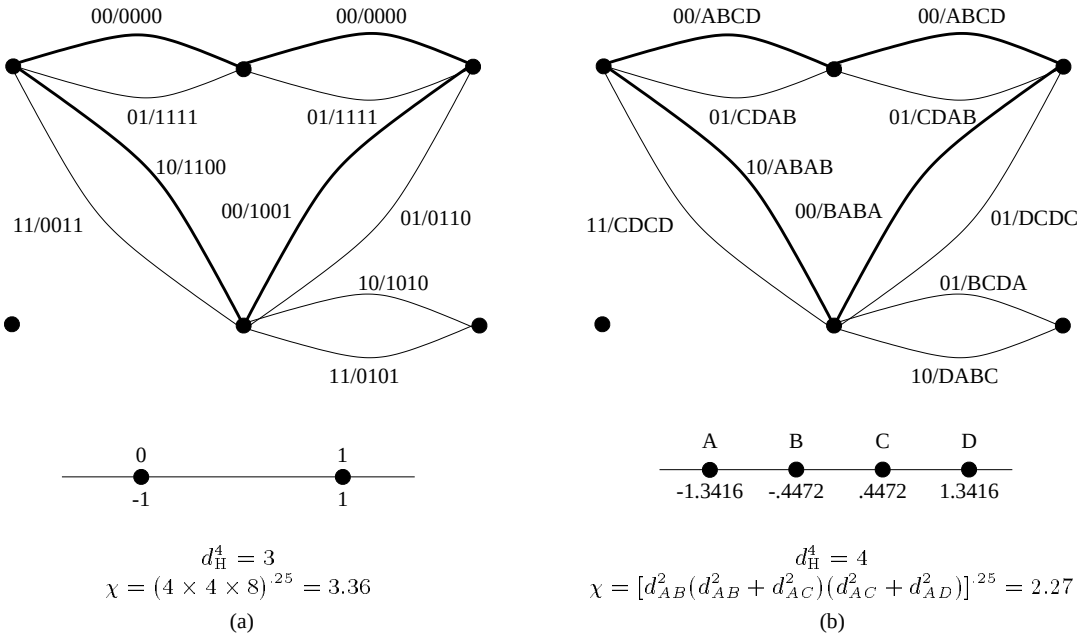

Figure 5.13: Two–state trellis code examples

meet the Singleton bound for $F = 4$, but suffer from small values of χ. If we compare the quaternary code, however, to a repetition code over the AM alphabet, there is an improvement in χ since in the latter case, it would simply be the minimum distance of the constellation $\chi_{\min} = d_1^2 = .8$. Extending this approach to larger values of F and more states becomes an exceedingly difficult and unrewarding task, since it is unclear how to choose the sets associated with the parallel transitions to jointly maximize d_{H}^F and χ. Moreover, using parallel transitions is not a good idea since χ will be limited. Another interesting approach for small values of F would be to use a trellis code with output on each branch coming from a (small) multidimensional constellation with maximal diversity. This would assure that the code has maximum diversity and χ would be significantly higher. We have opted to take a rather brute–force approach at finding more powerful trellis codes by performing extensive computer searches.

Code search for binary modulation

We have performed a code search using d_{H}^F as a primary performance criterion rather than d_{free} for binary rate $1/n$ trellis codes so that the diversity order of the code is maximum. At the same time we determine the number of states needed to achieve the maximum diversity indicated by the Singleton bound. We focused on maximum diversity rate 1/4, 1/3 and 1/2 codes for a varying numbers of blocks and states. The

results are summarized in Tables 5.1–5.3, where we have followed the convention of [LC83] regarding the octal representation of the generator polynomials. The table lists the codes which maximize d_{H}^F first and then χ as a secondary requirement and those marked in bold type meet the Singleton bound. We should note that searching for these codes is more computationally intensive than for those maximizing d_{free} since a simple dynamic–programming approach cannot be used to determine the minimum d_{H}^F path in the trellis because of the finite–depth interleaving. As a result of this and the fact that the trellis must be scanned to a very low depth to assure that there are no low diversity codewords, it is difficult to search for low–rate codes with many states. The search procedure was reduced somewhat by ruling out catastrophic codes.

As a first example, consider the case of $R = .5$ bits/dim with $F = 8$. We can achieve maximum diversity with an eight–state code, and moreover, it turns out that it does not exhibit maximum free Hamming distance ($d_{\mathrm{free}} = 5$, not 6). It is the only such code, so that it is a perfect example of the danger of using codes designed for ergodic channels. It is interesting to note that the GSM standard uses a 16–state maximum free Hamming distance code, which offers a slightly larger χ than its 8–state couterpart. The 16–state code listed in the table has a slightly larger χ than the GSM code, but we have found that the performance improvement is negligible. For the case of $F = 4$, maximum diversity can be obtained with a 4–state code, whereas in the GSM standard a 64–state code is used.

There are other important issues requiring the use of more complex codes. For instance, the 16-state code used in full–rate GSM achieves maximum diversity with $F = 2, 4, 6$ and 8, whereas the 8–state code achieves maximum diversity only with $F = 2, 4, 8$. This is important since in a frequency–hopping system, the number of hopping frequency is left up to the operator. Although we have not considered this issue, it would be interesting to determine "universally" good codes which achieve acceptable performance for many different values of F. The more important reason for increasing complexity, as we will see in section 5.3, is that larger values of $\chi_{\min}$ can yield significant coding gain in the frame error–rate performance.

Binary trellis codes with non–binary modulation

Since the first and most important goal is to maximize d_{H}^F we will consider linear binary trellis codes as before with an appropriate mapping of adjacent output bits to the non–binary constellation, $|\mathcal{S}|$. We have, therefore, that groups of $\log_2 |\mathcal{S}|$ adjacent bits are mapped into one symbol from $\mathcal{S}$. The interleaving is done on a symbol basis so that F adjacent symbols at the output of the encoder are transmitted in different blocks. We show two examples with 4–AM modulation in figure 5.14 which have .5 and 1 bits/dim. The

	$F=2$			$F=4$		
States	d_{H}^2	$\chi_{\min}$	gen	d_{H}^4	$\chi_{\min}$	gen
4	**2**	**17.89**	**5,7,3,3**	**4**	**7.80**	**5,5,7,7**
8	**2**	**24.00**	**64,64,34,34**	**4**	**12.90**	**64,64,54,74**
	$F=6$			$F=8$		
	d_{H}^6	$\chi_{\min}$	gen	d_{H}^8	$\chi_{\min}$	gen
4	**5**	**12.26**	**5,7,7,5**	6	7.27	5,6,7,7
8	**5**	**17.77**	**54,74,74,64**	**7**	**7.81**	**44,70,64,54**
	$F=10$			$F=12$		
States	d_{H}^{10}	$\chi_{\min}$	gen.	d_{H}^{12}	$\chi_{\min}$	
4	7	11.80	2,7,5,7	8	6.14	5,6,5,7
8	**8**	**7.45**	**44,54,74,74**	9	5.04	24,70,64,74
	$F=14$			$F=16$		
States	d_{H}^{14}	$\chi_{\min}$	gen.	d_{H}^{16}	$\chi_{\min}$	gen.
4	9	4.32	5,7,6,7	9	5.04	5,6,7,7
8	10	5.28	24,54,64,74	10	5.66	44,70,64,54

Table 5.1: Rate 1/4 bits/dim trellis codes for binary modulation

	$F=2$			$F=4$		
States	d_{H}^2	$\chi_{\min}$	gen	d_{H}^4	$\chi_{\min}$	gen
4	**2**	**13.86**	**6,7,3**	**3**	**17.93**	**6,6,7**
8	**2**	**17.89**	**64,64,74**	**3**	**29.27**	**54,74,64**
16	**2**	**19.60**	**42,76,32**	**3**	**37.13**	**46,76,66**
32	**2**	**24.00**	**61,65,37**	**3**	**49.75**	**51,31,77**
	$F=6$			$F=8$		
States	d_{H}^6	$\chi_{\min}$	gen	d_{H}^8	$\chi_{\min}$	gen
4	**5**	**5.28**	**5,6,7**	**6**	**4.00**	**5,3,7**
8	**5**	**7.55**	**44,60,64**	**6**	**6.00**	**44,70,64**
16	**5**	**11.30**	**32,54,76**	**6**	**12.00**	**42,56,62**
32	**5**	**14.08**	**54,65,67**	**6**	**15.09**	**41,67,53**
	$F=10$			$F=12$		
	d_{H}^{10}	$\chi_{\min}$	gen.	d_{H}^{12}	$\chi_{\min}$	
4	6	6.35	5,6,7	7	4.00	5,6,7
8	**7**	**6.93**	**64,54,74**	8	4.00	44,64,54
16	**7**	**11.41**	**46,52,76**	8	6.26	62,66,76
32	**7**	**15.85**	**66,47,34**	**9**	**5.44**	**54,73,67**
	$F=14$			$F=16$		
States	d_{H}^{14}	$\chi_{\min}$	gen.	d_{H}^{16}	$\chi_{\min}$	gen.
4	7	5.38	7,5,7	8	4.00	5,7,7
8	8	8.54	44,64,74	9	4.00	11,51,71
16	9	5.44	62,72,56	10	4.00	72,62,56
32	9	8.48	54,27,35	10	5.72	51,37,76

Table 5.2: Rate 1/3 bits/dim trellis codes for binary modulation

	$F=2$			$F=4$		
States	d_{H}^2	$\chi_{\min}$	gen	d_{H}^4	$\chi_{\min}$	gen
4	**2**	**9.80**	**5,7**	**3**	**6.35**	**5,7**
8	**2**	**12.00**	**64,54**	**3**	**10.08**	**64,54**
16	**2**	**12.65**	**62,72**	**3**	**13.21**	**62,46**
32	**2**	**16.00**	**62,72**	**3**	**14.54**	**75,57**
64	**2**	**17.89**	**704,564**	**3**	**17.93**	**724,564**
	$F=6$			$F=8$		
States	d_{H}^6	$\chi_{\min}$	gen.	d_{H}^8	$\chi_{\min}$	gen.
4	**4**	**5.66**	**5,7**	4	5.66	5,7
8	**4**	**6.26**	**64,74**	**5**	**4.00**	**44,64**
16	**4**	**8.24**	**62,56**	**5**	**5.28**	**46,66**
32	**4**	**11.31**	**21,75**	**5**	**8.19**	**51,66**
64	**4**	**14.65**	**664,854**	**5**	**10.90**	**444,774**
	$F=10$			$F=12$		
States	d_{H}^{10}	$\chi_{\min}$	gen.	d_{H}^{12}	$\chi_{\min}$	gen.
4	5	4.00	5,7	5	4.00	5,7
8	5	5.28	64,74	6	4.00	64,54
16	5	7.55	62,46	6	4.00	42,76
32	**6**	**5.04**	**61,75**	**7**	**4.42**	**51,67**
64	**6**	**7.27**	**644,564**	**7**	**6.30**	**724,534**
	$F=14$			$F=16$		
States	d_{H}^{14}	$\chi_{\min}$	gen.	d_{H}^{16}	$\chi_{\min}$	gen.
4	5	4.00	5,7	5	4.00	5,7
8	6	4.00	64,54	6	4.00	64,54
16	6	5.04	62,66	7	4.00	62,66
32	7	5.38	51,67	8	4.00	75,57
64	7	6.30	604,634	8	4.76	704,564

Table 5.3: Rate 1/2 bits/dim trellis codes for binary modulation

use of binary linear codes simplifies the code search since d_{H}^F preserves the linearity of the code. To see this let $\mathbf{c}^{(a)}$ and $\mathbf{c}^{(b)}$ be any two output paths in the trellis. Since $\mathbf{c}^{(a)} \oplus \mathbf{c}^{(b)} = \mathbf{c}^{(q)}$, where $\mathbf{c}^{(q)}$ is some other path and $\oplus$ is binary addition, we have clearly that

$$d_{\mathrm{H}}^F(\mathbf{c}_a, \mathbf{c}_b) = d_{\mathrm{H}}^F(\mathbf{0}, \mathbf{c}^{(q)}). \tag{5.25}$$

This means that as far as the diversity order is concerned, it suffices to compute the Hamming weight of

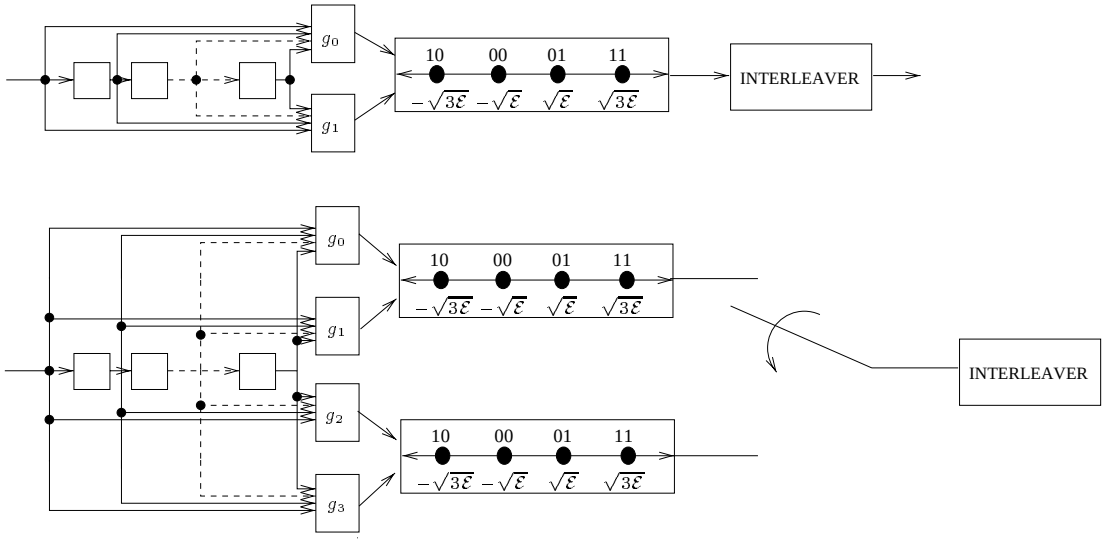

Figure 5.14: 4-AM Coding Example

each path as we did for the binary case, the only difference being that it must be performed on the symbol level. It is not necessary to consider all pairs of paths, which would greatly complicate the code search. The secondary performance measure in the PEP, $\chi_{\min}$ depends on the F Euclidean distances between the sub–codewords transmitted in each block. If we use *Gray coding* as in figure 5.14, then with 4–AM we cannot exploit the linearity of the code with respect to χ, but we can use it to lower bound χ as

$$\chi(\mathbf{c}^{(a)}, \mathbf{c}^{(b)}) \geq \chi^{\mathrm{lb}}(\mathbf{c}^{(a)}, \mathbf{c}^{(b)}) = \chi(\mathbf{0}, \mathbf{c}^{(a)} \oplus \mathbf{c}^{(b)}) \tag{5.26}$$

This lower bound is possible since under the Gray mapping $d^2(a,b) \geq d^2(0, a \oplus b), \forall a, b$ and in order to maximize it, we do not have to consider all pairs of paths in the trellis. This bound using the Gray mapping does not hold for larger AM constellations.

At the bottom of Table 5.4 we list some codes having $R = 1/2, 1$ bits/dimension for $F = 4, 8$. We must note that some of these codes were found with an incomplete search, due to the complexity of the search process (indicated in italics).

	$F=4$			$F=8$		
States	d_{H}^4	$\chi_{\mathrm{min}}^{\mathrm{lb}}$	gen.	d_{H}^8	$\chi_{\mathrm{min}}^{\mathrm{lb}}$	gen.
4	**3**	**1.6**	**5,7**	3	2.02	5,7
8	**3**	**2.02**	**44,64**	4	1.60	64,54
16	**3**	**2.78**	**26,76**	**5**	**1.27**	**26,74**
32	**3**	**3.33**	**51,76**	**5**	**1.84**	**75,23**
64	**3**	**4.25**	**364,574**	**5**	**2.21**	**744,634**

Table 5.4: Rate 1 bit/dim trellis–coded 4-AM modulations

	$F=4$			$F=8$		
States	d_{H}^4	$\chi_{\mathrm{min}}^{\mathrm{lb}}$	gen.	d_{H}^8	$\chi_{\mathrm{min}}^{\mathrm{lb}}$	gen.
4	**4**	**2.58**	**5,7,6,7**	6	2.02	5,7,6,7
8	**4**	**3.76**	**44,64,54,34**	**7**	**1.77**	**44,30,50,34**
16	**4**	**4.60**	**62,72,46,56**	**7**	**2.55**	**62,56,50,66**
32	*4*	*5.55*	*65,75,43,57*	*7*	*3.27*	*44,57,67,51*
64	*4*	*6.04*	*644,474,554,534*	*7*	*3.79*	*544,464,704,750*

Table 5.5: Rate 1/2 bits/dim trellis–coded 4-AM modulation

5.3 Computer simulation of various codes

We have found that a union–bound approach for assessing the performance analytically yields quite unfruitful results for trellis codes. The reason is that as we approach the maximum diversity F, the number of paths which share a given diversity level increases quickly as we progress through the code's trellis and enumerating them becomes difficult since they cannot be discarded. Another by–product of this effect which we remarked when the simulations were performed, is that error–patterns can be quite long (several times the constraint length) due to the limited diversity.

In our simulations, we assumed a block length $N = 100n/\log_2|\mathcal{S}|$ coded symbols, where n is the number of output bits of a rate $1/n$ binary trellis code. We used a one–shot Viterbi decoder with trellis termination. The channel is assumed to be a single–path Rayleigh fading channel and soft–decision decoding is performed with perfect channel state information. The results are shown in figure 5.15–5.26 and cover a wide range of systems. We considered systems with $F = 4$ and $F = 8$ blocks, information rates from .25 bits/dim to 1 bit/dim and simulated both frame and bit–error rates. We remark in general that for the frame error–rates, performance increases as we increase the complexity since the value of $\chi_{\min}$ increases. Since the block–length is fairly long, we may justifiably compare these results to the information outage probabilities we computed earlier. It is rather remarkable that we can come so close to the theoretical limit with reasonably simple codes. The binary code used in the half–rate GSM standard is less than one half of a decibel off from the information outage curve. We remark that this code is not the one listed in the tables since it has a $\chi_{\min}$ slightly less than the optimal code. Their performances are indistiguishable however. For $F = 8$, there is more of a gap between the codes and the theoretical limit. This can be explained by the fact that the channel is becoming more ergodic than with $F = 4$ and the code has to work much harder to get closer to the information outage probability. Examining the 4AM codes, the increase in diversity is evident. For low SNR, however, the frame–error rate performance is not significantly better than the binary codes. The performances of the 64–state codes for both $F = 4$ and $F = 8$ fall within two decibels of the information outage curves.

In terms of the bit–error rate performances, increasing complexity has less of an effect, especially for the case $F = 4$. We have observed that although less frame errors occur, the erroneous sequences tend to be much longer for the more complex codes and as a result contain many bit errors. We see that constellation expansion yields much more significant gains here than in the frame–error rate performance.

5.4 Chapter Summary

This chapter considered coding for block–fading channels with a small number of blocks. This channel model has significant practical importance for delay–constrained block–oriented communications, a category in which many mobile radio systems fall. The slow frequency–hopping scheme used in the current GSM mobile radio systems is a prime example. It is reasonable to assume that next generation systems will also use similar, and perhaps more complex techniques.

We focused our attention on the attainable diversity due to coding. We showed that there is a upper–limit to the diversity which depends on the number of blocks, the code rate and the size of the signaling constellation. This was shown in two ways; the first was based on the computation of the information outage probability for various constellations. We then computed a bound, which turns out to be a disguised version of the Singleton bound, which indicates the maximum achievable asymptotic diversity for a code of a given rate and constellation size. Both methods indicate that diversity is limited and that it can be increased by constellation expansion. A rather unfortunate result is that for high spectral–efficiency systems, in order to achieve a high asymptotic diversity level, very large constellations are required.

We gave examples of block and trellis codes, with more of an emphasis on the latter, which achieve maximum diversity. An important result is that maximum diversity can be achieved with rather simple codes and that, in terms of bit error–rate performance, increased complexity may not yield significant gains. This is not true, however, for the frame–error rate performance, which is often important in both speech and data applications.

We gave a few examples of trellis–coded AM modulation schemes which yield a higher level of diversity than binary modulation schemes of equal information rate. This is an area for further research, since similar higher spectral–efficiency schemes should be found with more appropriate modulation methods.

The channel model and codes covered in this chapter can be applied to several types of situations. For instance, a coded wideband multitone system or a partially interleaved narrowband channel. The performance analysis would be different since the blocks may be correlated, but the central conclusions of this chapter would remain valid.

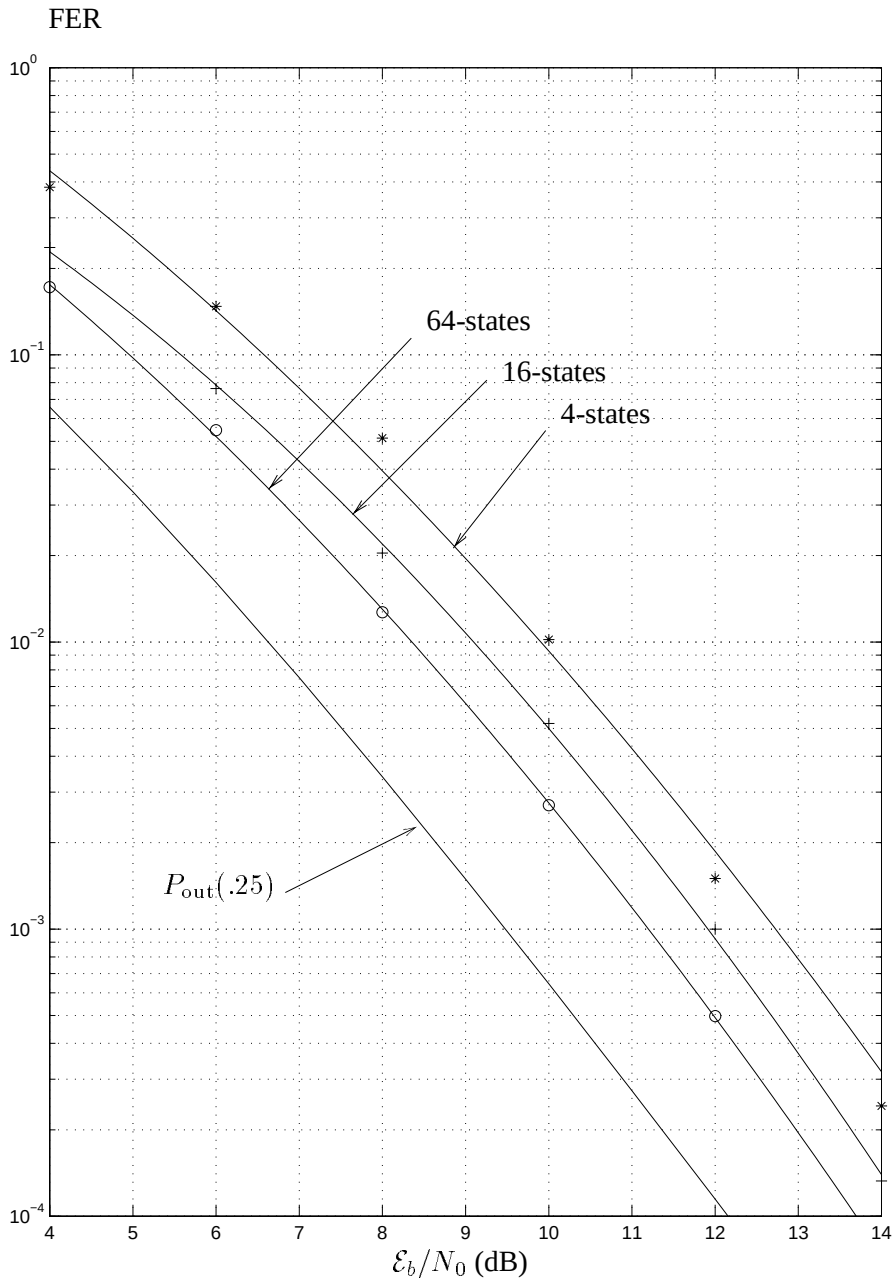

Figure 5.15: Frame Error Probabilities for $F = 4$ and $R = .25$ bits/dim (antipodal modulation)

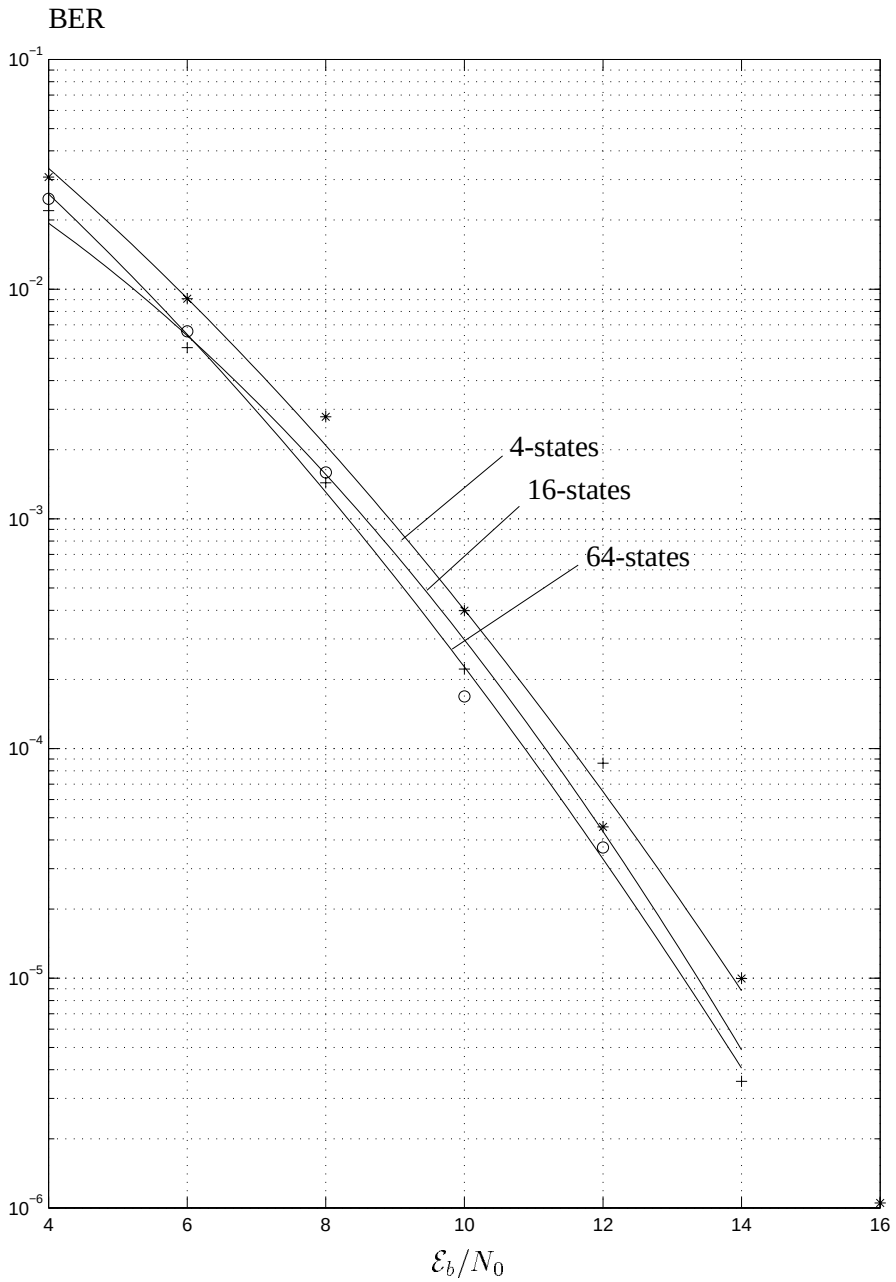

Figure 5.16: Bit Error Probabilities for $F = 4$ and $R = .25$ bits/dim (antipodal modulation)

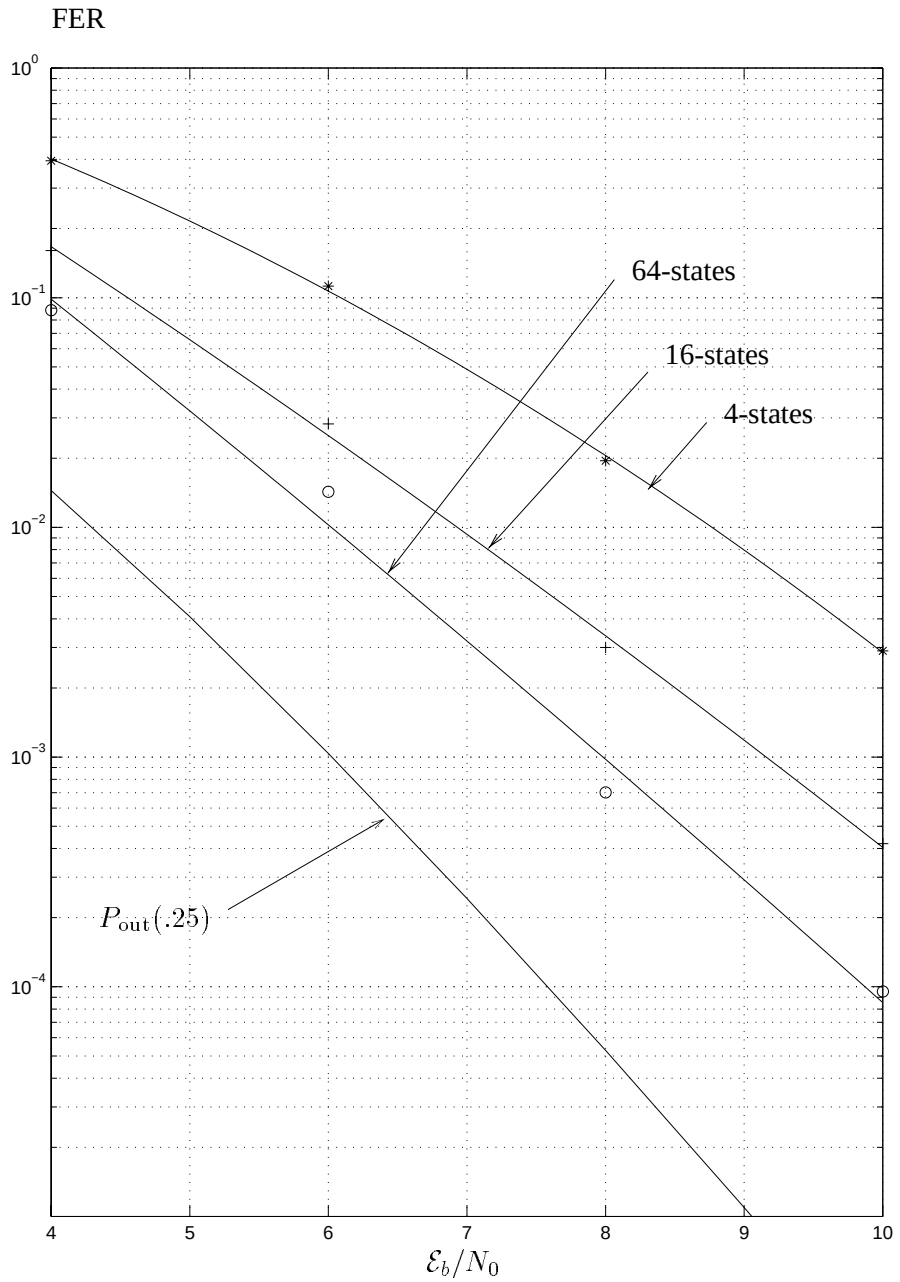

Figure 5.17: Frame Error Probabilities for $F = 8$ and $R = .25$ bits/dim (antipodal modulation)

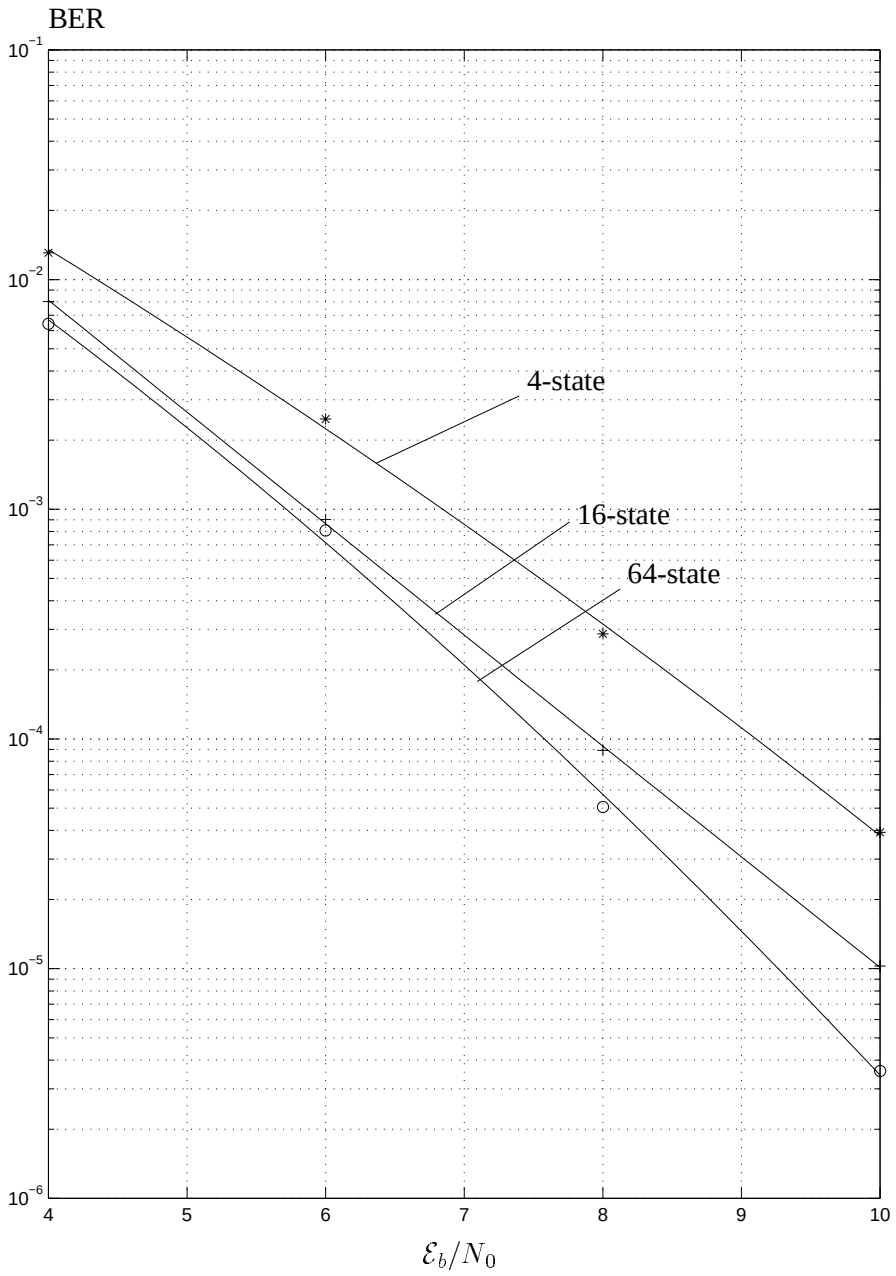

Figure 5.18: Bit Error Probabilities for $F = 8$ and $R = .25$ bits/dim (antipodal modulation)

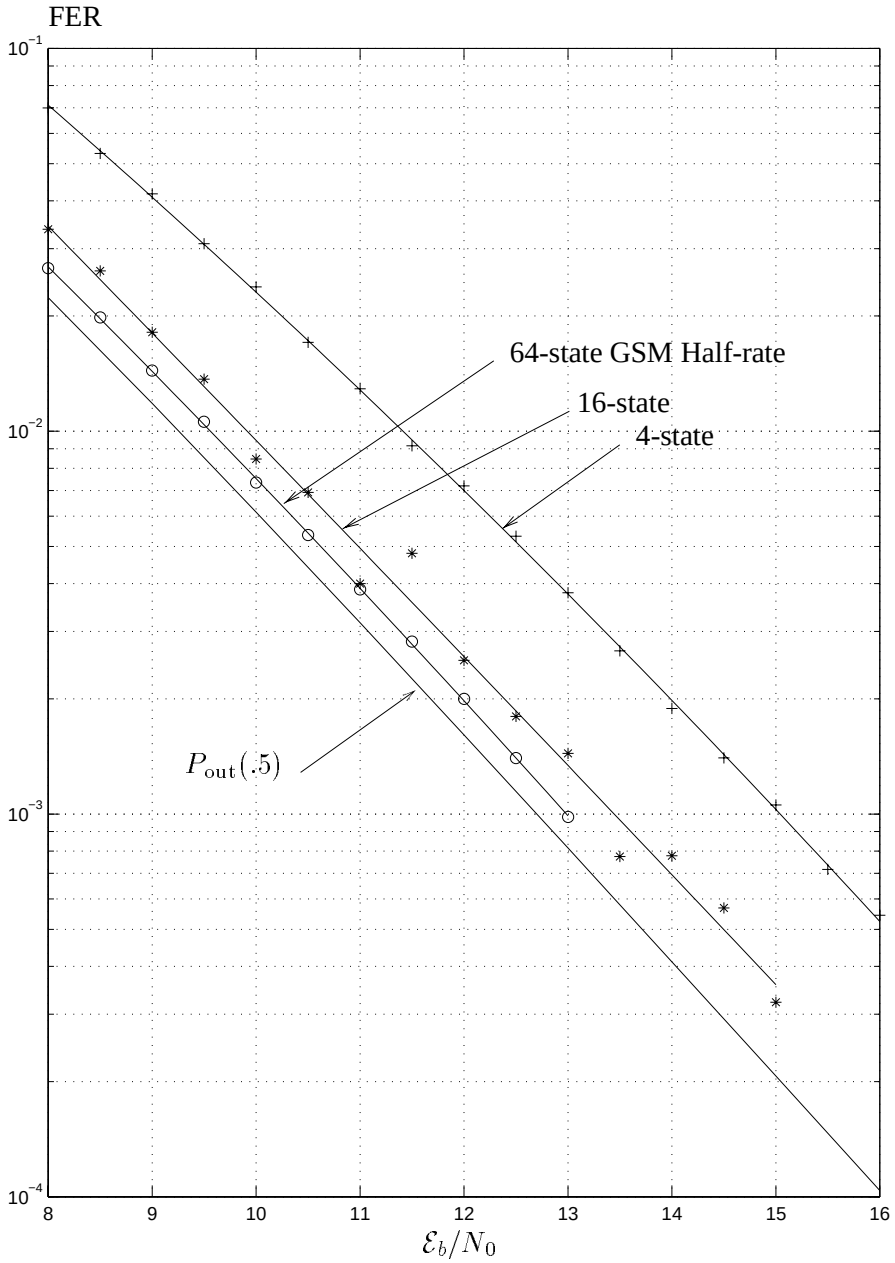

Figure 5.19: Frame Error Probabilities for $F = 4$ and $R = .5$ bits/dim (antipodal modulation)

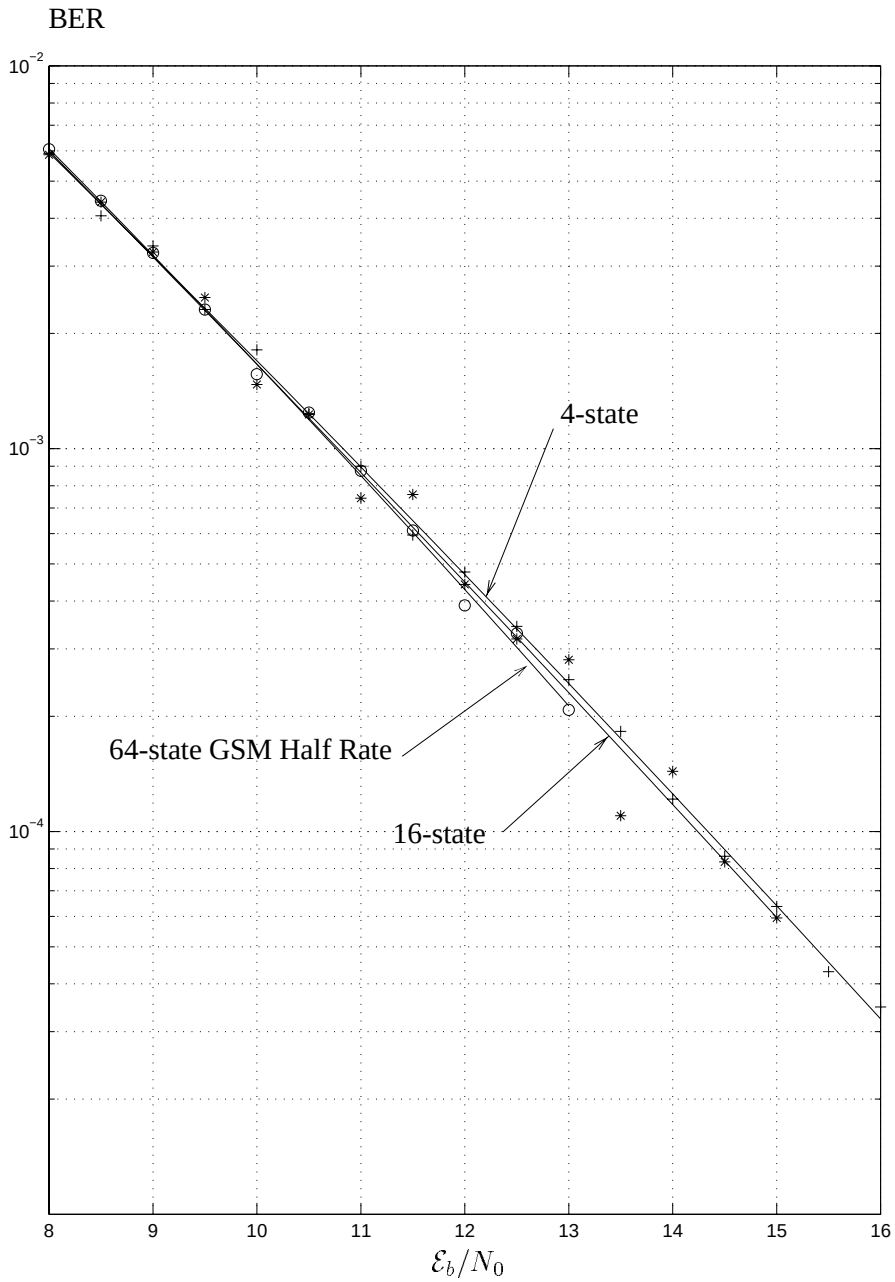

Figure 5.20: Bit Error Probabilities for $F = 4$ and $R = .5$ bits/dim (antipodal modulation)

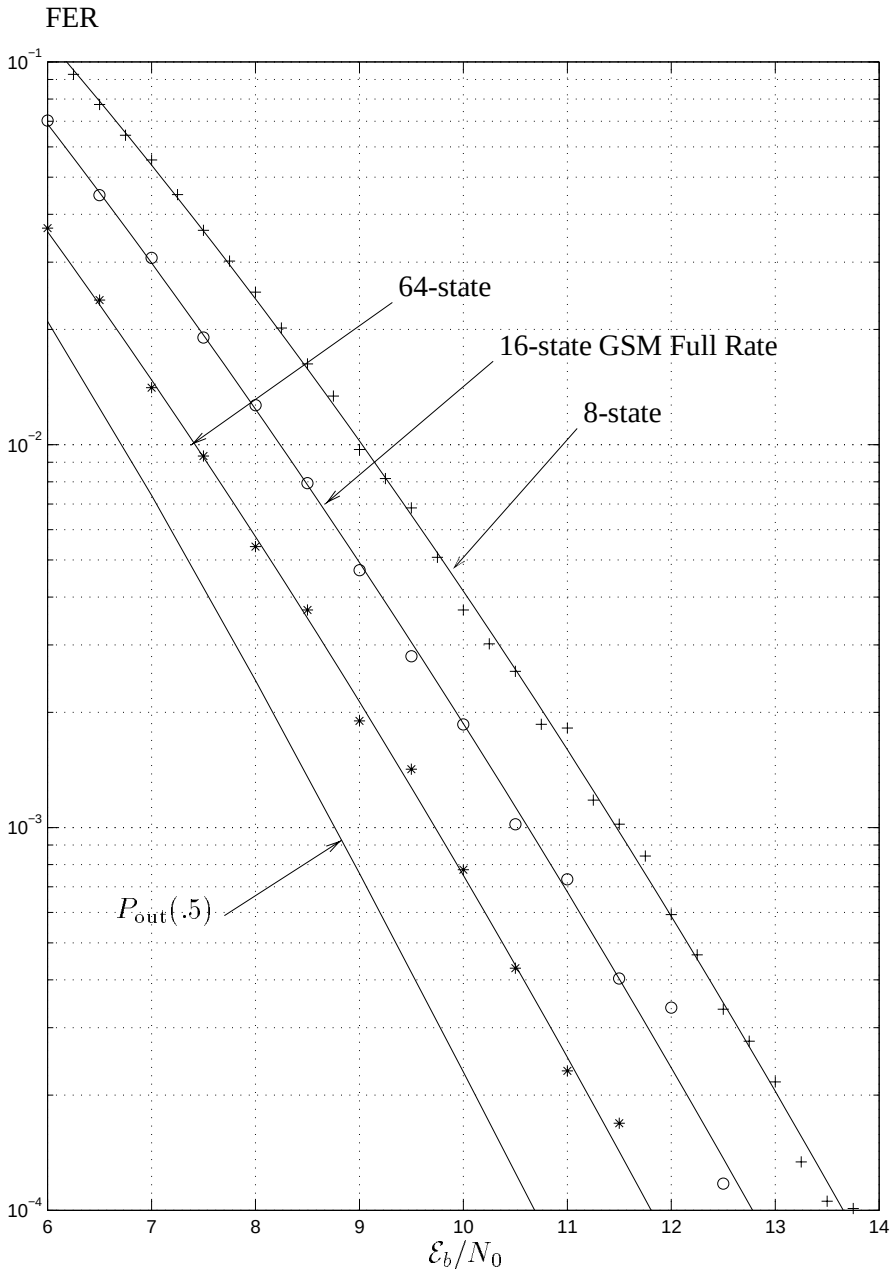

Figure 5.21: Frame Error Probabilities for $F = 8$ and $R = .5$ bits/dim (antipodal modulation)

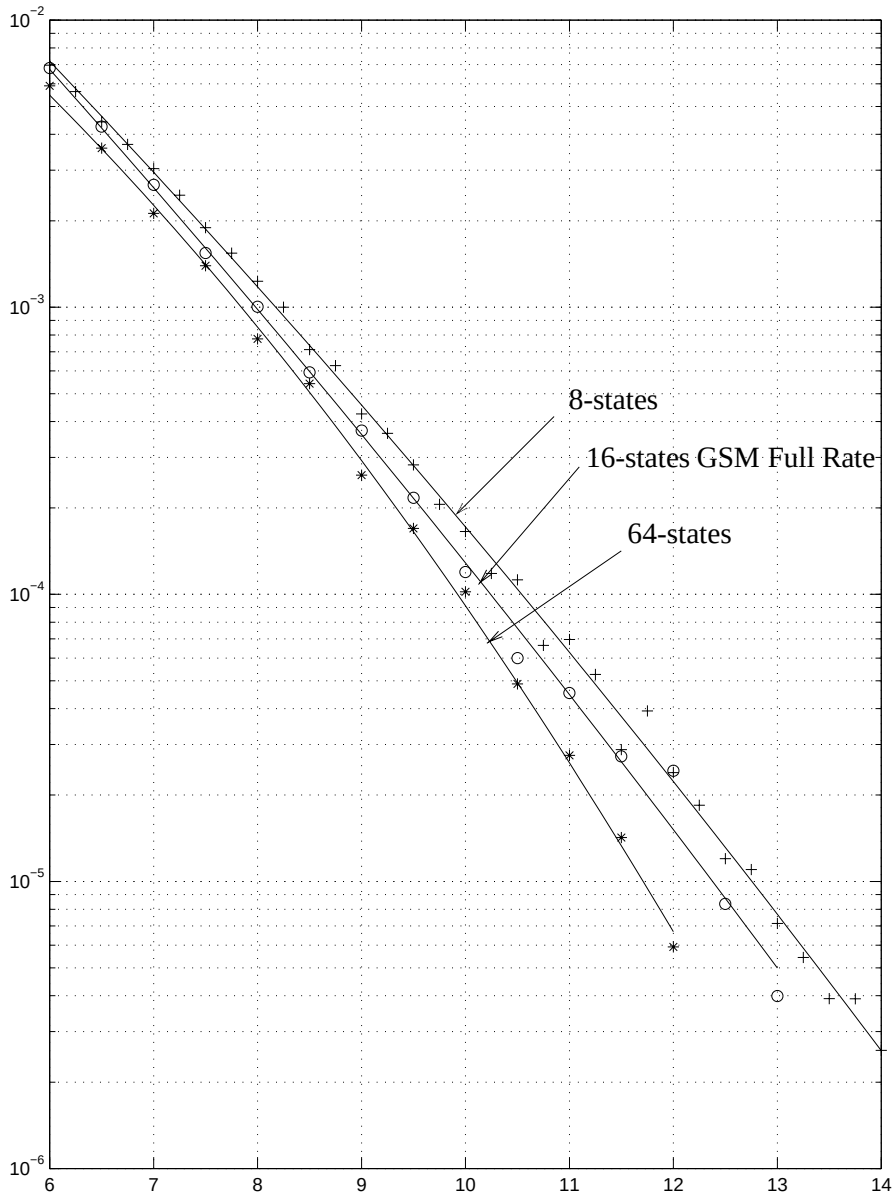

Figure 5.22: Bit Error Probabilities for $F = 8$ and $R = .5$ bits/dim (antipodal modulation)

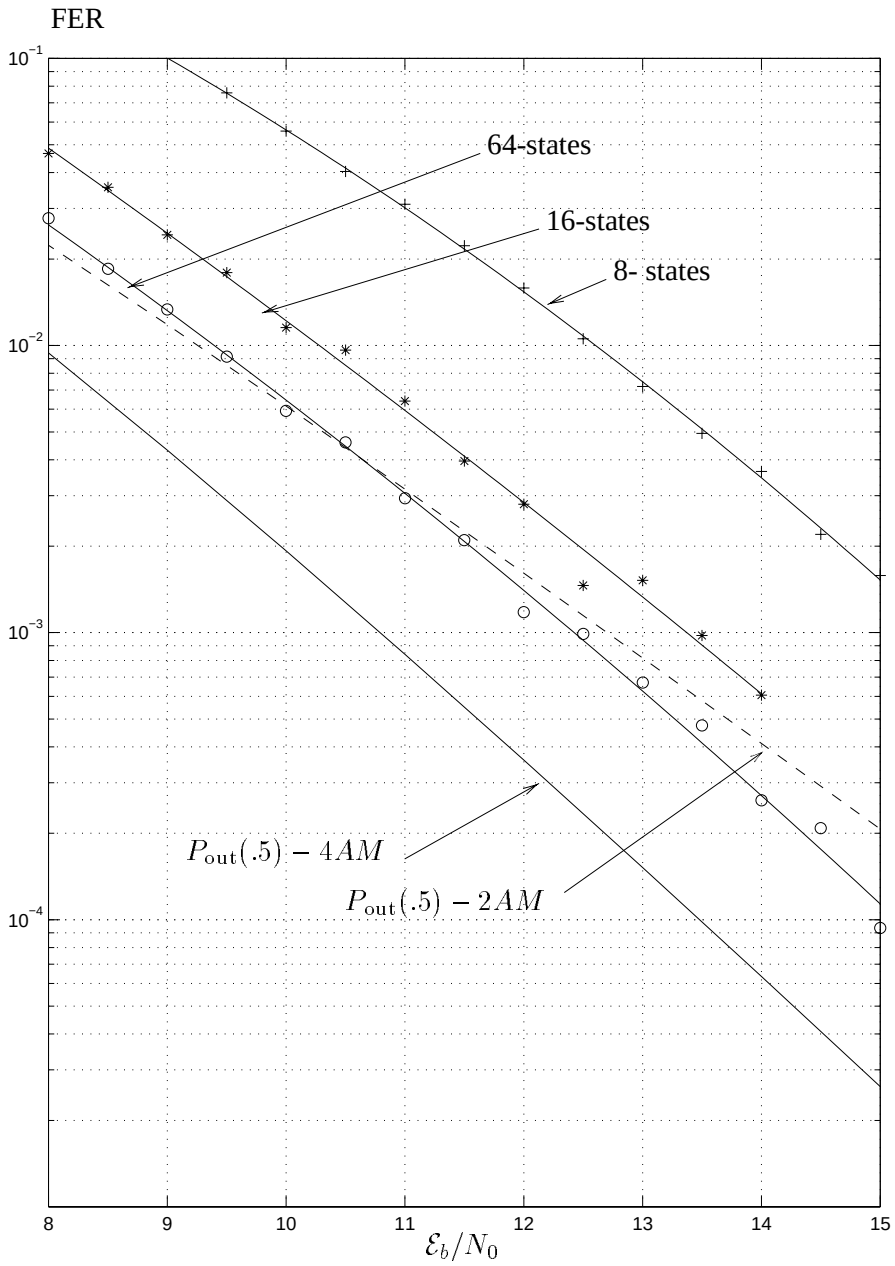

Figure 5.23: Frame Error Probabilities for $F = 4$ and $R = .5$ bits/dim (4 AM modulation)

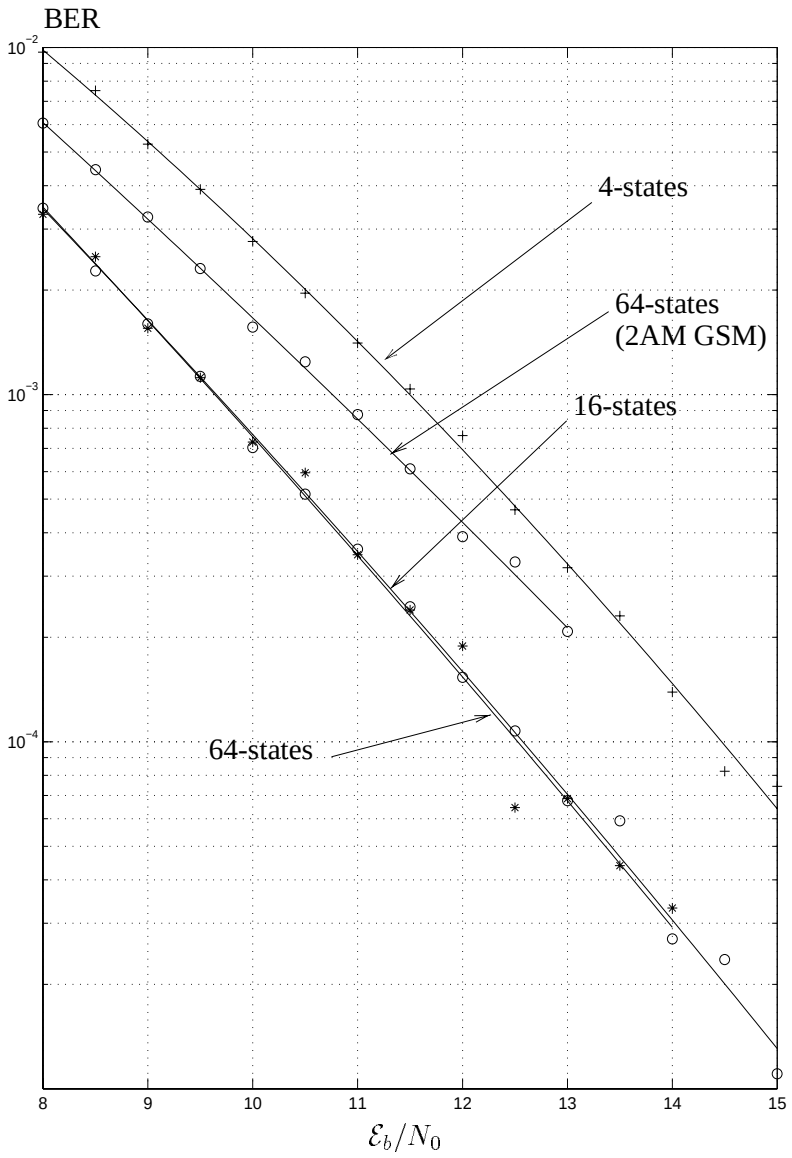

Figure 5.24: Bit Error Probabilities for $F = 4$ and $R = .5$ bits/dim (4 AM modulation)

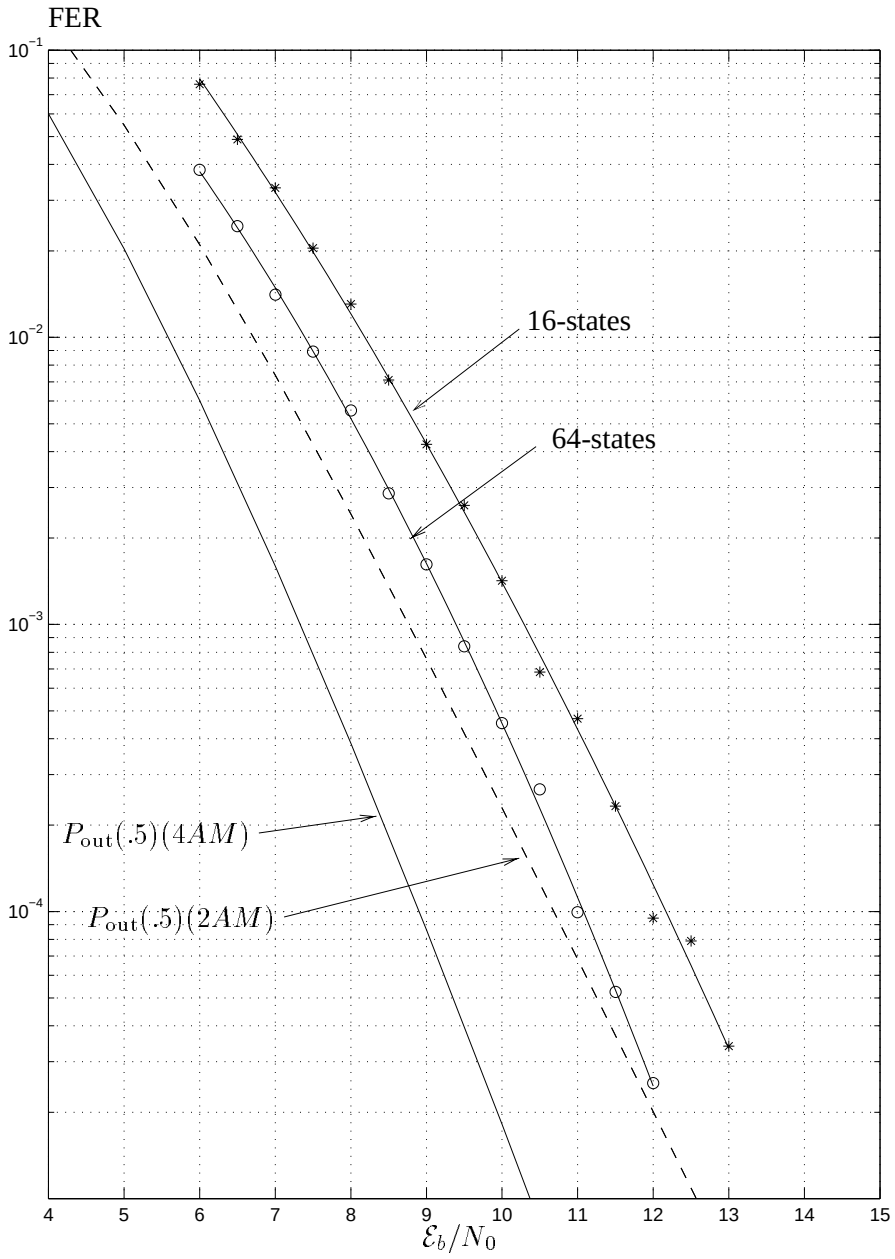

Figure 5.25: Frame Error Probabilities for $F = 8$ and $R = .5$ bits/dim (4 AM modulation)

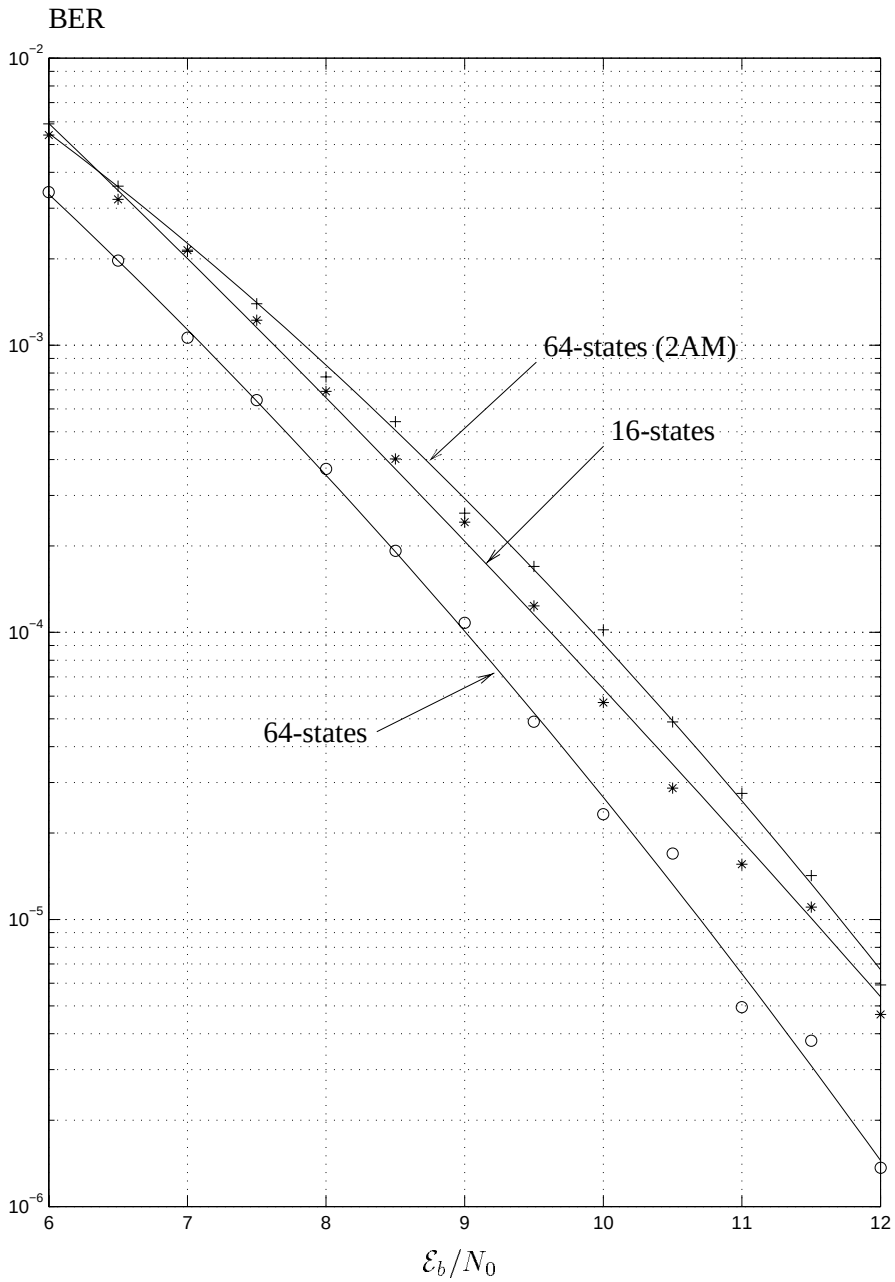

Figure 5.26: Bit Error Probabilities for $F = 8$ and $R = .5$ bits/dim (4 AM modulation)

Chapter 6

Systems Exploiting Channel State Feedback

In this chapter we consider the possibility of having *channel state feedback* (also known as *side information*) available at the transmission end so that outages at the receiver can be avoided. This includes adjusting the transmit power (*fast power control*) or the information rate (*variable–rate coding*). The IS95 system employs a feedback path for fast power control, which is critical in a CDMA system because of the near–far problem and fading [GJP+91]. Moreover, the updating is performed 800 times per second, so that accurate tracking of the channel state is feasible. We note, however, that the availability of channel state information does not necessarily imply a feedback path. In two–way wireless communication channels the up-link and down-link are often multiplexed in time. If this is the case and the channels do not vary too quickly, the signal arriving from the opposite link can be used to measure the channel(s). The *Digital European Cord-less Telecommunications System (DECT)* [Rap96b] and the *Personal Handy phone System (PHS)* [PHS95] already use some channel state information in this fashion. The mobile station uses the downlink signal which broadcasts across the entire system bandwidth to request allocation to the available channel in which his response is strongest. Some indoor cordless telephone systems also perform similar dynamic channel selection strategies.

We examine the role of fast power–control for both delay sensitive systems (section 6.1) and those which can tolerate long decoding delays (section 6.2). The average data–rate of a system employing variable–rate coding is presented. We show that this is completely equivalent to coding over an infinite number of degrees of freedom, from the point of view of spectral efficiency. We present an example of a simple two rate scheme which performs reasonably close to an optimal system.

The last part of this section deals with packet transmission over fading channels with a retransmission protocol, so that outages are corrected by an *Automatic Repeat reQuest (ARQ)* scheme [BG92]. We examine the maximum average information rate that can be expected on a collision–free channel, where outages are purely due to deep fades. This type of system is already in use in the data transmission mode of the GSM standard.

6.1 Variable Power Constant Rate Systems

When the transmitted signal can be tailored to the channel response, its statistics should be chosen to maximize average mutual information. Normally this maximum is given the name *channel capacity*, since this is the absolute maximum information rate at which communication can take place. Throughout this section we will assume that codewords are transmitted continuously across static multipath channels (for the duration of a codeword). The codewords are subject to the following average energy constraint

$$\mathrm{E}\, S_{x,n}(f) \leq \frac{P}{W} \tag{6.1}$$

where $S_{x,n}(f)$ is the power spectral density during the transmission of codeword n. We now adjust the power spectrum of the n^{th} codeword according the state of the channel, $H_n(f)$, as $S_{x,n}(f) = \mathcal{P}(H_n(f))$ such that the average mutual information at the receiver is constant and maximum for each codeword. This is known as the *delay–limited* capacity, defined by Hanly and Tse [HT96], which can be written explicitly as

$$C_d = \max_{\mathcal{P}} \int_{-W/2}^{W/2} \log_2 \left(1 + \frac{|H_n(f)|^2 \mathcal{P}(H_n(f))}{N_0}\right) df \quad \mathrm{bits/s} \tag{6.2}$$

subject to $\mathrm{E}_H \mathcal{P}(H_n(f)) \leq \frac{P}{W}$. It was given this name since the tolerable decoding delay is assumed to be small so that ergodic channel arguments cannot be used.

6.1.1 Multiple Receivers in Single–Path Rayleigh Fading

Let us consider the simplest case, namely frequency–flat channels. We may write the maximization problem as

$$C_d = \max_{\mathcal{P}} W \log_2 \left(1 + \frac{P}{W N_0} \alpha_n \mathcal{P}(\alpha_n)\right) \quad \mathrm{bits/s} \tag{6.3}$$

subject to $\int_0^\infty \mathcal{P}(u) f_\alpha(u) du = 1$. Clearly the only power control function which yields a constant average mutual information is $\mathcal{P}(u) = K/u$ so that

$$C_d = W \log_2 \left(1 + \frac{P}{WN_0} \frac{1}{\int_0^\infty f_\alpha(u) \frac{du}{u}} \right) \quad \text{bits/s.} \tag{6.4}$$

This expression was also found by Goldsmith in her doctoral thesis [Gol94]. We see, therefore, that in this simple case, the optimal delay–limited power control function is nothing but a perfect power controller, which attempts to keep the received SNR constant. If we use the Rayleigh fading model in (6.4) we see immediately that $C_d = 0$ since $K = \int_0^\infty e^{-u} \frac{du}{u} = \mathrm{E}_1(0) = \infty$ and therefore outages are inevitable. For systems employing some diversity this will not be the case, and outages can be avoided at the expense of transmitting at a high power when the channel state is weak. Let us examine simple multiple–antenna diversity schemes with maximal–ratio combining in Rayleigh fading. Assuming a system with L receivers the density function of the received energy is given by

$$f_\alpha(u) = \frac{u^{L-1}}{(L-1)!} e^{-u}, \; u \geq 0 \tag{6.5}$$

so that

$$K = \left(\int_0^\infty f_\alpha(u) \frac{du}{u} \right)^{-1} = L - 1 \tag{6.6}$$

and

$$C_d = W \log_2 \left(1 + (L-1) \frac{P}{WN_0} \right), \tag{6.7}$$

If there were no fading, the capacity of the multichannel system would be

$$C(L) = W \log_2 \left(1 + L \frac{P}{WN_0} \right), \tag{6.8}$$

so that for large L, the fading channel with power control loses very little in terms of spectral efficiency.

In order to better appreciate the effect of power control, let us compute the information outage probability for this example using (4.33) for $L = 2$ which yields

$$P_{\text{out}}(R) = 1 - \left(1 + (2^R - 1) \frac{WN_0}{P} \right) \exp \left(- \frac{WN_0}{P} \left(2^R - 1 \right) \right). \tag{6.9}$$

The power controlled information rate C_d for $\frac{P}{WN_0} = 10$ dB is plotted alongside (6.9) in Figure 6.1. We see that power control has a very significant effect since the outage probability is very high (.3) at $R = C_d$, which means that rates much less than C_d can be expected for practical outage rates. This outage rate is even close to a system without diversity which is shown in the second curve. The explanation for

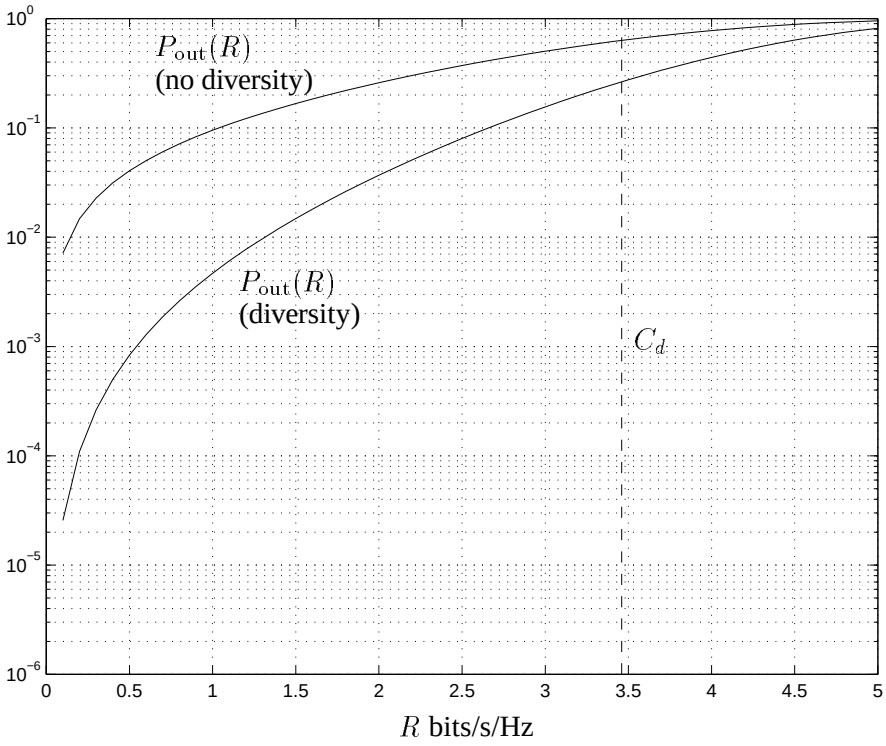

Figure 6.1: A delay–limited power control example

the effect of power control is that there is a much higher probability of having a signal amplitude above average in the diversity system. As a result, power is saved for when the signal amplitude falls below average, which also occurs less frequently than without diversity. We have not considered the selection diversity case since it will be treated in Chapter 6 when we treat multiuser systems.

6.1.2 Spread–Spectrum

Let us consider the case where we use power control in a spread–spectrum system (i.e. CDMA). This will be similar to the L receiver case, except that the each channel will be correlated and have different average strengths. As before we will use the the multi-tone model with maximal–ratio combining of the sub-bands as in (4.47) so

$$K = \frac{1}{\int_0^\infty \sum_{s=0}^{S-1} \frac{A_s}{\lambda_s} e^{-u/\lambda_s} \frac{du}{u}}. \tag{6.10}$$

From (4.48) we have that the capacity with power control is

$$C_d = \frac{1}{S} \log_2 \left(1 + \frac{KP}{WN_0} \right). \tag{6.11}$$

The values for K in dB as a function of S for the TU12 channel are -1.2860, 7.3224, 15.8094, and 19.6477 for $S = 4, 16, 64, 128$. If there were no fading, K would be equal to the number of sub–bands S so that the losses due to fading in dB are 7.3066, 4.7188, 2.25 and 1.42. As in the multichannel case, the diversity brings the performance of the system much closer that of the non–fading channel as the number of degrees of freedom increases.

We compare the information outage rates from (4.50) with C_d in figure 6.3 for the ETSI TU12 channel. As before we assume the bandwidth is SW_B with $W_B = 9.6$kHz and an SNR of $\frac{P}{WN_0} = 0$ dB. We see that as the bandwidth increases, the diversity has the effect of bringing the outage curve closer to C_d, so that power control has less of an effect. The reason for this is that the output of the maximal–ratio combiner tends quickly to 1 with increasing diversity, so that outages do not occur as frequently. For low diversity, as in the previous example we see that power control has a dramatic effect, even if the loss with respect to a non–fading channel is substantial. Even when the channel is more or less flat, for instance for $S = 4$, the second eigenvalue, which is almost insignificant (see Table 4.1), forces the density function of the channel gain to zero at the origin. This is shown in figure 6.2. As a result, outages can be effectively avoided by power control.

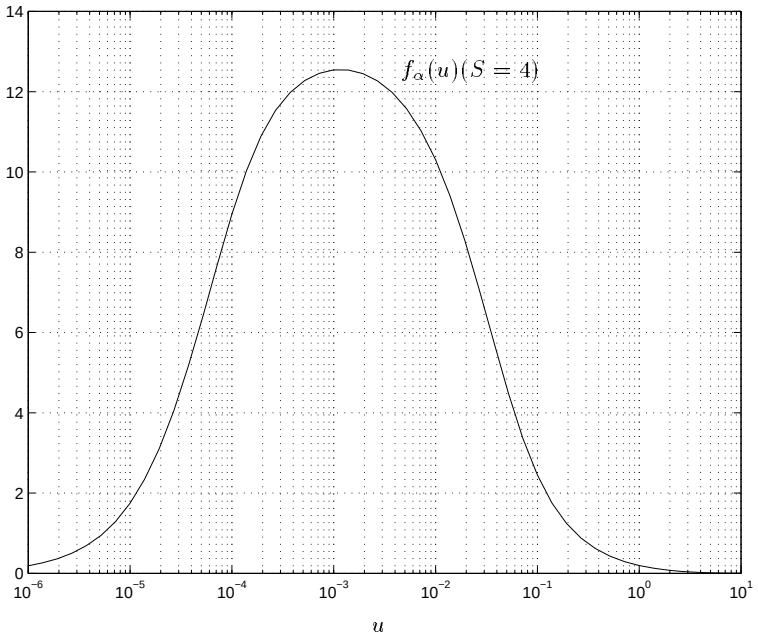

Figure 6.2: Probability density of channel gain for $S = 4$

The constraint (6.1) allows the transmit power of each codeword to vary according to the channel state, so that at certain times it can be quite high, in order to compensate for a poor channel state. If the

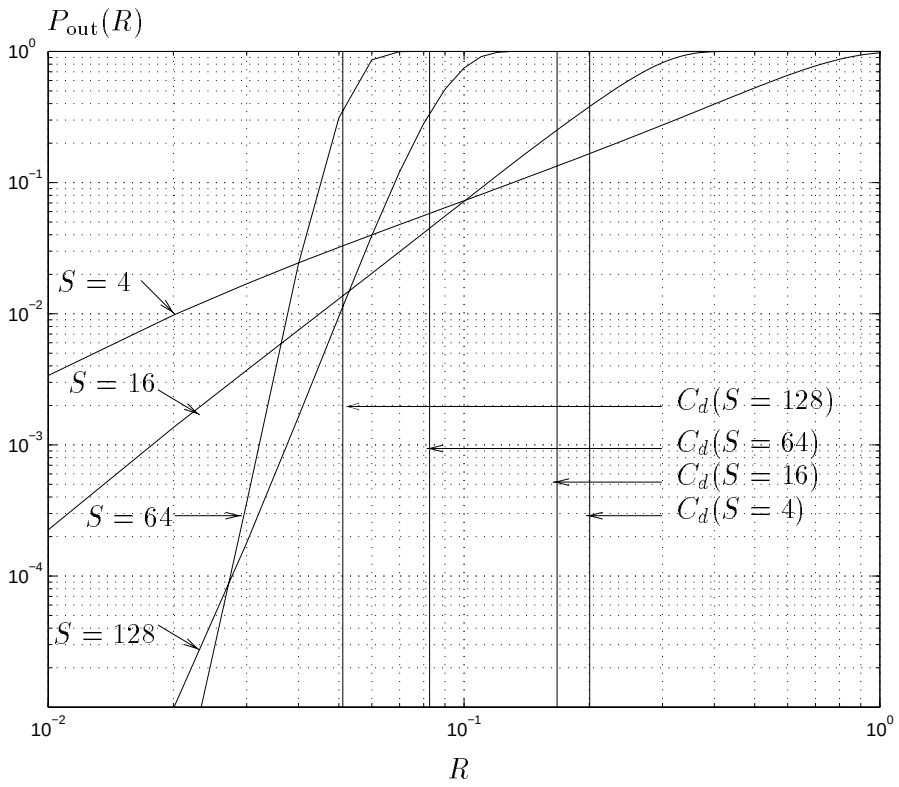

Figure 6.3: Comparison of spread–spectrum outage rates with C_d for $P/WN_0 = 0$ dB

transmitter has a peak–power limitation, there will always be times when it will be exceeded, thereby forcing the receiver into an outage situtation. In such cases, where outages can be controlled, it would be more wise to halt transmission and conserve power for when the channel state becomes acceptable. We will consider schemes such as this in section 6.2.

6.2 Variable Rate Schemes

6.2.1 Average Information Rates

Now let us assume that we can allow the average mutual information for each codeword to change, the goal being to maximize its average value. We saw earlier, that if we relaxed the decoding delay constraint in the block–fading channel (i.e. $F \to \infty$) we can communicate at any information rate less than I_∞ in (4.17). Suppose now we assume a constant power for each codeword (i.e. $S_{x,n}(f) = P/W$) and because of channel knowledge at the transmitter we choose the information rate

$$R_n = I_{H_n} = \int_{-W/2}^{W/2} \log_2 \left(1 + \frac{P}{WN_0}|H_n(f)|^2\right) df \quad \text{bits/s} \tag{6.12}$$

for codeword n. This assures that we never have an outage at the receiver. In practice, outage–like events still occur since when the channel is very weak R_n would be close to zero. The resulting average information rate is

$$\overline{R} = \lim_{N\to\infty} \frac{1}{N} \sum_{n=0}^{N} R_n = \overline{W \log_2 \left(1 + \frac{P}{WN_0}|H_n(f)|^2\right)} = I_\infty \tag{6.13}$$

which in Rayleigh fading is also given by (4.52). The integral in (6.12) can be removed since the statistics of $H_n(f)$ are invariant with frequency. We see, therefore, that a variable–rate system has the same average performance as a system which codes over an infinite number of degrees of freedom (i.e. infinite interleaving). As a result, the effects of frequency–selectivity are also averaged–out. The amount of time needed to achieve the average data rate I_∞ in a variable–rate scheme is equivalent to the depth of the interleaving (or number of uncorrelated carriers in frequency–hopping systems) needed to achieve I_∞ in a fixed rate scheme.

6.2.2 Water–Filling

Realizing the equivalence of variable–rate and long–term coding with interleaving, let us now consider the case when we can change the power spectrum for each codeword (block) according to the average constraint in (6.1). The goal is to choose $S_{x,n}(f)$ to maximize the conditional average mutual information (or the average information rate.) We refer to the maximum value as the *average channel capacity*, C_∞, which is solution to following maximization problem

$$C_\infty = \max_{S_{x,n}(f)} \overline{W \log_2 \left(1 + \frac{P}{WN_0} S_{x,n}(f)|H_n(f)|^2\right)} \text{ bits/s} \tag{6.14}$$

subject to (6.1). The solution for a frequency–flat channel was found by Goldsmith [Gol94] and is completely analogous to the water–filling solution for time–invariant non–fading channels [Gal68]. Generalizing this result, we have that the form of the optimal power spectrum for each block (codeword) is

$$S_{x,n}(f) = \begin{cases} B - \left(\frac{WN_0}{P}\right) \frac{1}{|H_n(f)|^2} & |H_n(f)|^2 \geq \frac{WN_0}{BP} \\ 0 & \text{otherwise} \end{cases} \tag{6.15}$$

where B is the solution to

$$\int_{\frac{WN_0}{PB}}^{\infty} \left(B - \left(\frac{WN_0}{P}\right)\frac{1}{\alpha}\right) f_{|H|^2}(\alpha) d\alpha = 1 \tag{6.16}$$

The corresponding average channel capacity is therefore

$$C_\infty = \int_{\frac{WN_0}{B}}^{\infty} \log_2 \left(B \frac{P}{WN_0} \alpha \right) f_{|H|^2}(\alpha) d\alpha \quad \text{bits/s.} \tag{6.17}$$

The general form of the optimal power spectrum is shown in figure 6.4. We see that more power is allocated when the channel is strong and less when it is weak and, moreover, outages are created. This is completely opposite from the delay–limited case with frequency–flat fading. Since no delay constraint is imposed on the problem, we are willing to wait forever for the channel to become acceptable. The best thing to do, therefore, is to save energy when the channel is weak so we can use more when it is strong. We effectively blast information through the channel when the fading state is favourable and turn it off when it is not. The name *water–filling* stems from the fact that the amount of energy allocated to each frequency can be calculated by inverting the channel response and pouring water on top of the curve until its level reaches B. Since this optimization is over all possible power spectra, it includes the one corresponding to the delay–limited case and consequently $C_d \leq C_\infty$.

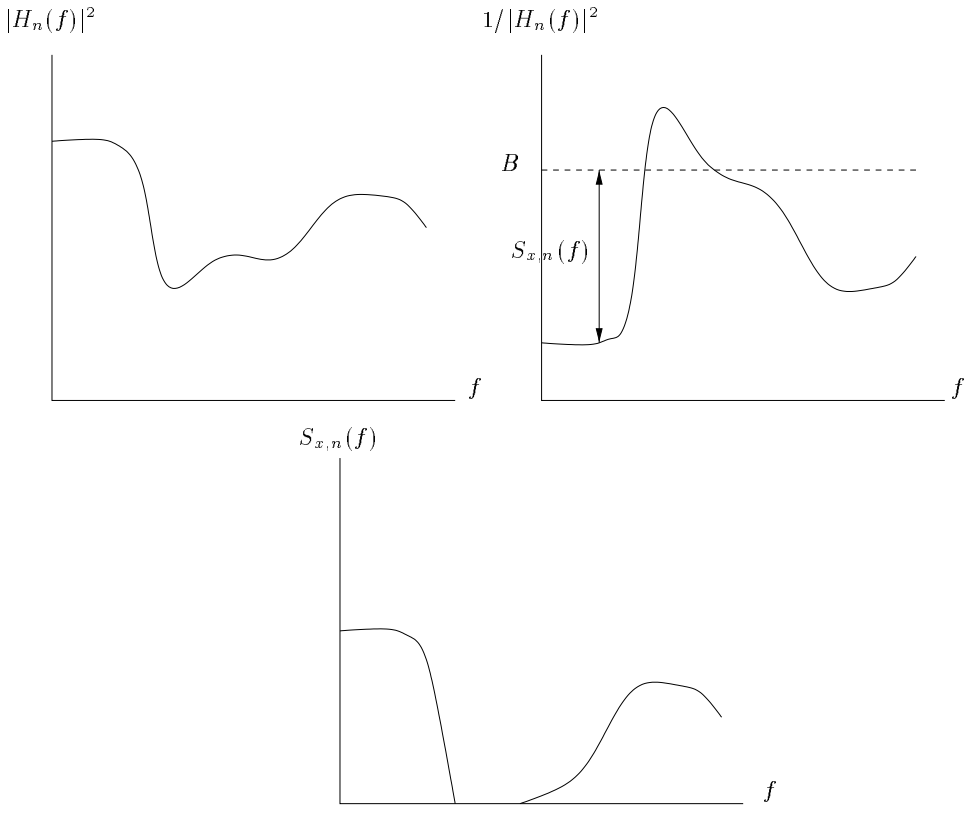

Figure 6.4: Graphical interpretation of water–filling

Using [GR80] it can be shown that (6.17) in Rayleigh fading can be expressed as

$$C_\infty = \frac{W}{\ln 2}\mathrm{E}_1\left(\frac{WN_0}{PB}\right) \quad \text{bits/s} \tag{6.18}$$

where B is the solution to

$$Be^{-\frac{WN_0}{BP}} - \frac{WN_0}{BP}\mathrm{E}_1\left(\frac{WN_0}{BP}\right) = 1. \tag{6.19}$$

Since $\lim_{a\to 0}\mathrm{E}_1(a)/a = 0$, we have that for large SNR $B \approx 1$ and consequently $C_\infty \approx We^{\frac{WN_0}{P}}\mathrm{Ei}\left(\frac{WN_0}{P}\right) = I_\infty$. This means that fast power control has almost no effect on an ergodic Rayleigh fading channel which is quite contrary to what we found for the non–ergodic case in section 6.1. This result is true for coded systems but we will see later that without coding, power control can have a noticeable effect. In figure 6.5 we show the constant B as a function of the SNR in Rayleigh fading. This is the peak–to–average power ratio which we see is not excessive for practical values of the SNR. In figure 6.6 we show C_∞, I_∞ and C_G as a function of the SNR. As we mentioned, fast power control has little effect in terms of capacity, except at very low SNR where it actually exceeds that of the Gaussian channel.

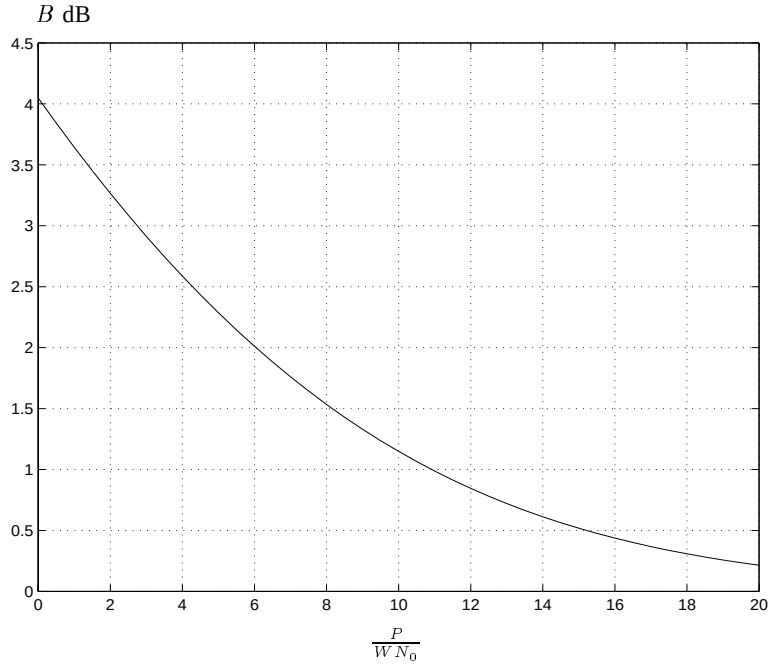

Figure 6.5: Peak–to–average power ratio in Rayleigh fading

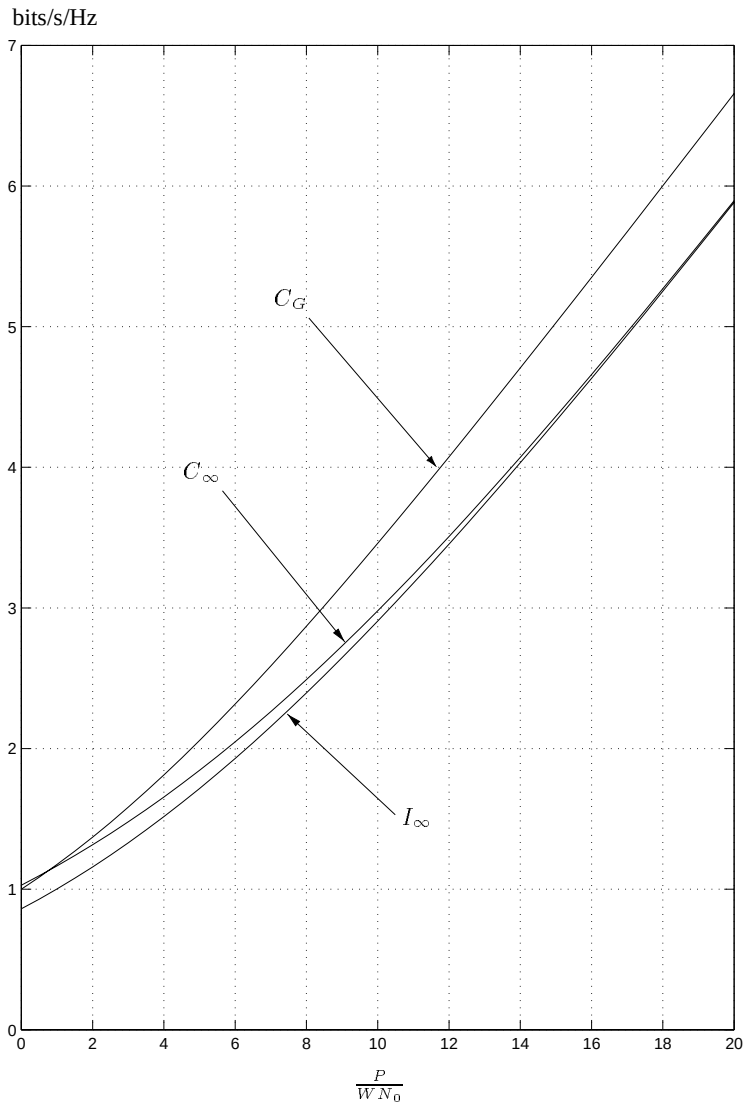

Figure 6.6: C_∞, I_∞ and C_G *vs.* SNR

6.3 Simple two–rate schemes with and without power control

Let us now consider a simple two–rate scheme with narrow–band signals, so we can assume the channel is frequency–flat. This would be the case for systems a large amount of narrowband channels which are allocated dynamically. We will consider these issues more in the following chapter. The channel response is characterized by two states, good and bad. We say the channel is good when the response, α, is greater than some nominal value $\alpha_{\min}$ and otherwise it is bad. When in the good state, we transmit with rate R and in the bad state we turn the transmitter off. We consider two different such schemes. The first transmits with a constant power when in the good state, so there is no power control. The

second, described by Goldsmith [Gol94], uses power control to keep a constant received power when transmission takes place.

Chua and Goldsmith[CG96][CG97] have considered variable rate schemes with more than two rates and find that average spectral efficiencies very close to I_∞ can be expected with and without additional coding. These results are also obtained with reasonable outage rates (on the order of 10^{-2}). The need for additional coding depends on the target bit–error rate of the system. Here we will show that the same is possible with uncoded two–rate transmission, if the system can spend large amounts of time in the outage state.

Scheme 1: Constant Transmit Power

In this scheme, the transmitter chooses to use the channel it knows that there will not be an outage at the receiver. The power control is of the form

$$\mathcal{P}(\alpha) = \begin{cases} \frac{1}{1-F_\alpha(\alpha_{\min})} & \alpha > \alpha_{\min} \\ 0 & \alpha \leq \alpha_{\min} \end{cases} \tag{6.20}$$

so that its average value is unity. The transmitter uses an information rate

$$R = W \log_2 \left(1 + \frac{P}{WN_0} \frac{\alpha_{\min}}{1 - F_\alpha(\alpha_{\min})}\right) \text{ bits/s} \tag{6.21}$$

when in the good channel state, so that as long as $\alpha \geq \alpha_{\min}$ we are guaranteed not to have an outage at the receiver. The average information rate is therefore

$$\overline{R} = R(1 - F_\alpha(\alpha_{\min})) \tag{6.22}$$

and the peak–to–average power ratio is $1 - F_\alpha(\alpha_{\min})$. We now maximize (6.22) with respect to $\alpha_{\min}$ by setting $\partial\overline{R}/\partial\alpha_{\min} = 0$ yielding the non–linear equation

$$\frac{\frac{P}{WN_0} e^{\alpha_{\min}}(1 + \alpha_{\min})}{1 + \frac{P}{WN_0}\alpha_{\min} e^{\alpha}_{\min}} = \ln\left(1 + \frac{P}{WN_0}\alpha_{\min} e^{\alpha_{\min}}\right) \tag{6.23}$$

for Rayleigh fading.

Scheme 2: Constant Received Power

Now we assume a power controller of the form

$$\mathcal{P}(\alpha) = \begin{cases} \frac{K(\alpha_{\min})}{\alpha} & \alpha \geq \alpha_{\min} \\ 0 & \alpha < \alpha_{\min} \end{cases} \tag{6.24}$$

so that the received power is constant when the channel is in the good state. This was considered by Goldsmith in her thesis [Gol94]. The information rate in the good state is given by

$$R = W \log_2 \left(1 + \frac{P}{WN_0} K(\alpha_{\min}) \right) \tag{6.25}$$

and the average information is again given by (6.22). As in earlier sections, we choose $K(\alpha_{\min})$ to yield a unit average power control level as

$$K(\alpha_{\min}) = \left(\int_{\alpha_{\min}}^{\infty} f_{\alpha}(u) \frac{du}{u} \right)^{-1}. \tag{6.26}$$

The peak–to–average power ratio is $K(\alpha_{\min})/\alpha_{\min}$. Again we maximize (6.22) with respect to $\alpha_{\min}$ which in Rayleigh fading yields the non–linear equation governing the optimal $\alpha_{\min}$

$$\frac{P}{WN_0} \frac{e^{-\alpha_{\min}}}{\alpha_{\min} \left(\mathrm{E}_1(\alpha_{\min}) \right)^2} = \left(1 + \frac{P}{WN_0} \frac{1}{\mathrm{E}_1(\alpha_{\min})} \right) \ln \left(1 + \frac{P}{WN_0} \frac{1}{\mathrm{E}_1(\alpha_{\min})} \right) \tag{6.27}$$

We note that in Rayleigh fading

$$K(\alpha_{\min}) = \frac{1}{\mathrm{E}_1(\alpha_{\min})}. \tag{6.28}$$

We compare the two schemes in figures 6.7–6.9 for Rayleigh fading. We see that with power control and moderate SNR, the two–rate scheme comes very close to optimal performance, which in terms of implementation complexity is an important result. Without power control there is a more significant loss. The peak–to–average power of scheme 2 is higher, but at the same time is rather invariant with respect to the average SNR. If we consider the peak–to–average power ratio for scheme 2, $1/(\alpha_{\min}\mathrm{E}_1(\alpha_{\min}))$, as shown in figure 6.10 we see that the optimized scheme operates in the vicinity of the minimum, 5.5 dB. If we consider the optimal threshold level for both cases in figure 6.10, we remark the two schemes work quite differently. With scheme 1, the variation of the threshold with the average SNR is significant, and more importantly the transmitter is turned off more often than with scheme 2. Scheme 2, on the other hand, has a more or less constant threshold and transmits around 75% of the time.

6.3.1 BER Comparison for Uncoded Transmission

The previous results on average information rates assumes the use of some form of error–control coding. Let us now consider the same two–rate channel control schemes without any coding at all. We will use different size QAM constellations to achieve average information rates of 1 and 2 bits/s/Hz and compare their performance to uncoded BPSK and QPSK.

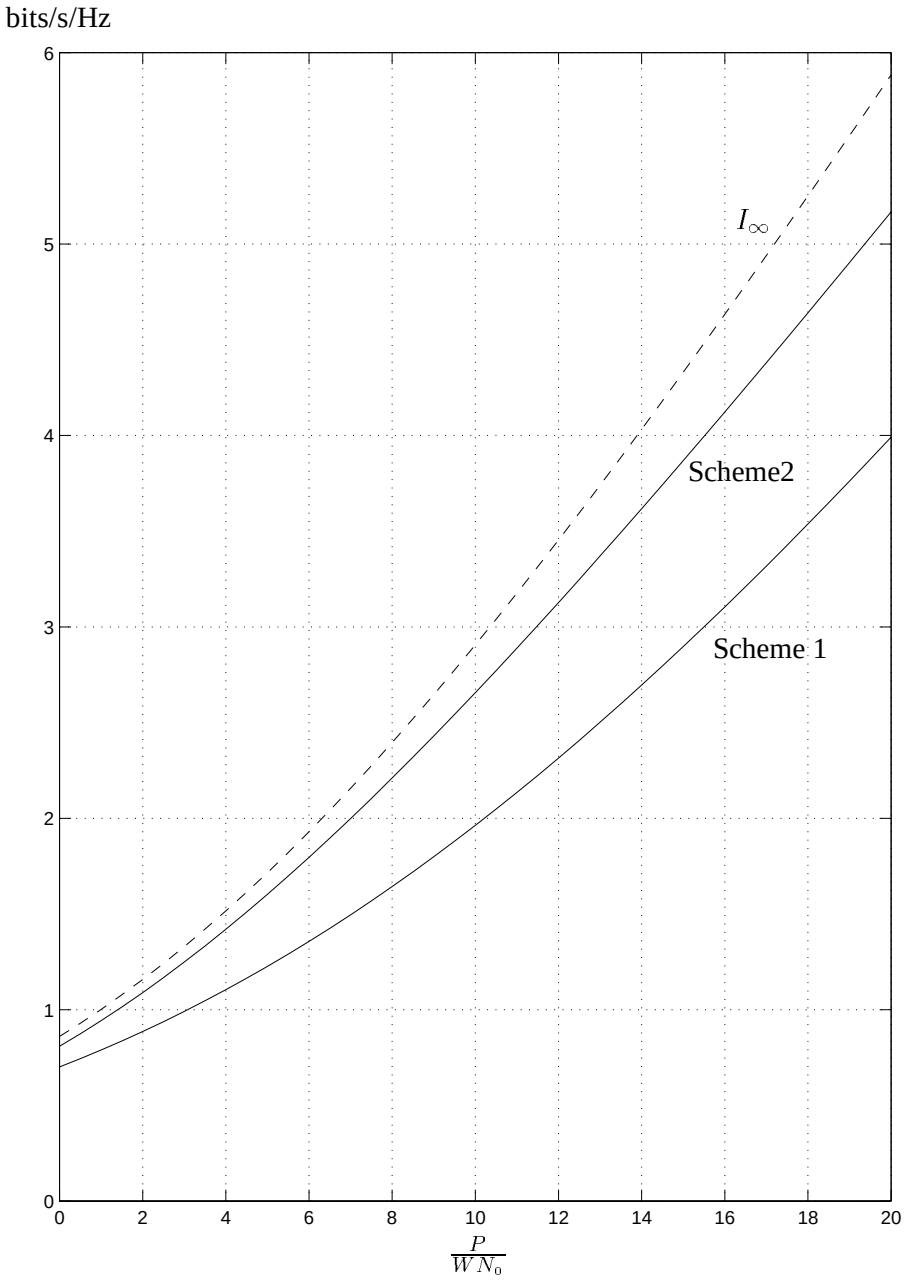

Figure 6.7: Average data rates of both two–rate schemes

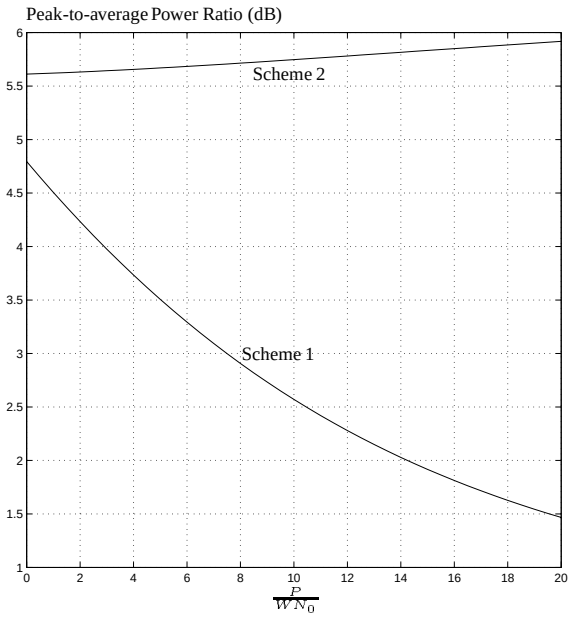

Figure 6.8: Peak–to–average Power Ratios

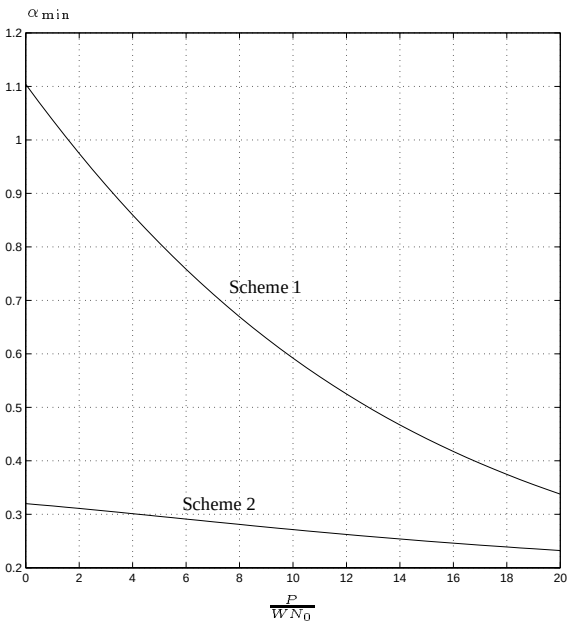

Figure 6.9: Threshold Comparison

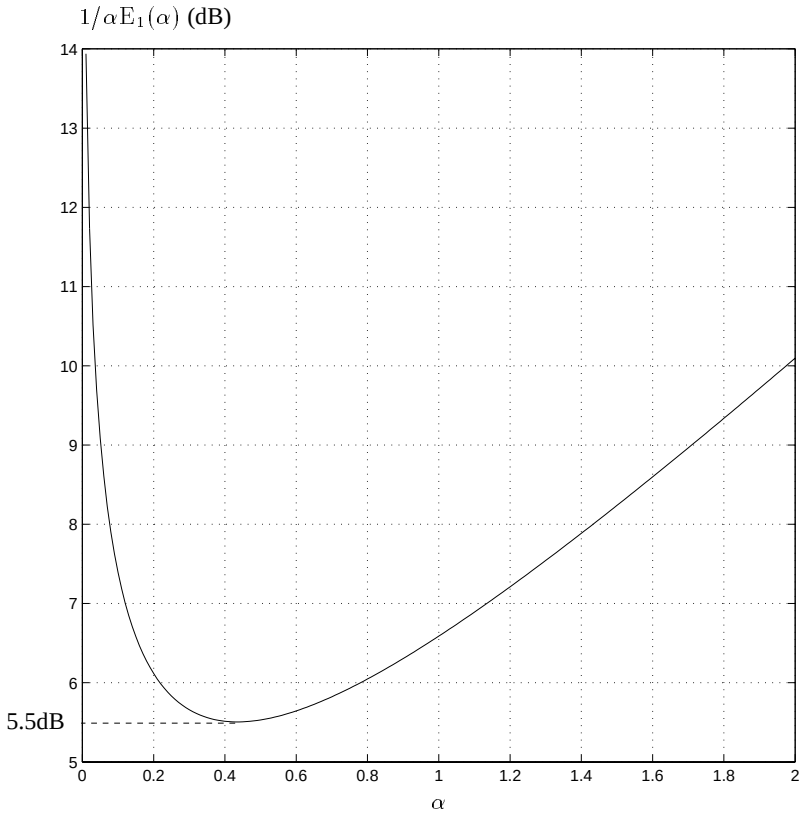

Figure 6.10: Minimum–Peak to Average Power Ratio for Scheme 2

We choose 4 different modulation schemes for numerical computations: BPSK ($R = 1$ bit/s/Hz), QPSK ($R = 2$ bits/s/Hz), 8-PSK ($R = 3$ bits/s/Hz) and 16-QAM ($R = 4$ bits/s/Hz). The BER conditioned on the channel strength α for the these QAM modulations are (from Proakis [Pro95])

$$\begin{aligned} P_{b|\alpha}^{\text{BPSK}} = P_{b|\alpha}^{\text{QPSK}} &= \text{Q}\left(\sqrt{2\mathcal{P}(\alpha)\alpha\frac{\mathcal{E}_b}{N_0}}\right) \\ P_{b|\alpha}^{8-\text{PSK}} &\approx \frac{1}{3}\text{Q}\left(\sqrt{.8787\mathcal{P}(\alpha)\alpha\frac{\mathcal{E}_b}{N_0}}\right) \\ P_{b|\alpha}^{16-\text{QAM}} &= \frac{3}{8}\text{Q}\left(\sqrt{.8\mathcal{P}(\alpha)\alpha\frac{\mathcal{E}_b}{N_0}}\right)\left[1-\frac{3}{8}\text{Q}\left(\sqrt{.8\mathcal{P}(\alpha)\alpha\frac{\mathcal{E}_b}{N_0}}\right)\right] \end{aligned} \tag{6.29}$$

We take three values for $\alpha_{\min}$ such that $1 - F_\alpha(\alpha_{\min}) = 1/2, 1/3, 1/4$, which in Rayleigh fading are $\alpha_{\min}(1/2) = \ln 2 = .6931,\ \ \alpha_{\min}(1/3) = \ln 3 = 1.0986,\ \ \alpha_{\min}(1/4) = \ln 4 = 1.3863$. These are simply the proportion of time communication is allowed. In order to calculate the average BER we use the density

$$f'_\alpha(\alpha') = \begin{cases} \frac{1}{1-F_\alpha(\alpha_{\min})} f_\alpha(\alpha'), & \alpha' \geq \alpha_{\min} \\ 0 & \text{otherwise} \end{cases}$$

which is the density of α conditioned on $\alpha \geq \alpha_{\min}$, or equivalently the time when transmission takes place.

Under scheme 1, the peak–to–average power ratios ($1 - F_\alpha(\alpha_{\min})$ for the three choices of $\alpha_{\min}$ are 3 dB, 4.77 dB and 6 dB. Using QPSK with $\alpha_{\min}(1/2)$ and 8–PSK with $\alpha_{\min}(1/3)$ for an average spectral spectral efficiency of 1 bit/s/Hz we have the BERs

$$\begin{aligned} P_b^{\text{QPSK}} &= e^{\alpha_{\min}} \int_{\alpha_{\min}(1/2)}^{\infty} \text{Q}\left(\sqrt{2e^{\alpha_{\min}(1/2)}\frac{\mathcal{E}_b}{N_0}\alpha'}\right) e^{-\alpha'} d\alpha' \\ &= \text{Q}\left(\sqrt{2.7724\frac{\mathcal{E}_b}{N_0}}\right) - 2\sqrt{\frac{\mathcal{E}_b/N_0}{.5+\mathcal{E}_b/N_0}}\text{Q}\left(\sqrt{1.3862\left(1+2\frac{\mathcal{E}_b}{N_0}\right)}\right) \end{aligned} \tag{6.30}$$

$$\begin{aligned} P_b^{8-\text{PSK}} &\approx \frac{1}{3}e^{\alpha_{\min}(1/3)} \int_{\alpha_{\min}(1/3)}^{\infty} \text{Q}\left(\sqrt{.8787e^{\alpha_{\min}(1/3)}\frac{\mathcal{E}_b}{N_0}\alpha'}\right) e^{-\alpha'} d\alpha' \\ &= \frac{1}{3}\left[\text{Q}\left(\sqrt{2.8960\frac{\mathcal{E}_b}{N_0}}\right) - 3\sqrt{\frac{\mathcal{E}_b/N_0}{.7587+\mathcal{E}_b/N_0}}\text{Q}\left(\sqrt{2.1972\left(1+1.3180\frac{\mathcal{E}_b}{N_0}\right)}\right)\right] \end{aligned} \tag{6.31}$$

We have used the fact that

$$\int_\alpha^\infty \text{Q}\left(\sqrt{\beta x}\right) e^{-x} dx = e^{-\alpha}\text{Q}\left(\sqrt{\beta x}\right) - \sqrt{\frac{\beta}{\beta+2}}\text{Q}\left(\sqrt{(\beta+2)x}\right). \tag{6.32}$$

We note that the uncoded BER for BPSK/QPSK can be found from (6.32) by setting $\alpha = 0$ and $\beta = 2\mathcal{E}_b/N_0$ yielding

$$P_b^{\mathrm{B/QPSK}} = .5\left(1 - \sqrt{\frac{\mathcal{E}_b/N_0}{1+\mathcal{E}_b/N_0}}\right). \tag{6.33}$$

For 16–QAM with $\alpha_{\min}(1/4)$ and $\alpha_{\min}(1/2)$ for average spectral efficiencies of 1 bit/s/Hz and 2 bit/s/Hz respectively, the BERs must be computed numerically.

Examining now scheme 2 in Rayleigh fading, we have that the power control constant K for the three values chosen for $\alpha_{\min}$ is $K(1/2) = 2.6406,\ \ K(1/3) = 5.3644,\ \ K(1/4) = 8.4274$. These correspond to peak–to–average power ratios ($K/\alpha_{\min}$) of 5.80 dB, 6.89 dB and 7.83 dB. For transmission at an average spectral efficiency of 1 bit/s/Hz we have the three average error probabilities of

$$P_b^{\mathrm{QPSK}} = \mathrm{Q}\left(\sqrt{2K(1/2)\frac{\mathcal{E}_b}{N_0}}\right) = \mathrm{Q}\left(\sqrt{5.2812\frac{\mathcal{E}_b}{N_0}}\right) \tag{6.34}$$

$$P_b^{8-\mathrm{PSK}} = \mathrm{Q}\left(\sqrt{.8787K(1/3)\frac{\mathcal{E}_b}{N_0}}\right) = \mathrm{Q}\left(\sqrt{4.6161\frac{\mathcal{E}_b}{N_0}}\right) \tag{6.35}$$

$$P_b^{16-\mathrm{QAM}} = \mathrm{Q}\left(\sqrt{.8K(1/4)\frac{\mathcal{E}_b}{N_0}}\right) = \mathrm{Q}\left(\sqrt{6.7419\frac{\mathcal{E}_b}{N_0}}\right) \tag{6.36}$$

and similarly at 2 bits/s/Hz we have

$$P_b^{16-\mathrm{QAM}} = \mathrm{Q}\left(\sqrt{.8K(1/2)\frac{\mathcal{E}_b}{N_0}}\right) = \mathrm{Q}\left(\sqrt{2.1125\frac{\mathcal{E}_b}{N_0}}\right) \tag{6.37}$$

We plot the BER for the two schemes at 1 and 2 bits/s/Hz in figures 6.11 and 6.12 where we notice that both have comparable performance, with a slight advantage for scheme 2 at 1 bit/s/Hz. The most important practical conclusion to be drawn from this analysis is that exploitation of channel state information is a very efficient means for achieving acceptable performance on a fading channel, when we do not have decoding delay constraints. We see that we can even achieve an SNR gain with respect to a non–fading channel *without coding*. This is possible by taking advantage of the time–varying nature of the fading channel by transmitting with a higher rate constellation when the attenuation is greater than unity. We will meet this effect again in Chapter 6 when we treat the multiuser channel. In that case, we do not even require constellation expansion to achieve an SNR gain without coding. Provided channel state information exploitation is feasible for given system parameters, it is a much simpler solution than using error–control codes with interleaving.

Here we have achieved an SNR gain at the expense of transmitting very infrequently on a single channel. In future (and already in some current) wireless systems, the transmitter may have access

to many channels, say L, over which to transmit information. These on/off schemes would be very attractive in this type of scenario. Suppose we choose some proportion of time, p, where the transmitter remains silent on any given channel and that when transmitting on a given channel we use rate R. The total average rate would be $LR(1-p)$ and the instantaneous number of channels in use, assuming all channels had uncorrelated strengths (i.e. carrier spacings much greater than the coherence bandwidth), is a binomial random variable with density

$$\text{Prob}(C_n = c) = \binom{L}{c}(1-p)^c p^{L-c}. \tag{6.38}$$

By choosing L to be large enough and p small enough, we have a variable–rate scheme with L rates and outage probability p^L, which is small. We will come across these types of allocation strategies in the following chapter.

6.4 Average information rate with retransmissions

We now consider a single–user system with an *Automatic Repeat reQuest (ARQ)* mechanism as shown in figure 6.13. The transmitter generates packets continuously which are stored in a buffer of unlimited size. We interpret each packet as a separate codeword which, after having been transmitted, remains in the buffer until an acknowledgment of successful decoding is returned by the receiver. Furthermore, we assume that the feedback path is error–free which is somewhat unrealistic on wireless channels. Using the information outage probability we have, for reasonable packet sizes, that the probability of correctly decoding the packet is $1-P_{\text{out}}(R)$. In a mobile environment where the channel state changes from packet to packet it is reasonable to assume that it is independent for each transmission of the same packet. Under this assumption, the average number of transmissions necessary to transmit the packet is

$$(1-P_{\text{out}}(R))\sum_{i=1}^{\infty} i[P_{\text{out}}(R)]^{i-1} = \frac{1}{1-P_{\text{out}}(R)} \tag{6.39}$$

yielding an average data rate of

$$\overline{R} = R(1-P_{\text{out}}(R)) \ \text{ bits/s}. \tag{6.40}$$

This type of system is very similar to scheme 1 in the previous section. The main difference is that instantaneous channel knowledge at the transmitter allows for power conservation by detecting the outage before it happens. Here the transmitter only learns of the outage by virtue of the repeat request. In a multiuser system this difference would be more important, since the *a priori* channel knowledge would

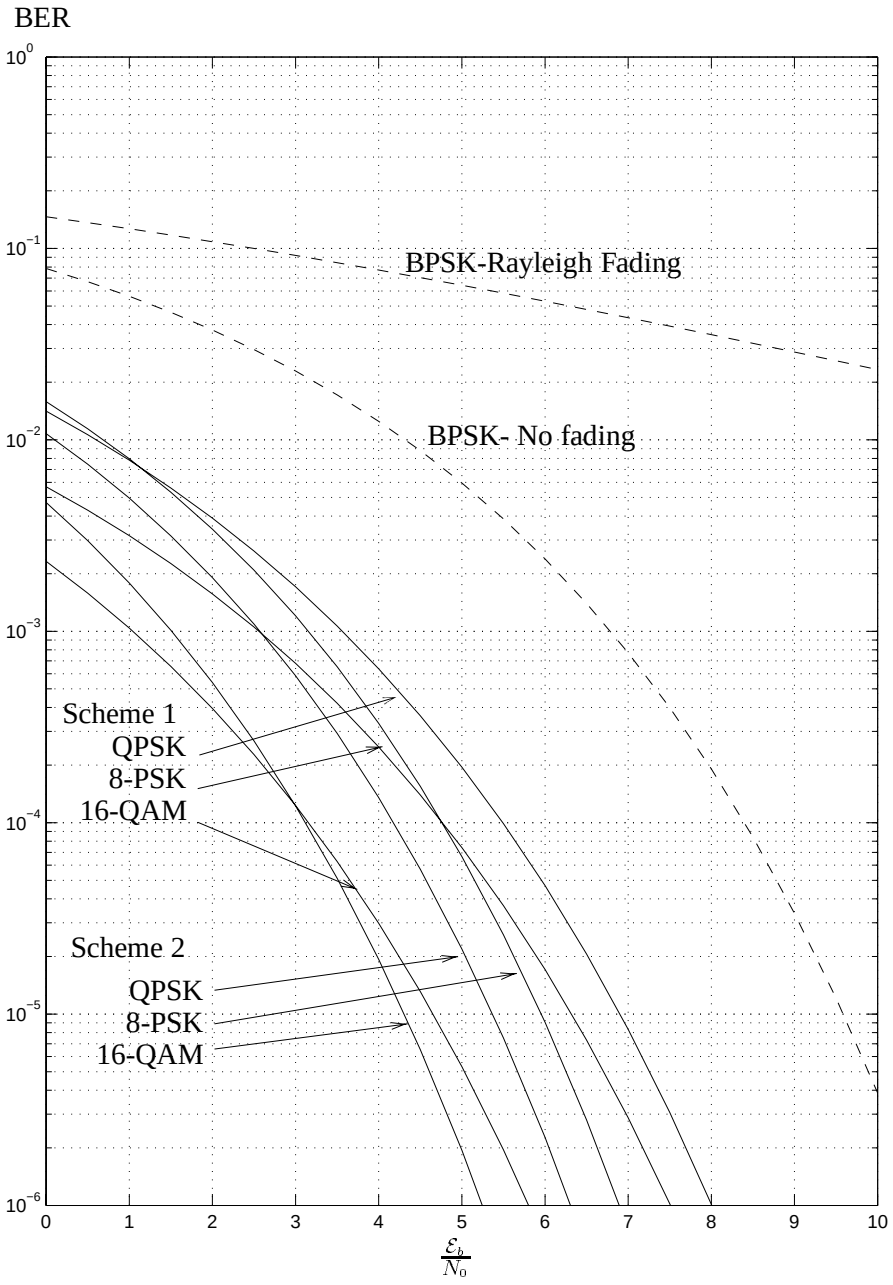

Figure 6.11: BER for 1 bit/s/Hz variable rate schemes

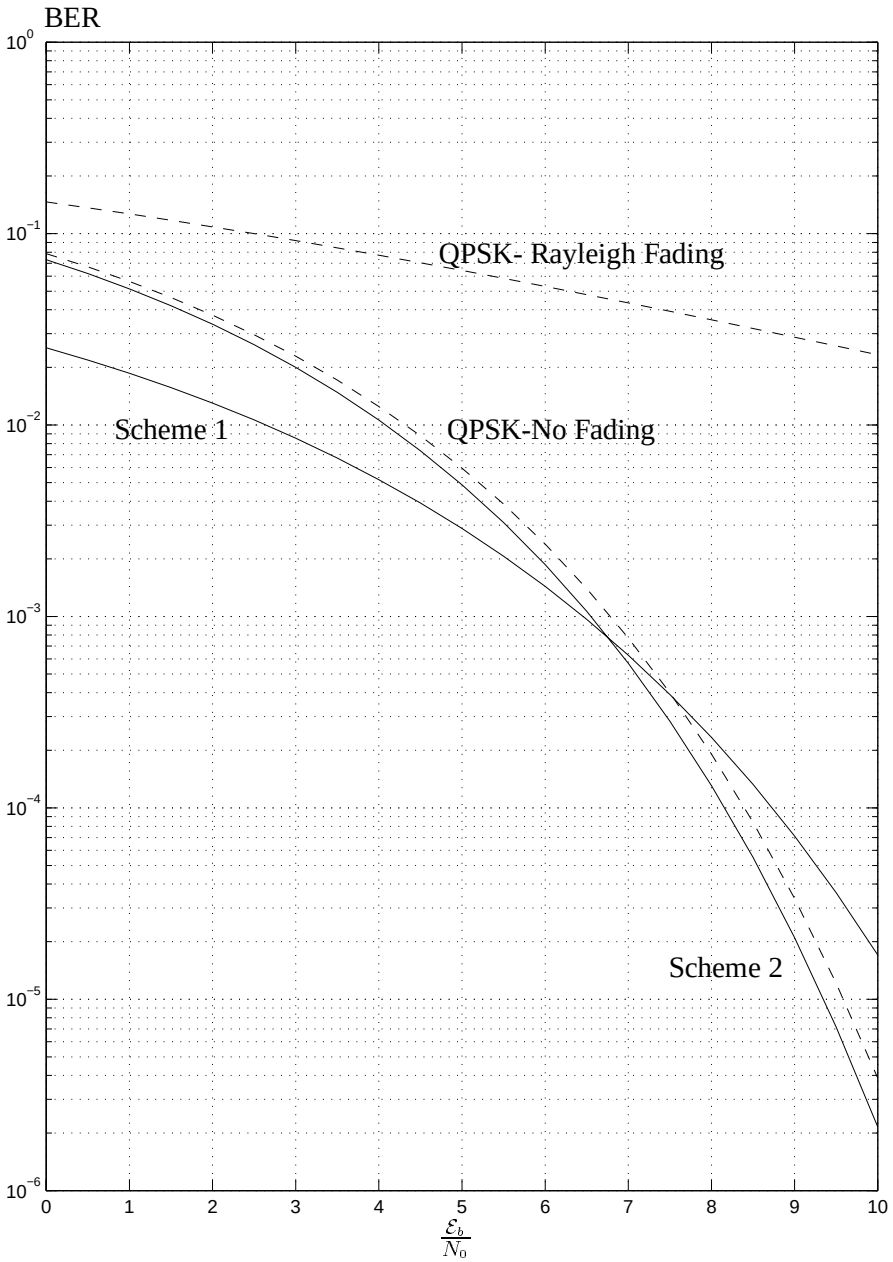

Figure 6.12: BER for 2 bit/s/Hz variable rate schemes

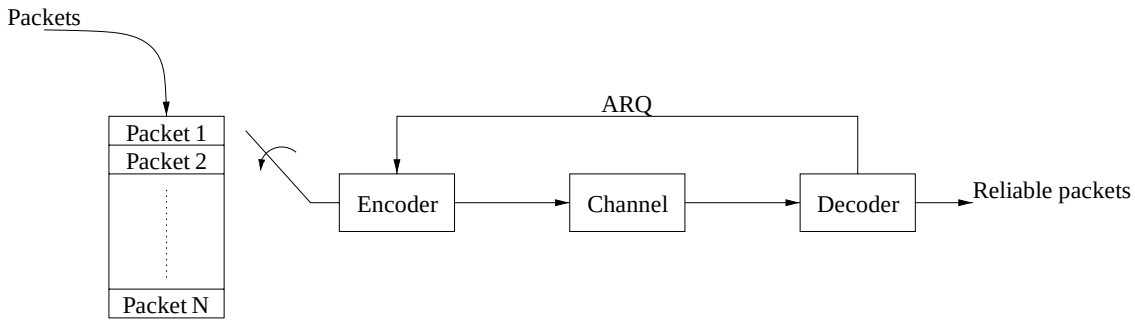

Figure 6.13: System model with repeat requests

also reduce the number of collisions as well as allow for a higher transmit power. We do not consider this effect here.

We plot $\overline{R}$ vs. R for single–path Rayleigh fading with $\frac{P}{WN_0} = 10$ dB in figure 6.14 where we see that there is an operating information rate at which $\overline{R}$ is maximum. By straightforward maximization we find using (4.34) that $R_{\rm opt}$ is the solution to

$$R_{\rm opt} 2^R = \frac{P}{WN_0} \ln 2. \tag{6.41}$$

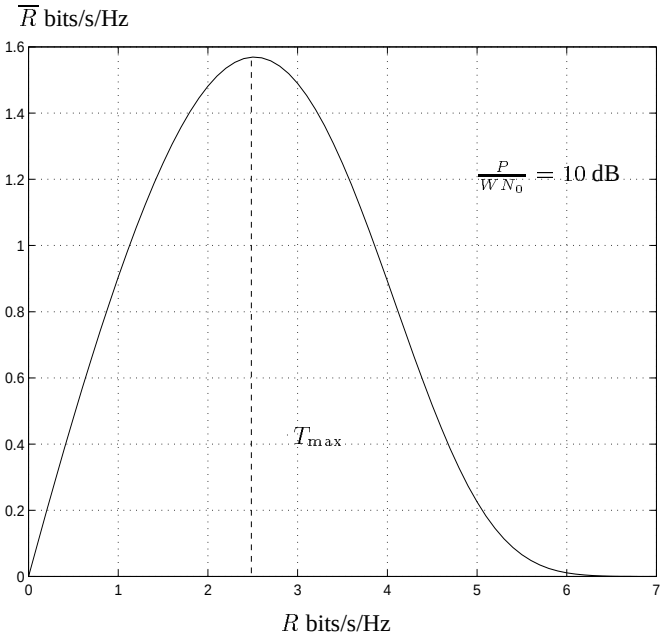

Figure 6.14: Reliable throughput as a function of R in Rayleigh fading

We now consider a system which employs some diversity. This can be achieved via slow–frequency hopping for instance, where a packet is split and transmitted in different parts of the spec-

trum. The multiple–access protocol considered by Humblet *et al* in [HHR96], which we depict in figure 6.15, uses a similar approach. Here the packet is transmitted with a sweeping carrier frequency in order to exploit diversity. This has the effect of turning a frequency–selective channel into a narrowband time–selective channel. It also has the advantage that several users can transmit concurrently without collisions, provided their sweeps do not overlap at the outset. This situtation is reduced by introducing a header at a given frequency which indicates when a user is about to begin transmission of the packet. As long as users do not initiate transmissions within a time–period equal to the header length they will

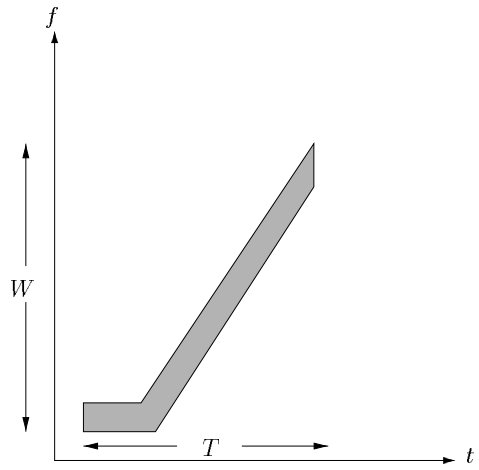

Figure 6.15: Frequency–sweeping transmission scheme

not collide. The bandwidth of the wideband system, either with a frequency–sweep or with frequency–hopping will be characterized by a certain number of degrees of freedom, but we simplify the problem by considering it as a block fading channel with F independent blocks, where F will be proportional to the available bandwidth. The optimal information rates R_{opt} can be calculated numerically using the results of section 3.6. In figure 6.16 we show $\overline{R}_{\max}$ as a function of the SNR and F and in figure 6.16 we show the information outage rate which yields $\overline{R}_{\max}$.

We see that the average data rate increases as a function of the diversity order, except it does so rather slowly. If we consider the optimal information outage rates, we see that they are all quite high, and they decrease with increasing diversity. This means that we are effectively using the channel at a very high information rate when it is favourable. This result was shown by Knopp and Humblet in [KH96]. This is not surprising, since it is exactly the same effect as with variable–rate coding. The merits of variable–rate coding and long decoding delays (i.e. interleaving) are clear, since I_{∞} is noticeably higher than any of the diversity–based systems with ARQ. Nevertheless, an ARQ–based system in Rayleigh fading can still offer spectral efficiencies exceeding 2 bits/s/Hz for reasonable signal–to–noise ratios.

6.5 Chapter Summary

In this chapter, we considered the exploitation of channel knowledge at the transmission end, either in the form of fast power control or variable–rate coding, in order to eliminate or exploit information outages. This can be achieved in practice in two–way systems either by a feedback mechanism or by measuring the channel response of the opposite link when time–division duplex is used. We first considered the delay–constrained case for narrow–band signals with optimal perfect power control, under an average power constraint. Using the definition of *delay–limited capacity* we showed that when some form of diversity can be exploited, not only can outages be eliminated, but significantly higher information rates can be expected. The price to be paid for using such a scheme is an unlimited peak–to–average power ratio. We then considered the case where the information rate of each codeword could be adjusted to avoid outages. We showed that this is completely equivalent to coding over a very large number of independent channel states, which in practice can be achieved by interleaving. When the power of each codeword can also be tailored to the channel response, the optimal power allocation scheme is *water–filling* in time and frequency, which effectively uses a high power when the channel is in a favourable state (so that a large amount of information can be transmitted) and halts transmission when the channel is weak. The optimal strategy suffers from outages, in the sense that no information is conveyed, but uses them to conserve energy for future transmissions, which occur at a much higher rate. It does not suffer, however, from an excessive peak–to–average power ratio. In Rayleigh fading an optimal power allocation scheme has little advantage over one which keeps the transmit power constant, and therefore over an optimal ideally interleaved coded system, since they offer practically identical average spectral efficiencies.

We considered simple two–rate sub–optimal power control schemes for narrow–band channels which work along the lines of the optimal scheme. They use a fixed information rate when the channel response is above a certain threshold and halt transmission when it falls below this threshold. We have, therefore, a system which controls outages.

The first scheme keeps the transmitter power constant when not in a outage state, has an average data rate which depends on the information rate agreed upon by the communicating parties. This rate is chosen to maximize the average spectral efficiency, which is on the order of 2 bits/s/Hz at an average SNR of 10dB. The second scheme keeps the received power constant when transmitting using a perfect power controller, and the outage threshold is chosen to maximize the average information rate. Such a scheme becomes possible in Rayleigh fading for peak–to–average power ratios which exceed 5.5 dB,

and the optimal operating point is always around this value. For average signal–to–noise ratios on the order of 10 dB it is possible to achieve average spectral efficiencies on the order of 2.5 bits/s/Hz which are only slightly less than optimal. For higher average signal–to–noise ratios the loss is more significant.

We considered the bit error–rate of the two simple schemes with uncoded QAM modulation. The main conclusion is that significant performance gains can be had in comparison to an uncoded system without channel state feedback without the need for channel coding/interleaving. Practically speaking, this says that by exploiting channel state feedback we can avoid complex coding/interleaving schemes altogether.

Finally we considered an ARQ–based single–user scheme, as is already used in the data transmission mode of the GSM standard. We showed that this scheme is identical to the second of the two–rate coding schemes considered previously, except for the fact that the power cannot be conserved during an outage event since the transmitter does not have this information at its disposal. The only means to avoid outages is by requesting retransmissions. The maximum average data rate is also found by choosing an optimum information rate which is effectively used only when the channel state is favourable. We computed these rates for block–fading channels, using $F = 1, 2, 4, 8$ blocks, and results indicate that average spectral efficiencies on the order of 2 bits/s/Hz in Rayleigh fading could be expected even with ARQ, and that diversity (i.e. number of independent blocks) increases the average spectral efficiency slowly. The outage rates are quite high ranging from 40% ($F = 1$) down to 10% ($F = 8$) at an SNR of 10 dB.

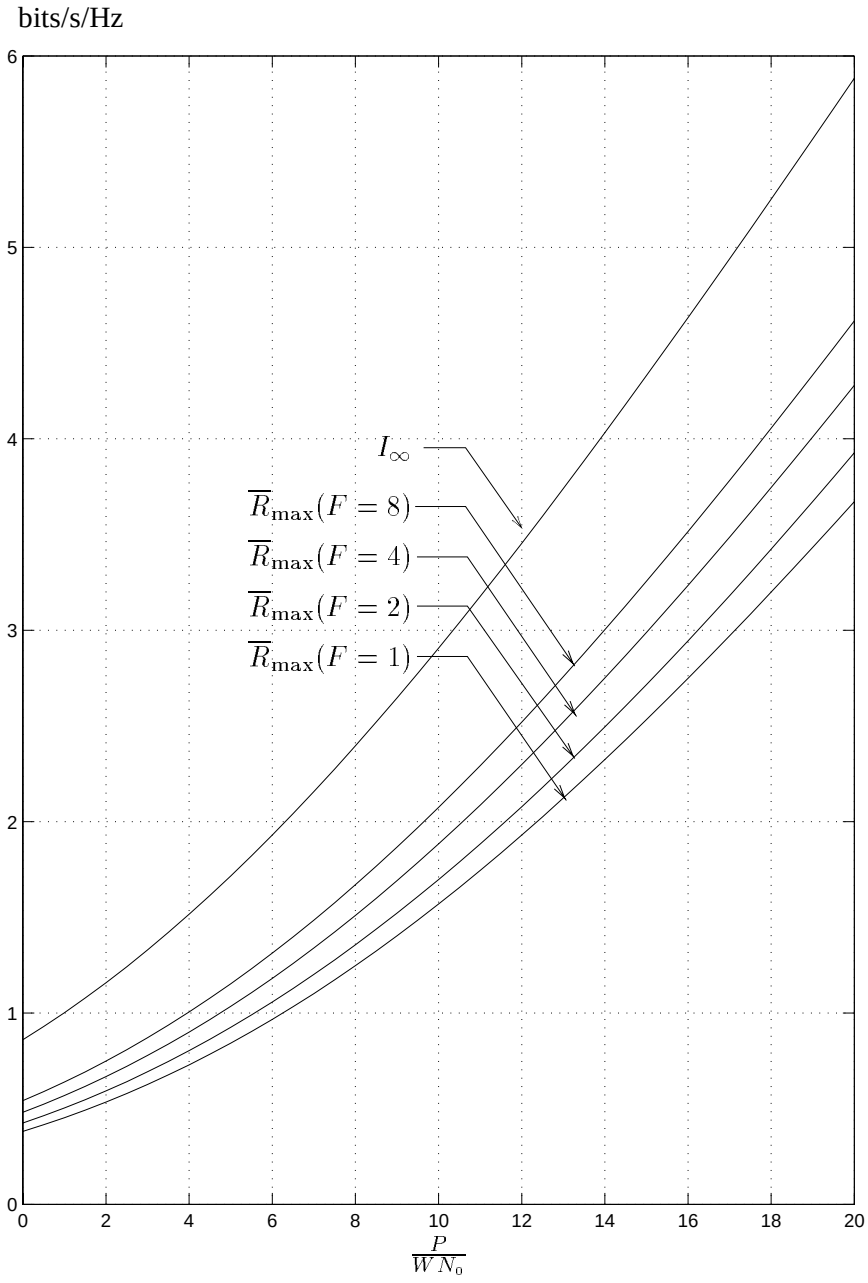

Figure 6.16: Average throughput in Rayleigh fading

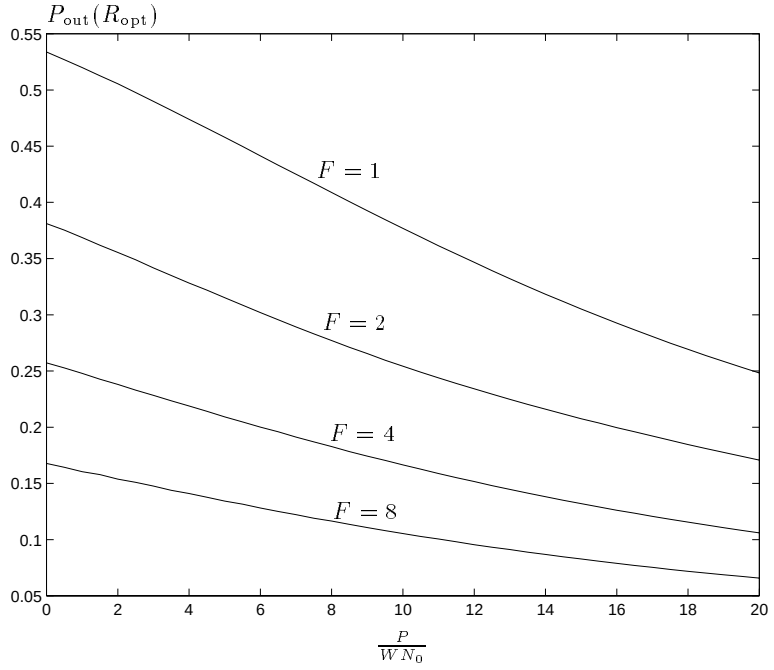

Figure 6.17: Optimal information outage rates as a function of R and F

Chapter 7

Multiuser Channels and Multiuser Diversity

In the multiuser cellular systems in use today, there are two primary communication links between the users located in the cell and the cell's central base station as shown in Figure 7.1. The *up-link* refers to the information flow from the users to the base station and is an example of a classic *multiple–access channel (MAC)*, or a many–to–one communication problem. The down-link refers to the opposite situation, namely the flow of information from the base station to the users. This is an example of a *broadcast channel* or a one–to–many communication problem. There has been much recent interest in determining which types of multiple–access methods are best, and this chapter we examine such issues, albeit in a rather general sense. Here we will concern ourselves only with case of the MAC. Another important aspect of multiuser cellular systems which we do not consider here is adjacent cell interference. Our results, therefore, apply mainly to single–cell systems (i.e. when there is only one base station) or also for systems where inter-cell–interference can be ignored. An information–theoretic treatment of Cellular systems without fading are given in [Wyn94]

We begin this chapter with a discussion of the Gaussian MAC without fading to familiarize ourselves with the different types of multiple–access schemes. One of the main goals of this is to illustrate that a multiple-access scheme is simply a way of sharing dimensions and distributing energy in such a way that the receiver can distinguish between different users. We introduce the basic information–theoretic tools needed to handle these systems and and we use them to analyze a specific example with multipath fading.

We then turn our attention to the average information rates that can be expected with different

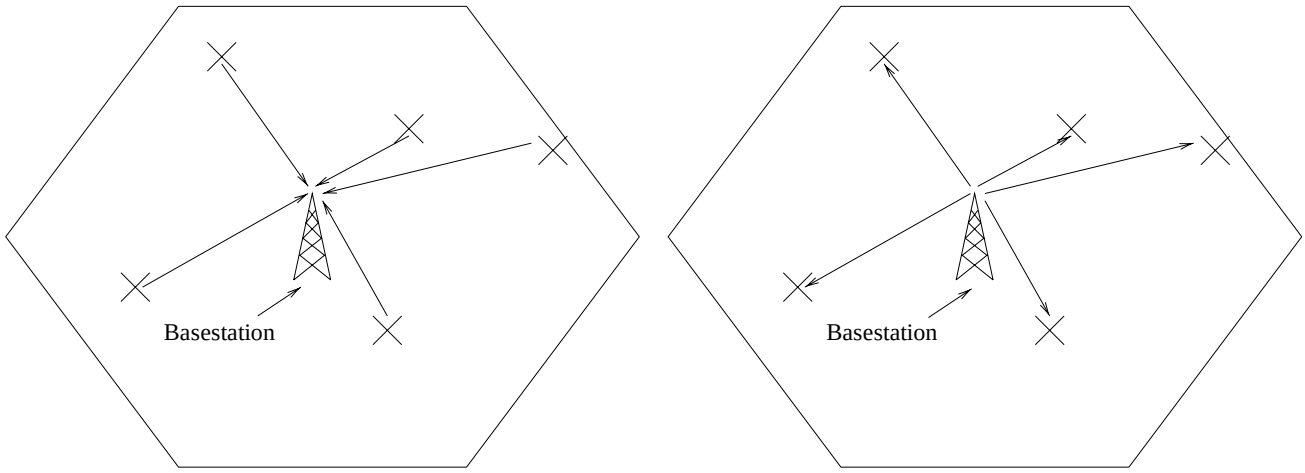

Figure 7.1: Communication Links in Cellular Systems

multiple–access schemes over fading channels. In the case where the system has access to channel state information either via feedback path or in time–division duplex, the users can allocate the power according to their channel and the channels of the other users. We show that when this is feasible, we have an inherent diversity effect that is due the nature of the time/frequency–varying MAC which was not present in the single–user channel we treated in Chapter 3. This effect can yield significant increases in the achievable data rates.

7.1 Multiple–Access Channels without fading

In order to familiarize the reader with the basic ideas in multiple–access communications we begin with a short treatment for a non–fading Gaussian channel. Consider the simple discrete–time channel

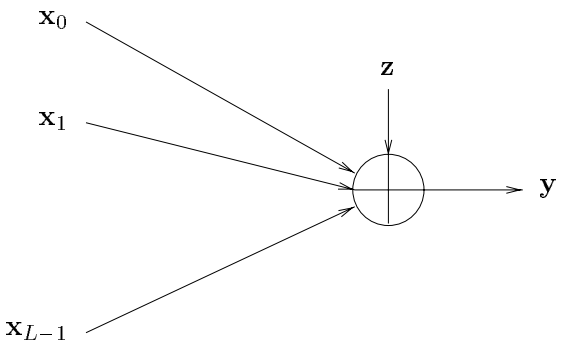

Figure 7.2: Gaussian Multiple–Access Channel (MAC)

model in Figure 7.2 which is known as the L–user Gaussian *multiple–access channel* with input output relationship

$$\mathbf{y} = \sum_{i=0}^{L-1} \mathbf{x}_i + \mathbf{z}. \tag{7.1}$$

We assume that each user signal $\{\mathbf{x}_i, i = 0, \cdots, L-1\}$ occupies N dimensions and belongs to $\mathbb{R}^N$. The noise is Gaussian and white with variance $N_0/2$ in each dimension. The information rate for user i is denoted by R_i bits/dim. We may write the users signals as

$$\mathbf{x}_i = \sum_{j=0}^{D_i-1} u_j \boldsymbol{\xi}_{i,j} \tag{7.2}$$

where D_i is the dimension of the subspace in which user i's signal lies and $\{\boldsymbol{\xi}_{i,j}\}$ is an orthonormal basis for this subspace. Each user's signal is constrained in energy as

$$\sum_{i=0}^{N-1} \overline{x_i^2} = \sum_{i=0}^{D_i-1} \overline{u_i^2} \leq NP_i. \tag{7.3}$$

It may sometimes be the case that users are distinguishable by the subspace in which they lie. In this case, decoding amounts to projecting the received signal on each subspace and decoding each users signal independently of the others. This is important since the coding and decoding processes need not be done jointly between users signals. We now consider two cases where this is possible.

7.1.1 Orthogonal Multiplexing

The first way of allocating dimensions to different users is *orthogonal multiplexing* which is achieved by making the subspaces orthogonal to one another. We have, therefore, that $\boldsymbol{\xi}_{i,j}^{\mathrm{T}} \boldsymbol{\xi}_{k,l} = 0, \forall j, l, i \neq k$ and consequently the achievable data rate of user i is bounded by

$$R_i \leq \frac{1}{2N} \sum_{j=0}^{D_i-1} \log_2 \left(1 + \frac{2NP_i}{N_0 D_i}\right) = \frac{D_i}{2N} \log_2 \left(1 + \frac{2NP_i}{N_0 D_i}\right) \quad \text{bits/dim}. \tag{7.4}$$

We have expressed the information rates in terms of the total number of dimensions of the signal space, and not the number of dimensions which the user actually uses. This allows for a fair comparison between systems in which all users use all the dimensions or those where the users share the total number of dimensions. By choosing D_i subject to $\sum_{i=0}^{N-1} D_i = N$ we can change the achievable rates allocated to each user. For example consider the two–user case with equal transmit powers $P_i = P$. We have the

following pair of bounds

$$R_0 \leq \frac{\alpha}{2}\log_2\left(1+\frac{2P}{\alpha N_0}\right) \quad \text{bits/dim}$$
$$R_1 \leq \frac{(1-\alpha)}{2}\log_2\left(1+\frac{2P}{(1-\alpha)N_0}\right) \quad \text{bits/dim} \tag{7.5}$$

where $\alpha = D_0/N$ is a parameter varying between 0 and 1. If we plot the upper–bounds in the R_0, R_1 plane as a function of α we obtain a region, $\mathcal{R}$, where every rate pair is achievable. This is shown in Figure 7.3 for a signal to noise ratio of $P/N_0 = 10$ dB. It is known as an *achievable rate region* or cases where the transmitters have *a priori* information about the states of the channels, a *capacity region*.

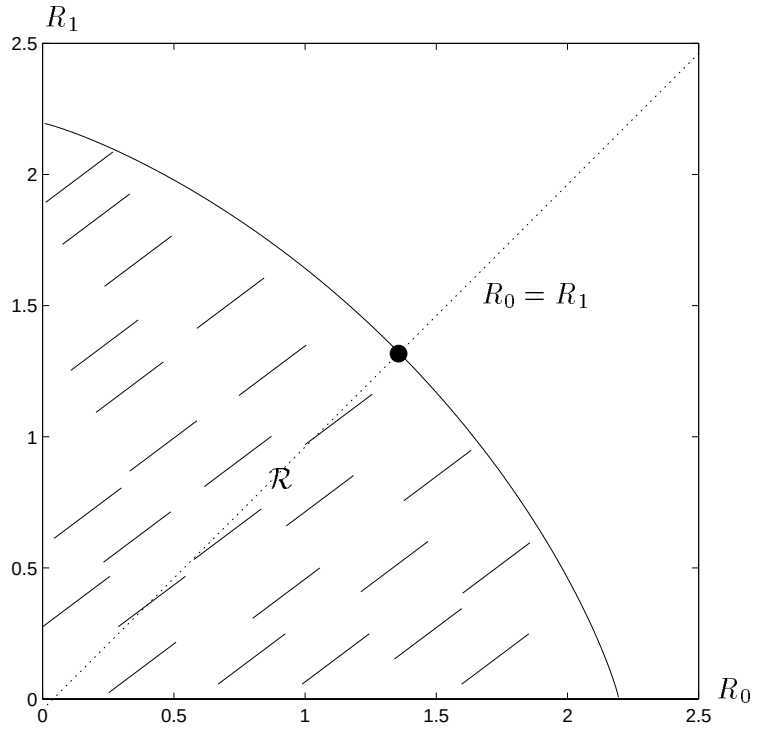

Figure 7.3: Achievable Rate Region with Orthogonal Multiplexing

In practice, orthogonal multiplexing can be achieved in the ways shown in figure 7.4. The first option is *Frequency–Division Multiple Access (FDMA)* where each user transmits in a frequency–band of bandwidth W/L all the time with power P. Another is *Time–Division Multiple Access (TDMA)*. If we assume a certain system bandwidth W then each user is allocated $2W/L$ dimensions per second and transmits with power LP. It is also possible to combine the two schemes. The third option is *synchronous Direct–Sequence Code–Division Multiple Access (DS-CDMA)* on frequency–flat channels where each user is assigned a wide-band spreading sequence which is orthogonal to those of all the other

users. This is more difficult to illustrate since users occupy all frequencies and all times and is therefore not included in the figure. It can be achieved using orthogonal spread–spectrum pulse shapes and can be defined either in the frequency–domain using a multi-tone approach [Van95] or in the time–domain with a classical direct–sequence approach.

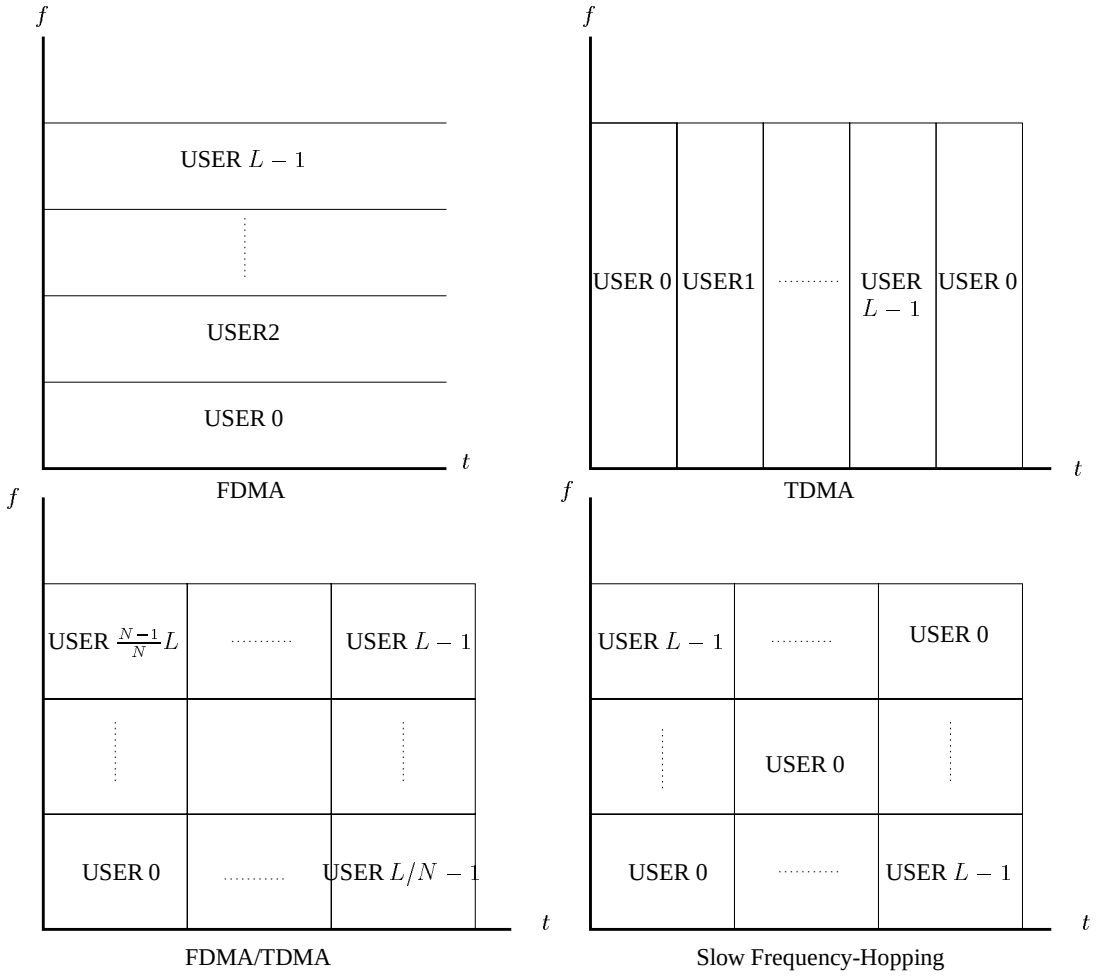

Figure 7.4: Orthogonal Multiplexing Schemes

7.1.2 Non–Orthogonal Multiplexing

When orthogonality cannot be achieved, or is avoided on purpose then the inter-user interference must be handled in some fashion. The simplest way is to have a bank of L decoders where each user is decoded separately treating the others as part of the background noise. We will refer to this type of decoding as *single–user decoding*. The received signal treated by decoder i is

$$\mathbf{y} = \mathbf{x}_i + \mathbf{z}_i \tag{7.6}$$

with

$$\mathbf{z}_i = \sum_{j \neq i} \mathbf{x}_j + \mathbf{z}. \tag{7.7}$$

Let us first consider the case where all users occupy the entire signal space so that $\boldsymbol{\xi}_{i,j} = \boldsymbol{\xi}_{k,j}, \forall i,k$, which is the most general type of coding scheme. If users transmit Gaussian signals, then in this case the achievable rate of each user is bounded by

$$\begin{aligned} R_i &\leq \frac{1}{N} \mathrm{I}(\mathbf{Y}; \mathbf{X}_i) \\ &= \frac{1}{2} \log_2 \left(1 + \frac{2P_i}{N_0 + 2\sum_{j \neq i} P_j} \right). \end{aligned} \tag{7.8}$$

We note that a Gaussian input distribution is not optimal. As the number of users increases, however, the statistics of the interference term quickly approach a Gaussian distribution, so that Gaussian signals are asymptotically optimal. Finding the best input distribution for this channel is essentially the same problem as with the Gaussian interference channel [CT91]. We notice in (7.8) that if $P_i = P, \forall i$ then as L increases $R_i \to 0$ but the total rate sum

$$R_{\text{sum}} = \sum_{i=0}^{L-1} R_i \tag{7.9}$$

tends to $\lim_{L\to\infty} L\frac{1}{2}\log_2\left(1 + \frac{2P}{N_0+2(L-1)P}\right) = 1/(2\ln 2) = .7213$ bits/dim which was first remarked in [Hui84]. With single–user decoding, therefore, we can never expect high spectral efficiencies.

Let us now consider the case of a completely synchronous DS–CDMA where each user signal is of reduced dimensionality as shown in figure 7.5. We will assume the system uses a spreading factor S

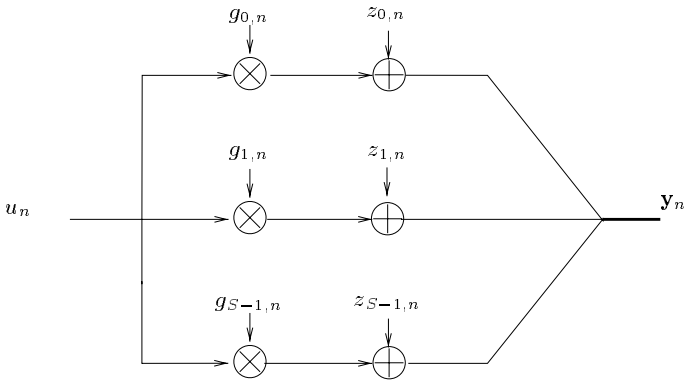

Figure 7.5: A Synchronous DS–CDMA System

which is not necessarily equal to the number of users, L. The received signal for every S dimensions can

be written as

$$\mathbf{y}_n = \sum_{i=0}^{L-1} \mathbf{g}_{n,i} u_{n,i} + \mathbf{z}_n, n = 0, \cdots, N/S - 1, \tag{7.10}$$

where $\mathbf{g}_{n,i}$ is a zero–mean $\pm\sqrt{1/S}$ random sequence which is independent between users and from one input symbol to the next. In practice, this is normally chosen from a pseudo–noise sequence with a very long period [IS992]. The receiver for user i correlates the received signal $\mathbf{y}_n$ with $\mathbf{g}_{n,i}$ yielding

$$y_{n,i} = u_{n,i} + \sum_{j \neq i} \mathbf{g}_{n,i}^{\mathrm{T}} \mathbf{g}_{n,j} u_{n,j} + z_n. \tag{7.11}$$

where z_n is Gaussian with variance $N_0/2$. For simplicity we assume that all users have the same power so that $\overline{u_i^2} = SP_i = SP$ (see (7.3) with $D_i = N/S$.) Since the receiver knows the spreading code for each user and the spreading sequences are truly random from symbol to symbol, the achievable data rate for each user assuming Gaussian input symbols (u_n) is bounded by

$$\begin{aligned} R_i &\leq \lim_{N\to\infty} \frac{1}{2N} \mathrm{I}\left(\{\mathbf{Y}_n, n = 0, \cdots, N/S-1\}; \{\mathbf{U}_n, n = 0, \cdots, N/S-1\} | \{Q_n = q_n,\ n = 0, \cdots, N/S-1\}\right) \\ &= \frac{1}{2N} \sum_{n=0}^{N/S-1} \mathrm{I}(Y_n; U_n | Q_n = q_n) \\ &= \frac{1}{2S} \mathrm{E}_{q_n} \log_2 \left(1 + \frac{2SP}{N_0 + 2SPq_n}\right) \quad \text{bits/dim} \end{aligned} \tag{7.12}$$

where

$$q_n = \sum_{j \neq i} \left(\mathbf{g}_{n,i}^{\mathrm{T}} \mathbf{g}_{n,j}\right)^2 = \sum_{j \neq i} q_{n,j} \tag{7.13}$$

and $q_{n,j}$ has density (for S even)

$$f_{q_{n,j}}(a) = \binom{S}{S/2} 2^{-S} \delta(a) + \sum_{k=1}^{S/2} \binom{L}{L/2+k} 2^{1-S} \delta\left(a - \frac{4k^2}{S^2}\right). \tag{7.14}$$

The density of q can be computed easily from (7.14) using numerical methods which can be applied to (7.12) to compute R_i.

As an approximation for large L we may invoke the central limit theorem [Pap82] and approximate the interference term in (7.11), $\sum_{j\neq i} \mathbf{g}_{n,i}^{\mathrm{T}} \mathbf{g}_{n,j} u_{n,j}$ by a Gaussian random variable with mean zero and variance $(L-1)P/S$. The achievable information rate for each user is therefore bounded by

$$R_i \leq \frac{1}{2N} \sum_{i=0}^{N/S-1} \log_2 \left(1 + \frac{2SP}{N_0 + 2(L-1)P}\right) = \frac{1}{2S} \log_2 \left(1 + \frac{2P}{N_0/L + 2\left(\frac{L-1}{L}\right)P}\right). \tag{7.15}$$

We see right away that if S is finite, in the limit of large L, the total rate sum LR_i also tends to .7213 bits/dim. If, on the other hand, $L/S = K$ then LR_i tends to $.5\log_2\left(1+1/K\right)^K \leq .7213$ bits/dim. In the special case where $K = 1$ (i.e. the spreading gain is equal to the number of users), we see that the total rate sum tends to .5 bits/dim. In figure 7.6 we plot $R_{\rm sum}$ for both types of systems with and without the approximation for $P/N_0 = 10$dB for the special case $K = 1$ in the DS–CDMA system. We see that both decrease to their asymptotic values quite quickly. The central limit theorem approximation is only slightly pessimistic for reasonable L. We may conclude, therefore, that on a Gaussian channel there is an advantage to using a low–rate coding scheme as opposed to simple DS–CDMA. We note also the non–optimality of Gaussian signals when the number of users is small, since the DS–CDMA system has a larger total sum rate. The transmitted signal for each user for each symbol is $u_{n,i}\mathbf{g}_{n,i}$ which is not Gaussian.

The issue of spreading *vs.* low–rate coding was first considered by Hui [Hui84] and later by Viterbi [Vit90]. Hui suggested that users should each use different low–rate convolutional codes with no (or very little) PN spreading. Viterbi's approach uses the same low–rate code for each user whose output modulates a very–long period and user–dependent PN sequence which may or may not provide additional bandwidth expansion. The PN sequences distiguish the users and allows each to use the same code. The coding scheme is based on mapping the output of a convolutional code to large set of Walsh–Hadamard sequences. We will soon see that the advantage of using such low–rate coding schemes is even greater on a multipath channel.

7.1.3 Joint Detection on the MAC

When the receiver can decode the signals jointly, Liao [Lia72] and Ahlswede [Ahl71] showed that the achievable rate region for two users is defined by

$$\begin{aligned} R_0 &\leq \mathrm{I}(\mathbf{Y};\mathbf{X}_0|\mathbf{X}_1) \leq \max_k \mathrm{I}(\mathbf{Y};\mathbf{X}_0|\mathbf{X}_1=\mathbf{x}_{1,k}) \\ R_1 &\leq \mathrm{I}(\mathbf{Y};\mathbf{X}_1|\mathbf{X}_0) \leq \max_k \mathrm{I}(\mathbf{Y};\mathbf{X}_1|\mathbf{X}_0=\mathbf{x}_{0,k}) \\ R_0+R_1 &\leq \mathrm{I}(\mathbf{Y};\mathbf{X}_0,\mathbf{X}_1) \end{aligned} \tag{7.16}$$

which generalizes for L users as

$$\mathcal{R} = \bigcap_{U\subseteq\mathcal{U}} \left\{ \sum_{i\in U} R_i \leq \mathrm{I}(\mathbf{Y};\{\mathbf{X}_i, i\in U\}|\{\mathbf{X}_j, j\in\overline{U}\}) \right\}, \quad \mathcal{U}=\{0,1,\cdots,L-1\} \tag{7.17}$$

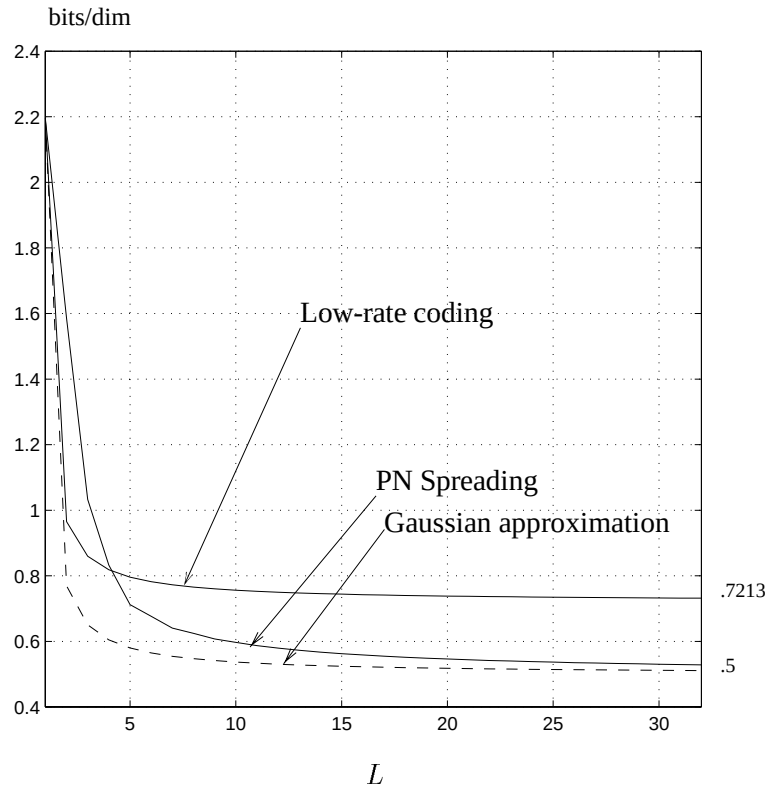

Figure 7.6: Total Sum of Rates Comparison for Low–Rate Coded CDMA and PN Spreading

This region is shown for $L = 2$ in Figure 7.7 and is known as the *Cover–Wyner pentagon*. We remark that its shape is quite different from the region for orthogonal multiplexing. For a Gaussian MAC the achievable rate region can be shown to be [CT91]

$$\bigcap_{U \subseteq \mathcal{U}} \sum_{i \in U} R_i \leq \frac{1}{2} \log_2 \left(1 + \frac{2}{N_0} \sum_{i \in U} P_i \right) \tag{7.18}$$

This results from the fact that the conditional mutual information functionals in (7.17) are maximum when the power of all the conditioned users is zero. The region in (7.17) corresponds to the case where all users occupy the entire signal space so that the region of a DS–CDMA system, which is a special case, will necessarily lie within. The practical interpretation of the corner points of the region is important, since it can be shown that they can be achieved by single–user decoding. The basic idea is that the codeword for a given user is decoded considering the other users as part of the noise, as we did earlier. His codeword is recreated and subtracted from the received signal and the next user is decoded in a similar fashion. The different rates achieved by these corner points depends on the order in which the successive decoding algorithm is performed. By changing the decoding order periodically, any point on the rate region boundary can be achieved. This assumes, of course that the users change their transmission rates

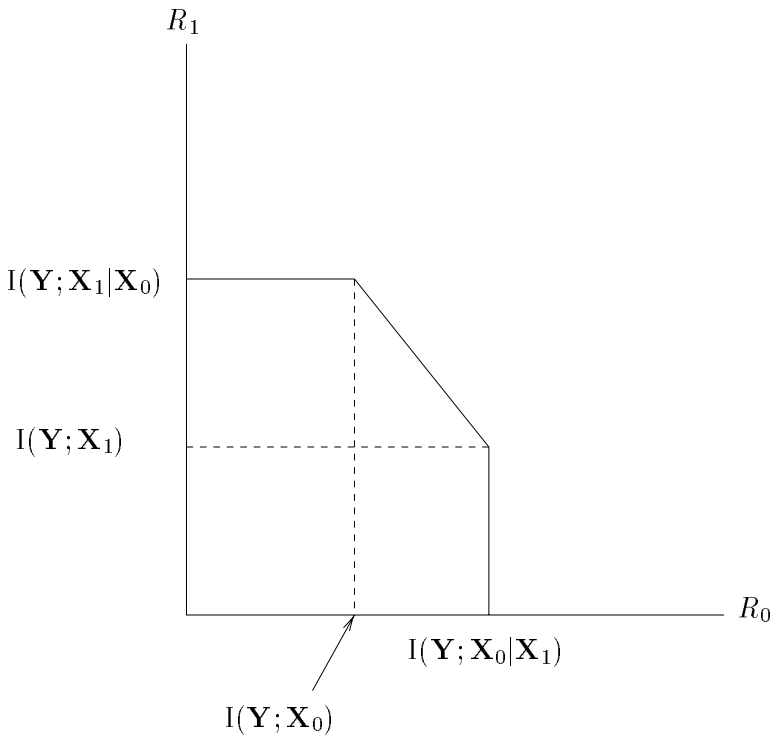

Figure 7.7: The Cover–Wyner Pentagon

according to the decoding order used at that time instant.

Another recent and promising technique for achieving any point on the rate region was developed by Rimoldi and Urbanke [RU96]. Here each user but one splits his source into two separate sources whose outputs are added before transmitting across the channel. By controlling the relative rates of the split sources, any point on the achievable rate region lying between the corner points can be used with single–user successive decoding. Practically speaking, this is very important since neither the decoding order nor the code rates need to be changed during transmission. The disadvantage of this technique, however, is that the decoding complexity is twice as high.

We show the Cover–Wyner pentagon compared to orthogonal multiplexing for equal signal–to–noise ratios $P_i/N_0 = 10$ dB in Figure 7.8. We see that orthogonal multiplexing is optimal at the equal–rate point when we have equal transmitter powers. The total rate sum also increases without bound with the number of users which was not the case when single–user decoding was performed.

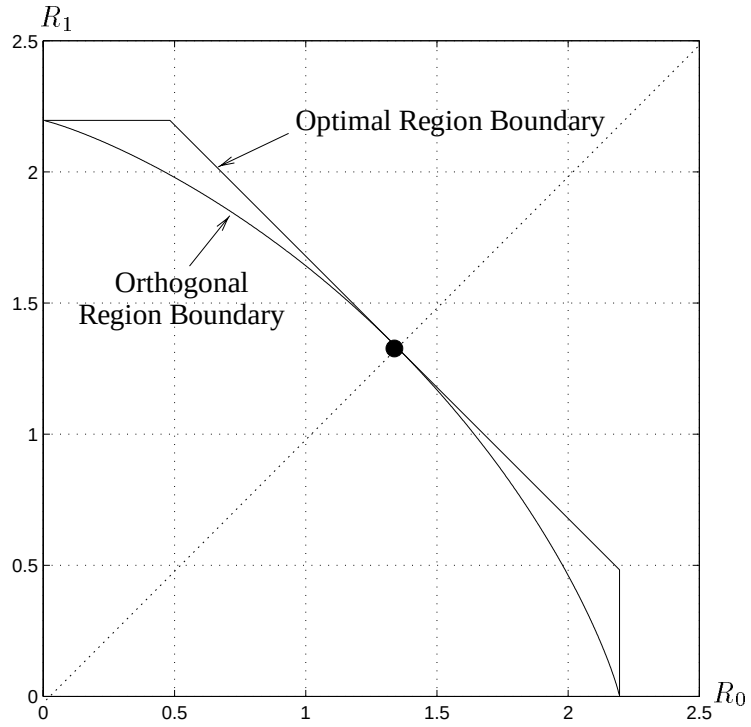

Figure 7.8: Comparison of the Optimal Rate Region with Orthogonal Multiplexing

DS–CDMA with Joint Detection

If we consider the perfectly symmetric power case, we can compute the total rate sum for joint detection of a synchronous DS–CDMA system. We may write (7.10) equivalently as

$$\mathbf{y}_n = \begin{pmatrix} \mathbf{g}_{0,n} & \mathbf{g}_{1,n} & \cdots & \mathbf{g}_{L-1,n} \end{pmatrix} \begin{pmatrix} u_{0,n} \\ u_{1,n} \\ \vdots \\ u_{S-1,n} \end{pmatrix} + \mathbf{z}_n, \quad n = 0, 1, \cdots, N/S - 1$$

$$= \mathbf{W}_n \sqrt{\mathbf{\Sigma}_n} \mathbf{V}_n^{\mathrm{T}} \begin{pmatrix} u_{0,n} \\ u_{1,n} \\ \vdots \\ u_{L-1,n} \end{pmatrix} + \mathbf{z}_n, \tag{7.19}$$

where $\mathbf{W}_n$ and $\mathbf{V}_n$ are unitary matrices and $\sqrt{\mathbf{\Sigma}_n}$ is a diagonal matrix containing the singular values of the $L \times S$ matrix, $\mathbf{G}_n = \mathbf{W}_n \sqrt{\mathbf{\Sigma}_n} \mathbf{V}_n^{\mathrm{T}}$, whose columns are the spreading sequences for symbol n. We may therefore consider the equivalent decomposed channel

$$y'_{n,i} = \sqrt{\lambda_{n,i}} u'_{n,i} + z'_{n,i}, \quad n = 0, \cdots, N/L - 1, \quad i = 0, \cdots, L - 1 \tag{7.20}$$

where $\overline{u'_{n,i}{}^2} = LP$. The total rate sum (for large N/S) is

$$R_{\text{sum}} = \frac{1}{N} \sum_{n=0}^{N/S-1} \text{I}(\mathbf{Y}_n; U_n | \mathbf{G}_n = \mathbf{G}_n)$$
$$= \frac{1}{2L} \text{E}_{\lambda_{n,i}} \sum_{i=0}^{S-1} \log_2 \left(1 + \frac{2\lambda_{n,i} P}{N_0}\right). \tag{7.21}$$

This can be computed numerically by Monte–Carlo averaging. We show the comparison between the total rate sum R_{sum} for the two non–orthogonal approaches with joint detection in Figure 7.9 for an SNR of $P/N_0 = 10$ dB and assuming $S = L$. As was the case for single–user decoding, we can achieve higher data rates with low–rate coding than with DS–CDMA.

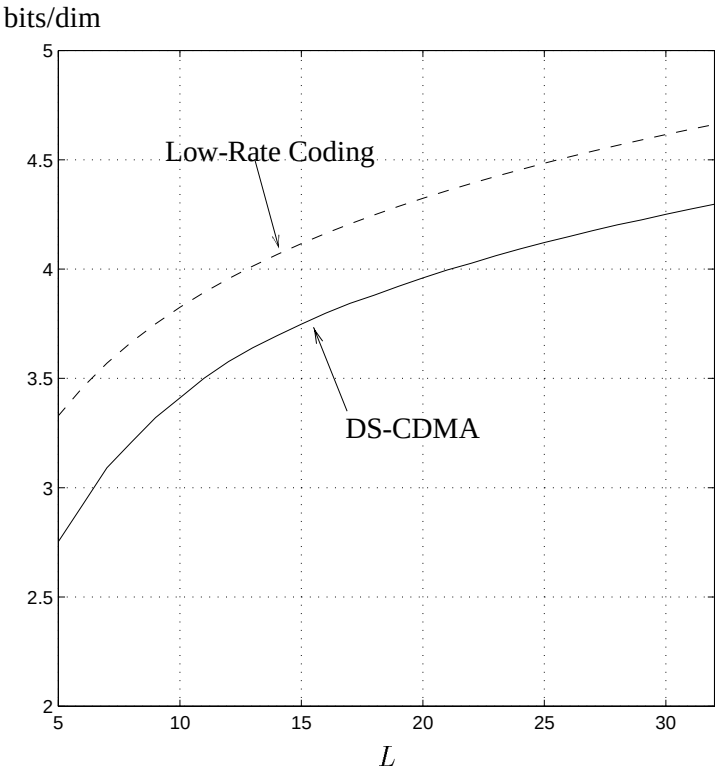

Figure 7.9: Comparison of Joint Detection of DS–CDMA and Low–Rate Coding Systems

There has been a great deal of research in the last ten years on joint detection schemes for the multiuser channel, the majority of which deal with the DS–CDMA case. A recent review of these techniques is given in [BJK96]. These were sparked by the work of Verdú in [Ver86] who considered the optimal joint detection of asynchronous DS–CDMA on a Gaussian channel.

7.2 Outage Probability Analysis of Single–User Decoding in the Multiple–Access Channel with Multipath Fading

In this section we consider three possible multiplexing strategies over multipath channels

1. Coding all users over all dimensions simultaneously (i.e. general CDMA)
2. A combination of spreading and coding (DS–CDMA)
3. Orthogonal multiplexing where each user's signal occupies each part of the spectrum equally so as to exploit all the degrees of freedom the channel has to offer (pure TDMA or frequency–hopping).

We will assume single–user decoding.

In general, since TDMA uses the entire bandwidth the available diversity significantly reduces the outage probability. Moreover, by adding guard intervals which slightly lowers the average information rate, orthogonality can be maintained even in the presence of multipath and slight user asynchronism. It has the disadvantage that the peak–to–average power ratio is high since it is inherently bursty. FDMA transmits with a constant power but does not benefit as much from frequency–selectivity. Perfect orthogonality is also difficult to achieve since the passband filters are never perfect and adjacent channel interference is inevitable. Some systems such as GSM combine FDMA and TDMA in order to lower the peak–to–average power ratio. In addition, one can perform slow–frequency hopping to take advantage of frequency–selectivity using the coding techniques we considered in Chapter 4 without losing orthogonality. This is also shown in figure 7.4. The price to be paid for this approach is a slightly longer decoding delay. Orthogonal DS-CDMA suffers to a certain extent on wireless multiple–access channels since multipath and user asynchronism removes perfect orthogonality between the signals.

Here we examine only the case of single–user receivers without any channel state feedback. In order to simplify the analysis we will use the multi-tone signal model described in Chapters 2 and 3. This allow us to capture several important characteristics of multiuser systems, most notably the reduced dimensionality of spread–spectrum waveforms and user asynchronism.

Recall that under the model we have $NS = WT$ dimensions where signals are approximately time–limited to $[-T/2, T/2]$ seconds and strictly band-limited to $[-W/2, W/2]$ Hz. The multiuser case is simply a combination of (4.38) and (7.1) so that its input–output relationship for each dimension is

$$y_{s,n} = \sum_{l=0}^{L-1} h_{l,s} x_{l,s,n} + z_{s,n}, \tag{7.22}$$

where l,s and n are the user,sub-band and time indices respectively and the $\{z_{s,n}\}$ are i.i.d. zero–mean circular–symmetric complex Gaussian random variables with variance N_0. The power constraint for each user is

$$\sum_{s=0}^{S-1}\sum_{n=0}^{N-1}\overline{|x_{l,s,n}|^2} \leq PT \tag{7.23}$$

so that under the assumption of independent $x_{l,s,n}$ and that users transmit Gaussian signals, the mutual information conditioned on *all* of the channel realizations for user 0 is

$$I_H = \frac{1}{NS}\sum_{s=0}^{S-1}\sum_{n=0}^{N-1}\log_2\left(1+\frac{\overline{|x_{s,n}|^2}|h_{0,s}|^2}{N_0+\sum_{l=1}^{L-1}\overline{|x_{l,s,n}|^2}|h_{l,s}|^2}\right) \quad \text{bits/dim} \tag{7.24}$$

$$= \frac{W}{NS}\sum_{s=0}^{S-1}\sum_{n=0}^{N-1}\log_2\left(1+\frac{\overline{|x_{s,n}|^2}|h_{0,s}|^2}{N_0+\sum_{l=1}^{L-1}\overline{|x_{l,s,n}|^2}|h_{l,s}|^2}\right) \quad \text{bits/s.} \tag{7.25}$$

As in the single–user case, we assume a flat signal spectrum with $\overline{|x_{l,s,n}|^2} = \frac{PT}{NS} = \frac{P}{W}$ so that

$$I_H = \frac{1}{S}\sum_{s=0}^{S-1}\log_2\left(1+\frac{P|h_{0,s}|^2}{WN_0+P\sum_{l=1}^{L-1}|h_{l,s}|^2}\right) \quad \text{bits/dim} \tag{7.26}$$

$$= \frac{W}{S}\sum_{s=0}^{S-1}\log_2\left(1+\frac{\frac{P}{WN_0}|h_{0,s}|^2}{1+\frac{P}{WN_0}\sum_{l=1}^{L-1}|h_{l,s}|^2}\right) \quad \text{bits/s.} \tag{7.27}$$

Now let us consider the DS–CDMA case, where we now choose a spreading factor S and spreading sequences of the form

$$\mathbf{g}_{l,n} = \sqrt{\frac{1}{S}}\begin{pmatrix} e^{j\phi_{l,n,0}} & e^{j\phi_{l,n,1}} & \dots & e^{j\phi_{l,n,S-1}}\end{pmatrix} \tag{7.28}$$

where $\phi_{l,n,k}$ are independent uniformly distributed random variables between $[0,2\pi)$. This is the frequency analog of classical DS–CDMA and is much simpler to analyze on multipath channels. The received signal for each time dimension is therefore of the form

$$\mathbf{y}_n = \sum_{l=0}^{L-1} u_{l,n}\mathbf{g}\otimes\mathbf{h}_{l,n} + \mathbf{z}_n \tag{7.29}$$

where $\mathbf{g}\otimes\mathbf{h}_{l,n} = \begin{pmatrix} g_{l,0,n}h_{l,0} & g_{l,1,n}h_{l,1} & \cdots & g_{l,S-1,n}h_{l,S-1}\end{pmatrix}$.

Similarly to the simple case described section 7.1.2, the receiver decodes each user by first correlating the received signal by the *combined* spreading sequence channel response (i.e. a frequency–domain RAKE receiver) for the user in question followed by conventional single–user decoding. We have for user 0

$$y_{0,n} = \frac{1}{S}\sum_{s=0}^{S-1}|h_{0,s}|^2 u_{0,n} + \sum_{l=1}^{L-1}\sum_{s=0}^{S-1} g^*_{0,n,s}g_{l,n,s}h^*_{0,s}h_{l,s}u_{l,n} + z_{0,n} \tag{7.30}$$

where $z_{0,n}$ is a complex circular symmetric Gaussian random variable with mean zero and variance $\frac{1}{S}\sum_{s=0}^{S-1}|h_{0,s}|^2$. We have, therefore, that the average mutual information conditioned on the channel realizations and the spreading sequences is

$$I_H = \frac{1}{S}\log_2\left(1+\frac{\frac{P}{WN_0}Sk_0}{1+\frac{P}{WN_0}j_0}\right) \quad \text{bits/dim} \tag{7.31}$$

where $k_0 = \frac{1}{S}\sum_{s=0}^{S-1}|h_{0,s}|^2$ and $j_0 = \sum_{l=1}^{L-1}\sum_{s=0}^{S-1}\sum_{s'=0}^{S-1} e^{j(\phi_{l,s,n}-\phi_{0,s',n})}h_{0,s}^* h_{l,s}^*/k_0$. The basic difference between (7.31) and (7.27) is the type of averaging which is performed. In the DS–CDMA case, both the averaging over fading (k_0) and over interference (j_0) are achieved by lowering the information rate in a rather brute–force fashion. Note the presence of $1/S$ outside the logarithm. The averaging effect is reduced since it is inside the logarithm. In the general low–rate coding case, the achievable code rate is raised/lowered by the extent of the fading and interference and not by an imposed by a particular coding scheme.

The information outage probabilities in both cases must be calculated by Monte Carlo integration. This has been done using for the same system parameters as in Chapter 3 (i.e. $S = 128$, $W = 1.2288$ MHz, ETSI TU12 channel) for different numbers of users and an SNR of $P/WN_0 = 10$ dB. The results are shown in Figure 7.10 where we plot the information outage probability *vs.* the total rate sum LR. We see that fairly low spectral efficiencies can be expected but that those where low–rate codes are used as opposed to PN spreading are significantly higher. We note that as the number of users increases, the total sum rate increases in the DS system. This is because the signal space is being used more efficiently as the number of users increases (i.e. the factor $1/F$ in front of the mutual information functional gradually disappears.)

Let us now use the IS-95 CDMA system as a means for comparison. The data rate is 9.6kb/s and the maximum number of users per 1.2288MHz is 64. With a voice activity factor of .5 (i.e. at any given time about half the users are actually transmitting and the signals for the others are squelched) this corresponds to a total rate sum spectral efficiency of 9.6*32/1229 = .25 bits/s/Hz. The information outage rate curve for 32 users crosses .25 bits/s/Hz at around $P_{\text{out}}(.25) = 10^{-2}$ which is an acceptable frame error rate for modern vocoders [1]. This shows that our analysis is not that far off from reality.

We also plot the single–user information outage we computed in Chapter 3 which corresponds to the total rate sum for an orthogonal multiplexing system which uses the entire bandwidth. We see that it is noticeably lower (i.e. that higher spectral efficiencies can be expected.)

[1] the GSM vocoder is designed to operate at this speech frame error rate

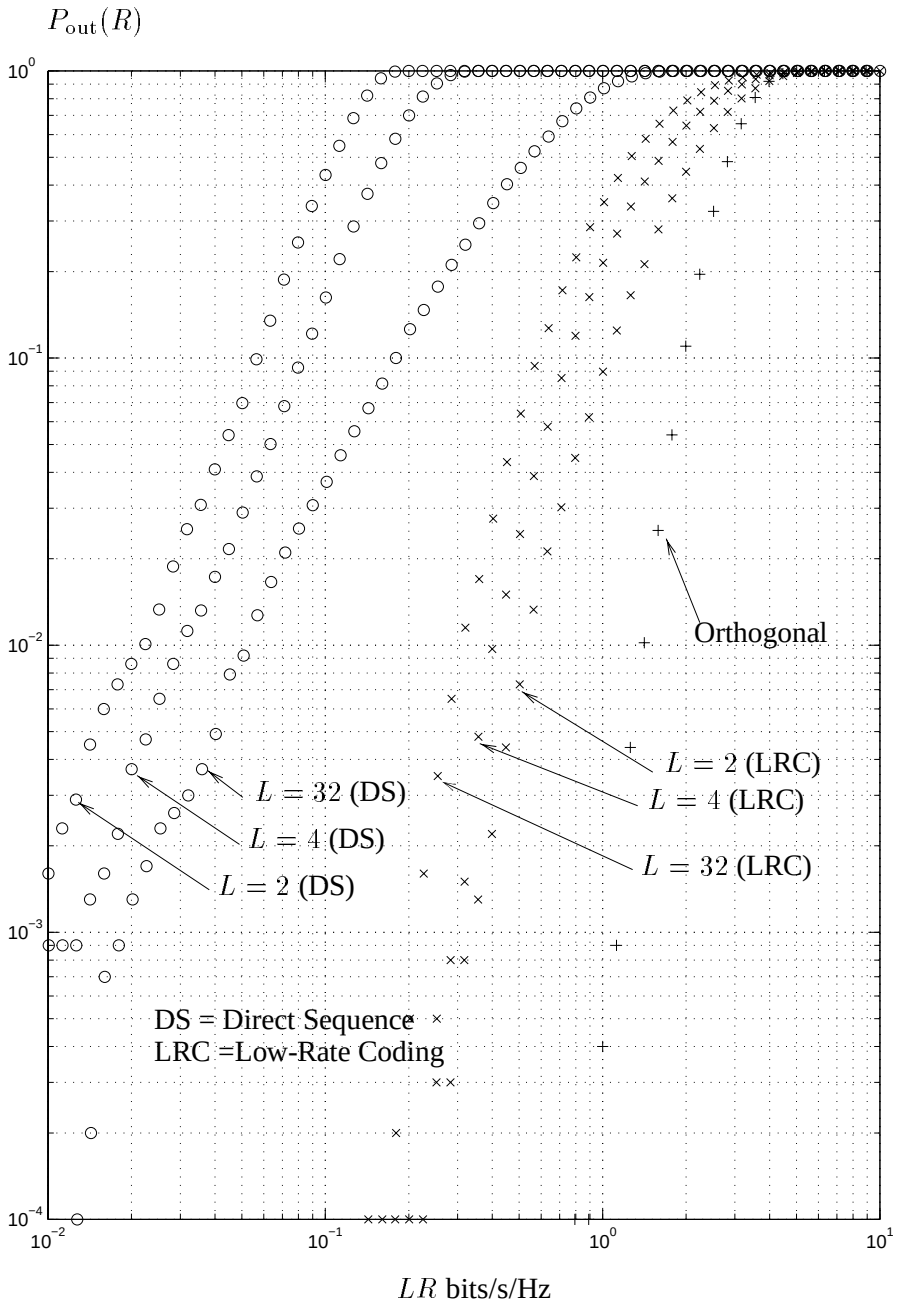

Figure 7.10: Comparison of Low–Rate Coding and Direct–Sequence CDMA schemes

For a single–cell system such as this we really must question the use of a non–orthogonal approach such as CDMA. Even if we could perform joint detection which would be a difficult task in a multipath fading environment, the amount that has to be gained to catch up to an othogonal scheme (with diversity) is huge. The real advantage of CDMA comes in cellular systems where co–channel interference is a significant problem [GJP+91]. Here the orthogonal scheme is at a real disadvantage since frequency–reuse must be used which significantly reduces system capacity. The effect of co–channel interference in CDMA is simply a slight reduction of the signal–to–noise ratio so that it does not suffer to a great extent. It has recently been shown [PC95][CKH97] that orthogonal schemes need not be limited by co–channel interference and that frequency–reuse may not be necessary. Moreover, they can offer system capacities comparable with CDMA, at the expense of increased decoding delay.

7.3 Average Information Rates - Multiuser Diversity

In Chapter 3 we considered average information rates and showed that they can be achieved in two ways. The first was by coding over a long time-scale (i.e. over an infinite number of degrees of freedom of the channel process) without the need for channel state information at the transmission end. The second was by variable–rate coding when channel state information is available. These results relied on the fact that the channel was block stationary, and that coding or channel control was performed over many such blocks. As a result, ergodic arguments could be used to determine the average or long–term information rates at which reliable communication is possible. We now generalize these ideas to the Gaussian MAC.

7.3.1 Generalizing the Single–User Average Mutual Information for the Fading MAC

We generalize the single user waveform channel from Chapter 3 to the L–user channel as

$$y_n(t) = \sum_{l=0}^{L-1} \int_{-T/2}^{T/2} x_{n,l}(\tau) h_{n,l}(t,\tau) d\tau + z_n(t), \quad t \in [-T_o/2, T_o/2] \tag{7.32}$$

where $h_{n,l}(t,\tau)$ is now the response of user l's channel at time t to an impulse at time τ. The subscript n in all the signals denotes the n^{th} realization or block of the corresponding process. We assume that the difference between the durations of the output signal and input signals $T_o - T$ is larger than all the delays due to multipath propagation and user asynchronism. The noise process is again a zero–mean, circular symmetric, white complex Gaussian process with power spectral density N_0 and the channel responses

are assumed to be stationary during the transmission of each block as

$$h_l(t,\tau) = \begin{cases} h_l(t-\tau) & -T/2 \le \tau \le T/2,\ -T_o/2 \le t \le T_o/2 \\ 0 & \text{elsewhere} \end{cases} \tag{7.33}$$

For the Gaussian MAC we are interested in the average mutual information functionals

$$I_{T,H,U} = \frac{1}{T}\mathrm{I}(Y(t); B_U(t)|B_{\overline{U}}(t), \{H_l(t,\tau) = h_l(t,\tau), l = 0, \cdots, L-1\})),\ \ \forall U \in \mathcal{U}\ \ \text{bits/s} \tag{7.34}$$

where $b_U(t) = \sum_{l\in U} \int_{-T/2}^{T/2} x_l(\tau) h_l(t,\tau) d\tau$. We now perform a Karhunen–Loève expansion on the $b_U(t)$ as

$$b_U(t) = \sum_{i=0}^{\infty} b_{U,i}\phi_i(t : U, T, H) \tag{7.35}$$

where the $\mathrm{E}\ |b_{U,i}|^2 = \lambda_i(U,T,H)$ and $\phi_i(t : U,T,H),\ -T_o/2 \le t \le T_o/2$ are the solution to

$$\lambda_i(U,T,H)\phi_i(t : U,T,H) = \int_{-T_o/2}^{T_o/2} K_b(t,u : U,T,H)\phi_i(u : U,T,H)du \tag{7.36}$$

and

$$K_b(t,u : U,T,H) = \sum_{l\in U} \int_{-T/2}^{T/2}\int_{-T/2}^{T/2} K_{x_l}(\tau,\tau')h_l(t,\tau)h_l(u,\tau')d\tau d\tau'. \tag{7.37}$$

We have assumed that the users signals are independent. In a mean–square sense we have with Gaussian signals that

$$I_{T,H,U} = \frac{1}{T}\sum_{i=0}^{\infty} \log_2\left(1 + \frac{\lambda_i(U,T,H)}{N_0}\right)\ \ \text{bits/s} \tag{7.38}$$

As was the case in Chapter 4, in the limit of large T we obtain, via the Szegö eigenvalue distribution theorem [GS83], the following lower–bound for (7.34)

$$I_{T,H,U} \ge I_{H,U} = \int_{-W/2}^{W/2} \log_2\left(1 + \frac{1}{N_0}\sum_{i\in U} S_{i,n}(f)|H_{i,n}(f)|^2\right),\ \ \forall U \in \mathcal{U}\ \ \text{bits/s} \tag{7.39}$$

and, under the assumption of bandlimited transmitted signals, the corresponding average power constraint is

$$\mathrm{E}\int_{-W/2}^{W/2} S_{i,n}(f)df = P_i. \tag{7.40}$$

The signals are band–limited to $[-W/2, W/2]$ and $S_{i,n}(f)$ is the power spectrum of user i in block n. If the time–bandwidth product is large, as in the single–user case $I_{T,H} \approx I_H$.

7.3.2 Systems Without Fast Power Control

Let us now compare two alternative systems. The first is orthogonal multiplexing where each user uses shares bandwidth/time equally. For FDMA each user would use a bandwidth W/L and transmit all the time. The F block average mutual information conditioned on the channel realizations for user i with FDMA is

$$I_{i,H}^{\text{orth}} = \frac{1}{F}\sum_{n=0}^{F-1}\int_{-W/L}^{W/L} \log_2\left(1+\frac{1}{N_0}S_{i,n}(f)|H_{i,n}(f)|^2\right) \text{bits/s}. \tag{7.41}$$

Let us assume that the users have flat input spectra so $S_{i,n}(f) = LP_i/W$ and that F is large so that the rate sum for any $U \subseteq \mathcal{U}$ tends to

$$I_{U,H}^{\text{orth}} = \sum_{i\in U}\frac{W}{L}\text{E}_{h_i}\log_2\left(1+\frac{LP_i}{WN_0}h_i\right) \quad \text{bits/s} \tag{7.42}$$

where h_i is the random variable describing the channel strength $|H_{i,n}(f)|^2$ which is assumed to be identically distributed at each frequency and in each block and independent from user to user. This allows us to remove the integral in (7.41). Note that (7.41) holds for slow–frequency hopping as well as long as the statistics of the different frequency bands where the signal hops are identical. The TDMA case is also given by (7.42) since each user would use bandwidth W with power LP_i a fraction $1/L$ of the time.

Now consider the general non–orthogonal approach which has the rate sum taken over a large number of blocks and using uniform power spectra

$$I_{U,H}^{\text{opt}} = W\text{E}_{\{h_i,\, i\in U\}}\log_2\left(1+\frac{1}{WN_0}\sum_{i\in U}P_ih_i\right) \text{bits/s}. \tag{7.43}$$

By virtue of the concavity of the logarithm and Jensen's inequality [CT91] we have that

$$I_{U,H}^{\text{orth}} \le \frac{W|U|}{L}\text{E}_{\{h_i,\, i\in U\}}\log_2\left(1+\frac{L}{|U|WN_0}\sum_{i\in U}P_ih_i\right) \quad \text{bits/s} \tag{7.44}$$

which, using the fact that $x\log_2(1+b/x)$ is increasing for any $b>0$, can be bounded further as

$$I_{U,H}^{\text{orth}} \le W\text{E}_{\{h_i,\, i\in U\}}\log_2\left(1+\frac{1}{WN_0}\sum_{i\in U}P_ih_i\right) = I_{U,H}^{\text{opt}} \ \text{bits/s} \tag{7.45}$$

with strict inequality unless $|U| = L$.

These important results are due to Gallager [Gal94] and show that the achievable rate region for orthogonal multiplexing (when users share the dimensions on an equal basis) always lies within that of an

optimal scheme which codes users over all the dimensions. Moreover, they are valid for TDMA,FDMA or slow–frequency hopping systems. Let us examine the implication of these results with a numerical example, by assuming that the fading process is Rayleigh distributed and $P_i = P,\ \forall i$. This symmetric situation arises in practice if we have a perfect *slow* power controller which assures that the average received SNR remains constant and equal for every user. This is important since it assures an equal quality of service (on a long–term basis) for all users. In this case, all the channel strengths h_l are exponentially distributed as

$$f_h(\alpha) = e^{-\alpha}, \alpha \geq 0 \tag{7.46}$$

so that the rate sums are

$$I_{U,H}^{\text{opt}} = W \int_0^\infty \log_2 \left(1 + \frac{P}{WN_0} a\right) f_{\beta_{|U|}}(a) da \ \ \text{bits/s} \tag{7.47}$$

where $\beta_{|U|} = \sum_{i \in U} h_i$ is the sum of the channel strengths in U, which is an *Erlang* random variable with density

$$f_{\beta_{|U|}}(a) = \frac{a^{|U|-1}}{(|U|-1)!} e^{-a}, a \geq 0. \tag{7.48}$$

The rate sums in (7.47) can be expressed in terms of the *Meijer G-function*[GR80] but are simpler to calculate via numerical integration. The orthogonal rates are just the single–user rates as in Chapter 3

$$I_{U,H}^{\text{orth}} = \frac{W|U|}{L \ln 2} e^{WN_0/(LP)} \text{E}_1 \left(\frac{WN_0}{LP}\right). \tag{7.49}$$

In figure 7.11 we show the achievable rate regions for three two–user systems, the two we just described and an orthogonal scheme where we can adjust the proportion of the total dimensions allocated to each user. This was described in section 7.1.1 and for the fading case, we simply have

$$\begin{aligned} R_1 &\leq \frac{(1-\alpha)W}{\ln 2} \exp\left((1-\alpha)\frac{WN_0}{P}\right) \text{E}_1 \left((1-\alpha)\frac{WN_0}{P}\right) \\ R_2 &\leq \frac{\alpha W}{\ln 2} \exp\left(\alpha \frac{WN_0}{P}\right) \text{E}_1 \left(\alpha \frac{WN_0}{P}\right) \end{aligned} \tag{7.50}$$

We chose a signal to noise ratio $P/(WN_0) = 10$ dB. We see that there is a significant increase in spectral efficiency for the non–orthogonal scheme even at the equal rate point, which shows that the fading channel behaves quite differently than the non-fading channel. As pointed out by Gallager a rather peculiar result is that L users transmitting over L different channels can transmit more total average information than a single user transmitting over one channel using L times as much power. This

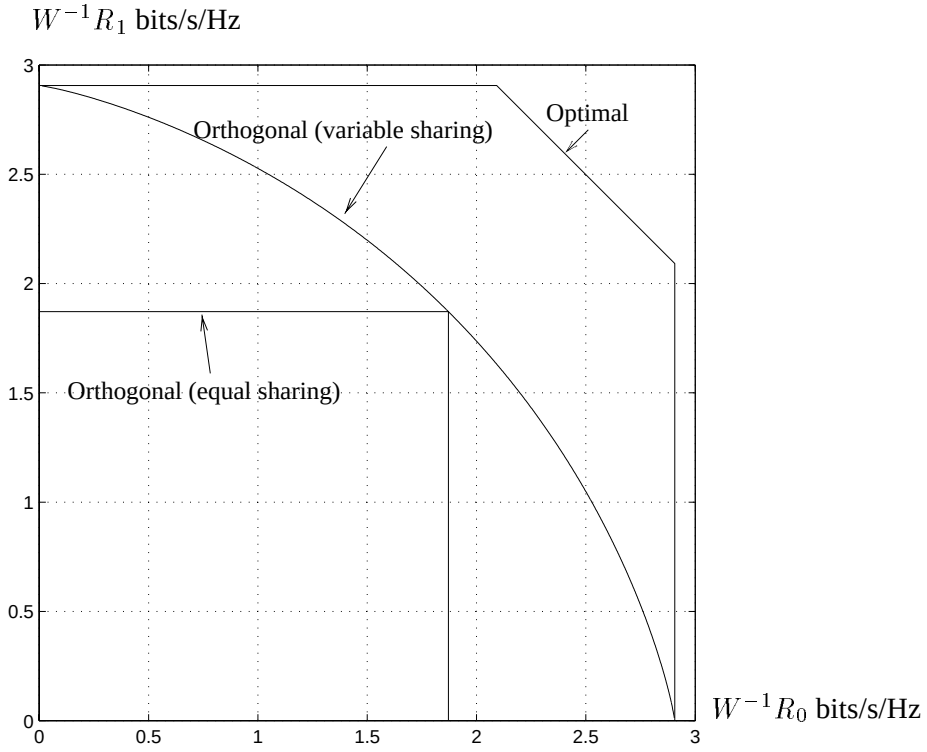

Figure 7.11: Two–user Rate Regions in Rayleigh Fading

is due to an averaging effect inside the logarithm in the multiuser case since the sum signal has a total received energy which has L degrees of freedom and not a single one as would be the case with one user. This can be made more clear if we consider the special case where the bandwidth is proportional to the number of users, say $W = LW_B$, where W_B can be thought of as the bandwidth per user. If we focus on the total rate sum (i.e. when $U = \mathcal{U}$), the orthogonal schemes with equal transmitted powers will have

$$I_{\mathcal{U},H}^{\text{orth}} = LW_B \mathrm{E}_h \log_2 \left(1 + \frac{P}{W_B N_0} h\right) \tag{7.51}$$

and the optimal scheme will have

$$I_{\mathcal{U},H}^{\text{opt}} = LW_B \mathrm{E}_{\beta_L} \log_2 \left(1 + \frac{P}{W_B N_0} \frac{\beta_L}{L}\right). \tag{7.52}$$

We note that for $L \to \infty$, the random variable β_L/L is 1 with probability 1 since the h_i are independent and consequently the total rate sum tends to L times the Gaussian channel capacity given by

$$C_G = LW_B \log_2 \left(1 + \frac{P}{W_B N_0}\right) \text{bits/s}. \tag{7.53}$$

If we now compute the difference in spectral efficiency on a per user level between the Gaussian channel capacity and orthogonal multiplexing on a Rayleigh fading channel, we have that [AS65]

$$\begin{aligned}(LW_B)^{-1}(C_G - I_{\mathcal{U},H}^{\text{orth}}) &= \log_2 \left(1 + \frac{P}{W_B N_0}\right) - \exp\left(\frac{W_B N_0}{P}\right) \mathrm{E}_1 \left(\frac{W_B N_0}{P}\right) / \ln 2 \\ &= \log_2 \left(1 + \frac{P}{W_B N_0}\right) - \\ &\quad \exp\left(\frac{W_B N_0}{P}\right) \left(-\gamma - \ln\left(\frac{W_B N_0}{P}\right) - \sum_{n=1}^{\infty} \frac{(-1)^n \left(\frac{W_B N_0}{P}\right)^n}{nn!}\right) / \ln 2 - \quad \text{bits/s/Hz}\end{aligned} \tag{7.54}$$

which for large $\frac{P}{W_B N_0}$ tends to $-\gamma/\ln 2 = .8327$ bits/s/Hz, where $\gamma = .57721$ is *Euler's constant*. This shows that the most that can be gained by using a non–orthogonal scheme such as CDMA on a multipath channel as opposed to any type of orthogonal multiplexing is .8327 bits/s/Hz. It assumes, of course, that we have a coding scheme with no delay constraint and that some optimal successive decoding scheme, such as *onion peeling* [RU96] can be used.

7.3.3 Channel State Feedback and Multiuser Diversity

We now move on to the case when channel knowledge is available at the transmission end and some form of channel control can be performed. When we considered this possibility for the single–user case we were only able to control the transmitter power and the code rate. On the multiuser channel we have one more possibility, the allocation strategy. We begin with a simple example.

A Two–User Frequency Flat Channel

Let us assume we have a two–user system and that we wish to allocate users equally in time using TDMA. We know that each user will transmit half the time with a peak–to–average power ratio of 2. Normally, we would alternate between the users every T seconds as shown in figure 7.12(a). Now let us assume that the transmitters have knowledge of *both* channel responses at any instant in time and the user with the stronger received signal strength is allocated to the channel. This is shown in 7.12(b). We no longer have a regular allocation strategy, but if both users have equal average received strengths then they will share the channel equally just like with regular TDMA, and will transmit with the same peak–to–average power ratio. Again we will assume that the channel stays constant for reasonably long periods of time

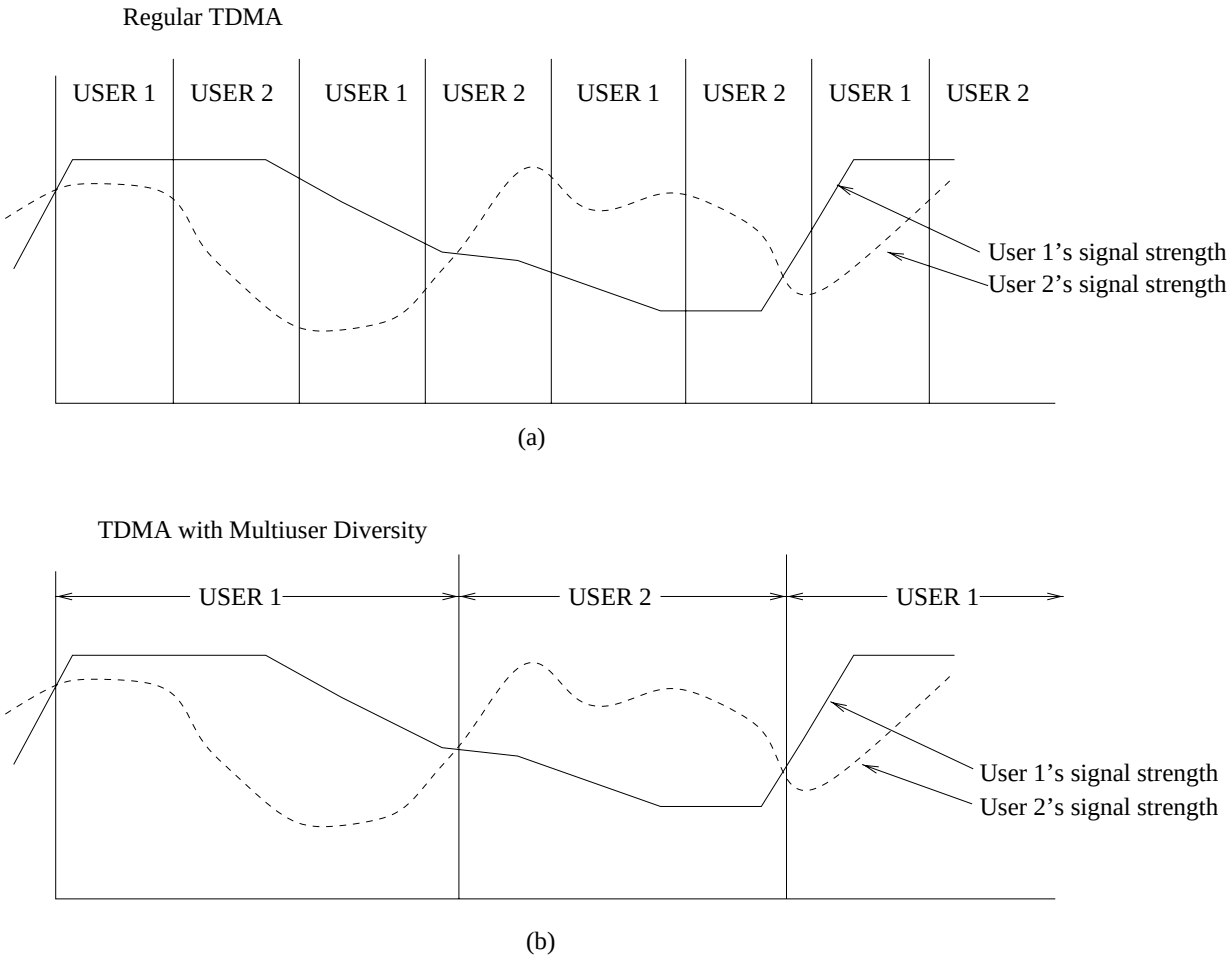

Figure 7.12: Illustrating Multiuser diversity

so that we can use the block–fading assumption. The average mutual information for regular TDMA is

given by

$$I_H^{\mathrm{TDMA}} = \frac{W}{2}\mathrm{E}_h \log_2\left(1 + \frac{2P}{WN_0}h\right) \quad \mathrm{bits/s/Hz}. \tag{7.55}$$

In the second case, when a given user is transmitting, we are sure to have a channel attenuation $h = \max\{h_0, h_1\}$ so that its statistics are quite different. Its average mutual information is still given by (7.55) but with a different distribution function for h. We see that this channel allocation strategy has given us a form of diversity which does not exist in the single–user case. We have given it the name *multiuser diversity* although it is simply selection diversity *performed at the transmission end.* This has the effect of a power boost at the receiver since the mean of h will be greater than the means of h_0 and h_1 (for this example the mean channel strength is 1.5 and not 1). Let us see what effect this has on the average mutual information. We saw in Chapter 2, that the density function of a 2–channel selection diversity system was given by

$$f_H(u) = 2e^{-u} - 2e^{-2u} \tag{7.56}$$

so that the average mutual information in Rayleigh fading is given by

$$I_H^{\mathrm{TDMA-div}} \frac{W}{\ln 2}\left(\exp\left(\frac{WN_0}{2P}\right)\mathrm{E}_1\left(\frac{WN_0}{2P}\right) - \exp\left(\frac{WN_0}{P}\right)\mathrm{E}_1\left(\frac{WN_0}{P}\right)\right) \quad \mathrm{bits/s}. \tag{7.57}$$

We plot (7.57) and (7.55) along with the Gaussian channel capacity for a two–user TDMA system

$$C_G^{\mathrm{TDMA}} = \frac{W}{2}\log_2\left(1 + \frac{2P}{WN_0}\right) \tag{7.58}$$

in figure 7.13 as a function of the signal–to–noise ratio P/WN_0. We see that not only is an improvement over the regular TDMA case, but the performance even surpasses that of a non–fading Gaussian channel. The reason for this is the power boost from the selection diversity, which forces the transmitter to operate only when the channel strength is above average. Unlike the single–user case, there is no penalty in using the channel only part of the time since it must be shared between the two users.

7.3.4 The Fading Channel Capacity Region

In order to explain the effect of multiuser diversity more carefully, we must compute the capacity region of the multiple–access channel with fading, since this will tell us the optimal channel–control policy, in the sense of maximum average information rates. In Chapter 5 we saw that there were two basic types of channel capacity and they were achieved by adjusting the power spectra of the user according to the channel state.

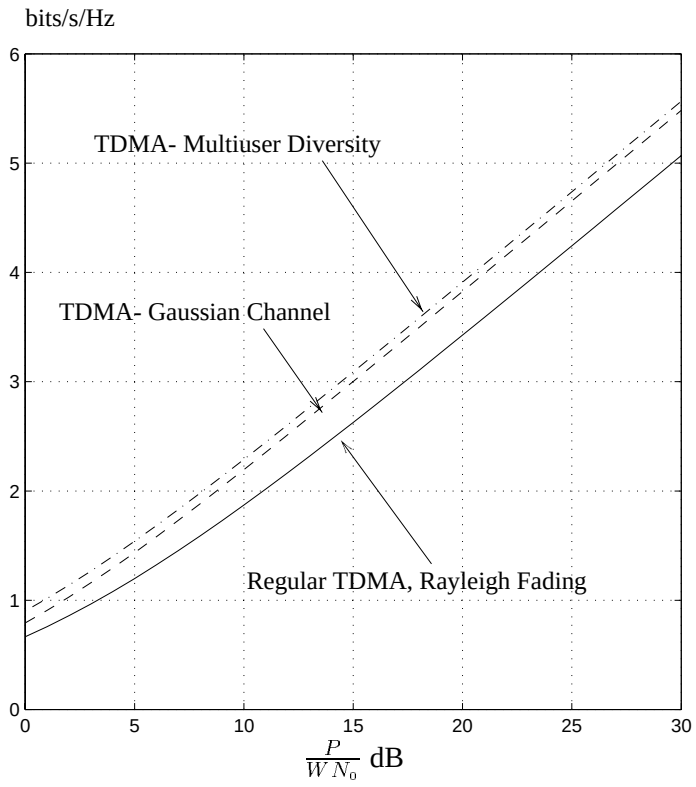

Figure 7.13: Mutual Information for Different 2-User Multiuser Channel Allocation Strategies

The first was the *delay–limited capacity* where the power was adjusted such that the average mutual information was constant and maximum at the receiver. This idea was also very recently generalized to the multiuser channel by Hanly and Tse in [HT96], where they define a *delay–limited capacity region* in the same way, which insures that the receiver is operating at a fixed set of data rates at any given time instant. They show that any point on the delay–limited capacity region can be achieved by a successive decoding strategy whose decoding order depends on the channel states of the different users, but their rates remain fixed in time. This is a particularly appealing result since as in Rimoldi's rate–splitting approach to the Gaussian MAC [RU96], no variable rate coding schemes are necessary.

The other type of capacity was the *average capacity*, where either the code rate was variable or the code extended across the different channel realizations. We will focus on this case and show that under some circumstances the optimal channel control scheme is orthogonal multiplexing with dynamic allocation as in the simple example we just outlined. In general, we are interested in letting the users adjust their power spectra assuming they have *a priori* knowledge of *all* the channel responses.

The complete capacity region for this problem has recently been found by Tse and Hanly [TH96]. They generalized the techniques of Cheng and Verdu in [CV93] who solved the problem for the non–

fading two–user Gaussian MAC with intersymbol interference. Tse and Hanly's result exploits the polymatroidal structure of the capacity region and describes the power control policies for an arbitrary number of users. An important result is that it is a convex region traced out from all possible combinations of power control strategies satisfying the energy constraints in (7.40). For each set of power control policies, the achievable rate region will be a Cover–Wyner pentagon, so that the capacity region will be the supremum of all the corner points from these pentagons. We illustrate this for two users in figure 7.14. They

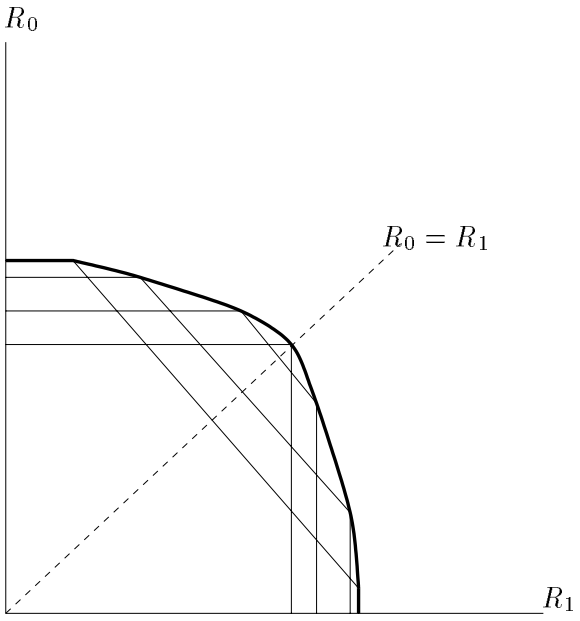

Figure 7.14: Fading Channel Capacity Region

also show that any point on the boundary of the region can be achieved by successive decoding without having to change the decoding order, the averaging effect achieved by timesharing on the Gaussian MAC is taken care of by the variations of the channel in the fading MAC.

In most cases, we are interested only in the situation where all users have the same average power at the receiver, which would be accomplished in practice using some form of slow power control. As we already mentioned, this would be to assure the same long–term quality of service for each user. If this is the case, all the power constraints in (7.40) will be the same and under the reasonable assumption of identical channel statistics, all power controllers will also be the same. In terms of the capacity region, we see that it is symmetric [TH96] around the equal rate line. If we focus on this case, the only quantity to maximize is the total rate sum which corresponds to the equal rate point on the capacity region boundary (i.e. $R_0 = R_1 = \cdots = R_{L-1}$). This maximization was first done by Knopp and Humblet

[KH95a][KH95b]. Here we must maximize

$$R_{\text{sum}} = \sum_{l=0}^{L-1} R_i = \int_{-W/2}^{W/2} \mathrm{E}_{\{H_0,\cdots,H_{L-1}\}} \log_2 \left(1 + \frac{1}{N_0} \sum_{i=0}^{L-1} S_{i,n}(f)|H_{i,n}(f)|^2\right) df \tag{7.59}$$

subject to (7.40), with $P_i = P, \ \forall i$. Introducing a single Lagrange multiplier (since the problem is symmetric) $1/B$ and by applying the Kuhn–Tucker conditions for the maximization of a concave cost function [Gal68], we have the following set of inequalities governing the optimal $S_{i,n}(f)$

$$\frac{\partial}{\partial S_{i,n}(f)} \log_2 \left(1 + \frac{1}{N_0} \sum_{i=0}^{L-1} S_{i,n}(f)|H_{i,n}(f)|^2\right) - \frac{1}{B} \frac{\partial}{\partial S_{i,n}(f)} \left(S_{i,n}(f) - \frac{P}{W}\right) \leq 0 \tag{7.60}$$

with equality if and only if $S_{i,n}(f) > 0$. Rearranging terms we have that the solution must be of the form

$$S_{i,n}(f) = \begin{cases} B - \frac{N_0}{|H_{i,n}(f)|^2} & |H_{i,n}(f)|^2 \geq \frac{N_0}{B}, |H_{i,n}(f)|^2 \geq |H_{j,n}(f)|^2, j \neq i \\ 0 & \text{otherwise} \end{cases} \tag{7.61}$$

where B satisfies the power constraints and is the solution to

$$\int_{N_0/B}^{\infty} \left(B - \frac{N_0}{\alpha}\right) f_\alpha(\alpha) d\alpha = \frac{LP}{W} \tag{7.62}$$

and $h = \max\{|H_0(f)|^2, \cdots, |H_{L-1}(f)|^2\}$. The total rate sum is therefore

$$R_{\text{sum}} = W \int_{N_0/B}^{\infty} \log_2 \left(B \frac{\alpha}{N_0}\right) f_h(h) dh. \tag{7.63}$$

This power control scheme is nothing but a generalization of the water–filling scheme described in Chapter 5 but has a very important practical implication. It says that at any given frequency in any given block, the only user who should be transmitting is the one with the strongest response at that frequency, provided his channel strength is greater than a threshold N_0/B. We illustrate this for a two–user system in figure 7.15. This scheme is another form of orthogonal multiplexing combined with dynamic frequency allocation. As in the Gaussian MAC, the equal rate point is achieved by orthogonal multiplexing, *when channel knowledge is available at the transmitters*. This is critical since no joint decoding is required to operate at this point. It can be seen as a TDMA system for each frequency where the allocation method is virtually the same as the simple example we used to introduce this section, except for the water–filling power allocation similar to the single–user case. This type of time–varying TDMA would be difficult to achieve if the channel changes too rapidly for accurate estimation to be performed.[2] The latter would

[2] In the IS-95 standard [IS992], channel state estimation is performed 800 times/sec in order to update the power control.

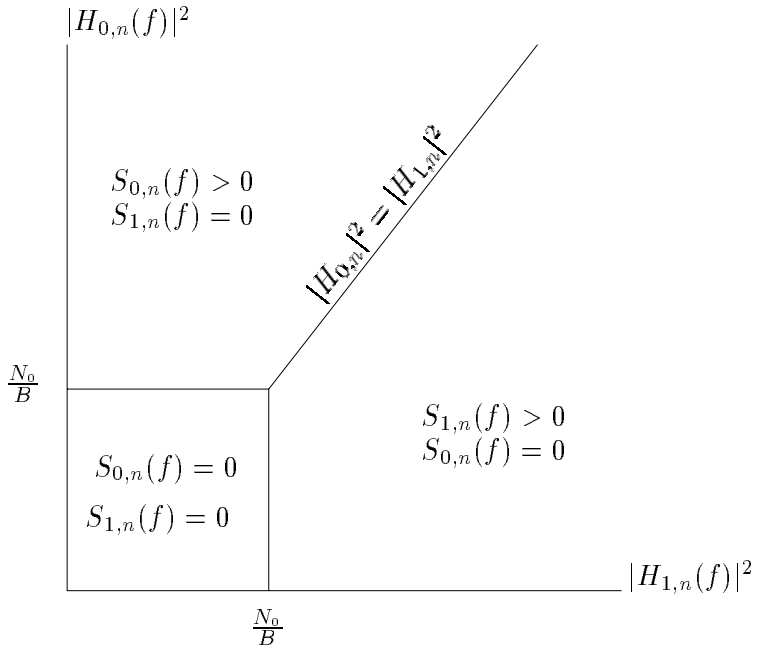

Figure 7.15: Illustrating the Optimal Power Controllers for a Two–User System

cause problems since as the number of users increases, the amount of time any one user remains in a given frequency would decrease. In addition, it should be evident the fading must not be too slow, so as to insure that the average time any user accesses a given frequency band is not too long so that others waiting for service do not get back-logged. This scheme may not be suitable for voice transmission because of the uncertainty in the channel access time. For bursty data, however, this may pose less of a problem.

Optimal bandwidth partitioning based on channel state information being available at the transmission end would be hard to achieve in practice. A more realistic alternative would be to divide the entire bandwidth into N equal size sub-bands and allocate a single user to each of these sub-bands based on the instantaneous frequency responses of all the users. The DECT system employs a technique along these lines. In this system, the available bandwidth is divided into several sub-bands, which we assume to be frequency flat. The users measure the strength of each sub-band, and choose the best available sub-band on which to transmit. In our case, the user with the best channel response in a particular sub-band uses that sub-band alone. This need not require too much effort to put into practice. As we already mentioned in Chapter 3, two–way systems which operate in a time–division duplex fashion can estimate the strengths of their channels via the opposite link, provided the channel responses do not change too quickly. This could be used in the following fashion: the users waiting for service would measure their

own channels from the down-link signal and compare the strengths to those of the currently active users which could be broadcast by the base-station on some control channel. Once they have detected a sub-band where their channel strength is maximum they request allocation to that band, and the base-station decides.

If the subbands are not flat, as is the case in a system like GSM, a time/frequency allocation strategy such as this would still benefit from multiuser diversity but to a lesser extent. The diversity factor gained from using a medium or wide–band signal would tend to reduce the variance of the set of channel strengths over which the selection is performed. At the same time, the average power of each users signal when transmitting would be reduced since the channel strength with diversity would have a much lower probability of being above average. This has a very important practical implication: if the system designer's goal is to maximize the average data rates, we must use narrowband signals with dynamic time/frequency allocation in order to benefit from multiuser diversity.

The type of system is very similar to the on/off multiple channel scheme briefly described in the last chapter. Suppose a user has S uncorrelated frequency bands at his disposal and multiuser diversity among L users is performed on each. The probability of a given user occupying a particular band is $1/L$. The number of bands, N_b, occupied by this user at any given time is binomial with density

$$\text{Prob}(N_b = n_b) = \binom{S}{n_b} \left(\frac{1}{L}\right)^{n_b} (1 - 1/L)^{S-n_b}. \tag{7.64}$$

The outage probability is $(1 - 1/L)^S$ which is approximately $e^{-S/L}$ if L is large. Thus, when $S \gg L$ we have effectively no outages.

Numerical Results in Rayleigh Fading

Let us now compute the total rate sum for Rayleigh fading statistics. We have, therefore, that each of the channel responses are exponentially distributed. It follows that the random variable

$$h = \max\{|H_0(f)|^2, \cdots, |H_{L-1}(f)|^2\} \tag{7.65}$$

has a probability distribution function given by

$$F_h(u) = \text{Prob}\,(h < u) = (1 - e^{-u})^L \tag{7.66}$$

so that its density is

$$f_h(u) = Le^{-u}(1 - e^{-u})^{L-1} = \sum_{k=1}^{L} (-1)^{k-1} \binom{L-1}{k-1} e^{-ku}, \tag{7.67}$$

which is nothing but traditional selection diversity [WJ65]. The total sum of rates is therefore

$$\begin{aligned} R_{\text{sum}} &= LW \sum_{k=1}^{L} (-1)^{k-1} \binom{L-1}{k-1} \int_{N_0/B}^{\infty} e^{-ku} \log_2(\frac{B}{N_0}u) du \\ &= LW \sum_{k=1}^{L} (-1)^{k-1} \binom{L-1}{k-1} \frac{B}{N_0} \int_{1}^{\infty} e^{-kN_0 Bu} \log_2(u) du \\ &= \frac{W}{\ln 2} \sum_{k=1}^{L} (-1)^{k-1} \binom{L}{k} \mathrm{E}_1\left(\frac{kN_0}{B}\right) \quad \text{bits/s} \end{aligned} \tag{7.68}$$

and the constant B is the solution to

$$\begin{aligned} \frac{LP}{W} &= \sum_{k=1}^{L} (-1)^{k-1} \binom{L-1}{k-1} \int_{N_0/B}^{\infty} e^{-ku} \left(B - \frac{N_0}{u}\right) du \\ &= \sum_{k=1}^{L} (-1)^{k-1} \binom{L}{k} \int_{N_0/Bk}^{\infty} e^{-u} \left(B - \frac{kN_0}{u}\right) du \\ &= \sum_{k=1}^{L} (-1)^{k-1} \binom{L}{k} \left(Be^{-\frac{N_0}{B}k} - kN_0 \mathrm{E}_1\left(\frac{N_0 k}{B}\right)\right). \end{aligned} \tag{7.69}$$

If we make the substitution $A = BW/P$ then we have

$$R_{\text{sum}} = \frac{W}{\ln 2} \sum_{k=1}^{L} (-1)^{k-1} \binom{L}{k} \mathrm{E}_1\left(\frac{kWN_0}{PA}\right) \quad \text{bits/s} \tag{7.70}$$

and A is the solution to

$$\sum_{k=1}^{L} (-1)^{k-1} \binom{L}{k} \left(Ae^{-\frac{WN_0}{PA}k} - k\left(\frac{WN_0}{P}\right) \mathrm{E}_1\left(k\frac{N_0 W}{PA}\right)\right) = L. \tag{7.71}$$

We see that as the signal to noise ratio P/WN_0 increases A tends to L. If we again consider the case when the bandwidth is proportional to the number of users, $W = LW_B$, we may compare the spectral efficiencies on an equal footing. This is shown in figure 7.16.

We see two things as the number of users increases. First, for the case of no channel state feedback, the sum capacities for the optimal non–orthogonal scheme in (7.52) quickly rise to the Gaussian channel capacity. The difference between their performance and that of orthogonal multiplexing is also around .8327 bits/s/Hz as predicted. The second observation is that multiuser diversity has an enormous effect at increasing achievable data rates. With $L = 16$ users we are around 1.5 bits/s/Hz higher than the Gaussian channel which is quite remarkable. For low SNR the sum capacity is double that of the Gaussian channel. Moreover, the curves will continue to rise, although slowly, with the number of users since the mean of the channel strength with multiuser diversity is unbounded.

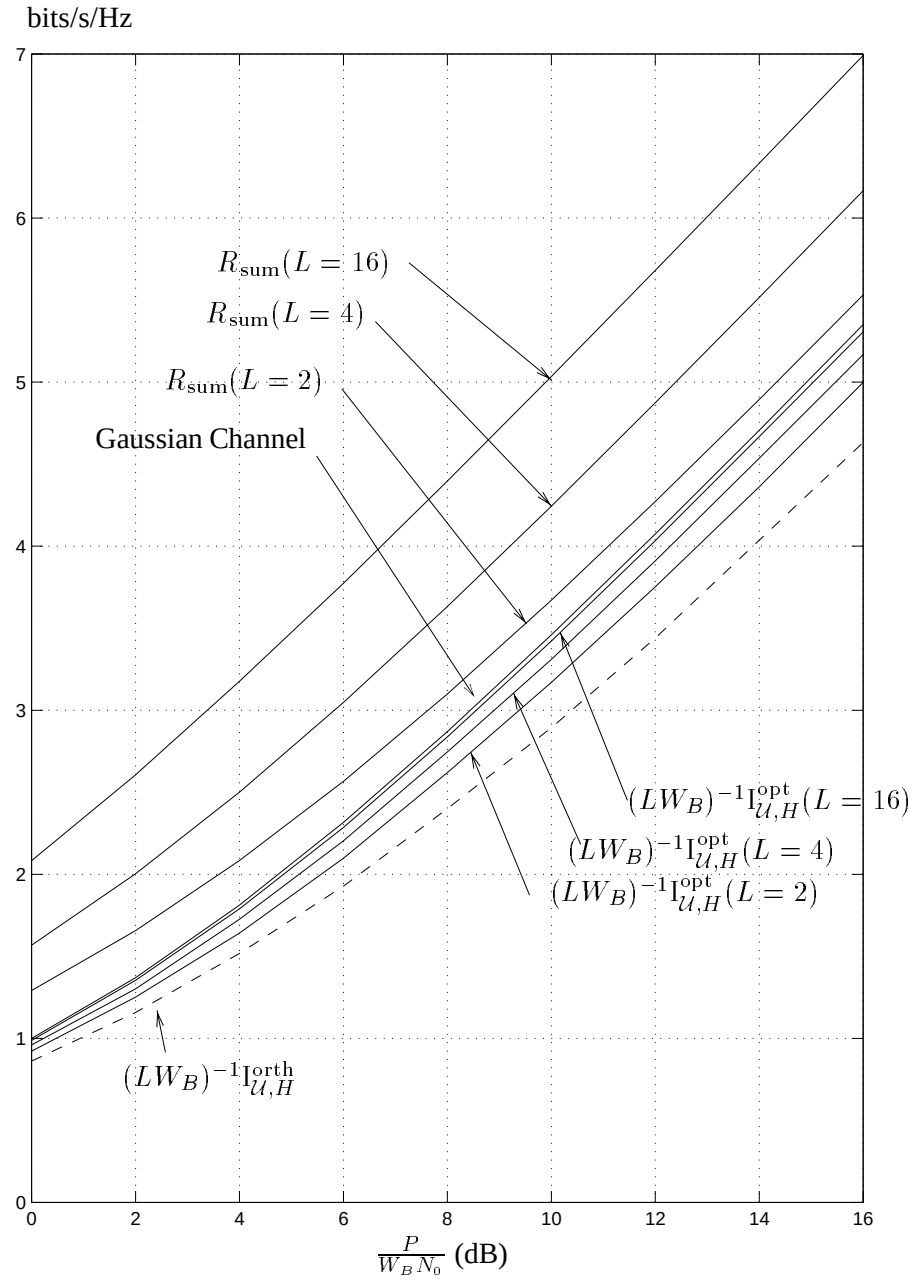

Figure 7.16: Comparison of Different Spectral Efficiencies with and without Channel Control

7.3.5 Multiuser Diversity with Perfect Power Control

Let us now examine the achievable rates for a system which employs multiuser diversity and keeps the received signal–to–noise ratio constant while transmitting (i.e. no water–filling). We considered such schemes for the single–user channel in section 6.1. We will assume that sub–bands in which users signals lie are small enough to be considered frequency–flat.

If we denote the signal attenuation for each user by h_i, the attenuation for the user currently active in a given sub–band is $h = \max\{h_0, h_1, \cdots, h_{L-1}\}$. We employ a perfect power controller

$$\mathcal{P}(h) = \frac{K(L)}{h} \tag{7.72}$$

so that the instantaneous transmit power is $P_T = PK(L)/h$. As before, we choose $K(L)$ such that $\overline{\mathcal{P}(h)} = 1$. The constant received power is $P_R = K(L)P$ so that $K(L)$ becomes the gain/loss with respect to a non–fading channel Gaussian channel. For Rayleigh fading with multiuser (selection) diversity we have [GR80]

$$\begin{aligned} K(L) &= \left(\int_0^\infty L e^{-u}(1-e^{-u}) \frac{du}{u} \right)^{-1} \\ &= \left(\int_0^1 L(-1)^L (u-1)^{L-1} \frac{du}{\ln u} \right)^{-1} \\ &= \left(\sum_{l=1}^{L} (-1)^l \binom{L}{l} l \ln l \right)^{-1}, \quad L > 1. \end{aligned} \tag{7.73}$$

which we plot in figure 7.17. We see that the gain increases with L but not linearly as was the case for the multichannel maximal–ratio combining in Chapter 4. This is due to the fact that the mean channel strength for selection diversity does not increase linearly with L. We must keep in mind, however, that multiuser diversity can be exploited without multiple receivers, if we are willing to wait for adequate channel conditions in order to perform optimal allocation.

Peak–Power Outage Probability

We saw in Chapter 4 that power controllers were subject to outages due to peak–power violations. The same will be true of a system exploiting multiuser diversity. For a maximum peak–to–average transmit power $P_{\max}$ the peak–power outage probability will be

$$P_{\text{out}}(L, P_{\max}) = \text{Prob}\left(h \leq \frac{K(L)}{P_{\max}} \right) \tag{7.74}$$

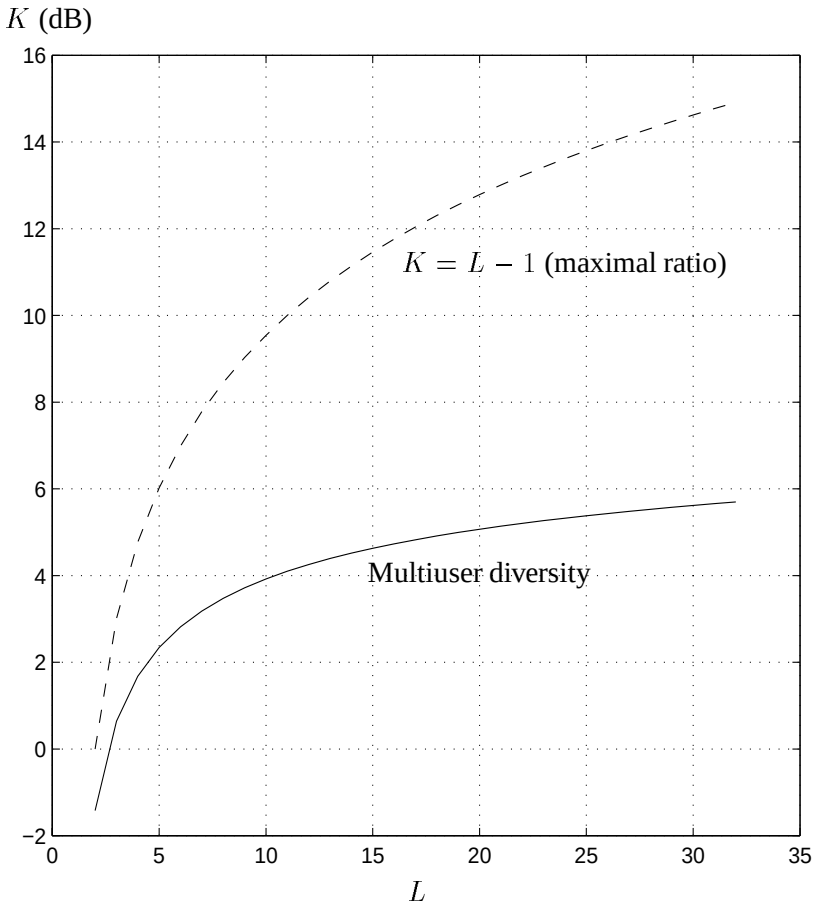

Figure 7.17: Multiuser Diversity Gain over Non–Fading Channel

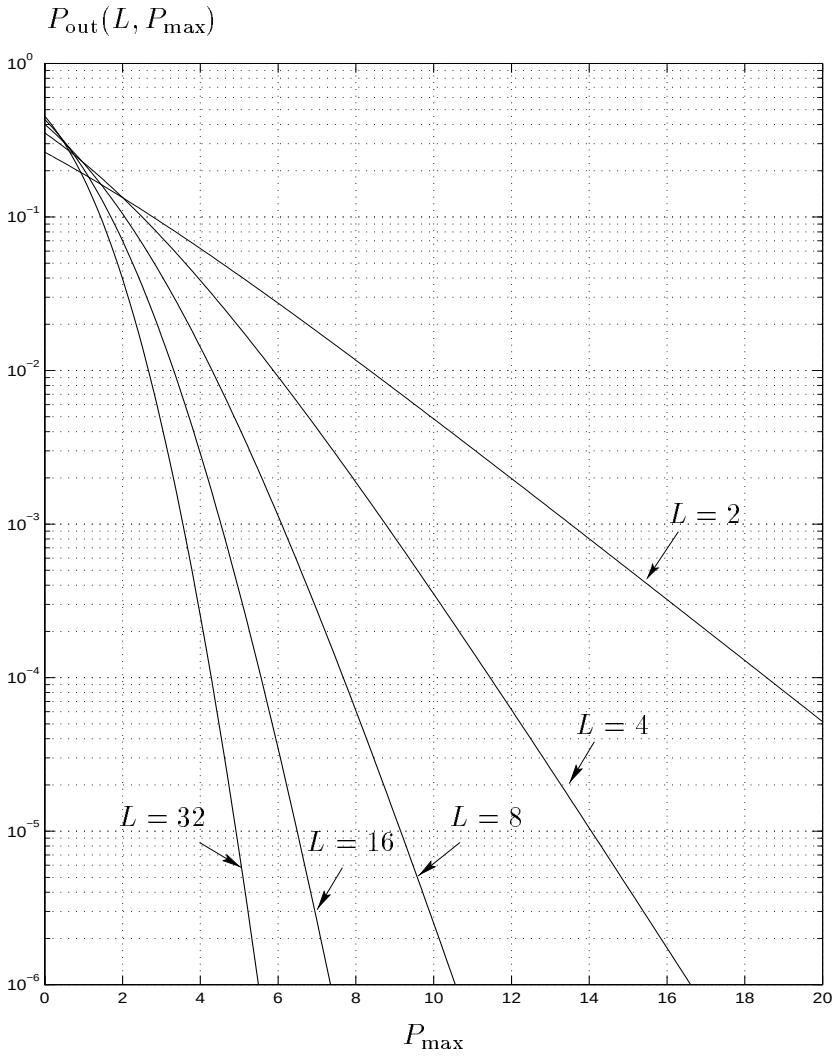

Figure 7.18: Peak–power Outage Probability with Multiuser Diversity

which for unit–mean square Rayleigh fading is

$$P_{\text{out}}(L, P_{\max}) = \left(1 - e^{-\frac{K(L)}{P_{\max}}}\right)^L. \tag{7.75}$$

We plot $P_{\text{out}}(L)$ as a function of $P_{\max}$ in figure 7.18.

Bit Error–Probability for Uncoded BPSK with Multiuser Diversity

As an example of using multiuser diversity with common signaling schemes, let us consider uncoded BPSK with and without power control. When no power control is employed, we have that the error probability conditioned on the maximum channel state h is

$$P_{b|h} = \text{Q}\left(\sqrt{2h\frac{\mathcal{E}_b}{N_0}}\right) \tag{7.76}$$

where $\mathcal{E}_b$ is the energy per information bit. Averaging over h in (7.67) yields

$$P_b = \text{E}_h P_{b|h} = .5\sum_{l=1}^{L}(-1)^{l-1}\binom{L}{i}\left(1 - \frac{1}{\sqrt{1 + i\frac{N_0}{\mathcal{E}_b}}}\right) \tag{7.77}$$

For the case with power control we have the following average error probability

$$P_b = (1 - P_{\text{out}}(L, P_{\max}))\text{Q}\left(\sqrt{2K(L)\frac{\mathcal{E}_b}{N_0}}\right) + \int_0^{K(L)/P_{\max}} \text{Q}\left(\sqrt{2u\frac{\mathcal{E}_b}{N_0}}\right) f_h(u)du \tag{7.78}$$

The bit–error–rates are shown in figures 7.19 and 7.20 for a varying number of users and peak–to–average power ratios $P_{\max}$. We see that in the case of no power control, we have performance superior to that of a non–fading channel for $L \geq 8$ at practical signal–to–noise ratios. In the case with power control, even better performance is possible. Moreover, for $L \geq 4$ we notice that peak–power constraints do not pose a significant problem.

The important conclusion to be drawn from this analysis is that channel state feedback, as in the single–user case, has a dramatic effect and that it may be a simpler option than sophisticated coding schemes for achieving acceptable performance on fading multiuser channels. Moreover, with multiuser diversity we do not need large QAM alphabets to improve performance as for single–user channels.

7.4 Chapter Summary

This chapter was concerned with multiuser communications and we focused on the up-link direction, which is appropriately modeled by a Gaussian multiple access channel. We began with a general discussion about the Gaussian MAC without fading and described the different dimension allocation strategies

that are available. These were orthogonal multiplexing, which includes TDMA, FDMA and combinations of the two. We also considered a simplified CDMA systems and the two main types of coding strategies, namely PN spreading or low–rate coding. An approach based on decoding a particular user's signal while considering other users as background noise was examined for the two cases and we showed that the low–rate coding alternative has some advantage.

We described the achievable rate region for the Gaussian MAC. In order to operate at an arbitrary set of rates on the boundary of this region one is forced to decode the users signals jointly, which is an arduous task. In the special case of equal transmitter powers, orthogonal multiplexing achieves the equal rate point on the region, and for this point is optimal.

We then moved on to the fading channel by first considering a comparison of single–user decoding for CDMA. We used the multi-tone model with the TU12 channel to compare a DS–CDMA approach to a general low–rate coding scheme. We found that much higher spectral efficiencies are attainable with low–rate coding. The results we obtained are comparable to the performance of the IS95 system in use today, indicating that our analysis approach is not that far off from reality.

The last section dealt with average information rates, which as in the case of the single–user channel can be achieved by either tolerating a long decoding delay or by performing variable–rate coding. In both cases, the quantities of interest are long–term average rates. We showed that the achievable rate region for an optimal joint coding scheme without channel control lies strictly outside the region of orthogonal multiplexing schemes, unlike the Gaussian MAC. Furthermore, for Rayleigh fading we showed that the total sum rate for a large number of users and a high signal–to–noise ratio exceeds that of orthogonal multiplexing by .8327 bits/s/Hz.

We then turned our attention to systems employing channel control. We showed that there is another inherent feature in multiuser systems which allows for very efficient exploitation of channel state information at the transmission end. This aspect is called multiuser diversity and arises from the fact that the medium must be shared by the users. With channel state information for all channels available at the user terminals, they can choose to transmit when their channels are stronger than all the rest. This is an inherent form of selection diversity and yields significant increases in the achievable data rates. In Rayleigh fading, the data rates even exceed a non–fading Gaussian channel. While schemes employing this form of diversity may not be suitable for delay constrained traffic, such as voice, some data communication systems may be able to benefit greatly from such schemes. An important result is that even without any error–control coding, the bit–error–rate of systems employing multiuser diversity is comparable to a non–fading channel. If, in addition, we employ power control, significantly lower

BER can be expected with respect to an uncoded non–fading channel. The performance is also rather insensitive to peak–power constraints.

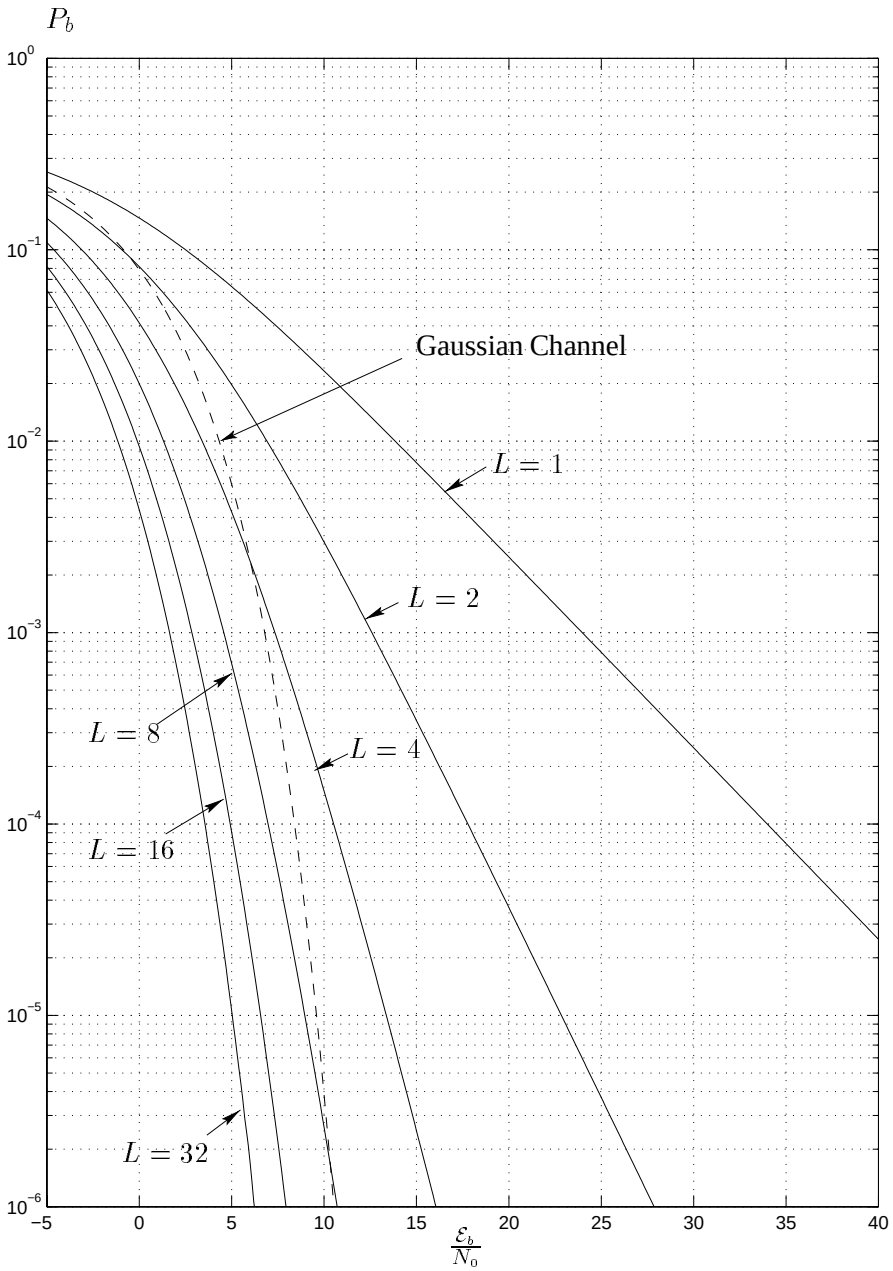

Figure 7.19: BER for Different Multiuser Diversity Systems without Power Control

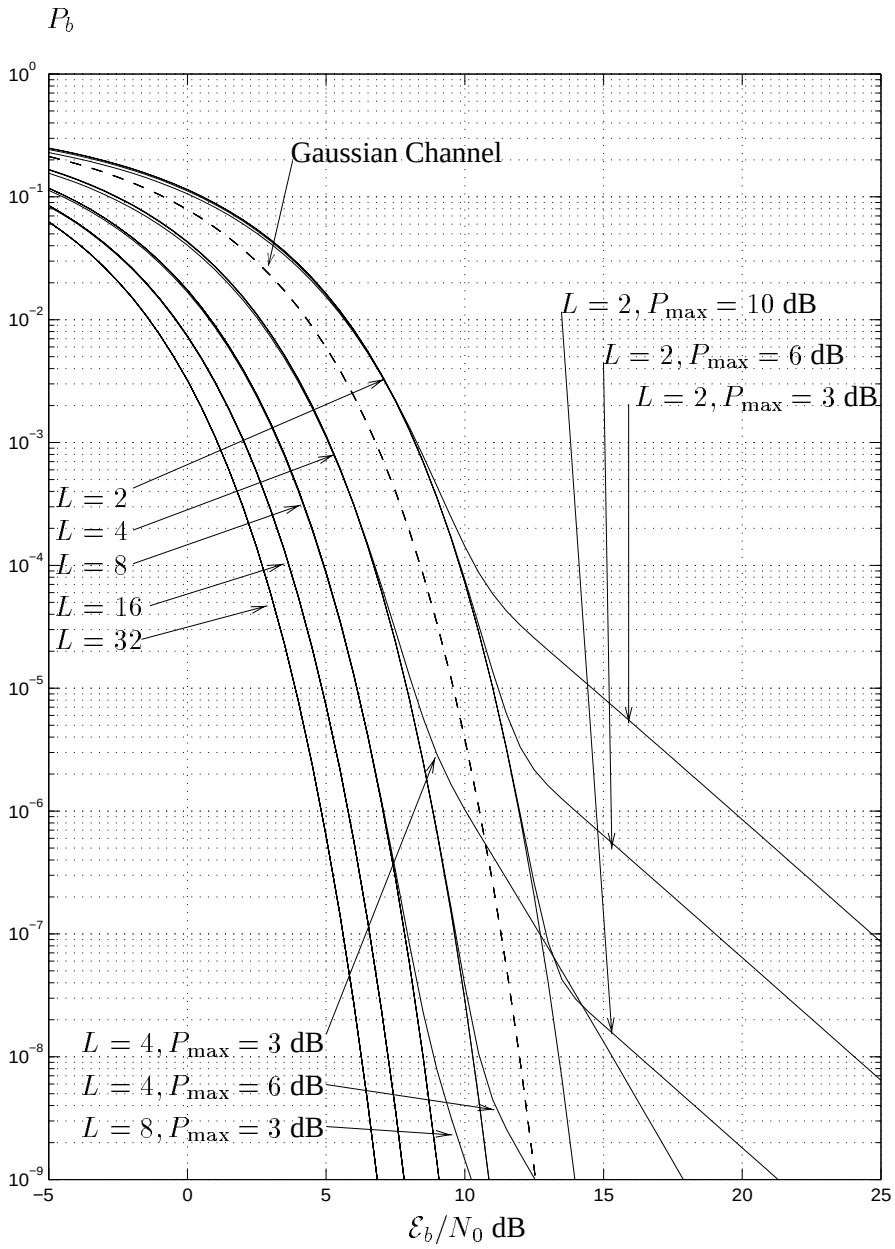

Figure 7.20: BER for a Multiuser Diversity Systems with Power Control

Chapter 8

Conclusions and Areas for Further Research

8.1 Conclusions

We now summarize the main results of this thesis. In Chapter 3 we showed that the communication problem over fading channels with a small number of degrees of freedom, or stated otherwise, independent realizations of a random process, is fundamentally limited by a quantity $P_{\rm out}(R)$, or the information outage rate. This quantity defines the minimum achievable probability of codeword error. We have applied these ideas to practical situations and have drawn a number of conclusions regarding what can be expected in terms of attainable performance. Even for high diversity systems, we should not expect to be able transmit at more than 1 bit/s/Hz for modest signal–to–noise ratios (on the order of 10 dB). We demonstrated that for spread–spectrum signals there is a large performance difference between using a direct–sequence and a very low rate coding technique. The latter approach benefits greatly in terms of spectral efficiency.

In chapter 4 we tackled the coding problem for channels with a small number of degrees of freedom by modeling them as block–fading channels. We have shown that diversity is limited not only by the number of degrees of freedom, but also by the size of the signaling constellation and the desired code rate. The Singleton bound turns out to be the tool which gives us this information. We found that both the Singleton bound and the information outage probability are linked in the sense that they predict the achievable diversity for any coding system over a finite number of degrees of freedom. Examples of block and trellis codes were given which attain maximum diversity. We have found, by computer

search, a wide variety of practical coding schemes for spectral efficiencies less than or equal to 1 bit/dim which, in some cases, achieve close to optimal performance. Their performance has been verified by computer simulation, both in terms of bit and frame error rates. It seems that the bit error rate is much less sensitive to the complexity of the coding scheme than the frame error rate. An important conclusion is that information outage probability is a good indicator of practical frame error rates.

Chapter 5 treated systems which employ channel state information at the transmission end in order to control or eliminate outages. This can be achieved either by fast power control or variable rate coding. We showed that systems with some diversity, such as multiple receivers or spread–spectrum signaling, can benefit tremendously with fast power control. Not only are outages eliminated but performance quickly approaches that of the non–fading channel with increasing diversity. For systems employing variable–rate coding, we found that simple two–rate schemes with power control can provide close to optimal performance. In the case of uncoded transmission, these simple schemes achieve performance comparable (or even better) than the uncoded AWGN channel without fading. This is important since it shows that channel state feedback can play the role of sophisticated coding/interleaving schemes over *ergodic* fading channels. We ended the chapter with a demonstration that the use of ARQ protocols on fading channels can achieve high average data rates, although slightly lower rates than for systems exploiting *a priori* channel knowledge. The key is to operate at a high spectral efficiency and high information outage rate (on the order of 50The downside is that the ARQ protocol has to work very hard to achieve these average rates.

Finally, in Chapter 6, we considered single–cell multiuser channels. After an introduction where we treated non–fading AWGN channels we examined different multiple–access approaches for single–user decoding of a wide–band (1.2288MHz) multiuser channel. We found, using the information outage probability, that a low–rate coding based CDMA system is far superior in terms of spectral efficiency to a direct–sequence based system. Moreover, we showed that our analysis is very accurate at predicting the spectral efficiency of practical CDMA systems such as IS95. In a single–cell system, the spectral–efficiency of an orthogonal scheme such as TDMA or FDMA/TDMA with frequency–hopping is much higher than CDMA. We then turned to average information rates, where it was found that the spectral efficiency of an optimal jointly–decoded CDMA system exceeds than of any orthogonal multiplexing system by .8723 bits/s/Hz for a large number of users and signal–to–noise ratio. For systems exploiting channel state feedback, we demonstrated that there is an inherent feature in multiuser systems which allows for significantly higher average data rates than even a non–fading channel. We have called this effect multiuser diversity, although it is simply selection diversity at the transmission end. Schemes

employing are potentially optimal for symmetric multiuser channels (i.e. where the average received power of all users is equal.) It allows for a completely orthogonal dynamically allocated FDMA/TDMA multiplexing so joint detection is not required. While systems employing this type of diversity may not by suitable for delay–constrained traffic, such as voice, some data communication systems may be able to benefit greatly from it. An important result is that even without any error–control coding, the bit error–rate of systems employing multiuser diversity is comparable (or even lower) than a non–fading channel. This is true both with and without power control.

8.2 Areas for further research

We have been unable to find construction methods for coding schemes with higher spectral efficiencies for the block–fading channel model and a small number of degrees of freedom. This is an important area for further research, since data systems working at higher signal–to–noise ratios (e.g. wireless local–area networks) will definitely require such coded–modulation schemes. The codes found in Chapter 4 should be analyzed for both partially–interleaved and multi-tone systems. In addition, for fast–fading channels, concatenation of these codes with multiple–symbol non–coherent detection would be an interesting problem to pursue.

We have completely ignored multiuser cellular systems where interference from other cells is an important issue. In some cases these can also be characterized using information outage techniques. An initial step in this direction has been taken in [CKH97]. As far as coding is concerned, the techniques from Chapter 4 should be applied to systems such as those described in [CKH97] and [PC95].

For the results on channel state feedback exploitation, we have not considered the channel estimation problem which, of course, is critical. At the same time practical protocols for exploiting multiuser diversity should be found and analyzed. These ideas must also be applied to interference–limited systems.

Bibliography

[ACM88] H.W. Arnold, D.C. Cox, and R.R Murray. "Macroscopic diversity performance meansured in the 800–MHz portable radio communications environment". *IEEE Trans. Antennas Propagat.*, 36:277–280, February 1988.

[Ahl71] R. Ahlswede. "Multi-way Communication Channels". In *Proc. 2nd. Int. Symp. Information Theory(Tsahkadsor, Armenian S.S.R)*, pages 23–52, Prague, 1971. Publishing House of the Hungarian Academy of Sciences.

[AS65] M. Abramovitz and I.A. Stegun. *Handbook of Mathematical Functions*. Dover, 1965.

[Aul79] T. Aulin. "A Modified Model for the Fading Signal at a Mobile Radio Channel". *VT*, 28(3):182–203, 1979.

[BB92] K. Boullé and J.C. Belfiore. "Modulation Scheme Designed for the Rayleigh Fading Channel". In *Proc. CISS '92, Princeton, N.J.*, March 1992.

[BCTV96] E. Biglieri, G. Caire, G. Taricco, and J. Ventura. "Simple Method for Evaluating Error Probabilities". *Electronic Letters*, 32(3):191–192, feb 1996.

[BDMS91] E. Biglieri, D. Divsalar, P.J. McLane, and M.K. Simon. *Introduction to Trellis–Coded Modulation with Applications*. MacMillan, New York, 1991.

[BG92] D.P. Bertsekas and R.G. Gallager. *Data Networks*. Prentice Hall, 1992.

[BGT93] C. Berrou, A. Glavieux, and P. Thitimajshima. "Near Shannon Limit Error–Correcting Coding and Decoding: Turbo–Codes". In *Proc. IEEE ICC '93*, May 1993.

[BJK96] P.W. Baier, P. Jung, and A. Klein. "Taking the challenge of multiple access for third-generation cellular mobile radio systems-a European view". *IEEE Communications Magazine*, 34(2):82–89, February 1996.

[Bla87] R.E. Blahut. *Principles and Practice of Information Theory.* Addison-Wesley, Reading, Massachusetts, 1987.

[BR97] T.E. Bell and M.J. Riezenman. "Communications". *IEEE Spectrum*, 34(1):27–37, January 1997.

[Bul87] R.J.C. Bultitude. "Measurement, Characterization and Modeling of Indoor 800/900 MHz Radio Channels for Digital Communications". *IEEE Commun. Mag.*, 25(6):5–12, 1987.

[BVRB96] J. Boutros, E. Viterbo, C. Rastello, and J.C. Belfiore. "Good Lattice Constellations for Both Rayleigh Fading and Gaussian Channels". *IEEE Transactions on Information Theory*, 42(2):502–518, March 1996.

[CG96] S.G. Chua and A. Goldsmith. "Variable–Rate Variable–Power MQAM for Fading Channels". In *Proc. VTC*, pages 815–819, April 1996.

[CG97] S.G. Chua and A. Goldsmith. "Adaptive Coded Modulation for Fading Channels". In *Proc. ICC*, pages 1488–1492, 1997.

[CKH97] G. Caire, R. Knopp, and P.A. Humblet. "System Capacity of F-TDMA Cellular Systems". *submitted to IEEE Trans. on Comm.*, March 1997.

[Cla68] R.H. Clarke. "A Statistical Theory of Mobile Radio Reception". *Bell Systems Technical Journal*, 47:957–1000, 1968.

[CT91] T. Cover and J. Thomas. *Elements of Information Theory*. John Wiley and Sons, New York, 1991.

[CV93] R.S. Cheng and S. Verdú. "Gaussian Multiaccess Channels with Capacity Region and Multiuser Water–Filling". *IEEE Transactions on Information Theory*, 39(3), may 1993.

[DR58] W.B. Davenport Jr. and W.L. Root. *An Introduction the the Theory of Random Signals and Noise*. McGraw Hill, New York, 1958.

[DS88] D. Divsalar and M.K. Simon. "The Design of Trellis Coded MPSK for Fading Channels: Performance Criteria". *IEEE Transactions on Communications*, 36:1004–1012, 1988.

[DS90] D. Divsalar and M.K. Simon. "Multiple–Symbol Differential Detection of MPSK". *IEEE Transactions on Communications*, 38:300–308, 1990.

[Eri70] T. Ericson. “A Gaussian Channel with Slow Fading”. *IEEE Transactions on Information Theory*, 1970.

[Feh95] K. Feher. *Wireless Digital Communications*. Prentice Hall, 1995.

[FL96] B.H. Fleury and P.E. Leuthold. “Radiowave Propagation in Mobile Communications: An Overview of European Research”. *IEEE Comm. Mag.*, pages 70–81, February 1996.

[For73] G.D. Forney Jr. “The Viterbi Algorithm”. *Proceedings of the IEEE*, 61(3):268–278, March 1973.

[For91] G.D. Forney Jr. “Geometrically Uniform Codes”. *IEEE Transactions on Information Theory*, 37:223–236, September 1991.

[Gal68] R.G. Gallager. *Information Theory and Reliable Communication*. John Wiley and Sons, 1968.

[Gal94] R.G. Gallager. “An Inequality on the Capacity Region of Multiaccess Multipath Channels”. In U. Maurer, T. Mittelholzer, G.D. Forney, and R.E. Blahut, editors, *Communications and Cryptography – Two Sides of One Tapestry–*, pages 129–139. Kluwer Academic Publishers, 1994.

[GB96] X. Giraud and J.C. Belfiore. “Constellations Matched to the Rayleigh Fading Channel”. *IEEE Transactions on Information Theory*, 42(1):106–115, January 1996.

[GJP+91] K. Gilhousen, I. Jacobs, A. Padovani, A.J. Viterbi, L. Weaver, and C. Wheatly. “On the Capacity of a Cellular CDMA System”. *IEEE Transactions on Vehicular Technology*, 40(2):303–312, 1991.

[Gol94] A. Goldsmith. *Design and Performance of High-Speed Communication Systems over Time–Varying Radio Channels*. PhD thesis, University of California at Berkeley, 1994.

[GP89] R. Ganesh and K. Pahlavan. “On the Arrival of the Paths in Multipath Fading Indoor Radio Channels”. *IEE Electr. Lett.*, 25:763–765, 1989.

[GR80] I. Gradsteyn and I. Ryzhik. *Tables of Integrals, series and products*. Academic Press, New York, 1980.

[GS83] U. Grenander and G. Szegö. *Toeplitz Forms and their Applications*. Chelsea, 1983.

[GSM90] European Telecommunications Standards Institute. *European Digital Cellular Telecommunications System : Physical Layer on the Radio Path (GSM 05.02)*, 1990.

[Gud91] M. Gudmundson. "Correlation Model For Shadow Fading in Mobile Radio Systems". *Elec. Lett.*, 27:2145–2146, Nov. 7 1991.

[Has79] H. Hashemi. "Simulation of the Urban Radio Propagation Channel". *VT*, 28(3):213–225, 79.

[Hat80] M. Hata. "Empirical Formula for Propagation Loss in Land Mobile Radio Services". *VT*, 29(3):317–325, 1980.

[HH89] J. Hagenauer and P. Heoher. "A Viterbi Algorithm with Soft–Decision Outputs and its Applications". In *Proceedings of IEEE Globecom*, pages 47.1.1–47.1.7, Dallas, Tx, feb 1989. IEEE.

[HHR96] P.A. Humblet, S. Het́huin, and L. Ramel. "A multiaccess protocol for high-speed WLAN". In *Proceedings of IEEE VTC '96*, May 1996.

[HT96] S.V. Hanly and D.N. Tse. "Multi–Access Fading Channels: Part II: Delay–Limited Capacities". Technical Report UCB/ERL M96/69, Electronics Research Laboratory, College of Engineering, University of California, Berkeley, 1996.

[Hui84] J.Y.N. Hui. "Throughput Analysis for Code Division Multiple Accessing of the Spread Spectrum Channel". *IEEE Journal on Selected Areas in Communications*, 2:482–486, July 1984.

[Hum85] P.A. Humblet. "Error Exponents for a Direct Detection Optical Channel". In *Proc. 23rd Allerton Conference on Communication, Control, and Computing*, October 1985.

[IS592] Telecommunications Industry Association. *EIA/TIA Interim Standard, Cellular System Dual mode Mobile-Station Base-Station Compatibility Standard IS-54B*, 1992.

[IS992] Proposed EIA/TIA Interim Standard. *Wideband Spread Spectrum Digital Cellular System Dual–Mode Mobile Station–Base Station Compatibility Standard*, 1992.

[IYTU84] F. Ikegami, S. Yoshida, T. Takeuchi, and M. Umehira. "Propagation Factors Controlling Mean Field Strength on Urban Streets". *IEEE Trans. on Antennas and Propagation*, 1984.

[Jak74] W.C. Jakes, editor. *Microwave Mobile Communications*. John Wiley and Sons, New York, 1974.

[KCW93] T. Kürner, D. Cichon, and W. Wiesbeck. "Concepts and Results for 3D Digital Terrain–base Wave Propagation Models: An Overview". *IEEE Transactions on Communications*, COM-11:1002–1012, September 1993.

[Ker96] K.J. Kerpez. "Radio Access System with Distributed Antennas". *IEEE Transactions on Vehicular Technology*, 45(2):265–275, May 1996.

[KH95a] R. Knopp and P.A. Humblet. "Information Capacity and Power Control in Single–Cell Multiuser Communications". In *Proc. IEEE ICC'95, Seattle, Wa.*, June 1995.

[KH95b] R. Knopp and P.A. Humblet. "Multiple–Accessing over Frequency–Selective Fading Channels". In *Proc. IEEE PIMRC'95, Toronto, Ont.*, Sept. 1995.

[KH96] R. Knopp and P.A. Humblet. *Multiacces, Mobility and Teletraffic for Mobile and Personal Communications*, chapter Channel Control and Multiple Access. Kluwer, 1996.

[Kim97] M. Kimpe. "A Fast Algorithm for Computerized Indoor Radio Channel Estimation". In *Proc. IEEE ICC'97, Montreal, Canada*, pages 66–70, June 1997.

[KL94] R. Knopp and H. Leib. "M–ary Phase Coding for the Non–Coherent AWGN Channel". *IEEE Transactions on Information Theory*, 40(6):1968–1984, November 1994.

[KSS95] G. Kaplan and S. Shamai (Shitz). "Error Probabilities for the Block–Fading Gaussian Channel". *Archiv für Elektronik und Übertragungstechnik*, 49(4):192–205, 1995.

[KSSK95] G. Kaplan, S. Shamai (Shitz), and Y. Kofman. "On the Design and Selection of Convolutional Codes for and Uninterleaved, Bursty Rician Channel". *IEEE Transactions on Communications*, 23(12), 1995.

[KZS97a] Y. Kofman, E. Zehavi, and S. Shamai(Shitz). "nd–Convolutional Codes- Part I: Performance Analysis". *IEEE Transactions on Information Theory*, 43(2):558–575, March 1997.

[KZS97b] Y. Kofman, E. Zehavi, and S. Shamai(Shitz). "nd–Convolutional Codes- Part I: Structural Analysis". *IEEE Transactions on Information Theory*, 43(2):576–589, March 1997.

[KZZ71] T.T Kadota, M. Zakai, and J. Ziv. "Capacity of a continuous memoryless channel with feedback". *IEEE Transactions on Information Theory*, 17:372–378, 1971.

[Lap94] A. Lapidoth. "The Performance of Convolutional codes over the Block Erasure Channel Using Various Finite Interleaving Techniques". *IEEE Transactions on Information Theory*, 40(5), 1994.

[LC83] S. Lin and D.J. Costello Jr. *Error Control Coding: Fundamentals and Applications*. Prentice Hall, Englewood Cliffs, New Jersey, 1983.

[Lee82] W.C.Y. Lee. *Mobile Communications Engineering*. McGraw Hill, New York, 1982.

[Lee90] W.C.Y. Lee. "Estimate of Channel Capacity in Rayleigh Fading Environment". *IEEE Transactions on Vehicular Technology*, 39(3):187–189, August 1990.

[Lia72] H. Liao. *Multiple Access Channels*. PhD thesis, University of Hawaii, Dept. of Electrical Engineering, Honolulu, 1972.

[LP91] H. Leib and S. Pasupathy. "Optimal Noncoherent Block Demodulation of Differential Phase Shift Keying". *Archiv für Elektronik und Übertragungstechnik*, 45:299–305, 1991.

[LWK93] Y.S. Leung, S.G. Wilson, and J.W. Ketchum. "Multi-frequency Trellis Coding with Low-Delay for Fading Channels". *COM*, 41(10):1450–1459, October 1993.

[Mas74] J.L. Massey. "Coding and Modulation in Digital Communications". In *Proc. Int. Zürich Sem. Digital Commun.*, Zürich, Switzerland, March 1974.

[Med95] M. Medard. *The Capacity of Time–Varying Multiple–User Channels in Wireless Communications*. PhD thesis, Massachusetts Institute of Technology, 1995.

[ML97] E. Malkamäki and H. Leib. "Rate $1/n$ Convolutional Codes with Interleaving Depth of n over a Block-Fading Ricean Channel". In *Proc. IEEE Vehicular Technology Conference*, pages 2002–2006, May 1997.

[MS84] R. McEliece and W.E. Stark. "Channels with Block Interference". *IEEE Transactions on Information Theory*, 30(1):44–53, January 1984.

[Nak60] M. Nakagami. "The M–distribution. A General Formula of Intensity Distribution of Rapid Fading". In W.C. Hoffman, editor, *Statistical Methods in Radio Wave Propagation*. Pergamon Press, 1960.

[OOKF68] Y. Okumura, E. Ohmori, T. Kawano, and K. Fukuda. "Field Strength and its Variability in the VHF and UHF Land Mobile Radio Service". *Review Elec. Commun. Lab.*, 16(9–10):825–873, 1968.

[OSSW94] L. Ozarow, S. Shamai (Shitz), and A.D. Wyner. "Information Theoretic Considerations for Cellular Mobile Radio". *IEEE Transactions on Vehicular Technology*, 43(2):359–378, May 1994.

[Pap82] A. Papoulis. *Probability, Random Variables and Stochastic Processes*. McGraw Hill, New York, 1982.

[Par92] D. Parsons. *The Mobile Radio Propagation Channel*. Pentech Press, London, England, 1992.

[PC95] G. Pottie and R. Calderbank. "Channel Coding Strategies for Cellular Mobile Radio". *IEEE Transactions on Vehicular Technology*, 44(4):763–769, November 1995.

[PHS95] ARIB. *Personal Handy Phone System ARIB Standard, version 2*, 1995.

[Pro95] J.G. Proakis. *Digital Communications*. McGraw Hill, New York, third edition, 1995.

[Rap96a] D. Raphaeli. "Non–Coherent Coded Modulation". *IEEE Transactions on Communications*, 44(2):172–183, 1996.

[Rap96b] T. Rappaport. *Wireless Communications*. Prentice Hall, Englewood Cliffs, New Jersey, 1996.

[RH92] T.S. Rappaport and D.A. Hawbaker. "A Ray Tracing Technique to Predict Path Loss and Delay Spread Inside Buildings". In *Proc. IEEE GLOBECOM '92*, pages 649–653, December 1992.

[RU96] B. Rimoldi and R. Urbanke. "A Rate–Splitting Approach to the Gaussian Multiple–Access Channel". *IEEE Transactions on Information Theory*, 42(2):364–375, March 1996.

[SBS66] M. Schwartz, W.R. Bennett, and Stein S. *Communication Systems and Techniques*. McGraw Hill, New York, 1966.

[SC89] C. Schlegel and D.J. Costello Jr. "Bandwidth Efficient Coding for Fading Channels: Code Construction and Performance Analysis". *IEEE Journal on Selected Areas in Communications*, 7(9), December 1989.

[Sha48a] C.E. Shannon. “A Mathematical Theory of Communication: Part I”. *Bell Systems Technical Journal*, 27:379–423, jul 1948.

[Sha48b] C.E. Shannon. “A Mathematical Theory of Communication: Part II”. *Bell Systems Technical Journal*, 27:353–355, oct 1948.

[Shn89] D.A. Shnidman. “The Calculation of the Probability of Detection and the Generalized Marcum Q–Function”. *IEEE Transactions on Information Theory*, 35(2):?, March 1989.

[Sin64] R.C. Singleton. “Maximum Distance q–Nary Codes”. *IEEE Transactions on Information Theory*, 10:116–118, 1964.

[Suz77] H. Suzuki. “A Statistical Model for Urban Multipath Propagation”. *COM*, 25(7):673–680, 77.

[SV87] A.A.M. Saleh and R.A. Valenzuela. “A Statistical Model for Indoor Multipath Propagation”. *IEEE Journal on Selected Areas in Communications*, 5:127–137, February 1987.

[TCJ+72] G.L. Turin, F.D. Clapp, T.L. Johnston, S.B. Fine, and D. Lavry. “A Statistical Model of Urban Multipath Propagation”. *VT*, 21(1):1–9, 72.

[TH96] D.N. Tse and S.V. Hanly. “Multi–Access Fading Channels: Part I: Polymatroidal Structure, Optimal Resource Allocation and Throughput Capacities”. Technical Report UCB/ERL M96/69, Electronics Research Laboratory, College of Engineering, University of California, Berkeley, 1996.

[Ung82] G. Ungerböck. “Channel Coding with Multilevel/Phase Signals”. *IEEE Transactions on Information Theory*, 28:55–67, January 1982.

[Van95] L. Vandendorpe. “Multitone Spread Spectrum Communications Systems in a Multipath Rician Fading channel”. *IEEE Transactions on Vehicular Technology*, pages 327–337, May 1995.

[Ver86] S. Verdú. “Minimum Probability of Error for Asynchronous Gaussian Multiple–Access Channels”. *IEEE Transactions on Information Theory*, 32(1), January 1986.

[Vit79] A.J. Viterbi. “Spread–Spectrum Communications- Myths and Realities”. *IEEE Comm. Mag.*, 4:11–18, May 1979.

[Vit90] A.J. Viterbi. "Very Low–Rate Convolutional Codes for Maximum Theoretical Perofmance of Spread–Spectrum Multiple–Access Channels". *IEEE Journal on Selected Areas in Communications*, 8(4), May 1990.

[VN96] R. Van Nee. "OFDM Codes for Peak–to–Average Power Reduction and Error Correction". *Proceedings of IEEE Globecom*, November 1996.

[VT68] H.L. Van Trees. *Detection, Estimation and Modulation Theory: Part I*. John Wiley and Sons, New York, 1968.

[VT72] H.L. Van Trees. *Detection, Estimation and Modulation Theory: Part III*. John Wiley and Sons, New York, 1972.

[VT95] G. Vitetta and D.P. Taylor. "Maximum Likelihood Decoding of Uncoded and Coded PSK Signal Sequences Transmitted over Rayleigh Flat–Fading Channels". *IEEE Transactions on Communications*, 43(11):2750–2758, November 1995.

[WB88] J. Walfisch and H.L. Bertoni. "A Theoretical Model of UHF Propagation in Urban Environments". *IEEE Trans. Antennas and Propagation*, AP-38:1788–1796, December 1988.

[Wil96] S.G. Wilson. *Digital Modulation and Coding*. Prentice Hall, Englewood Cliffs, New Jersey, 1996.

[WJ65] J. Wozencraft and I. Jacobs. *Principles of Communication Engineering*. John Wiley and Sons, New York, 1965.

[WJ95] T. Wilkinson and A. Jones. "Minimization of the Peak–to-Mean Envelope Power Ratio of Multicarrier Transmission Schemes by Block Coding". *Proceedings of the IEEE International Conference on Vehicular Technology*, July 1995.

[Wol69] J.K. Wolf. "Adding Two Information Symbols to Certain Non–Binary BCH Codes and Some Applications". *Bell Systems Technical Journal*, 48:2405–2424, 1969.

[Wol78] J. Wolfowitz. *Coding Theorems of Information Theory*. Springer–Verlag, 1978.

[Wyn94] A.D. Wyner. "Shannon–Theoretic Approach to a Gaussian Cellular Multiple–Access Channel". *IEEE Transactions on Information Theory*, 40(6), November 1994.